UNIVERSITAT DE BARCELONA

Molecular Mechanisms of the Ubiquitin Ligase HERC2 in Cell Signalling: Implications in Cellular Stress, Autophagy and Proteasome Assembly

Joan Sala Gastón

UNIVERSITAT DE BARCELONA

DOCTORAL PROGRAM in BIOMEDICINE

Molecular Mechanisms of the Ubiquitin Ligase HERC2 in Cell Signalling: Implications in Cellular Stress, Autophagy and Proteasome Assembly

---

Doctoral thesis submitted by:

Joan Sala Gaston

Thesis conducted under the direction of:

Dr. José Luis Rosa López

Departament de Ciències Fisiològiques
Facultat de Medicina i Ciències de la Salut
Campus Bellvitge - Universitat de Barcelona - 2022

TABLE OF CONTENTS

INDEX OF FIGURES

INDEX OF TABLES

Abbreviations and acronyms

53BP1	TP53-binding protein 1
ADRM1	Proteasomal ubiquitin receptor ADRM1
ALP	Autophagy-Lysosome Pathway
ALS	Amyotrophic lateral sclerosis
AMP	Adenosine monophosphate
AMPK	5'-AMP-activated protein kinase
A-RAF	Serine/threonine-protein kinase A-Raf
ARE	Antioxidant Response Element
ASK	Apoptosis Signal-Regulating Kinase
ASPM	Abnormal spindle-like microcephaly-associated protein
ATF	Activating Transcription Factor
ATG	Autophagy-Related Gene
ATM	Serine-protein kinase ATM
ATP	Adenosine triphosphate
ATP	Adenosine triphosphate
ATR	Serine/threonine-protein kinase ATR
BARD1	BRCA1-associated RING domain protein 1
BCA	Bicinchoninic Acid Assay
BH3	Bcl2-homology domain 3
^{bio}Ub	biotin-tagged ubiquitin
BirA	Biotin protein ligase
BLM	RecQ-like DNA helicase BLM
B-RAF	Serine/threonine-protein kinase B-raf
BRCA1	Breast cancer type 1 susceptibility protein
BSA	Bovine Serum Albumin
BTF3	Transcription factor BTF3

bvg3	HERC2 polyclonal antibody
CAT	Catalase
CHC	Clathrin Heavy Chain
CHK1	Serine/threonine-protein kinase Chk1
CHOP	C/EBP-homologous protein / DNA damage-inducible transcript 3 protein
CMA	Chaperone-Mediated Autophagy
COVID-19	Coronavirus disease 2019
CP	Core Particle
CP110	Centriolar coiled-coil protein of 110 kDa
CPH	Conserved domain within Cul7, PARC and HERC2
CR	Conserved Region
C-RAF	RAF proto-oncogene serine/threonine-protein kinase
CRD	Cysteine-Rich Domain
CUL3	Cullin-3
Cul7	Cullin7
Cyt b5	cytochrome b5-like region
DLK1	Protein delta homolog 1
DMEM	Dublecco's Modified Eagle's Medium
DNA	Desoxyribonucleic acid
DNA-PK	DNA-dependent protein kinase catalytic subunit
DSB	DNA double-strand break
DTT	Dithiothreitol
DUB	deubiquitylating enzyme
DUSP1	Dual specificity protein phosphatase 1
E1	Ubiquitin-activating enzyme
E2	Ubiquitin-conjugating enzyme
E3	Ubiquitin ligase
E6AP	Ubiquitin-protein ligase E3A

ECL	Enhanced Chemiluminescence
EDTA	Ethylenediaminetetraacetic acid
ELK1	ETS domain-containing protein Elk-1
ER	Endoplasmic Reticulum
ERK	Extracellular signal-Regulated Kinase
FBS	Fetal Bovine Serum
FBX15	F-box only protein 15
FIP200/RB1CC1	RB1-inducible coiled-coil protein 1
G4	G-quadruplex DNA secondary structures
GAP	GTPase-Activating Protein
GAPDH	Glyceraldehyde-3-Phosphate Dehydrogenase gene
GDP	Guanosine diphosphate
GEF	Guanine Exchange Factor
GFP	Green Fluorescent Protein
GPCR	G Protein-Coupled Receptors
GPX	Glutathione peroxidase
GRB2	Growth factor Receptor-Bound protein 2
GSH	Glutathione
GST	Glutathione S-Transferase
GTP	Guanosine triphosphate
GUSB	Beta-glucuronidase gene
H_2O_2	Hydrogen peroxide
HECT	Homologous to E6-AP carboxy terminus
HERC	RCC1-like domain-containing HECT proteins
HSC70/HSPA8	Heat shock cognate 71 kDa protein
HSP90	Heat shock protein 90
IFN-γ	Interferon gamma
IL	Interleukin

INH	Inhibitors
IP	Immunoprecipitation
IRP2	Iron-responsive element-binding protein 2
jdf2	juvenile development and fertility-2 syndrome
JNK	c-Jun N-terminal Kinase
KD	Knock-Down
kDa	Kilodalton
KEAP1	Kelch-like ECH-associated protein 1
KO	Knock-Out
LAMP2	Lysosome-associated membrane glycoprotein 2
LC3	Microtubule-associated proteins 1A/1B light chain 3
LC-MS/MS	Liquid Chromatography - Tandem Mass Spectrometry
LDS	Lithium Dodecyl Sulfate
LFQ	Label-Free Quantification
LIR	LC3-Interacting Region
LKB1	Serine/threonine-protein kinase STK11
lncRNA	long non-coding RNA
LRRK2	Leucine-rich repeat serine/threonine-protein kinase 2
MAPK	Mitogen-Activated Protein Kinase
MCM2	DNA replication licensing factor MCM2
MDM2	E3 ubiquitin-protein ligase Mdm2
MEFs	Mouse Embryonic Fibroblasts
MEF2	Myocyte-specific enhancer factor 2A
MEK	Dual specificity mitogen-activated protein kinase kinase
M-H	mind-bomb/HERC2 domain
MHC	Major Histocompatibility Complex
MLK	Mix Lineage Kinase
MP1	MEK-binding Partner 1

mRNA	Messenger RNA
MSK	Mitogen and Stress activated protein Kinase
mTORC1	Mammalian Target Of Rapamycin Complex 1
MW	Molecular Weight
MYC	Myc proto-oncogene protein
NBR1	Next to BRCA1 gene 1 protein
NC	Negative Control
NCOA4	Nuclear receptor coactivator 4
NDP52	Calcium-binding and coiled-coil domain-containing protein 2
NEURL4	Neuralized-like protein 4
NFE2L2	Nuclear factor erythroid 2-related factor 2 gene
NLK	Serine/threonine-protein kinase NLK
NLRC4	NLR family CARD domain-containing protein 4
NRF2	Nuclear factor erythroid 2-related factor 2
Nt-R	Amino-terminal arginine residue
NudCL2	NudC-like protein 2
O_2^-	Superoxide anion radical
OCA2	oculocutaneous albinism II gene
OH	Hidroxyl radical
OPTN	Optineurin
p62/SQSTM1	Sequestosome-1
PAAF1	Proteasomal ATPase-associated factor 1
PAC	Proteasome Assembly Chaperone
PAGE	Polyacrylamide Gel Electrophoresis
PARC	Parkin-like Cytoplasmic
PBS	Phosphate Buffered Saline
PCNA	Proliferating cell nuclear antigen
PCR	Polymerase Chain Reaction

PD	Pull-Down
PE	Phosphatidylethanolamine
PI	Preimmune serum
PI3K	Phosphoinositide 3-kinase/phosphatidylinositol 3-kinases
PI3KC3/VPS34	Phosphatidylinositol 3-kinase catalytic subunit type 3
PI3KC3-C1	Phosphatidylinositol 3-kinase class III complex 1
PI3KR4/VPS15	Phosphoinositide 3-kinase regulatory subunit 4
PI3P	Phosphatidylinositol-3-phosphate
PIAS4	E3 SUMO-protein ligase PIAS4
PKC	Protein Kinase C
POMP	Proteasome maturation protein
PSMC	26S proteasome regulatory subunit
PSMD	26S proteasome non-ATPase regulatory subunit
PSME	Proteasome activator complex subunit
PTM	post-translational protein modification
PVDF	Polyvinylidene difluoride
qRT-PCR	Quantitative Reverse Transcription PCR
RAP80	BRCA1-A complex subunit RAP80
Raptor	Regulatory-associated protein of mTOR
RBD	Ras Binding Domain
RBR	RING-in-Between-RING
RCC1	Regulator of chromosome condensation 1
Rheb	GTP-binding protein Rheb
RING	Really interesting new gene
rjs	runty, jerky, sterile syndrome
RLD	RCC1-Like Domain
RNA	Ribonucleic acid
RNF168	E3 ubiquitin-protein ligase RNF168

RNF8	E3 ubiquitin-protein ligase RNF8
ROS	Reactive Oxygen Species
RP	Regulatory Particle
RPA	Replication Protein A
RSK	Ribosomal S6 Kinase
RTK	Receptor Tyrosine Kinase
SAR	Selective Autophagy Receptors
SARS-CoV-2	Severe Acute Respiratory Syndrome CoronaVirus 2
SCF	Skp, Cullin, F-box containing complex
SEM1	26S proteasome complex subunit SEM1
SH2	Src Homology 2
shRNA	Short Hairpin RNA
siRNA	Small-Interfering RNA
SLR	Sequestosome-1-Like Receptor
SNP	Single Nucleotide Polymorphism
SOD	Superoxide dismutase
SOS	Son Of Sevenless homolog
SPRY	SPla and ryanodine receptor domain
TAK1	Nuclear receptor subfamily 2 group C member 2
TAO	Serine/threonine-protein kinase TAO
TAX1BP1	Tax1-binding protein 1
TBK1	Serine/threonine-protein kinase TBK1
TBS-T	Tris-Buffered Saline and Tween 20
TF	Transcription Factor
TFEB	Transcription factor EB
TLR	Toll-Like Receptor
TNFα	Tumor necrosis factor alpha
tRNA	Transfer RNA

TSC2	Tuberin
TUBEs	Tandem Ubiquitin Binding Domains
TUSC4	GATOR complex protein NPRL2
Ub	Ubiquitin
Ubc13	Ubiquitin-conjugating enzyme E2 N
UBD	Ubiquitin Binding Domain
ULK	Unc-51-like kinase / Serine/threonine-protein kinase ULK
UPS	Ubiquitin-Proteasome System
USP16	Ubiquitin carboxyl-terminal hydrolase 16
USP20	Ubiquitin carboxyl-terminal hydrolase 20
USP33	Ubiquitin carboxyl-terminal hydrolase 33
WD40	Trp-Asp-rich 40-amino acid repeat
WHO	World Health Organisation
WIP1	Protein phosphatase 1D
WIPI	WD repeat domain phosphoinositide-interacting protein
WRN	Bifunctional 3'-5' exonuclease/ATP-dependent helicase WRN
WT	Wild-Type
XPA	DNA repair protein complementing XP-A cells
α-MEM	Alpha-modified Minimum Essential Medium

English abstract

Ubiquitylation is a posttranslational modification that consists in the attachment of ubiquitin to a substrate protein. During the process of ubiquitylation, the E3 ubiquitin ligases determine the specificity of the substrates, thus, they represent a crucial regulatory factor. Among them is the ubiquitin ligase HERC2, which belongs to the Large HERC protein family. HERC2 has been extensively studied for its implication in the regulation of genomic stability and p53 transcriptional activity. However, its involvement in other signalling pathways in which ubiquitylation also plays an important role remains fairly unexplored. Regarding the clinical relevance of HERC2, mutations in HERC2 gene in humans have been related to different pathologies such as a neurodevelopmental disorder known as HERC2 Angelman-like syndrome and several types of cancers. A better understanding of how pathologic HERC2 mutant variants affect intracellular signalling may aid definition of potential new therapies for these disorders.

In view of all this, the main objective of this thesis was to study the signalling pathways regulated by HERC2 and to characterize the molecular mechanisms behind. We focused on the MAPK and autophagy pathways, and analysed how these are deregulated in pathological contexts of HERC2 deficiency. For that, we studied patient-derived fibroblasts of individuals with the HERC2 Angelman-like syndrome, which present a marked reduction in HERC2 protein levels. We complemented the investigations using other human and mouse cellular models by knocking down HERC2 protein expression. On the other hand, we applied a proteomic approach to identify ubiquitylated proteins regulated by HERC2, which can help to unveil novel physiological functions of this ubiquitin ligase.

First, we studied MAPK signalling pathways in the patient-derived fibroblasts and observed increased levels of C-RAF protein and p38 phosphorylation. We showed that this occurs due to the fact that HERC2 regulates ubiquitin-mediated proteasomal degradation of C-RAF. Thus, in a context of HERC2 deficiency, C-RAF protein levels are upregulated. We found out that this upregulation triggers overactivation of a crosstalk between C-RAF and MKK3/p38 signalling pathways, which boosts the cellular response to oxidative stress through NRF2 and the expression of antioxidant genes.

Secondly, we focused on autophagy and observed that it was increased in HERC2 deficient cells. Moreover, we demonstrated that HERC2 regulates protein levels of the autophagy initiating kinase ULK1 and the deubiquitinating enzyme USP20, which stabilizes ULK1. Additionally, we showed that HERC2 interacts with USP20, and observed that this interaction is disrupted upon p38 phosphorylation. Taken together these results suggested that HERC2 regulates autophagy through modulating USP20/ULK1 axis and that this process might be fine-tuned by p38 activity.

In third place, we applied a proteomic approach to identify potential HERC2 ubiquitylation substrates. Results showed a functional enrichment of proteins related with the proteasome assembly pathway such as PSMC5 and PAAF1. We further confirmed that HERC2 interacts with these proteins in pull-down experiments.

Finally, we discussed the molecular mechanisms of HERC2 in the regulation of MAPK signalling, autophagy and the proteasome assembly pathway, trying to postulate a working model that adds the results obtained to the knowledge stablished so far in the scientific literature. In addition, we inquired about how these mechanisms fit with the pathophysiology of the HERC2 Angelman-like syndrome and cancer.

In conclusion, throughout this work we revealed previously unexplored functions of the ubiquitin ligase HERC2 in cell signalling. In particular, we described HERC2 as a regulator of: 1) the cellular response to oxidative stress through the C-RAF/MKK3/p38 pathway; 2) autophagy through the USP20/ULK1 axis; and 3) the proteasome assembly pathway through regulating ubiquitylation of proteins such as PSMC5 and PAAF1.

Resum en català

La ubiqüitilació és una modificació post-traduccional que consisteix en la unió d'una o més molècules d'ubiqüitina a una proteïna substrat. Durant el procés d'ubiqüitilació, les lligasses d'ubiqüitina E3 determinen l'especificitat dels substrats. Per aquesta raó, representen un factor regulador molt important. Una d'aquestes és la ubiqüitina lligassa HERC2, que pertany a la família de proteïnes anomenades "HERC grans". La proteïna HERC2 ha estat àmpliament estudiada per la seva implicació en la regulació de l'estabilitat genòmica i l'activitat transcripcional de p53. Tanmateix, la seva participació en altres vies de senyalització, en què la ubiqüitilació també hi té un paper regulador important, continua sent força desconeguda. Pel que fa a la rellevància clínica de l'HERC2, mutacions en el seu gen en humans s'han relacionat amb diferents patologies com ara amb un trastorn del neuro-desenvolupament similar a la síndrome d'Angelman que s'anomena "*HERC2 Angelman-like*", i també amb diversos tipus de càncers. Un millor coneixement de com les diferents mutacions patològiques del gen *HERC2* afecten a la senyalització intracel·lular ens pot ajudar a desenvolupar possibles noves teràpies per a les persones afectades per aquests trastorns.

Tenint en compte tot això, l'objectiu principal d'aquesta tesi doctoral va ser estudiar les vies de senyalització regulades per la proteïna HERC2 i caracteritzar-ne els mecanismes moleculars. Concretament, ens vam centrar en les vies de les MAPK i la via de l'autofàgia, analitzant també com aquestes es desregulen en contextos patològics de deficiència d'HERC2. Per assolir aquests objectius, vam estudiar fibroblasts humans derivats de pacients amb la síndrome *HERC2 Angelman-like*, els quals presenten una marcada reducció dels nivells de la proteïna HERC2. A més a més, vam complementar aquestes investigacions utilitzant altres models cel·lulars com ara cèl·lules humanes i de ratolí amb un silenciament de l'expressió de la proteïna HERC2. Per altra banda, també vam realitzar un estudi de proteòmica per identificar proteïnes ubiqüitilades que estiguin regulades per l'HERC2. Aquest enfocament ens pot ser molt útil per tal de descobrir noves funcions fisiològiques d'aquesta ubiqüitina lligassa.

Així doncs, primer vam estudiar les vies de senyalització de les MAPK en els fibroblasts derivats del pacient amb la síndrome *HERC2 Angelman-like* i vam observar que presentava uns nivells augmentats de la proteïna C-RAF, així com també de la fosforilació de p38.

Seguidament, vam demostrar que això es produeix perquè l'HERC2 regula la ubiqüitilació i posterior degradació via proteasoma de C-RAF. Així doncs, en un context de deficiència d'HERC2, els nivells de proteïna de C-RAF incrementen. A més a més, vam descobrir que aquest increment provoca la sobre-activació d'una comunicació entre les vies de senyalització de C-RAF i MKK3/p38, cosa que dispara la resposta cel·lular a l'estrès oxidatiu mitjançant el factor de transcripció NRF2 i l'expressió de gens antioxidants.

En segon lloc, ens vam centrar en la via de l'autofàgia i vam observar que aquesta està incrementada en les cèl·lules deficients d'HERC2. A més, vam demostrar que l'HERC2 regula els nivells de la cinasa iniciadora de l'autofàgia ULK1 i de l'enzim deubiqüitinant USP20, el qual pot estabilitzar ULK1. També, vam descobrir que l'HERC2 interacciona amb l'USP20 i vam observar que aquesta interacció es veu alterada per l'activació de p38. En conjunt, aquests resultats van suggerir-nos que l'HERC2 regula l'autofàgia mitjançant la modulació de l'eix USP20/ULK1 i que aquest procés pot estar ajustat per mitjà de l'activitat de p38.

A continuació, vam realitzar un estudi de proteòmica per identificar els possibles substrats d'ubiqüitilació de l'HERC2. Els resultats van mostrar-nos un enriquiment funcional de proteïnes relacionades amb la via del muntatge del proteasoma com ara PSMC5 i PAAF1. Seguidament, vam confirmar que l'HERC2 interacciona amb aquestes proteïnes amb uns experiments d'interacció.

Finalment, a l'apartat de discussió, plantegem quins són els mecanismes moleculars a través dels quals l'HERC2 regula les vies de les MAPK, l'autofàgia i la del muntatge del proteasoma, intentant postular un model que encaixi els resultats que hem obtingut amb el coneixement científic previ. A més a més, també debatem sobre com aquests mecanismes es poden relacionar amb la fisiopatologia de la síndrome *HERC2 Angelman-like* i el càncer.

En conjunt, durant aquest treball hem revelat funcions prèviament inexplorades de la lligasa d'ubiqüitina HERC2 en la senyalització cel·lular. En concret, hem descrit a l'HERC2 com a reguladora de diversos processos com ara: 1) la resposta cel·lular a l'estrès oxidatiu, a través de la via C-RAF/MKK3/P38. 2) L'autofàgia, a través de l'eix USP20/ULK1. 3) La via de muntatge del proteasoma, mitjançant la regulació de la ubiqüitilació de proteïnes com ara PSMC5 i PAAF1.

CHAPTER I. Introduction

Ubiquitylation

Ubiquitylation is a posttranslational modification that consists in the attachment of ubiquitin to a substrate protein. Ubiquitin can be linked as a single moiety or in the form of polymeric chains of different topologies. In addition, further modifications of polyubiquitin chains such as phosphorylation, acetylation, SUMOylation and NEDDylation can also occur. Similar to a code, different ubiquitin modifications lead to different outcomes in the cells. Ubiquitin E3 ligases are the enzymes that catalyse the transfer of ubiquitin to a protein substrate. Therefore, they determine the precise substrate specificity of ubiquitylation, and play essential roles in cell signalling networks mediated by ubiquitin. Accordingly, the Large HERC ubiquitin ligase HERC2, is involved in several cellular functions such as regulation of genomic stability, regulation of p53 transcriptional activity, neurodevelopment and centrosome function, among others.

The ubiquitylation cascade

Ubiquitin (Ub) is a small globular protein of 76 amino acid residues that was first identified in 1975 as a 8,5 kDa protein expressed in all eukaryotic cells [1]. The basic biological functions of ubiquitin and the components of the ubiquitylation pathway were discovered in the early 1980s. Avram Hershko, Aaron Ciechanover and Irwin A. Rose characterized the ATP-dependent, ubiquitin-mediated protein degradation system [2–4]. As a result of their pioneering findings on the field, Hershko, Ciechanover, and Rose were awarded the 2004 Nobel Prize in Chemistry “for the discovery of ubiquitin-mediated protein degradation” [5].

The most important features of ubiquitin are its flexible six-residue **C-terminal tail**, its **N-terminus residue methionine** and its **seven lysine residues**. Ubiquitin attaches to a substrate through the formation of a covalent bond between the Ub C-terminal tail and, typically, an internal lysine residue of the substrate. The Ub N-terminus residue (**Met1**) and the seven lysines (**Lys6, Lys11, Lys27, Lys29, Lys33, Lys48, Lys63**) are the attachment sites for chain assembly and they cover all surfaces of ubiquitin pointing to different spatial directions [6] (Figure 1A).

Ubiquitylation is a post-translational protein modification (PTM) that consists in the conjugation of ubiquitin to a substrate protein. This process requires a coordinated and

sequential enzymatic cascade that consists in a 3-step process and involves three types of enzymes: **ubiquitin-activating enzymes (E1)**, **ubiquitin-conjugating enzymes (E2)** and **ubiquitin ligases (E3)**. First, ubiquitin is activated by an E1 enzyme, which binds the ubiquitin to a cysteine residue within its structure in an ATP-dependent manner. Then, an E2 enzyme transfers the ubiquitin from E1 to the active site cysteine of the E2 in a process called conjugation. Finally, E3 ubiquitin ligases intervene in the last step of the ubiquitylation cascade, catalysing a covalent union between the C-terminal region of ubiquitin and, typically, a lysine residue of the target protein (Figure 1B). Thus, E3 ligases determine substrate specificity [7]. In humans, 2 E1s, 38 E2s and over 600 E3s have been identified [8].

Ubiquitylation can be reversed by **deubiquitylating enzymes (DUBs)**, which catalyse deconjugation of ubiquitin from the protein where it is attached (Figure 1B). To date, up to 100 different DUBs have been described in humans [9].

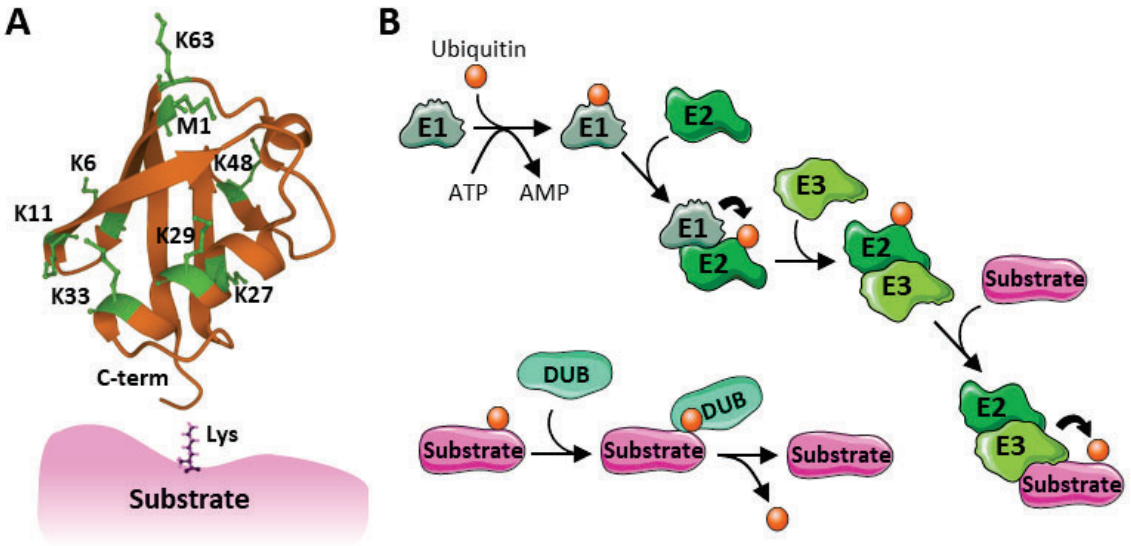

Figure 1. The ubiquitylation cascade. (A) Crystal structure of a ubiquitin monomer indicating its C-terminal tail (C term), the seven lysine residues (K6, K11, K27, K29, K33, K48, K63), and M1 residue. Residues depicted in green. Crystal structure obtained from Protein Data Bank (PDB), identification code 1UBQ (10.2210/pdb1UBQ/pdb). **(B)** Schematic representation of the ubiquitylation cascade. The ubiquitin is first activated by an E1 enzyme with ATP consumption. Then, ubiquitin is transferred to a E2 enzyme, which in turn binds to an E3 to mediate the ubiquitylation of the target protein. Deubiquitylating enzymes (DUBs) catalyse deconjugation of ubiquitin.

The ubiquitin code

Once attached to a substrate, ubiquitin can be exposed to additional modifications, thus creating different polymeric chains which encode information about the substrate's fate in the cell. This is known as the **ubiquitin code**. Ubiquitin can be ubiquitylated on the seven

lysine residues or the N-terminus methionine residue, which leads to the formation of polyubiquitin chains of different topologies. Over the years, it has been discovered that ubiquitin lysine residues can also be modified by ubiquitin-like molecules such as SUMO or NEDD8. In addition, further modification of ubiquitin with acetylation on Lys and phosphorylation on Ser, Thr or Tyr residues have also been identified (Figure 2). This expands the ubiquitin code with new layers of ubiquitin modifications and shows the complexity and potential versatility of the ubiquitin code in cell signalling [10].

Proteins can be ubiquitylated at one or multiple lysine residues with a single ubiquitin moiety. This is called **monoubiquitylation** or **multi-monoubiquitylation**, respectively, and has been associated with DNA repair, transcriptional regulation, membrane trafficking and proteasomal degradation, among other functions [11, 12]. The attachment of more than one ubiquitin moiety in a substrate protein forming a chain is called **polyubiquitylation**. Polyubiquitin chains can be formed with different length, linkage type and alignment (Figure 2). Indeed, all linkage(s) types are present in cells, corroborated by proteomic studies [13].

Ubiquitin chains that contain only one unique linkage type are called **homotypic** (Figure 2). The most predominant linkage type is **Lys48-linked ubiquitin chains** and its main biological outcome is to target the substrate protein to proteasome-dependent degradation. The second most abundant linkage type is the **Lys63-linked ubiquitin chains**. This linkage type does not primarily target proteins to proteasome degradation, instead, Lys63 Ub chains drive proteolysis by the autophagy-lysosome system and, in addition, have other non-proteolytic functions such as regulation of protein activity or transcription [10, 14]. The remaining homotypic polyUb chains (Lys6, Lys27, Lys29, Lys33 and Met1), although less studied and known as "**atypical ubiquitin chains**", are involved in different cell signalling functions such as cell cycle control and cytokine signalling [15].

On the other hand, ubiquitin chains that contain mixed linkages are known as **heterotypic**. These ones can also be branched if a ubiquitin molecule is ubiquitylated at two or more sites (Figure 2). Therefore, considering the eight linkages sites of ubiquitin, the possibility of forming branched structures and the new layers of the ubiquitin code including modifications by SUMMO, NEDD8, acetylation and phosphorylation, this generates a limitless amount of potential combinations, and highlights the complexity of the ubiquitin code [16].

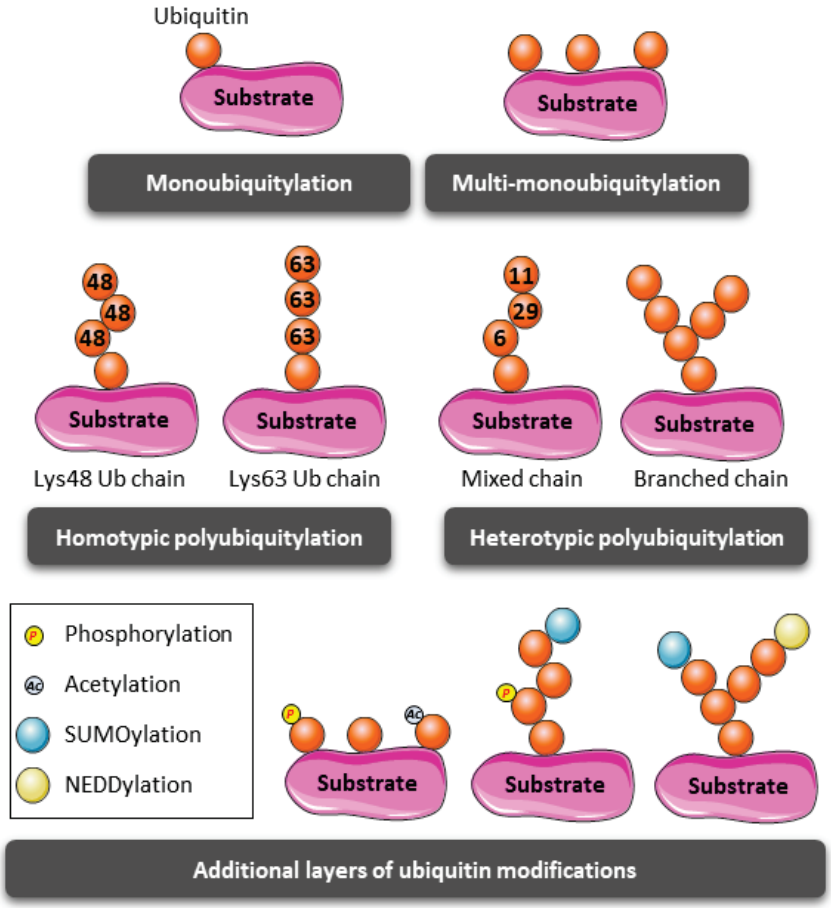

Figure 2. The complexity of the ubiquitin code. Schematic representation of different possible ubiquitin chain topologies on a substrate protein. Examples of monoubiquitylation, multi-monoubiquitylation, homotypic polyubiquitylation, heterotypic polyubiquitylation and the additional layers of ubiquitin modifications (phosphorylation, acetylation, SUMOylation and NEDDylation) are indicated.

Types of E3 ubiquitin ligases

As state above, E3 ubiquitin ligases determine substrate specificity by catalysing the transfer of ubiquitin to a specific substrate. They are currently classified in three main families according to their structure and mechanism of ubiquitin transfer: **RING E3s**, **HECT E3s** and **RBR E3s** (Figure 3). RING (Really Interesting New Gene) E3s are the most abundant class. Up to 600 different types have been described in humans. They are characterized by the presence of a RING or U-box domain. These domains bind the ubiquitin-charged E2 enzyme and catalyse the transfer of ubiquitin directly to the substrate. Therefore, they act as a scaffold positioning the E2 enzyme to the substrate protein (Figure 3A). Conversely, the HECT (Homologous to the E6AP carboxyl terminus) E3s, catalyse ubiquitin transfer to the substrate protein by a two-step reaction. To date, 28 different types have been identified in humans. Its specific mechanism is that first, the ubiquitin from the E2 enzyme is attached to a catalytic

cysteine on the E3 enzyme forming a thioester bond. Then, it is transferred to the substrate [17] (Figure 3B). RBR (RING-in-Between-RING) E3s represent the third class of E3 ligases. They are characterised by a mixed mechanism of ubiquitin transfer. They bind the E2 enzyme to a RING1 domain and transfer the ubiquitin to a second domain called RING2, which contains a catalytic cysteine. Then, the ubiquitin is transferred to the substrate protein. Despite being a small family, RBR E3s regulate different cellular process in human cells [18] (Figure 3C).

Focusing now on **HECT ubiquitin ligases**, they are characterized for the presence of a HECT domain in their C-terminal region. The HECT domain forms a bilobed structure that enables the transmission of the ubiquitin molecule to the target protein. Specifically, the first lobe (the one closest to the amino terminus) binds the E2 enzyme from which the ubiquitin is transferred to the catalytic cysteine located in the second lobe. Next, the conjugation of ubiquitin to the target protein is catalysed [19] (Figure 3B).

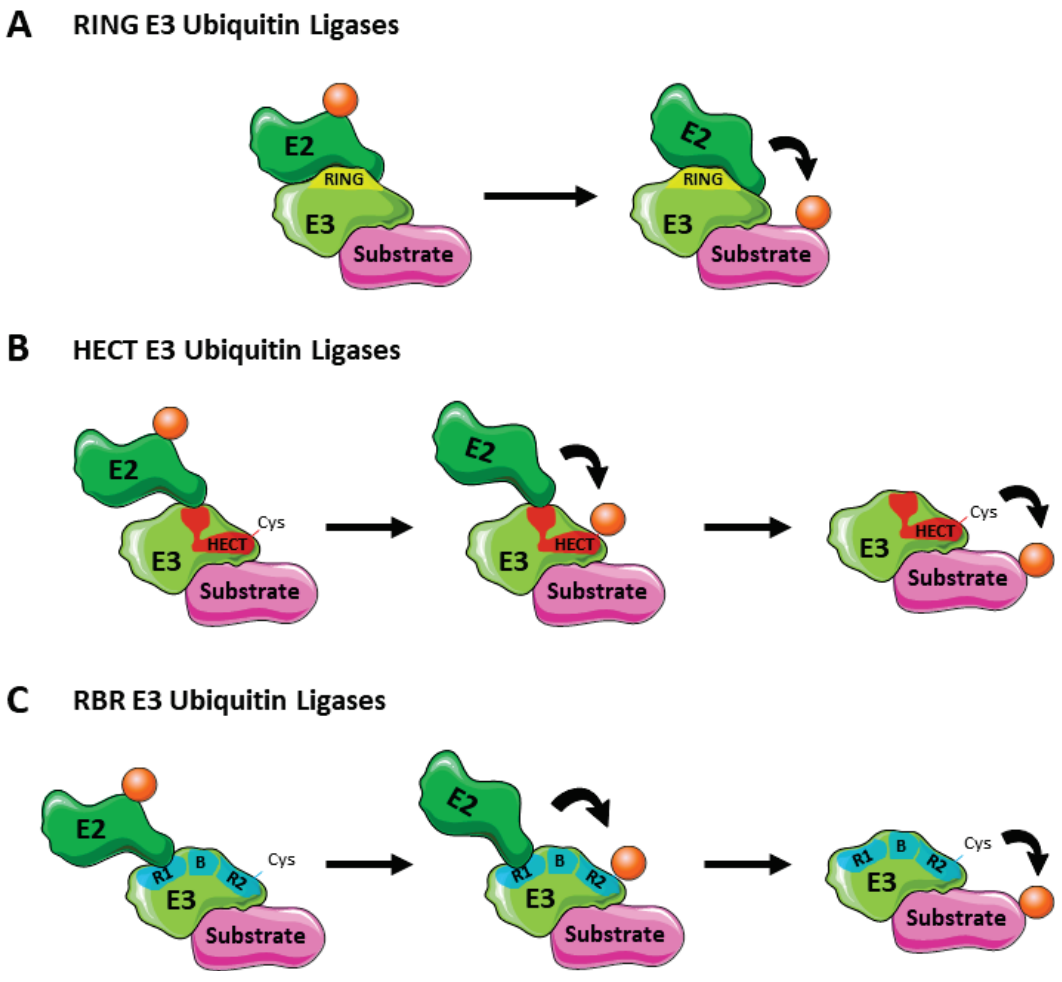

Figure 3. Figure caption on next page ▼

Figure 3 ▲. Types of E3 Ubiquitin Ligases. (A) The RING E3 ligases are characterized by the presence of a RING domain that binds the E2 enzyme. RING E3s mediate a direct transfer of ubiquitin from E2 to the substrate. **(B)** The HECT E3 ligases contain the conserved C-terminal HECT domain with bilobed structure. The first lobe of the HECT domain binds the E2 enzyme and then ubiquitin is transferred from the E2 to the catalytic cysteine located in the second lobe of HECT domain; afterwards, ubiquitin is transferred to the substrate. **(C)** The RBR E3 ligases consist of two RING domains (R1 and R2) separated by an in-Between domain (B). RING1 domain binds the E2 enzyme and ubiquitin is transferred from the E2 to the catalytic cysteine located in the RING2 domain. Then, ubiquitin is transferred to the substrate protein.

Traditionally, human HECT ubiquitin ligases have been classified in three different families: NEDD4-like E3s, which contain WW (tryptophan-tryptophan) domains; HERC E3s, harbouring RLDs (RCC1-Like Domains); and Single-HECT E3s, proteins lacking both of those domains [20, 21]. Nevertheless, sequence and structural comparison analysis showed a more complex division of the HECT family into 16 different subfamilies: **NEDD4-like** proteins, **Small HERCs**, **Large HERCs** and 13 different subfamilies formerly called "**other HECTs**" [22]. Small and Large HERCs were initially classified together and defined by the presence of an HECT domain and one or more RLD domains [23]. However, it was demonstrated that the RLD domains from Small and Large HERCs had significant structural differences [24], and that these domains were acquired by each subfamily in two independent events. Thus, the homology between Large and Small HERCs is due to a convergent evolution phenomenon rather to a common phylogenetic ancestor and, consequently, they should be classified in different protein subfamilies [22].

Large HERC family

The Large HERC protein family is characterized by the presence of an HECT domain in their C-terminal region, more than one RLD domains and several other conserved regions. This family is composed by two members: **HERC1** and **HERC2** (Figure 4). Due to their huge size they are designated as "Large" HERCs. HERC1 has 4861 amino acids with a molecular weight of 532 kDa, while HERC2 has 4834 amino acids and 528 kDa of molecular weight [23].

The ubiquitin ligase HERC1

HERC1 has multiple structural domains, including two RLD domains (**RLD1** and **RLD2**), a SPla and ryanodine receptor (**SPRY**) motif, a Bcl2-homology domain 3 (**BH3**), a Trp-Asp-rich 40-amino acid repeat (**WD40**) region and the C-terminal **HECT** domain [19, 23] (Figure 4).

The first ubiquitylation substrate of HERC1 that was identified is the serine/threonine protein kinase **C-RAF**. HERC1 ubiquitylates C-RAF targeting it to proteasomal degradation and

thus modulating ERK signalling pathway [25]. More recently, the subunit of the proteasome **PSMC5** has also been identified as a target for proteasomal degradation by HERC1. The authors proposed that HERC1 acts as a quality control factor during proteasome assembly by facilitating elimination of excess of PSMC5 intermediates [26].

The ubiquitin ligase HERC2

The structure of the ubiquitin ligase HERC2 include: three RLD domains (**RLD1, RLD2** and **RLD3**), a cytochrome b5-like region (**Cyt b5**), a mind-bomb/HERC2 (**M-H**) domain, a conserved domain within Cul7, PARC and HERC2 (**CPH**), a **ZZ-type zinc finger** region, a domain homologous to subunit 10 of APC (**DOC**) and the carboxyl-terminal **HECT** domain [19, 23] (Figure 4).

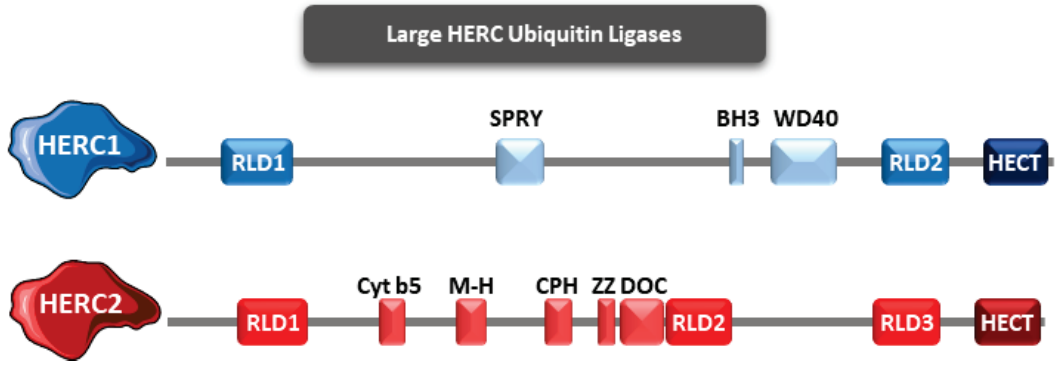

Figure 4. Large HERC Ubiquitin Ligases. Structural domains of the large HERC ubiquitin ligase HERC1 (in blue) and HERC2 (in red).

Looking in more detail at each of the domains, the RCC1-Like Domains (RLDs), as the name indicates, have a similar structure to Regulator of Chromosome Condensation 1 (RCC1), which is a guanine exchange factor (GEF) for the GTPase Ran, a nuclear import protein. However, for now, no GEF activities have been reported in HERC2. Still, the RLD2 domain of HERC2 was found to interact with E6AP ubiquitin ligase, thus stimulating its activity [19]. The DOC and M-H domains might contribute on the ubiquitin ligase activity of HERC2 [27, 28]. The CPH domain binds to the tumour suppressor protein p53 [29]. The ZZ Zinc finger region in HERC2 is a SUMO and histone H3 binding module implicated in the DNA damage response [30, 31]. In the cytoplasm of the cells, the ZZ domain recognizes the amino-terminal arginine residue (Nt-R) of proteins. The Nt-R is produced by proteolytic cleavage or enzymatically added by Arg-tRNA transferases and it acts as a specific degradation signal that can be recognized by ubiquitin ligases. Therefore, the ZZ domain of HERC2 might act as a receptor of arginylated substrates [32].

In contrast to HERC1, several substrates of HERC2 have been proposed. HERC2 regulates ubiquitylation and subsequent proteasomal degradation of several proteins involved in the DNA repair pathway such as **XPA** and **BRCA1**. Also of some deubiquitinating enzymes such as **USP33** and **USP20**, and of proteins involved in iron metabolism such as **FBX15** and **NCOA4**. In addition, HERC2 also promotes degradation of the protein kinase **LKB1** when acetylated, which is critical for a correct arterial remodelling process [19] (Figure 5). Moreover, HERC2 regulates ubiquitylation of **NEURL4** with non-proteolytic functions, instead implicated in centrosome architecture regulation [33].

Functional relevance of the ubiquitin ligase HERC2

Regulation of genomic stability

One of the most studied functions of HERC2 is its involvement in the **regulation of genomic stability**. As mentioned before, HERC2 regulates ubiquitylation and proteasome-dependent degradation of key regulators of DNA repair pathways (Figure 5). For instance, XPA is critical to the nucleotide excision repair machinery and it is ubiquitylated by HERC2 in a circadian-dependent manner [34]. Regulation of this process depends on the phosphorylation state of XPA. Its phosphorylation by the serine/threonine-protein kinase

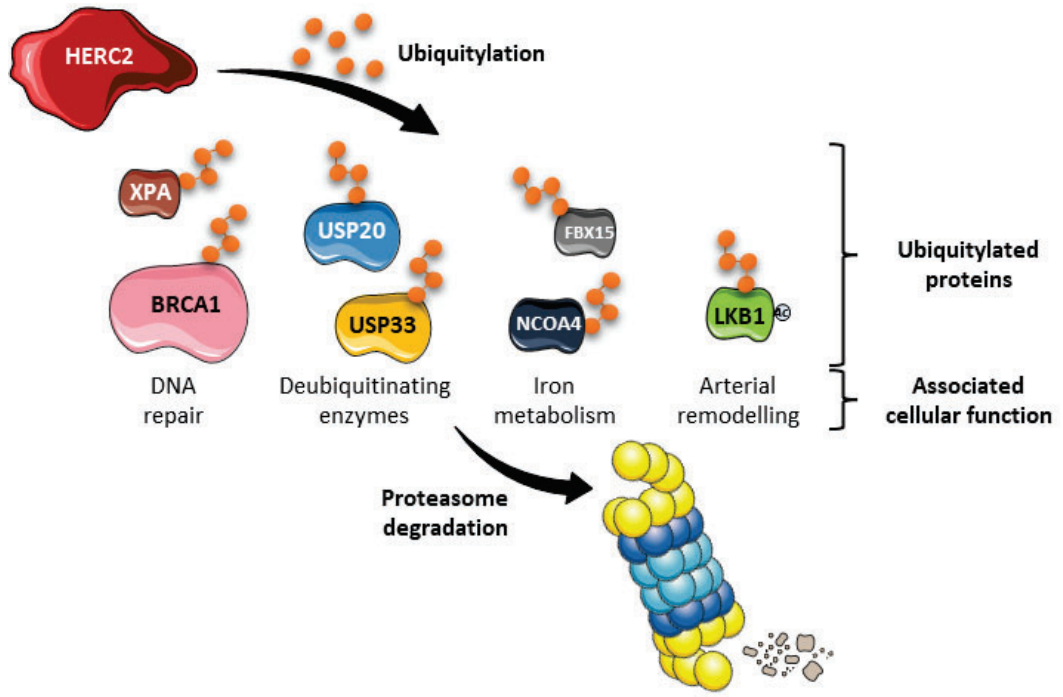

Figure 5. Ubiquitin-mediated proteasomal degradation regulated by HERC2. HERC2 regulates ubiquitylation of several proteins targeting them to proteasomal-dependent degradation. This has effects on various cellular pathways such as DNA repair, deubiquitylation, iron metabolism and arterial remodelling.

ATR prevents its ubiquitylation, while dephosphorylation by protein phosphatase 1D (also known as WIP1) enhances it [34, 35]. Another HERC2 degradation target is BRCA1 [36]. BRCA1 maintains genome stability by repairing double-strand breaks [37]. The HERC2-dependent degradation of BRCA1 is regulated by the binding of different protein interactors to HERC2 or BRCA1. For instance, BARD1 binds BRCA1, forming a heterodimer that protects BRCA1 from HERC2-dependent ubiquitylation. Likewise, TUSC4 binds to HERC2 and prevents BRCA1 degradation [36, 38]. Similarly, the mitotic spindle protein ASPM interacts with both HERC2 and BRCA1 thus protecting BRCA1 from HERC2-dependent ubiquitylation [39].

Also concerning the regulation of genomic stability, HERC2 is required for the **retention of DNA repair factors** such as 53BP1, RAP80, RNF168, and BRCA1 at sites of DNA damage in **response to double-strand breaks (DSBs)** [40]. Upon double-strand breaks, HERC2 is phosphorylated on T4827 by the serine-protein kinase **ATM** or other DNA damage-related kinases like **ATR** or **DNA-PK**. In addition, it is SUMOylated in its HECT domain by the E3 SUMO ligase **PIAS4** [30]. These posttranslational modifications are essential for the binding of HERC2 to **RNF8**, another ubiquitin E3 ligase involved in the DNA damage response. Mechanistically, HERC2 promotes the specific assembly of RNF8 with one of its E2 enzymes, **Ubc13**. Then, RNF8 catalyses the formation of **K63 polyubiquitin chains in H2A-type histones** flanking the double-strand break site. HERC2 therefore mediates the specificity of the interaction between the E2 enzyme Ubc13 and the E3 ligase RNF8, safeguarding the formation of K63 ubiquitin chains that are essential for recruiting repair factors to the damaged chromosomes. In addition, HERC2 can interact with, and stabilize, the E3 ligase **RNF168** that is responsible for amplifying the ubiquitin chain formation initiated in histones by RNF8 [30, 40]. Separately, levels of the deubiquitinating enzyme **USP16** increase in a HERC2-dependent manner during DNA damage, which negatively regulates H2A histone ubiquitylation to fine-tune polyubiquitin chain formation. Eventually, USP16 triggers the ubiquitylation signal termination once the damage is repaired (Figure 6). In conjunction these findings suggest that HERC2 has a central role in regulating and fine-tuning the DNA damage response pathway, being involved both in the initiation and termination processes [41].

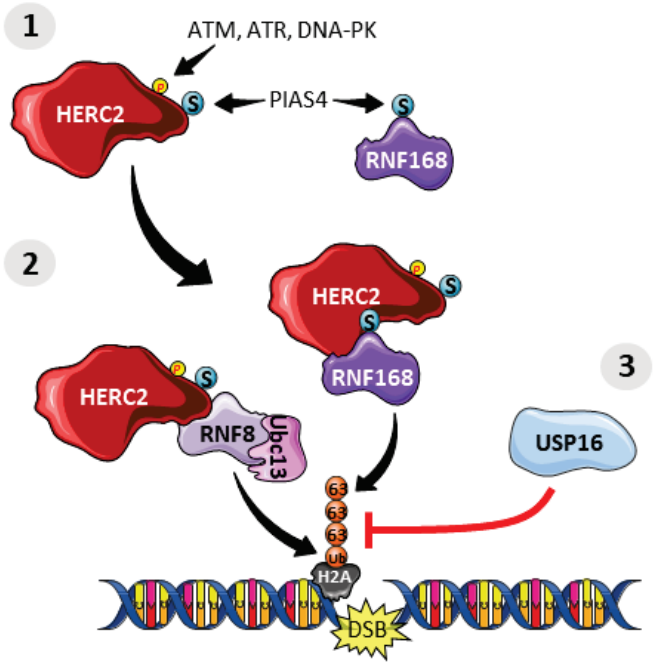

Figure 6. HERC2 regulates DNA double-strand break (DSB) repair. Upon double-strand break in the DNA, first HERC2 is phosphorylated (by ATM, ATR, or DNA-PK) and SUMOylated (by PIAS4). PIAS4 also SUMOylates the E3 ligase RNF168. Then, HERC2 binds to the E3 RNF8 and promotes the specific assembly of RNF8 with the E2 enzyme Ubc13. This allows the formation of K63 polyubiquitin chains in H2A-type histones flanking the double-strand break site. In addition, HERC2 interacts with and stabilizes SUMOylated RNF168. This amplifies ubiquitin chain formation in histones. By contrast, USP16 levels increase in a HERC2-dependent manner and negatively regulate H2A histone ubiquitylation to fine-tune chain formation and eventually trigger ubiquitylation signal termination.

Moreover, HERC2 interacts with Claspin, a protein essential for both G_2-M checkpoint activation and replication fork stability. Also with replication fork complex proteins such as PCNA. Indeed, by means of these mechanisms, HERC2 regulates **origin firing** and **replication fork progression** during DNA replication in the S-phase of the cell cycle. S-phase progression is regulated by two main mechanisms that must be correctly balanced: origin firing and elongation. **Claspin** and **CHK1** enhance elongation while they restrict origin firing. In contrast, ATR-mediated phosphorylation of **MCM2** recruits PLK1, which enhances origin firing to compensate stalled replication forks and recover DNA replication after replication stress. When cells are faced with **replication stress** that impairs DNA elongation, HERC2 facilitates ATR-mediated phosphorylation and activation of MCM2. Thus, origin firing is upregulated as a compensatory mechanism to recover from the replication blockade [42]. Additionally, upon replication stress, ATR phosphorylates **USP20**, a deubiquitinating enzyme which is a degradation target of HERC2. This phosphorylation disrupts HERC2-USP20 interaction, which leads to USP20 stabilization. In turn, USP20 deubiquitylates and stabilizes Claspin levels. Claspin can then interact with CHK1, promoting its activation by ATR-dependent phosphorylation. This, in turn, promotes checkpoint activation and genome stability [43, 44] (Figure 7).

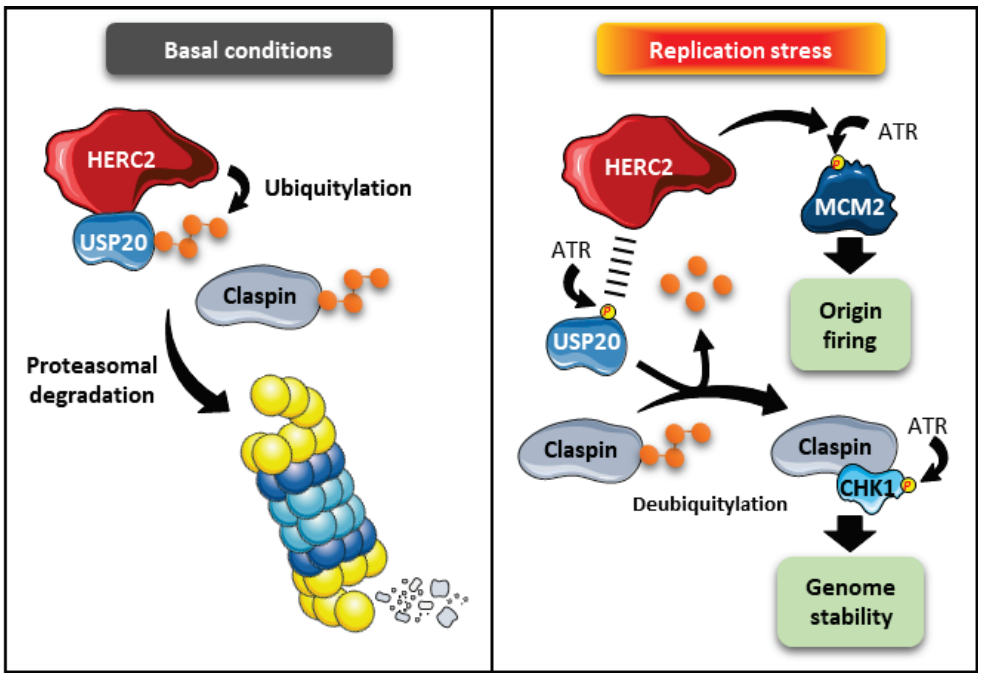

Figure 7. HERC2 regulates the cellular response to replication stress. In basal conditions, HERC2 ubiquitylates USP20 targeting it to proteasomal degradation. Claspin is also regulated by ubiquitin-mediated proteasomal degradation. Upon replication stress, HERC2 facilitates ATR-mediated phosphorylation and activation of MCM2, which leads to origin firing upregulation to compensate the stalled replication forks. In addition, ATR phosphorylates USP20. This disrupts HERC2-USP20 interaction thus stabilizing USP20 protein levels. In turn, USP20 deubiquitylates and stabilizes Claspin. Claspin facilitates ATR-dependent phosphorylation of CHK1, which promotes genome stability.

Some guanine-rich DNA sequences can fold into a secondary structure known as **G-quadruplex (G4)**. These structures are involved in transcriptional initiation and termination, replication initiation, and telomere maintenance. However, the deregulation of G4 can cause fork stalling during DNA replication that eventually causes DNA damage and genome instability. **Replication protein A (RPA)** is an heterotrimeric complex formed by **RPA1**, **RPA2**, and **RPA3**. It binds to single-stranded DNA and protects it from spontaneous annealing and G4 formation. RPA assembly to the RecQ DNA helicases **BLM** and **WRN** is essential for suppressing the formation of G4 DNA structures. HERC2 interacts with BLM and WRN helicases, and also with RPA2. Thereby, HERC2 promotes the assembly of the RPA complex with the helicases, which is indispensable to resolve the G4 structure. In detail, under conditions of replication stress, ATR phosphorylates RPA2 at Ser33 by an HERC2-dependent mechanism. Then, HERC2 ubiquitylates the phosphorylated form of RPA2, targeting it to proteasomal degradation [45]. Although the specific effects of RPA2 phosphorylation and its later degradation by HERC2 are not fully understood, both mechanisms are essential for HERC2 to function correctly in suppressing G4 structures. HERC2 may fine-tune the levels of

phosphorylated RPA2 by promoting its ATR-dependent phosphorylation and targeting it to proteasomal degradation through polyubiquitylation. This precise balance might be needed for the correct assembly of BLM and WRN helicases to the RPA complex, as well as for the subsequent suppression of G4 structures and the maintenance of genomic stability [46] (Figure 8). Further investigations also revealed that the ubiquitin ligase activity of HERC2 maintains BLM and WRN localized in the nucleolus in unstressed cells and that it is also needed for its relocalization to RPA nuclear foci in response to replication stress [47].

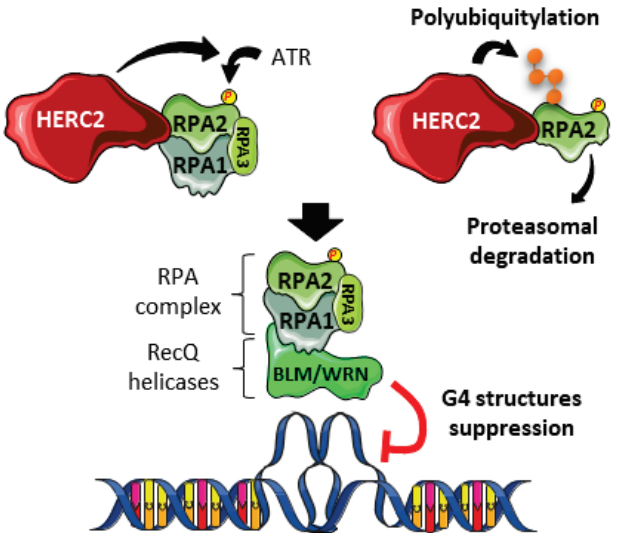

Figure 8. HERC2 regulates suppression of G4 DNA structures. G4 structures cause replication stress. Upon G4 formation, HERC2 promotes RPA2 phosphorylation via ATR. Also, HERC2 polyubiquitylates the phosphorylated form of RPA2, targeting it to proteasomal degradation. By this, HERC2 fine-tunes the total levels of phospho-RPA2. This mechanism is essential for assembling BLM and WRN RecQ helicases to the RPA complex, which is necessary to suppress G4 DNA structures.

Regulation of p53 transcriptional activity

Another important function of the ubiquitin ligase HERC2 is the **regulation of p53 transcriptional activity** [29]. Tetramerization of **p53** is a key step in its activation, and this oligomerization process is modulated by a complex formed by **NEURL4** and HERC2 [48]. Recently, it has been reported that **MDM2** is also present in this complex. In non-stressed cells, the ubiquitin ligase MDM2 keeps low protein levels of p53 by targeting it to proteasome-dependent degradation. Upon DNA damage, the DNA damage kinases such as ATM and ATR, phosphorylate MDM2, p53 and HERC2. Phosphorylated MDM2 is dissociated from the p53/HERC2/NEURL4 complex, which prevents the MDM2 ability to ubiquitylate p53 and induces its self-ubiquitylation and degradation. Oligomeric p53 is then acetylated in several C-terminal lysine residues by acetyltransferases such as p300. This is indispensable for its stabilization and activation. In addition, p53 acetylation increases sequence-specific DNA binding, moment at which p53 uncouples from the HERC2/NEURL4 complex. Activated

p53 binds to the p53-response elements in the promoters of its target genes such as *p21*. *MDM2* is another p53-activated gene. Therefore, as MDM2 expression increases, it binds to p53 targeting it to proteasomal degradation and stablishing a negative feedback loop [49]. Interestingly, the oncogene protein BTF3, was found to interact with HERC2 and p53, but its involvement in the p53 regulatory loop is not fully understood yet [50]. In conjunction, these findings highlight the importance of HERC2 in regulating the transcriptional program of the tumour suppressor protein p53 (Figure 9).

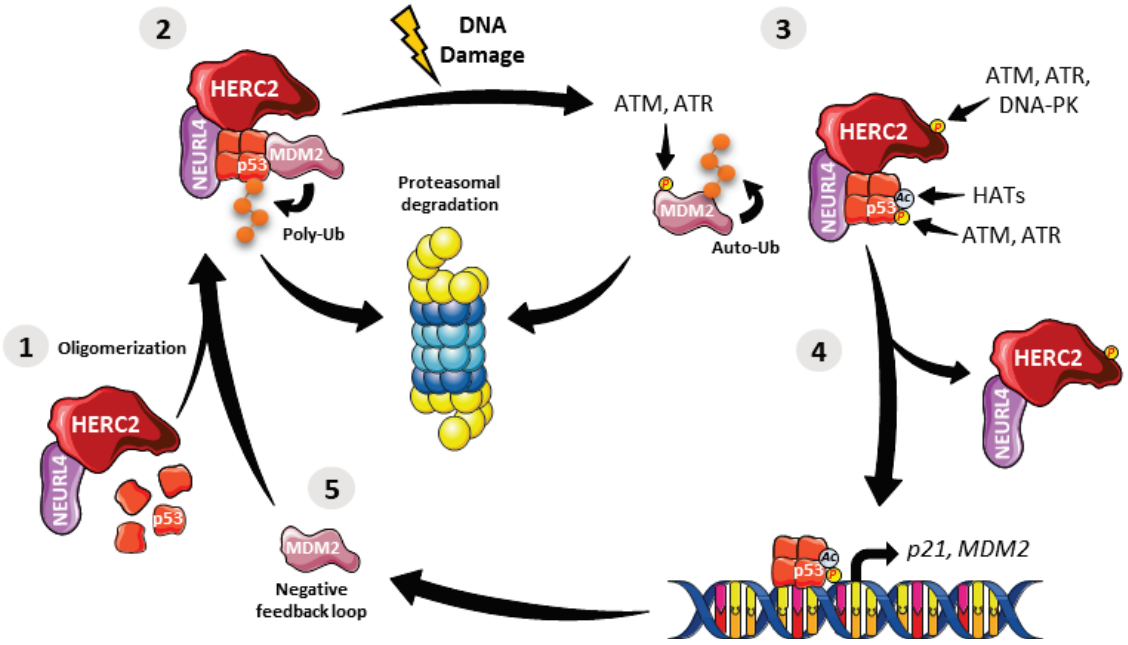

Figure 9. Regulation of the p53/MDM2 pathway by HERC2. Modulation of the p53 pathway by HERC2 occurs following a regulatory loop: (1) In basal conditions, HERC2 and NEURL4 regulate p53 transcriptional activity by promoting its oligomerization. (2) MDM2 maintains low levels of p53 by polyubiquitylating (Poly-Ub) and targeting it for proteasomal degradation. (3) Upon DNA damage, DNA damage kinases (ATM, ATR, DNA-PK) phosphorylate MDM2, HERC2 and p53. In addition, p53 is further activated by acetylation via histone acetyl transferases (HAT). The phosphorylated MDM2 is detached from the p53/HERC2/NEURL4 complex and is auto-polyubiquitylated (Auto-Ub) and subsequently degraded. (4) Activated p53 detaches from HERC2/NEURL4 complex and binds to the promoters of its target genes, such as p21 and MDM2. (5) Expression of MDM2 protein stablishes and a negative feedback loop.

Development and neurobiology

HERC2 is expressed in several tissues with a notable expression in the nervous system both in mice and humans. Indeed, mutations in its gene have been linked with hereditary neurodevelopmental disorders [23, 51].

In mice, mutations in *Herc2* gene are associated with a syndrome known as **runty, jerky, sterile (rjs)** or **juvenile development and fertility-2 (jdf2)**, characterized by reduced viability, growth defects, motor coordination disfunction and sterility [52, 53]. *Herc2*

knockout mice are not viable, showing that HERC2 is essential for embryonic development. However, mice with a targeted inactivation of *Herc2* in heterozygosis, named ***Herc2*$^{+/530}$ mice**, are viable. In these mice, HERC2 protein levels are reduced by one-half and they present motor coordination dysfunction. Morphological analysis revealed Purkinje cells degeneration with signs of increased accumulation of autophagosomes and lysosomes [54].

In humans, the *HERC2* gene locates to chromosome 15 among genes responsible for disorders such as Angelman and Prader-Willi syndromes and Autism spectrum disorders [55, 56]. Interestingly, HERC2 interacts and allosterically activates the ubiquitin ligase activity of E6AP, the principal protein involved in the pathogenesis of Angelman Syndrome. Indeed, biallelic mutations in the *HERC2* gene are associated with a neurodevelopmental disorder called **HERC2 Angelman-like syndrome** (autosomal recessive mental retardation type 38; OMIM # 615516). It is characterised by a global developmental delay, intellectual disability, autistic characteristics and movement disorders. The syndrome is caused by missense and frameshift loss-of-function mutations that result in a complete loss or markedly reduced levels of HERC2 protein. It was first described in Amish/Mennonite communities, associated with homozygosity for a *HERC2* (c.1781C>T) founder gene variant at increased frequency in the population. This gene variant encodes an HERC2 protein with an amino acid substitution (**p.Pro594Leu/P594L**) that makes it more unstable, thus reducing the total levels of HERC2 protein in cells of the affected individuals [57–61].

HERC2 could also be involved in other neurological diseases. For instance, Parkinson's disease-associated kinase LRRK2 binds to the HERC2-NEURL4 complex and regulates endosomal vesicular trafficking promoting the recycling of the Notch ligand Delta-like 1 (Dll1)/Delta (Dl). This process negatively regulates Notch signalling and impacts on adult dopaminergic neurons function and survival [62].

Regulation of centrosome function

HERC2 is also involved in the modulation of **centrosome architecture**. Interaction proteomics analysis identified HERC2 and NEURL4 as binding partners of the centrosomal protein **CP110**, which is a key regulator of centrosome biogenesis. Both HERC2 and NEURL4 localize to the centrosome and are necessary to maintain centrosome architecture. In addition, HERC2 regulates non-proteolytic NEURL4 polyubiquitylation, which biological

outcome needs to be further explored [63]. Besides, **NudCL2** protein, which is an HSP90 co-chaperone that localizes to centrosomes, is required for accurate centriole duplication. Mechanistically, NudCL2 interacts with and stabilizes HERC2. In turn, HERC2 regulates **USP33** protein levels by polyubiquitylation and subsequent proteasome-dependent degradation. USP33 is a centrosomal deubiquitinating enzyme that positively regulates centriole duplication. Thus, NudCL2 maintains correct centriole duplication by stabilizing HERC2 to restrain USP33 protein levels [64].

Other functions

Regarding other functions in which HERC2 is involved, noteworthy is its involvement in **iron metabolism** and **ferritinophagy**. HERC2 targets the iron regulator **FBXL5** for degradation. FBXL5 is the protein subunit responsible for substrate recognition of the ubiquitin ligase SCF, which targets iron regulatory protein 2 (IRP2) for proteasomal degradation [65]. Besides, when iron is available, HERC2 promotes **NCOA4** degradation. In contrast, when iron levels are low, HERC2-NCOA4 interaction is attenuated, which promote trafficking of ferritin to the lysosome, a process called ferritinophagy, in order to potentiate iron release [66].

Recently, HERC2 has also been related with **pyroptosis**, a form of cell death triggered by proinflammatory signals. Mechanistically, HERC2 interacts with **NLRC4**, targeting it to degradation through ubiquitylation. NLRC4 is a protein of the innate immune system that regulates activation of inflammatory responses. Interestingly, a long non-coding RNA (lncRNA) called **lncRNA-Fendrr** was found to bind HERC2. This affects HERC2 ability to ubiquitylate NLRC4, therefore enhancing NLRC4-mediated pyroptosis of microglia [67].

Finally, HERC2 has been widely associated with **human pigmentation** traits. The human *HERC2* locus is upstream of that of the *OCA2* gene, which is mutated in oculocutaneous albinism. Some SNPs in *HERC2* gene can interfere *OCA2*'s expression and affect eye, skin, and hair pigmentation [68].

Identification of ubiquitylated proteins by a proteomic approach

Given that E3 ubiquitin ligases determine substate specificity, identifying their protein substrates is of paramount importance to infer its physiological function. The development of strategies that allow studying ubiquitylated proteins and linking them with their specific

E3 ligases may help to meet this goal. However, for any given protein, only a fraction of the molecules are usually ubiquitylated. In addition, it is a labile post-translational modification subjected to further changes such as degradation or deubiquitylation. This poses a challenge in the study of ubiquitylated substrates. Different strategies have been developed for the enrichment of ubiquitylated proteins. One of the most common is based on antibodies that recognize the **diGly signature** that ubiquitylated proteins retain after digestion with trypsin [69]. Digestion of ubiquitylated proteins results in peptides that contain an ubiquitin remnant that derives from the ubiquitin C-terminus chain. The three last residues of ubiquitin are Arg-Gly-Gly, being the last Gly the one that conjugates to the lysine residue of the substrate protein. After trypsin digestion, ubiquitin is cleaved after arginine, which leaves a Gly-Gly mark on the conjugated lysine. Therefore, the diglycine-modified lysine serves as a signature of ubiquitylation and also identifies the specific substrate site where the modification occurs [70]. Another tool to identify ubiquitylated material are the TUBEs, tandem-repeated ubiquitin binding entities that capture ubiquitylated proteins. However their main limitation is that a plethora of proteins associated with the ubiquitylated material are also isolated, hampering the identification of true ubiquitylation substrates [14]. To overcome this limitation a novel approach has been developed called the **^{bio}Ub strategy**. This methodology is based on the *in vivo* biotinylation of ubiquitin. Due to the strength and specificity of the avidin-biotin interaction, the isolation and enrichment of ubiquitylated material with ^{bio}Ub can be done under high stringent conditions, thus significantly avoiding the contamination with non-ubiquitylated proteins. Ubiquitylated proteins can then be quantified and, importantly, identified, combining the ^{bio}Ub strategy and **mass spectrometry analysis** [71]. This approach had been successfully applied to identify putative ubiquitylation substrates of some E3 ligases such as Parkin, Ube3a and Ariadne-1. In brief, in cells, the approach consists in overexpressing the E3 ligase of interest and providing the cells with biotinylated ubiquitin molecules. This is achieved by transfecting the **(^{bio}Ub)$_6$-BirA construct**. This construct encodes a precursor polypeptide composed of six ubiquitin molecules, which had been modified in their N-terminus with a short biotinylatable peptide. In addition, the biotin ligase enzyme of *E.Coli* BirA is fused at the C-terminus of the precursor peptide. Once the (^{bio}Ub)$_6$-BirA construct is expressed in cells, it is digested by endogenous DUBs, releasing ubiquitins and enabling BirA to label them with biotin in its N-terminus. After that, cells are subjected to biotin pulldown using Avidin agarose to isolate the ubiquitylated material. Then, pulldowns

are analysed by liquid chromatography with tandem mass spectrometry (LC-MS/MS), which allows the identification and quantification of ubiquitylated proteins. Identifying which proteins are more ubiquitylated in E3 ligase overexpressing cells compared to control cells, allows the recognition of putative ubiquitin ligases' substrates [72–74] (Figure 10).

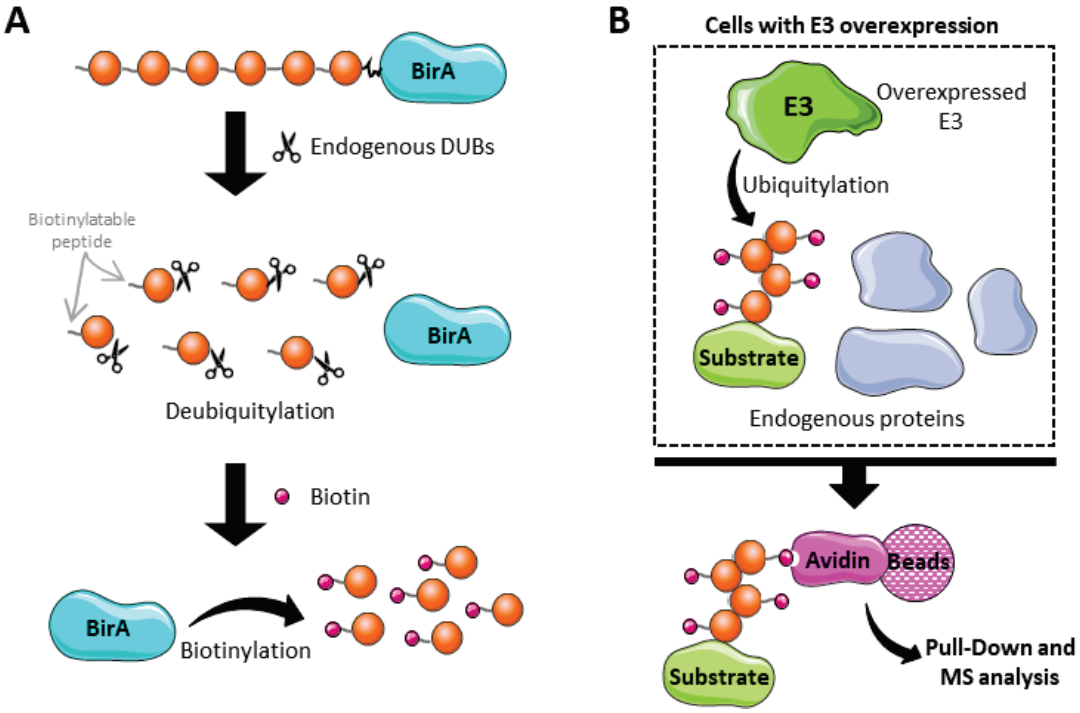

Figure 10. Study of ubiquitylated proteins with the ^{bio}Ub strategy. (A) Schematic illustration of the $(^{bio}Ub)_6$-BirA construct. The construct is expressed as a polyubiquitin chain of six ubiquitin motifs fused to the E.coli BirA enzyme. Once expressed in the cell, endogenous deubiquitylating enzymes (DUBs) digest the construct and release single ubiquitin molecules as well as BirA enzyme. Ubiquitin molecules from the construct contain a short biotinylatable peptide at its N-terminus. Next, BirA catalyses biotinylation of modified ubiquitin molecules. **(B)** Scheme of the strategy used to identify ubiquitylated proteins regulated by an E3 ligase of interest in cells. The E3 ligase of interest is overexpressed along with $(^{bio}Ub)_6$-BirA construct. Once expressed, the E3 ligase will regulate ubiquitylation of its substrates. Chains that are formed will contain biotinylated ubiquitin. Then, bio-ubiquitylated material is purified using Avidin beads. Isolated material is analysed by Mass Spectrometry (MS) to identify putative substrates of the E3 ligase of interest.

MAPK signalling and the oxidative stress response

MAPK pathways are cell signalling modules that relay, amplify and integrate signals from a diverse range of stimuli, and elicit an appropriate physiological response. Two of the most important pathways are ERK and p38 signalling cascades. While ERK is typically implicated in regulating cell growth and proliferation, p38 is strongly activated by environmental stresses and involved in the regulation of the cellular stress response. Of the different types of stress to which p38 responds, one of them is oxidative stress, which is defined as a cell's imbalance in which excessive reactive oxygen species (ROS) are produced. In response to this, activation of the transcription factor NRF2 is crucial, since it enhances transcription of several antioxidant enzymes. Ubiquitin modification of components of these signalling pathways modulates and affects downstream signalling. This highlights the important regulatory role that E3 ligases may have in these pathways.

Mitogen-activated protein kinases (MAPKs) signalling pathways are intracellular signal transduction cascades that in response to various extracellular signals elicit an appropriate intracellular response affecting different cellular processes such as cell growth, cell proliferation, differentiation, migration, stress responses, survival and apoptosis. MAPK cascades can be activated by several factors such as hormones, growth factors, inflammatory cytokines and different types of stress [75]. Each MAPK cascade consists of three core protein kinases: **MAPKKK (MAP3K)**, **MAPKK (MAP2K)** and **MAPK**, that are activated sequentially. In brief, in response to different stimuli, MAP3Ks are activated through phosphorylation, often as a result of their interaction with a small GTP-binding protein of the Ras/Rho family. MAP3K activation leads to the phosphorylation and activation of MAP2K, which then stimulates MAPK activity through phosphorylation. In turn, activated MAPKs eventually lead to the phosphorylation of target regulatory proteins in order to elicit an appropriate cellular response [76].

Currently, four main mammalian MAPK cascades have been identified, and named according to their central MAPK component. These are: **ERK1/2**, **p38**, **JNK** and **ERK5**. Of note, other kinases with structural and sequence similarities have been identified as well. These are termed as "**Atypical MAP kinases**" and comprise **ERK3/4**, **NLK** and **ERK7** [77].

ERK1/2 signalling pathway

The mammalian ERK1/2 signalling cascade consists of the MAP3Ks **A-RAF**, **B-RAF** and **C-RAF (RAF1)**; the MAP2Ks **MEK1** and **MEK2**; and the MAPKs **ERK1** and **ERK2**. This module is mainly activated by growth factors and hormones. It also responds to ligands for heterotrimeric G protein-coupled receptors (GPCRs), cytokines and osmotic stress. Typically it is activated by receptor tyrosine kinases (**RTKs**). Binding of ligands induce receptors dimerization. Then, the kinase domain of each receptor trans-phosphorylates tyrosine residues in the intracellular domain of the other receptor. These phosphorylated motifs serve as a specific binding-sites for proteins with phosphorylated-tyrosine binding domains such as the **Src-Homology 2 (SH2) domain**. **GRB2** is an adaptor protein that contains one SH2 domain, with which it binds to phosphorylated tyrosine sequences. GRB2 then recruits **SOS**, a guanine nucleotide exchange factor (GEF), to the plasma membrane. Next, SOS stimulates the exchange of GDP bound to RAS by GTP, that is necessary for the activation of this small GTPase. Activated **RAS-GTP** can then interact directly with its target effectors, one of which is RAF, the MAP3K that initiates the ERK1/2 signalling pathway. RAF dimerizes and phosphorylates and activates MEK, which in turn phosphorylates and activates ERK [78, 79]. Finally, ERK phosphorylates several substrate proteins both in the nucleus and cytoplasm. Some of them are other protein kinases such as MSK1/2 and RSK; or transcription factors such as ELK-1 and MYC. Thus, ERK regulates important cellular functions such as cell proliferation, cell survival, cell growth, metabolism, cell motility and cell differentiation [80] (Figure 11).

The three core members of the cascade typically assemble on a **scaffold protein**, that brings them closer for interaction and facilitates the activation process. The plasma membrane is a predominant ERK activation site, although it also occurs in the endoplasmic reticulum, endomembranes of the Golgi apparatus, endosomes and autophagosomes [81, 82]. Several scaffolding proteins have been proposed to bridge ERK with the other pathway components and to target them to specific cellular compartments. Some of them are Paxillin, ß-arrestins, MP1, among others. In detail, scaffold proteins regulate ERK signals by connecting the different components of the pathway into a multi-enzymatic complex. In addition, they provide a spatial regulation mechanism, delimiting the pathway to specific subcellular location. In this regard, depending on the subcellular localization from which the

activating signals originate, determined scaffolds specify which downstream substrates are potentially phosphorylated, thus defining a specific cellular response [82].

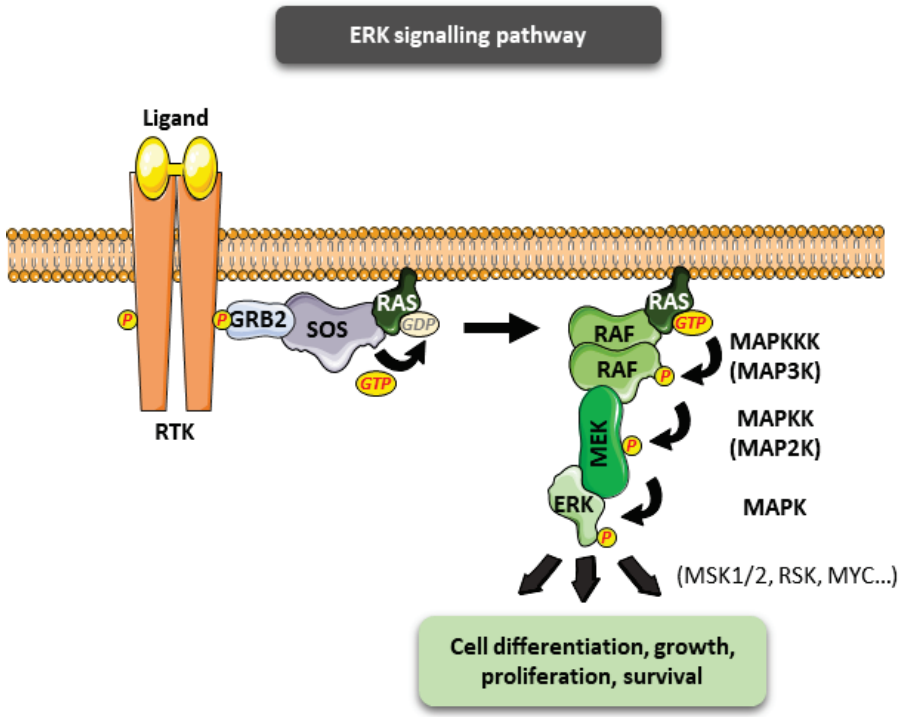

Figure 11. ERK signalling pathway. Ligand binding leads to the dimerization of two subunits of the receptor tyrosine kinase (RTK). At the inner site of the receptor tyrosine kinase domains are activated by trans-phosphorylation. Then GRB2 is recruited to the receptor. SOS binds to GRB2 and recruits RAS-GDP, catalysing the exchange of GDP to GTP. This leads to RAS activation. In its active state RAS binds the MAP3K RAF, which can form dimers, and activates it by phosphorylation. This triggers the start of the phosphorylation cascade: RAF activates MEK and MEK activates ERK, which in turn phosphorylates several substrates regulating cell differentiation, growth, proliferation and survival.

Focusing on the upper part of the triple cascade formed by the MAP3Ks, the **RAF family** of enzymes, which comprises A-RAF, B-RAF and C-RAF, share some structural characteristics. All three contain three conserved regions: **CR1**, **CR2** and **CR3**. The N-terminal CR1 contains the **RAS-binding domain (RBD)** and a **cysteine-rich domain (CRD)**; CR2 contains some regulatory phosphorylation sites; and CR3 contains the **kinase domain** [83] (Figure 12). The full activation of RAF requires the dimerization of the kinase domains. Interestingly, RAF can homo- and hetero-dimerize. In fact, the heterodimer B-RAF/C-RAF appears to be the most abundant in cells [84, 85].

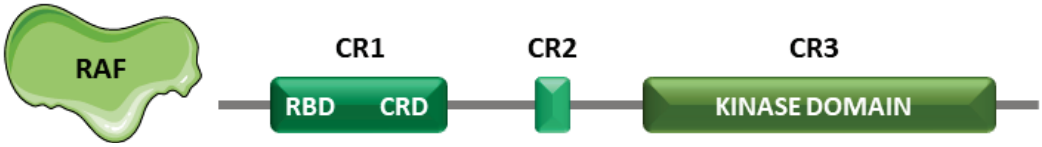

Figure 12. Domain structure of RAF proteins. RAF proteins share three conserved regions (CR1, CR2 and CR3). CR1 contains the RAS-binding domain (RBD) and a cysteine-rich domain (CRD). The kinase domain is contained in CR3.

p38 signalling pathway

The mammalian p38 MAPK signalling cascade consists of several MAP3Ks such as **ASK1/2**, **DLK1**, **TAK1**, **TAO1-3**, **MLK2/3** and **MAPKKK1-4** [86]. The different MAP3Ks can activate three different MAP2Ks: **MKK3**, **MKK6** and **MKK4**. These lasts converge in the activation of the **p38 MAPK protein family**. In mammals, there are four different isoforms of p38: **p38α**, **p38ß**, **p38γ** and **p38δ**. The four isoforms are encoded by different genes and present distinct tissue expression patterns. While p38α is ubiquitously expressed in different cell types, the other isoforms are more tissue-specific. For instance, p38ß in brain; p38γ in skeletal muscle; and p38δ in endocrine glands.

This module is strongly activated by **inflammatory cytokines** and **environmental stresses** such as **oxidative stress**, osmotic stress, UV irradiation, hypoxia, among others (Figure 13). The regulation of the cascade upstream MAP3Ks is complex and diverse. The diversity of these regulatory mechanisms provide the ability to respond to many different stimuli [87]. Activation of specific MAP3Ks have been linked to particular stimuli. For example, in mammalian cells, the apoptosis signal-regulating kinase 1 (ASK1) plays a central role in the activation of p38α by oxidative stress. The reduced form of thioredoxin binds to and inhibits ASK1. In presence of **reactive oxygen species (ROS)**, thioredoxin is oxidized. This triggers its dissociation from ASK1, allowing ASK1 homo-oligomerization and activation [88]. In addition, MAPKKK3 is also implicated in the response to oxidative stress. This kinase is activated by coupled oxidation-reduction modification of specific cysteine residues [89]. Thus, p38α activation by ROS seems to be crucial for the regulation of cellular viability, with largely different effects on the cells depending on the context. How ROS can lead to such different context-dependent responses is not yet understood but might involve activation of different components of the pathway [90].

Focusing now on other cues activating p38 kinases, **inflammatory cytokines** such as TNFα, IL-6 and IL-1ß bind to different surface receptors, which in turn lead to p38 phosphorylation. Typically, binding of IL-1ß or TNFα to its receptors lead to the MAP3K TAK1 activation. Infections also trigger p38 activation. Bacterial infection, through Toll-like receptors (TLRs), end up activating several MAP3Ks [90]. In addition, viral infections also activate p38. For instance, infection with SARS-CoV-2, the coronavirus strain that caused the

global COVID-19 pandemic declared by the World Health Organization (WHO) in 2020, promotes host p38 MAPK cascade activity [91].

The diversity in the upstream mechanisms allows the pathway to integrate a broad range of stimuli, providing versality to the response. Endogenous p38 is distributed both in the cytosol and nucleus in non-stimulated cells. Upon p38 activation by its upstream kinases, a pool of p38 translocates to the nucleus to access its nuclear substrates, while another pool preferentially accumulates in the cytosol [92] (Figure 13). Probably, the preferential activation of the nuclear or cytosolic pool might depend on the stimuli and the substrates to which p38 is directed [93]. In fact, a multitude of p38 downstream substrates have been identified. More than 100 proteins are directly phosphorylated by p38, which are located throughout the cell and regulate different cellular processes such as transcription, translation, protein degradation and localization, cell cycle, metabolism, etc. Some substrates are protein kinases, which in turn phosphorylate other proteins, expanding the versality of the pathway. For example, p38 regulates MSK1 and MSK2, which control gene expression by phosphorylating several transcription factors. In addition, p38 directly targets a large number of transcription factors such as MEF2, ATF-1/2/6, CHOP, p53, among others [94]. One of the main biological responses triggered by the activation of different p38 substrates is the **cellular stress response**, typically supporting cell survival via different mechanisms [95].

Signal termination is also a key regulatory step in p38 signalling, since p38 hyperactivation is usually detrimental for the cell. Therefore, mechanisms that ensure signal cessation are essential for cellular homeostasis. For instance, some phosphatases such as **DUSP1**, which dephosphorylate and inactivate p38, can be induced by p38 signalling stablishing a negative feedback loop [90] (Figure 13).

Recapitulating, signalling by p38 can regulate many cellular responses. Consequently, it has been linked to several human pathologies such as inflammatory, neurodegenerative, cardiovascular and metabolic diseases, as well as cancer [90]. For instance, activation of p38 is detected in early stages of Alzheimer disease, Amyotrophic lateral sclerosis (ALS), Parkinson disease and the autism spectrum disorder [96–99]. Concerning its implication in cancer, p38 plays tumour-suppressor roles in normal cells by contributing to cellular

homeostasis. However, some reports have showed that this pathway is often exploited by malignant cells to support survival and progression of tumour cells [100].

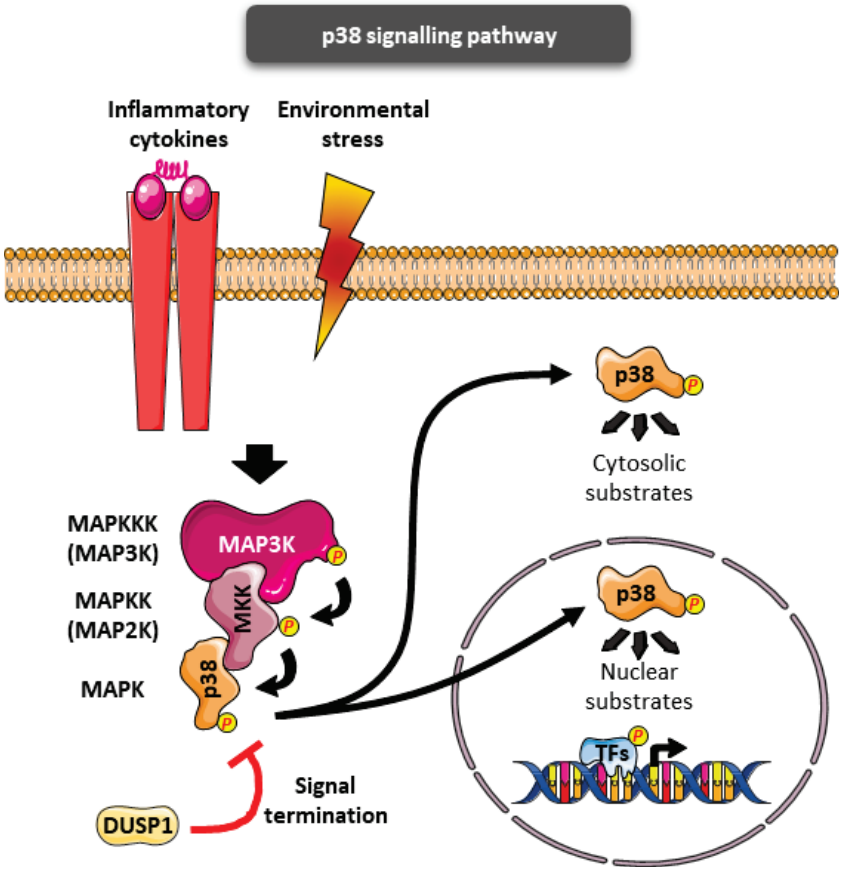

Figure 13. p38 signalling pathway. Different stimuli such as inflammatory cytokines and environmental stresses can activate p38 MAPK pathway. They converge in the activation of MAPKKK (MAP3K), which initiates the phosphorylation cascade leading to MKK activation and eventually to p38 activation. Once activated, p38 can accumulate in the cytosol where it phosphorylates several cytosolic substrates. In addition, a pool of phosphorylated p38 translocates to the nucleus to access different nuclear substrates such as transcription factors (TFs). Signal termination can be triggered by phosphatases as DUSP1, which dephosphorylates p38 inactivating it.

Regulation of MAPKs by the Large HERCs

Ubiquitin modification of components of MAPK signalling pathways by E3 ligases modulates and affects downstream signalling [101]. In this regard, Large HERCs have been associated with MAPK signalling regulation, particularly HERC1. Our knowledge of the regulation of MAPK by HERC1 has evolved grown in recent years. HERC1 controls cell proliferation through the regulation of ERK signalling. Mechanistically, HERC1 regulates protein levels of the MAP3K C-RAF by polyubiquitylation and subsequent proteasome-dependent degradation [25]. In addition, HERC1 also modulates the p38 signalling pathway, with implications in cell migration. This modulation occurs through a crosstalk between RAF and MKK3/p38 signalling modules. By regulating C-RAF protein stability, HERC1 controls

protein levels of MKK3, a MAP2K of the p38 signalling pathway. Thus, HERC1 regulates a previously unknown crosstalk between these two MAPK pathways [102] (Figure 14).

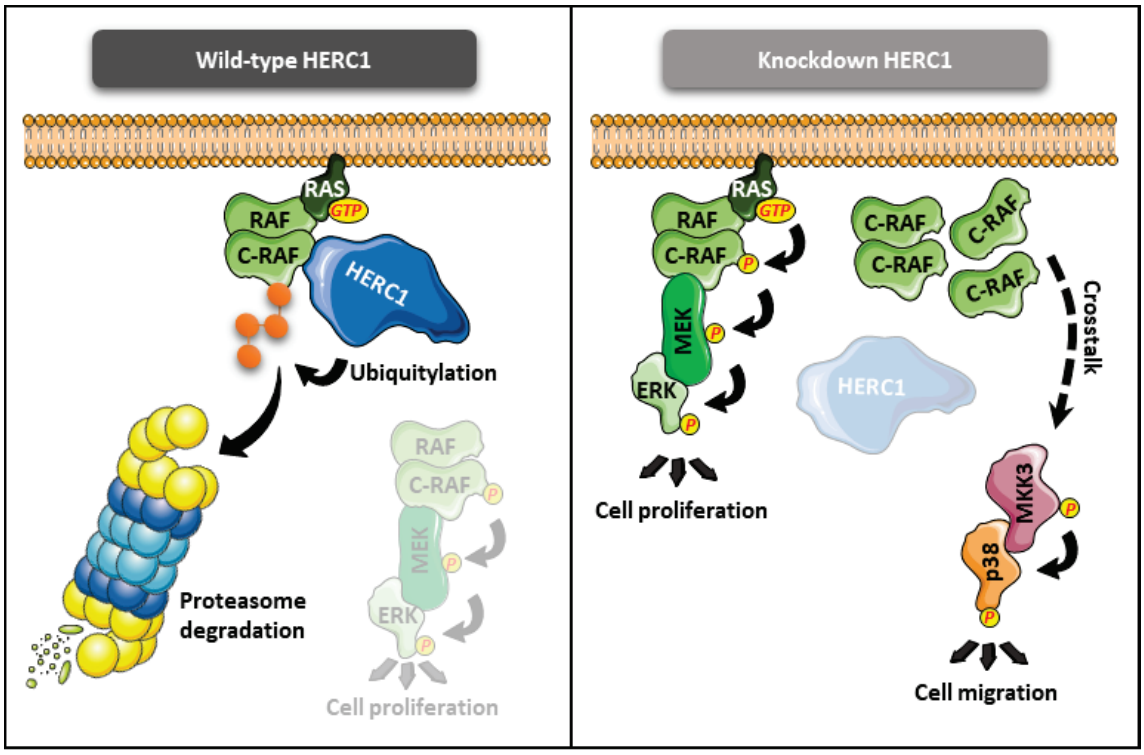

Figure 14. Regulation of ERK and p38 signalling by HERC1. HERC1 regulates ERK signalling by controlling protein levels of the MAP3K C-RAF via an ubiquitin-mediated proteasomal degradation mechanism. Knockdown of HERC1 causes accumulation of C-RAF protein levels. From one hand, this accumulation triggers overactivation of ERK signalling, thus enhancing cell proliferation. From the other hand, increased levels of C-RAF activate a crosstalk between ERK and p38 pathways at the level of MKK3. Hence, p38 is phosphorylated and activated, which eventually promotes cell migration.

The involvement of HERC2 in the regulation of MAPK signalling is more unknown. However, HERC2 has been reported to be part of a high-molecular-weight complex formed by E6AP/UBE3A, NEURL4, and the "atypical" MAPK ERK3 [33]. Some cellular functions that might be regulated by this complex involve transcription, protein translation, formation and transport of vesicles as well as metabolism [103]. To date, the precise molecular mechanism remains to be elucidated, necessitating further research. In addition, the participation of HERC2 in the regulation of "typical" MAPK signalling pathways such as ERK and p38 remains mainly unexplored.

Oxidative stress response

In a wide sense, **cellular stress** defines a condition in which cells confront and react to a non-homeostatic state. This imbalance or perturbation in the cellular homeostasis may originate through both extracellular and intracellular means. The **cellular stress response** is

the wide range of molecular changes that cells undergo to counteract this imbalance and recover cell homeostasis [104].

In particular, **oxidative stress** reflects a cell's imbalance in which excessive **reactive oxygen species (ROS)** are produced and the cellular system's ability to detoxify the reactive intermediates is insufficient. More simply, it is a disturbance in the balance between oxidant-antioxidant states, favouring the oxidant environment [105]. ROS include **superoxide anion radical ($\cdot O_2^-$)**, **hydroxyl radical ($\cdot OH$)** and **hydrogen peroxide (H_2O_2)** and are normally counteracted by cellular antioxidant proteins such as **superoxide dismutase (SOD)**, **catalase (CAT)**, **glutathione (GSH)**, **glutathione peroxidase (GPX)**, **thioredoxin** and **glutaredoxin**. ROS are constantly produced by a number of normal cellular events, a major source being aerobic respiration. However, these are generally counteracted by antioxidant proteins [106].

Several studies have demonstrated that exposure to ROS can induce MAPK pathways activation. For instance, exposure of cells to exogenous H_2O_2, to mimic oxidative stress conditions, leads to activation of several MAPK such as ERK and p38 [107]. The mechanisms by which ROS activate MAPK pathways are not well defined. Still, the oxidative modification of amino acid residues of signalling proteins is a plausible mechanism. Many growth factor and cytokine receptors have cysteine-rich motifs, the oxidation of which may induce MAPK pathway activation. ROS may also activate MAPK through direct oxidative modification of intracellular kinases such as ASK1. In conjunction, stimulation of these pathways mediates activation of a wide variety of cellular responses that might boost an appropriate cellular response to counteract oxidative stress induced by ROS [108].

A key factor in the regulation of the oxidative stress response is the **nuclear factor erythroid 2-related factor 2 (NRF2)**. It is considered the master regulator of the anti-oxidant response. NRF2, encoded by the ***NFE2L2* gene**, is a transcription factor that binds to **antioxidant response elements (AREs)** in the promoter regions of its target genes. In particular, NRF2 induces the expression of several antioxidant enzymes such as SOD, CAT, Glutathione S-transferase (GST) and GPX [109]. As a master regulator, its abundance and expression is tightly regulated to ensure that its activity increases only during redox perturbation. At post-translational level, NRF2 stability is strictly controlled by ubiquitylation and proteasomal degradation. Under homeostatic conditions, NRF2 is rapidly degraded.

Following translation, NRF2 binds with a KEAP1 homodimer. KEAP1 functions as an adaptor protein for the CUL3 E3 ubiquitin ligase, which constitutively ubiquitylates NRF2 targeting it to proteasomal degradation maintaining NRF2 basal levels low [110]. In response to oxidative stress, NRF2 escapes KEAP1-dependent inhibition by dissociating from the complex and entering the nucleus where it activates its target genes (Figure 15). The mechanism by which oxidative stress promotes NRF2-KEAP1 dissociation remains controversial. One model suggests that KEAP1 is the sensor of oxidative stress. In presence of ROS, it is oxidized at reactive cysteine residues, which results in KEAP1 inactivation and dissociation from NRF2. Another model postulates that upon oxidative stress, NRF2 is phosphorylated by protein kinase C (PKC), PI3 kinase and/or MAPKs ERK and p38. Following this modification, NRF2-KEAP1 interaction is disrupted and hence NRF2 activated and translocated to the nucleus [104].

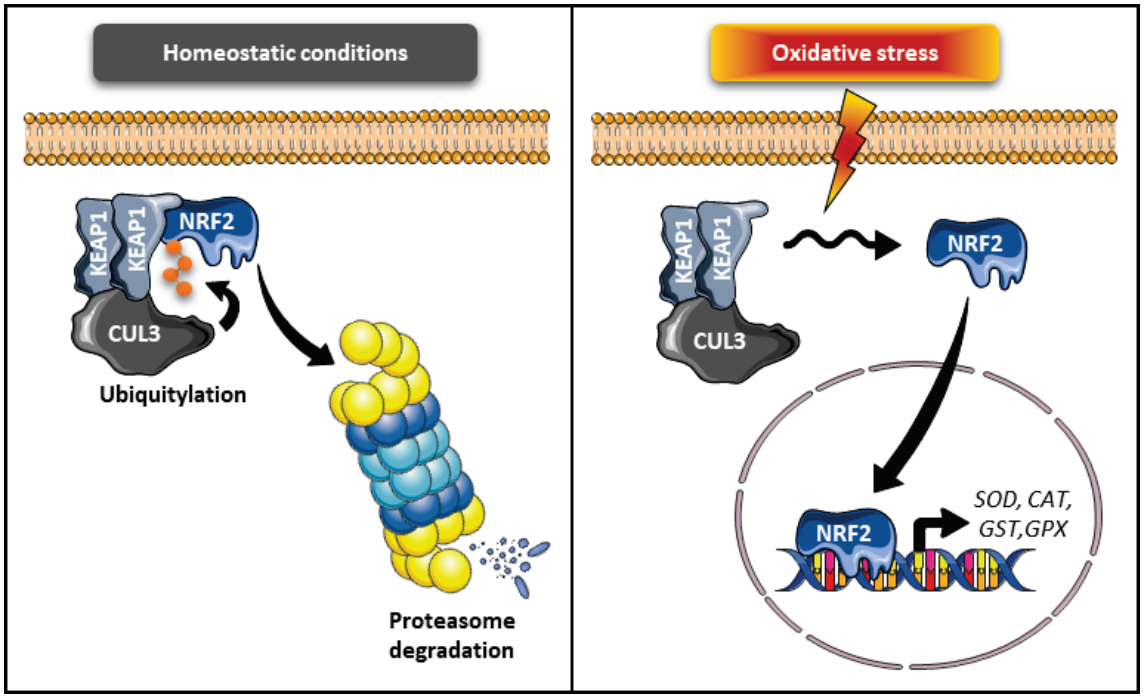

Figure 15. Regulation of the oxidative stress response by NRF2. Under homeostatic conditions, KEAP1 homodimers bind NRF2 and present it to the E3 ubiquitin ligase CUL3, which ubiquitylates NRF2 targeting it for proteasomal degradation. In response to oxidative stress, KEAP1-NRF2 interaction is disrupted, which leads to NRF2 stabilisation. Then, NRF2 induces expression of antioxidant genes such as SOD, CAT, GST and GPX, which defend the cell against the homeostatic failure.

Intracellular degradation machineries

Autophagy and the ubiquitin-proteasome system are the two major intracellular degradation and recycling machineries. As such, they act as quality control pathways favouring cell homeostasis. Autophagy is mainly involved in the elimination of long-lived proteins, insoluble protein aggregates and even organelles such as mitochondria or intracellular pathogens such as bacteria. On the other hand, the proteasome pathway is typically implicated in the degradation of short-lived proteins and soluble protein aggregates or misfolded peptides. Intriguingly, ubiquitylation is employed as a degradation signal in both systems, although implying different molecular mechanisms. Furthermore, there is accumulating evidence about additional links between autophagy and proteasome pathways, implying reciprocal regulation mechanisms to coordinate their actions in proteostasis and cellular homeostasis.

Upon cellular stress, such as oxidative stress, cells maintain cellular homeostasis by activating and appropriate response. A common hallmark of cellular damage triggered by different types of stress is protein aggregation, that is the accumulation of misfolded proteins. To deal with this situation, stressed cells activate protein degradation machineries in order to eliminate abnormal proteins by **autophagy-lysosome pathway (ALP)** and/or the **ubiquitin-proteasome system (UPS)**. If neither of these processes can alleviate the damage caused by the accumulation of protein aggregates, apoptosis and cell death will eventually be triggered [111]. Therefore, the maintenance of a healthy proteome, which is called **proteostasis**, is a key requirement for the well-being of any cell type. In this aspect, both ALP and UPS represent important intracellular machineries of protein quality control. In general, long-lived and insoluble protein aggregates are preferentially eliminated by autophagy, whereas short-lived and soluble misfolded or damaged proteins are targeted by UPS. Importantly, all of these systems are interconnected via different mechanisms. For instance, ubiquitylation is utilized as a degradation signal by both [112].

Molecular mechanisms of mammalian autophagy

Autophagy is a catabolic process that consists in delivering cytoplasmic components, known as **cargo**, to the lysosomes for degradation. In mammals there are three different types of autophagy: **macroautophagy**, **microatuophagy** and **chaperone-mediated autophagy (CMA)**. They differ in the mechanism by which the cargo is directed to the lytic

compartment [112]. The best described type of autophagy is **macroautophagy (hereafter called autophagy)**. It is characterized by the engulfment of cellular material by a double-membrane structure called **phagophore**, which eventually seals forming the **autophagosome**. Mature autophagosomes are transported along microtubules toward **lysosomes**, fusing with them and resulting in the degradation of the cargo [113]. Conversely, in **microautophagy,** the cargo is sequestered by a small invagination of the lysosomal membrane, that delivers it into the lumen for degradation [114]. Finally, during **CMA**, cytosolic components that bear a pentapeptide signature motif (KFERQ) are selectively recognized by the chaperone HSC70/HSPA8, which in turn binds to the lysosomal-associated membrane protein 2A (LAMP2A). Then, the target proteins are unfolded and translocated into the lumen of lysosomes for degradation [115].

Focusing now on **macroautophagy (autophagy)**, the cargos are not limited to proteins and include organelles and macromolecules. The core mammalian machinery consists of about 20 highly conserved **autophagy-related genes (*ATG*s)** that encode different proteins that can be divided into six functional groups: 1) the **ULK protein kinase complex**; 2) the **ATG9-containing vesicles**; 3) the **phosphatidylinositol 3-kinase class III complex 1 (PI3KC3-C1)**; 4) **ATG2A- or B-WIPI1-4 complex**; 5) the **ATG12-5:16L1 complex**; and 6) the **LC3 protein-lipid conjugation system**. The first three complexes (ULK, ATG9-containig vesicles and PI3KC3-C1) are involved in the initiation mechanisms, whereas the others regulate phagophores expansion [116]. Signals that activate the initiation of autophagy usually originate from various stress conditions such as starvation, oxidative stress, protein aggregation, hypoxia and others. Typically, all signalling cascades converge in the activation of the ULK complex, composed of four components (**ULK1/2**, ATG13, FIP200/RB1CC1 and ATG101). The ULK complex then phosphorylates and activates components of the PI3KC3-C1 complex (consisting of PI3KC3/VPS34, PI3KR4/VPS15, Beclin-1, ATG14L). This, in turn, activates local phosphatidylinositol-3-phosphate (PI3P) production at a structure of the endoplasmic reticulum called omegasome. Rise of PI3P levels recruits PI3P-binding proteins such as WIPI1-4 proteins. In the WIPI complexes, ATG2A/B act binding the ER membrane to the phagophore that is forming and mediating lipid transfer to facilitate its expansion [117]. The following mechanisms facilitating phagophore elongation and autophagosome maturation require two ATG conjugation systems. First, the E1 and E2 enzymes ATG7 and

ATG10 catalyse the conjugation of the ubiquitin-like protein ATG12 to a lysine residue in ATG5. Then the ATG12-ATG5:ATG16L1 complex is assembled and recruited to the nascent phagophore through direct binding between ATG16L1 and WIPI2. There, ATG12-ATG5:ATG16L1 complex acts as an E3 ligase to stimulate conjugation of **phosphatidylethanolamine (PE)** to a C-terminal glycine residue of the cytosolic form of LC3 protein (called **LC3-I**). Once conjugated to PE, the lipidated form of LC3 is bound to the autophagic membrane and named **LC3-II** [118]. Lipidated LC3 (LC3-II) proteins are essential for elongation and sealing of the phagophore membrane (Figure 16A). In addition, they act as adaptors to recruit other proteins containing a domain called **LC3-interacting region (LIR)**. These proteins can be components of the autophagic machinery but also cargo receptors that in turn bind specific degradation substrates, a key mechanism of the so called **selective autophagy** [119]. Mature autophagosomes are transported along microtubules and ultimately fuse with lysosomes resulting in the degradation of the cargo by lysosomal hydrolases (Figure 16B). The products resulting from the degradation, such as amino acids, are recycled back into the cytoplasm for reuse, which is important for cell survival during periods of nutrient deprivation. In addition, autophagy also provides a system for the elimination of damaged or unwanted cellular contents [112].

Autophagy is tightly connected to metabolism and growth. As stated above, ULK complex represents the most upstream kinase within the autophagy core machinery. Therefore, several signalling pathways converge in its activation. The most characterized trigger for autophagy induction is deprivation of amino acids, which results in inhibition of the serine/threonine kinase complex **mTORC1**. Under nutrient rich conditions, the members of the ULK complex ULK1 and ATG13 are bound to mTORC1, which phosphorylates and maintains them inactive. Upon starvation, inhibitory phosphorylation's of ULK1 are removed, which triggers its dissociation from mTORC1. Subsequently, ULK1 is auto-phosphorylated and next it phosphorylates ATG13 and FIP200, which eventually fully activates the ULK complex. Then the process of induction and phagophore nucleation is initiated [120]. Another key regulatory protein is the transcription factor TFEB. Similarly to ULK1 and ATG13, it is negatively regulated by mTORC1 and liberated upon starvation to regulate expression of genes involved in lysosomal biogenesis and lipid catabolism [121]. Autophagy can also be induced upon decreasing cellular energy levels, as in glucose starvation. This is sensed via a

decrease in the ATP:AMP ratio, which is detected by **5' AMP-activated protein kinase** (**AMPK**) and the **serine/threonine kinase LKB1**. Energy stress results in LKB1-dependent activation of AMPK, which directly phosphorylates both TSC2 and Raptor to inhibit mTORC1. In detail, TSC2 contains a GTPase activating domain that inactivates Rheb GTPase, which has been shown to directly activate mTORC1. Phosphorylation of TSC2 by AMPK enhances its activity, thus resulting in Rheb and consequently mTORC1 inhibition. On the other hand, Raptor is a subunit of the mTORC1 complex that acts as a scaffold recruiting downstream substrates. Its phosphorylation by AMPK stimulates its binding to 14-3-3, dissociating from mTORC1 complex which results in mTORC1 inhibition. In other words, AMPK activation results in autophagy stimulation by lifting the brake that exerts mTORC1 [122].

Autophagy was originally conceived as a nonselective bulk degradation process. Indeed, under nutrient or growth factor deprivation, autophagy is thought to be nonselective and committed to degrade any cytosolic protein or macromolecules in order to provide essential nutrients and building blocks to the cell. This process is known as **bulk autophagy**. Nevertheless, autophagy can also be a highly selective degradation pathway targeting not only specific proteins but also organelles, nuclear components, the proteasome or pathogens. In this context, selective autophagy functions as a defensive mechanism that can be activated in a nutrient-rich context by different stress signals [123]. Thus, **selective autophagy** can further be divided into different subtypes depending on the specific cargos that are degraded. For instance, **mitophagy (mitochondria)**, **xenophagy (pathogens)** or **aggrephagy (protein aggregates)**. The discovery of selective autophagy receptors, such as p62/SQSTM1, was key in the understanding of this concept of selective autophagy [124]. Hence, the main characteristic of selective autophagy is the use of these **selective autophagy receptors (SARs)**. SARs bind the cargo from one side and uses a LIR motif to interact with LC3-II on the inner membrane surface of the elongating phagophore. Thus, they facilitate encapsulation of the cargo (Figure 16B). The most-studied SARs in mammals are the **Sequestosome-1-like receptors (SLRs) p62, NBR1, NDP52, TAX1BP1** and **OPTN**. They are characterized by containing, in addition to the LIR domain, an ubiquitin-binding domain. So, the substrates targeted by SLRs are typically ubiquitylated proteins [116].

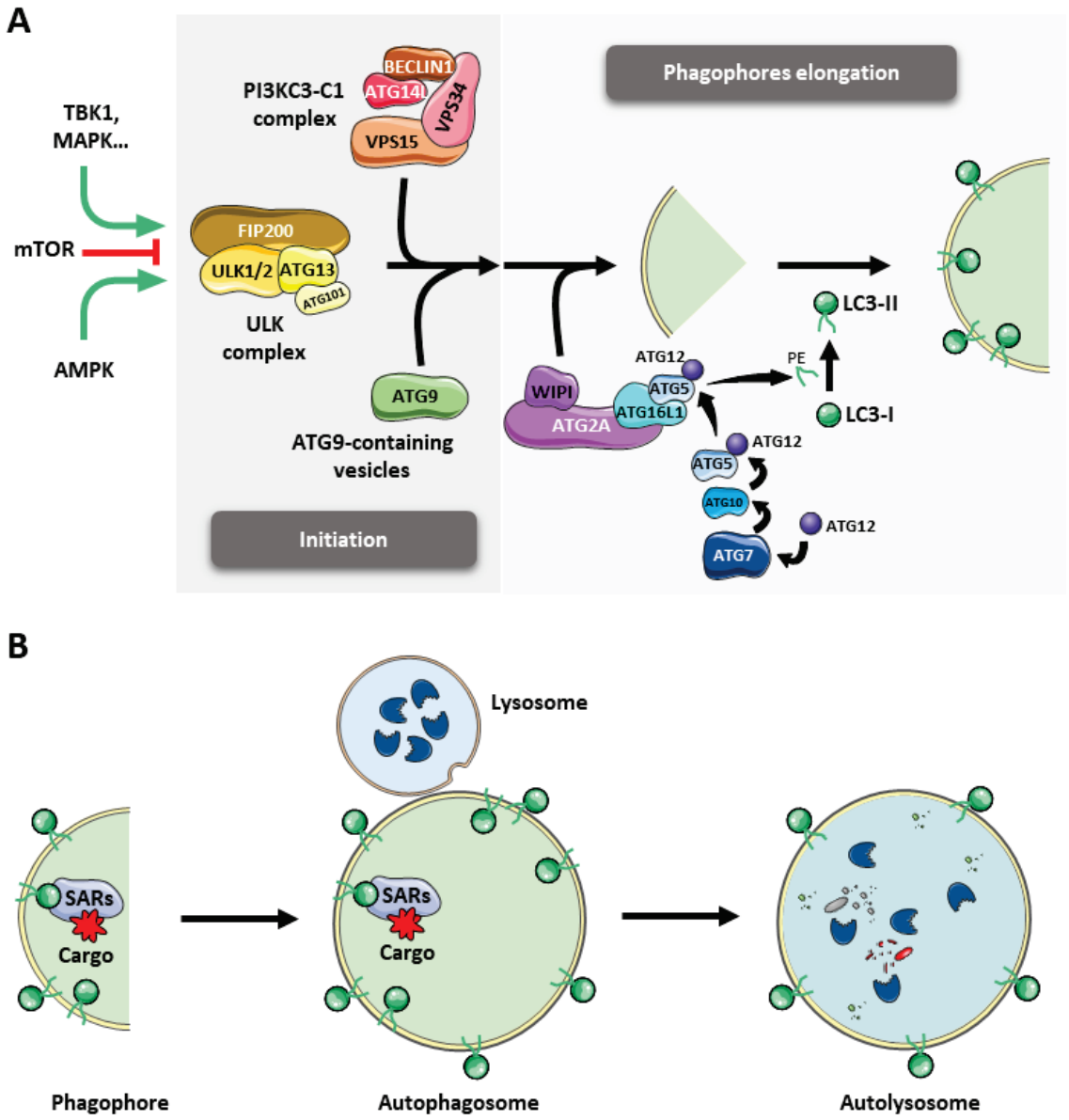

Figure 16. Schematic representation of the main regulatory machinery of macroautophagy (autophagy). **(A)** The metabolic sensor mTOR inhibits autophagy while AMPK activates it. Some kinases such as TBK1 or MAPK can also induce autophagy. They all converge in the activation of the ULK complex, which along with PI3KC3-C1 complex and ATG9-containing vesicles, promote autophagy initiation. For phagophore elongation, first the E1 enzyme ATG7 and the E2 enzyme ATG10 catalyse the conjugation of the ubiquitin-like protein ATG12 to ATG5. Then ATG12-ATG5 is recruited to the nascent phagophore through binding to ATG16L1, which in turn is attached to ATG2A and WIPI. There, ATG12-ATG5 acts as an E3 ligase to stimulate conjugation of phosphatidylethanolamine (PE) to the cytosolic form of LC3 protein (LC3-I). Once conjugated to PE, the lipidated form of LC3 (LC3-II) is bound to the autophagic membrane. **(B)** In selective autophagy, selective autophagy receptors (SARs) bind the cargo to be degraded from one site and from another site bind LC3-II proteins attached to the inner membrane of the nascent phagophore. Once the phagophore seals forms the autophagosome. Mature autophagosomes ultimately fuse with lysosomes resulting in the degradation of the cargo by lysosomal hydrolases.

In brief, SLRs, recognize cargos labelled with this “eat-me” signals, typically polyubiquitin chains, and recruit them to phagophore structures [116]. The prevailing model stablishes that the mechanism of autophagy induction in these cases of selective autophagy

differ from starvation-induced autophagy, since in selective autophagy ULK1 is activated independently of mTORC1 and AMPK. The precise mechanism still requires further characterization but the specific recruitment and activation of ULK1 to cargo by other signalling pathways seems critical to recruit the rest of the core autophagic machinery [125]. In this line, the serine-threonine kinase TBK1 phosphorylates several SLRs such as p62, NDP52, OPTN and TAX1BP1 [126]. In addition it facilitates recruitment and activation of ULK1 at the cargo [127]. Another example is the MAPK p38, which activity has been linked with the regulation of autophagy. Sustained activation of p38α triggers massive autophagosome formation and enhances the autophagic flux. Specifically, p38 phosphorylates ULK1, which contributes to autophagy induction [128].

Assembly and function of the 26S proteasome

The ubiquitin proteasome system (UPS) degrades thousands of short-lived and regulatory proteins in addition to damaged and misfolded polypeptides. Hence, it regulates several cellular functions such as cell survival, cell cycle, metabolism and protein quality control [129]. To achieve these key functions, its activity is tightly regulated. There are two main types of signals to target proteins for proteasome-dependent degradation: ubiquitylation, typically in the form of lysine 48-linked polyubiquitin chains; and the presence of an unstructured region in proteins [130]. In addition to selectively targeting proteins to the proteasome, cells regulate proteasomal degradation activity by adjusting proteasome abundance. This is highly controlled by different factors: 1) transcriptional regulation of genes encoding proteasomal subunits and assembly factors; 2) factors triggering degradation of proteasomes; and 3) posttranslational modifications that modulate assembly, localization and degradation capacity of proteasomes [112]. Notably, assembly of the fully functional proteasome following subunit synthesis is a complex process and crucial for its correct activity.

Proteasomes are multiprotein complexes. The most abundant proteasome in mammals is the **26S proteasome (the constitutive proteasome)**, which is comprised by a **20S core particle (CP)** and **19S regulatory particle (RP)**. While the 20S CP acts as the catalytic component of the 26S proteasome, the 19S RP is responsible for substrate recognition, deubiquitylation, protein unfolding and transferring to the 20S CP [131]. It is worth noting that, given that numerous studies of the proteasome structure are in yeast models, in the

scientific literature it is common to find the proteins that form the proteasome complexes designated with the name corresponding to the homologues in yeast. However, since we are focusing on the mammalian proteasome, the nomenclature corresponding to the human homologues will be used from now on. Still, a comparison between yeast and mammalian nomenclature is provided in Figure 17.

The 20S CP has a cylindrical structure, formed by two outer heptameric **α rings (α1-7)** and two inner heptameric **ß rings (ß1-7)**. It adopts a $\alpha_{1-7}ß_{1-7}ß_{1-7}\alpha_{1-7}$ structure (Figure 17). The α rings serve as gate keepers and the ß rings hold the catalytic activity, with caspase-like, trypsin-like and chymotrypsin-like activities [129].

On the other hand, 19S is composed by two substructures: the **base** and **lid** subcomplexes. The base comprises an heterohexameric ring of six **AAA$^+$ ATPases (PSMC1-6)**. The ATPases subunits are required not only for substrate unfolding with the energy liberated from hydrolysis of ATP, but also for α ring channel opening. Additionally, other non-ATPase proteins are also part of the base subcomplex (**PSMD1, PSMD2, PSMD4** and **ADRM1**). PSMD2, PSMD4 and ADRM1 recognize ubiquitylated proteins, while PSMD1 facilitates stabilization of the complex. The lid comprises nine proteins (**PSMD3, PSMD6, PSMD7, PSMD8, PSMD11, PSMD12, PSMD13, PSMD14** and **SEM1**), which are involved in the recruitment of ubiquitylated proteins, deubiquitylation of substrates and stabilizing the proteasome [131] (Figure 17).

Besides the 26S constitutive proteasome, cells have developed different proteasome complexes to control different substrate specificity. For instance, lymphoid tissues express high levels of ß1i, ß2i and ß5i, which are counterparts of the typical ß1, ß2 and ß5 catalytical subunits. These subunit variants, which are upregulated by IFN-γ, constitute the so called **immunoproteasome**, which mainly contributes to peptide generation for MHC class I antigen presentation. The immunoproteasomes can be regulated by the classical 19S RP or by the IFN-γ-induced PA28 complex (also known as REG or 11S). In mammals, PA28 comprises four **PA28α (REGα or PSME1)** and three **PA28β (REGβ or PSME2)** proteins organized as a heteroheptameric ring complex [132, 133].

Assembly of a 26S proteasome is a highly intricate process that requires numerous dedicated chaperones and maturation factors. Increasing evidence points to that cells

regulate proteasome abundance through the expression of proteasome subunits and assembly chaperones. In addition, the assembly mechanisms of the different subunits are key and well-controlled [129]. The assembly of multiprotein complexes, such as the proteasome, requires each subunit to be produced at a determined amount relative to its partners. Thus, a correct balance in the subunits protein levels is needed. Proportional synthesis as a result of a tightly regulated transcription and translation might be important to control the stoichiometry of the complex. Still, imbalances are inevitable, and the elimination of excess or orphan proteins, derived from unassembled intermediates, also plays an important role [134]. In addition, because proteasomal subunits share structural similarities, miss-assembly can occur, leading to aberrant assembly intermediates that interfere with the normal construction of the proteasome. For this reason, mechanisms to avoid the formation of dysfunctional intermediates and to remove orphaned or aberrant assembly intermediates are essential for maintaining a healthy proteasome pool [135].

CP assembly begins with the formation of individual α rings, which provide a scaffold in which ß subunits are incorporated. Initial assembly of the α ring is controlled by two hetero-dimeric chaperones called PAC1-PAC2 and PAC3-PAC4, which act as a platform onto which the α ring is assembled [136, 137]. Next, the proteasome maturation protein (POMP) recruits the ß subunits into the nascent complex and supports the final proteasome maturation [138] (Figure 17).

Unlike CP, which is composed exclusively of ring structures, the RP is more architecturally complex, with the base and the lid assembling in an independent way. Again, the role of different chaperones is crucial. Regarding the base assembly, four chaperones have been described: **PSMD9, PSMD10, PAAF1** and **PSMD5.** These chaperones independently bind to the C-terminal domain of a distinct AAA^+ ATPase protein of the base hetero-hexameric ring. In brief, PSMD5 binds PSMC2, PSMD9 binds PSMC3, PSMD10 binds PSMC4 and PAAF1 binds PSMC5. Their main function seems to be to ensure correct assembly of the hetero-hexameric ring. The ring is formed by joining three different dimers: PSMC2-PSMC1, PSMC5-PSMC4 and PSMC6-PSMC3. Next, the base non-ATPases PSMD2 and PSMD1 bind to the tips of PSMC2-PSMC1 and PSMC5-PSMC4, respectively. ADRM1 and PSMD4 complete the base sub-complex [135] (Figure 17).

Lid arrangement is initiated by the formation of two intermediates that self-assemble. One is composed of PSMD11, PSMD12, PSMD7, PSMD13 and PSMD14; and the other is composed of PSMD3, PSMD6 and SEM1. After formation of these two intermediates, the last lid subunit, PSMD8, is incorporated. This triggers conformational changes of the lid that enable binding to the base, thus forming a complete 19S RP [129] (Figure 17).

The association of the 19S RP at the end of the 20S CP is crucial for the function of the 26S proteasome since, as stated above, the RP controls essential steps in proteasomal degradation such as substrate recognition, deubiquitylation, unfolding and translocation to the CP gate. All these phases guarantee a selective degradation of proteins. Association between RP and CP is mediated by the attachment of C-terminal domains of base AAA^+-ATPases proteins into the α rings. Once this interaction occurs, there are several conformational changes of the CP that enable the channel formation and the opening of the CP gate when the substrates are incorporated [139].

As can be seen, proteasome assembly is a complex process involving a multitude of proteins that need to be correctly assembled in an adequate order and quantity. Indeed, chaperones help intermediates to bind correctly with each other but still, the cells need mechanisms to detect excess or orphaned intermediates and to eliminate them, so that they do not negatively interfere with proteasome assembly. That is, cells need quality control factors to supervise the assembly process. However, how cells detect these stalled orphaned assembly intermediates for selective degradation is not fully elucidated. In this aspect, HERC1 was identified as a possible quality-control factor responsible for marking certain unassembled intermediates of the proteasome for degradation. Specifically, HERC1 recognises PSMC5 when it is associated with its cognate assembly chaperone PAAF1. PAAF1 only dissociates from PSMC5 after assembly into the complex, therefore, chaperone association is what allows the identification of this unassembled intermediate as an orphan protein, that will then be ubiquitin-marked by HERC1 and subsequently degraded [26]. The involvement of HERC2 in this type of mechanisms remains unexplored.

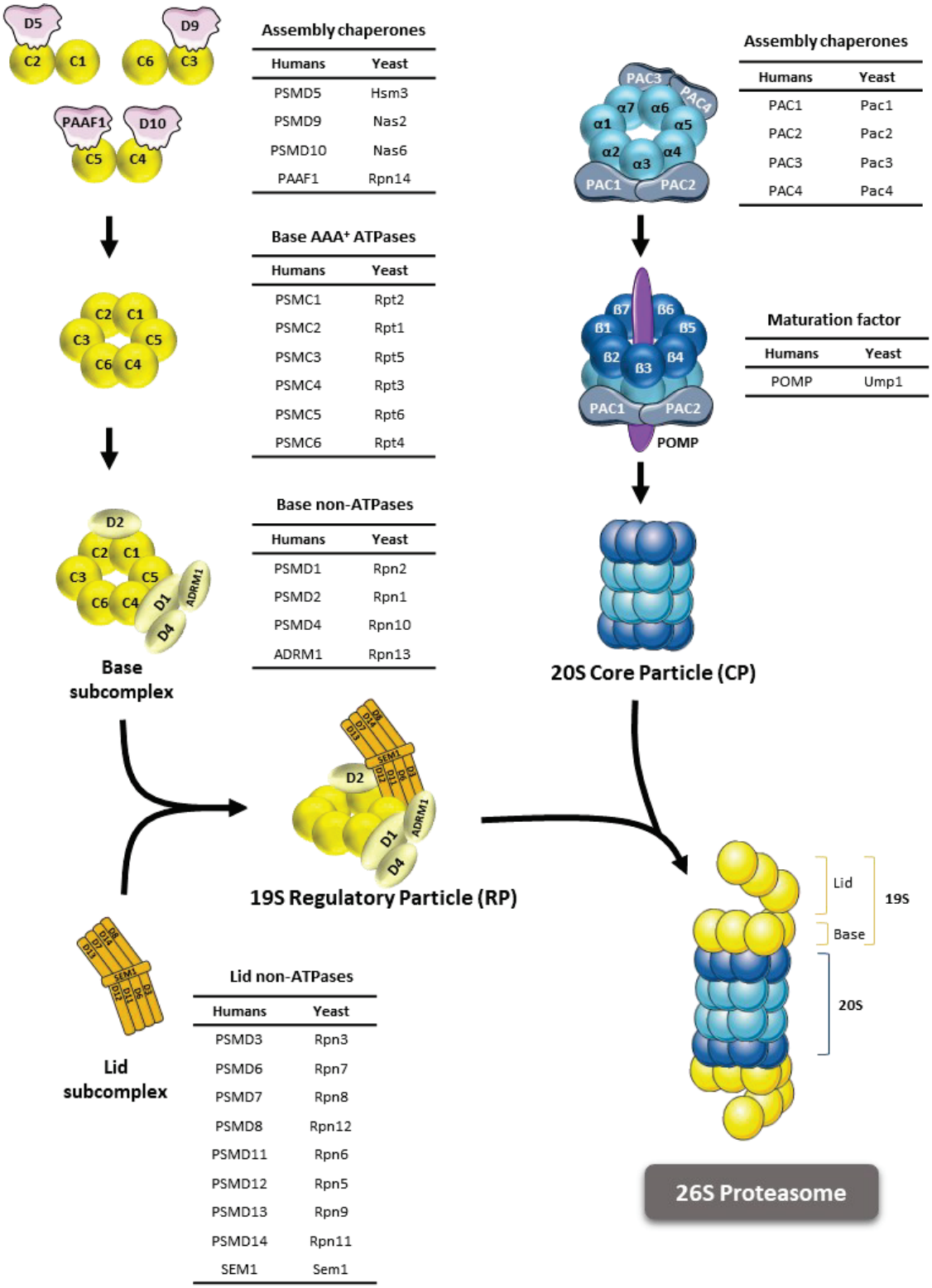

Figure 17. Proteasome structure and assembly. During assembly of 19S regulatory particle (RP) it is suggested that the base and the lid are assembled independently. The base assembly is mediated by four assembly chaperones. First, an heterohexameric ring of six base AAA+ ATPases is formed. Next, four base non-ATPases are joined constituting the base subcomplex. The lid is formed by nine non-ATPases and is suggested to self-assemble. The union of the base and lid subcomplexes give rise to the 19S regulatory particle. Regarding 20S core particle (CP) assembly, PAC1-PAC2 and PAC3-PAC4 heterodimers assist α-ring formation. Incorporation of ß-subunits is mainly mediated by the maturation factor POMP. Eventually the 20S core particle is assembled. Association of RP and CP forms the 26S proteasome.

Coordinated action of the UPS and autophagy in proteostasis

Both autophagy and the ubiquitin-proteasome system (UPS) represent the two major quality control pathways responsible for cellular homeostasis. In addition, both systems communicate and interconnect with each other at multiple points in order to coordinate their functions to promote proteostasis. Indeed, proteasome inhibition or overload induces autophagy in the majority of cell types, which provides a strong evidence of this functional interconnection. However, evidence for an opposite shift, that is, proteasome activation upon autophagy inhibition, is not as clear. Still, several reports indicate that both AMPK and mTORC1 can sense impaired proteasome activity thereby promoting autophagy as a compensatory mechanism [112]. Apart from this, the UPS and autophagy regulate each other through mutual control of the protein levels of their key regulators. For instance, upon oxidative stress, the autophagy receptor p62 facilitates autophagic turnover of KEAP1. This triggers NRF2 stabilization, since its ubiquitylation and proteasome degradation regulated by KEAP1 and CUL3 is avoided [140]. Another example is that the termination of autophagy is typically mediated by proteasomal degradation of ULK1 or other autophagy regulators [141].

The most obvious common feature between the two systems is the use of ubiquitylation as a labelling system for their substrates. Interestingly, most E3 ubiquitin ligases cannot be indubitably assigned to either the UPS or ALP. For instance, the E3 ligase Parkin plays a main role in mitophagy, regulates proteasomal degradation of multiple mitochondrial substrates and also mediates autophagic degradation of other different subset of substrates. In conjunction, a major future challenge is to reveal which factors define the specific degradation route that a given E3 ligase substrate will follow [112].

CHAPTER II. Hypothesis and Objectives

Ubiquitylation has emerged as an important cellular mechanism that regulates different signalling networks. In this process, the E3 ubiquitin ligases determine the specificity of the substrates, thus, they represent a crucial regulatory factor. The main line of research of our group is the functional characterization of the HERC family of ubiquitin ligases, to which HERC2 belongs. HERC2 has been widely studied for its implication in in the regulation of genomic stability and p53 transcriptional activity. However, its involvement in other signalling pathways, in which ubiquitylation also plays an important role, remains mainly unexplored. With regard to its clinical relevance, mutations in HERC2 are associated with the neurodevelopmental disorder known as HERC2 Angelman-like syndrome as well as with some tumours. A better understanding of how pathologic HERC2 mutant variants affect intracellular signalling may aid definition of potential new therapies for these disorders.

In view of all this, and considering the precedent findings on the role of the other Large HERC family member HERC1 in the regulation of MAPK signalling pathways, we hypothesized that HERC2 could also be involved in the modulation of these pathways. Secondly, given the evidence of an accumulation of autophagosomes and lysosomes in the Purkinje cells of the *Herc2*$^{+/530}$ mice model, we hypothesized that HERC2 could regulate the autophagy-lysosome pathway. Finally, as a result of the great scientific advances in the field of proteomics and the development of the ^{bio}Ub strategy, we hypothesized that we could use these approaches to identify potential HERC2 substrates and thus uncover as yet undescribed physiological functions of HERC2. Therefore, the main objective of this doctoral thesis was to study the signalling pathways regulated by HERC2 and to characterize the molecular mechanisms behind. To this end, we focused on three specific goals:

1. To assess how HERC2 deficiency affects MAPK signalling and to determine how HERC2-dependent MAPK regulation affects the cellular stress response.
2. To study the potential relationship between HERC2 and autophagy regulation.
3. To identify potential new substrates of HERC2 unveiling other possible physiological functions of HERC2 based on the putative substrates identified.

CHAPTER III. Materials and Methods

Cell lines, primary cultures, human samples and culture conditions

Different cell lines, primary cultures and human samples were used as an *in vitro* research model. Each of them is described in the table below (Table 1):

Table 1. Cell lines, human cell samples and mouse primary cultures.

Cells		Brief description
Cell lines	**U2OS**	Human tumour cell line derived from an osteosarcoma.
	H1299	Human tumour cell line derived from a non-small cell lung carcinoma. These cells have a homozygous partial deletion of the *TP53* gene, thus do not express p53 protein.
	A549	Human tumour cell line derived from a non-small cell lung carcinoma harbouring wild-type *TP53* gene.
	HeLa	Human tumour cell line derived from cervical cancer.
	HEK 293T	Non-tumour cell line derivative of the human embryonic kidney (HEK) 293 cell line. It was immortalized by expression of the large T antigen of simian virus 40 (SV40T).
	RAW 264.7	Mouse macrophage cell line derived from a tumour induced with the Abelson murine leukaemia virus.
Primary cultures	**Human skin fibroblasts**	Human skin fibroblasts were obtained from individuals with the pathological *HERC2* mutation c.1781C>T (p.Pro594Leu). Samples from parents and unaffected siblings with wild type *HERC2* were obtained and used as controls. All samples were obtained with approved informed consent as previously described [58].
	Mouse embryonic fibroblasts	Primary mouse fibroblasts prepared from mouse embryo.
	Mouse osteoblasts	Primary mouse osteoblasts derived from mice calvaria.

U2OS, H1299, A549, HeLa, HEK 293T, RAW 264.7, human skin fibroblasts and mouse embryonic fibroblasts were cultured in Dulbecco's Modified Eagle's Medium (DMEM) supplemented with 10% foetal bovine serum, 2 mM l-glutamine, 100 U/mL penicillin, and 0.1 mg/mL streptomycin sulphate. Mouse osteoblasts were cultured in alpha-modified

Minimum Essential Medium (α-MEM) with 10% FBS, 2 mM l-glutamine, 1 mM pyruvate, 100 U/ml penicillin, and 0.1 mg/ml streptomycin with 50 µg/ml ascorbic acid and 4 mM β-glycerophosphate. All cells were maintained in a humidified incubator at 37 °C and 5% CO_2.

Transfection methods

Transfection is a powerful experimental method that enables the study of the function of genes and gene products in cells. For gene overexpression experiments, a plasmid with a sequence encoding the protein of interest was incorporated into the cells following Lipofectamine LTX transfection. For gene interference, silencing RNAs were transfected using the calcium phosphate method.

Plasmid transfection with Lipofectamine LTX protocol

Plasmid transfection was performed following Lipofectamine® LTX DNA Transfection Reagent Protocol (Invitrogen, #15338100) with some modifications:

1- Seed the cells to one well per condition using a 6-well plate. Each well should be at approximately 70% of confluence the day of transfection.
2- The following day prepare one tube for each condition and add to each 200 µl of Opti-MEM™ (Gibco, #11058021), 1 µg of DNA and 1.25 µl of PLUS™ reagent.
3- Incubate for 5 min at room temperature.
4- Add to each tube 3.125 µl of Lipofectamine® LTX reagent.
5- Incubate each transfection mix for 20 min at room temperature.
6- Meanwhile, change the cell culture medium of the cells for one not supplemented with antibiotics (1 mL/well).
7- After the 20 min incubation, add 200 µl of each transfection mix to the corresponding well.
8- Incubate cells in presence of the transfection mix overnight.
9- The next day, remove the medium from the cells and add fresh medium (2 mL/well)
10- Incubate for 24 hours before proceeding to fixation, lysis, visualization or analysis.

High levels of expression of plasmids are observed after 48 hours post-transfection. A list of plasmids used in this work is provided in the following table. Plasmid's name, vector, description and references are indicated (Table 2).

Table 2. List of plasmids.

Plasmid	Description	Reference
Myc-HERC2 F1	HERC2 fragment tagged with Myc epitope. Amino acids from 1 to 1295.	Kindly provided by Dr. Ohta [36].
Myc-HERC2 F2	HERC2 fragment tagged with Myc epitope. Amino acids from 1224 to 2329.	Kindly provided by Dr. Ohta [36].
Myc-HERC2 F3	HERC2 fragment tagged with Myc epitope. Amino acids from 2292 to 2923.	Kindly provided by Dr. Ohta [36].
Myc-HERC2 F4	HERC2 fragment tagged with Myc epitope. Amino acids from 2893 to 3591.	Kindly provided by Dr. Ohta [36].
Myc-HERC2 F5	HERC2 fragment tagged with Myc epitope. Amino acids from 3559 to 4834.	Kindly provided by Dr. Ohta [36].
Myc-HERC2 F5CT	HERC2 fragment tagged with Myc epitope. Amino acids from 4252 to 4834.	Kindly provided by Dr. Ohta [36].
GFP-C-RAF CR1	C-RAF fragment tagged with GFP epitope. Amino acids from 1 to 200.	Previously generated in the lab [25].
GFP-C-RAF CR2	C-RAF fragment tagged with GFP epitope. Amino acids from 201 to 300	Previously generated in the lab [25].
GFP-C-RAF CR3	C-RAF fragment tagged with GFP epitope. Amino acids from 301 to 648.	Previously generated in the lab [25].
GFP-C-RAF FL	C-RAF full-length protein. Tagged with GFP epitope.	Previously generated in the lab [25].
Flag-HERC2 WT	Wild type HERC2 full-length protein. Tagged with Flag epitope	Addgene plasmid #55613 [142].
Flag-HERC2 C4762S	HERC2 with mutation Cys-4762Ser, to render HERC2 catalytically inactive. Tagged with Flag epitope.	Addgene plasmid #55614 [142].
His-Ubiquitin	Ubiquitin tagged with His epitope.	Kindly provided by Dr. Erazo [143].
mCherry-YFP-LC3	Tandem-tagged mCherry-YFP-LC3 used as a reporter to monitor autophagic flux	Kindly provided by Dr. Terje [144].
MKK6 (glu)	MKK6 with mutations Ser-207Glu and Thr-211Glu, to render MKK6 constitutively active.	Addgene plasmid #13518 [145].
GFP-PSMC5	PSMC5 protein tagged with GFP epitope.	Kindly provided by Dr. Edge [26].
Flag-PAAF1	PAAF1 protein tagged with Flag epitope.	Kindly provided by Dr. Edge [26].

Transfection of siRNAs with calcium phosphate protocol

Small interfering RNA (siRNA) is a double-stranded RNA typically of 20-24 base pairs that interferes with the expression of specific genes with complementary nucleotide sequences by degrading their mRNA. Thus, it is used to knockdown gene expression in cells. To transfect siRNAs into cells we used the calcium phosphate protocol as described below:

1- Seed cells to one well per condition using a 6-well plate. Each well should be at approximately 70% of confluence the day of transfection.
2- The following day prepare one tube for each condition and add to each 46 µl sterile Milli-Q water, 4 µl of 50 µM stock siRNA solution and 50 µl of CaBES solution (500 mM $CaCl_2$ and 100 mM BES, pH 6.95).
3- Next, while aerating the mix making bubbles with a glass Pasteur pipette attached to the pipettor, gently add dropwise 100 µl of BES solution (280 mM NaCl, 0.75 mM Na_2HPO_4, 0.75 mM NaH_2PO_4, and 50 mM BES, pH 6.9).
4- Incubate the transfection mix for 15 min at room temperature.
5- Meanwhile, change the cell culture medium of cells for one not supplemented with antibiotics (2 mL/well).
6- After 15 min, add 200 µl of the transfection mix to the indicated well. Note that the final concentration at which siRNAs are incubated is 100 nM.
7- Incubate the cells in presence of the transfection mix overnight
8- The next day, remove the medium from the cells and add fresh medium (2 mL/well)
9- Incubate for 48 hours before proceeding to fixation, cell lysis, visualization or analysis.

High silencing efficiency is observed after 72 hours post-transfection. This happens because siRNAs, apart from being expressed (high expression at 48h post-transfection), must be correctly processed and directed towards their target mRNA to induce gene silencing. Custom double-stranded siRNA oligonucleotides were obtained from GeneCust (Boynes, France). The specific forward sequences are indicated in the following table (Table 3).

Table 3. List of siRNAs and its specific sequence

siRNA	Forward sequence
Negative control (NC)	5'-UUCUCCGAACGUGUCACGU**TT**-3'
HERC2 (H2.2)	5'-GACUGUAGCCAGAUUGAAA**TT**-3'
HERC2 (H2.4)	5'-GGAAAGCACUGGAUUCGUU**TT**-3'
HERC1	5'-CGGCAUGGAUGAACAAAUU**TT**-3'
MKK3	5'-GGAAGAAGGAUCUACGGAU**TT**-3'
C-RAF	5'-UAGUUCAGCAGUUUGGCUA**TT**-3'
A-RAF	5'-AACAACAUCUUCCUACAUGAG**TT**-3'
B-RAF	5'-AAAGAAUUGGAUCUGGAUCAU**TT**-3'
p53	5'-GACUCCAGUGGUAAUCUAC**TT**-3'

Lentiviral particle production and infection of target cells

Several primary cells remain difficult to transfect with plasmid DNA using the before-mentioned methodologies (LTX and calcium phosphate protocols). This is mainly due to their fragility and low dividing rates. To overcome this limitation we implemented a lentiviral transduction protocol. First, we produced lentiviral vectors containing the insert of interest. Then, these vectors were used to infect target cells. Lentiviruses typically integrate into actively transcribed host genes, hence, the DNA product is produced using the cell's own machineries. We used this methodology to express a short hairpin RNA (shRNA) to induce gene silencing in mouse primary cultures.

Production of lentiviral particles

Lentiviral vectors were produced in HEK 293T cells. For lentivirus to be produced, cells were transfected with plasmids expressing the necessary lentiviral genes. These are three: the **envelope plasmid**, encoding the envelope protein (VSV-G); and the **packaging plasmid**, encoding packaging proteins (Gag, Pol, Rev, Tat). In addition, we transfected the **transfer plasmid**, encoding the insert of interest which in our case was either an empty sequence (plKO), used as a control, or a sequence encoding an shRNA against HERC2 (Figure 18).

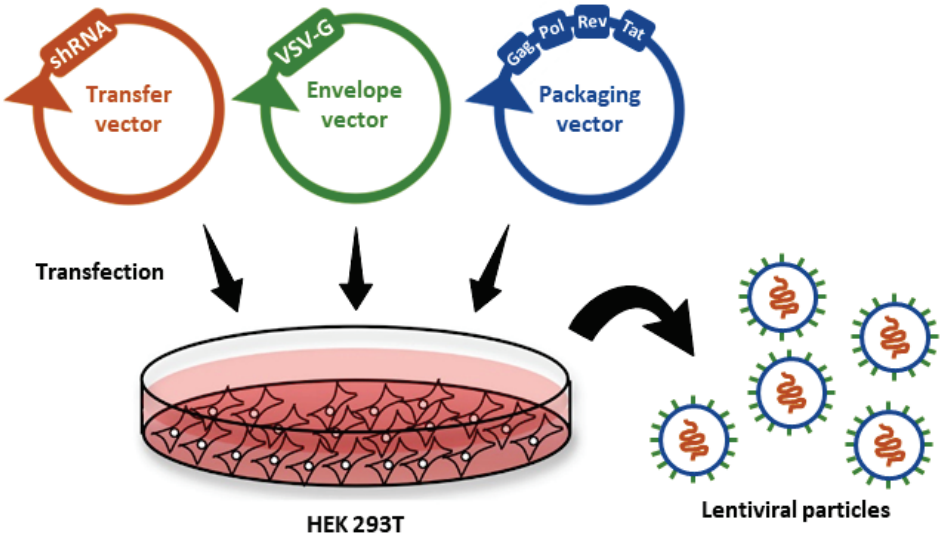

Figure 18. Lentiviral production scheme. HEK 293T were transfected with a transfer vector, encoding either an empty sequence (plKO) or an shRNA against HERC2; an envelope vector and a packaging vector. Lentivirus were collected from cells' supernatant medium.

The plasmids used for lentivirus production protocol are listed below. Plasmids, a brief description and references are indicated (Table 4).

Table 4. Plasmids used for lentivirus production.

Plasmid	Description	Reference
pMD2.G	VSV-G envelope expressing plasmid	Addgene plasmid #12259
psPAX2	Plasmid expressing lentivirus packaging genes (Gag, Pol, Rev, Tat)	Addgene plasmid #12260
plKO.1	Transfer vector with an empty coding region used as a negative control	Addgene plasmid #10879 [142].
shRNA HERC2	Transfer vector encoding an shRNA against mouse HERC2 mRNA sequence	MERCK MISSION shRNA (TRCN0000039444)

To transfect the vectors of envelope, packaging and transfer into cells we used the calcium phosphate protocol adjusted to a 10 cm cell culture dish as indicated as follows:

1- Seed HEK 293T cells on a 10 cm plate. They should be around 50-60% confluent the day of transfection.
2- The following day proceed to cell transfection following the calcium phosphate method. In brief, prepare one tube and add 7 µg of the transfer vector (either plKO or shRNA HERC2), 7 µg of the envelope vector and 7 µg of the packaging

vector. Add sterile Milli-Q water until you reach a total volume of 250 µL. Then, add 250 µl of CaBES solution (500 mM $CaCl_2$ and 100 mM BES, pH 6.95).

3- Next, while aerating the mix, add dropwise 500 µl of BES solution (280 mM NaCl, 0.75 mM Na_2HPO_4, 0.75 mM NaH_2PO_4, and 50 mM BES, pH 6.9).
4- Incubate the transfection mix for 15 minutes at room temperature.
5- Meanwhile, change the cell culture medium of cells for one not supplemented with antibiotics (9 mL/plate).
6- After the incubation, add 1 mL of the transfection mix to the 10 cm plate.
7- Mix gently and incubate cells overnight at 37 ºC, 5% CO_2 in a virus facility for 24h.
8- The next day aspirate the cell medium containing the transfection mix and add 5 mL of fresh medium not supplemented with antibiotics. Incubate for 24 hours.
9- Then, proceed to the first collection. Collect the medium of cells, which contains lentiviral particles (5 mL), and store it at 4 ºC. Subsequently add 5 mL of fresh medium not supplemented with antibiotics to cells.
10- Incubate for another 24 hours.
11- The following day proceed to the second collection. Collect the medium containing lentiviruses (5 mL) and mix it with the first collection medium stored at 4ºC.
12- Filter the collected medium using PVDF filters (Millex-HV filter 0.45um, Millipore #SLHV033RB). With the resulting filtrate (lentivirus mix) you can proceed to the infection step. The lentivirus mix can also be stored in aliquots at -80ºC.

Lentiviral transduction

Once lentivirus mixes were produced, these were used to infect target cells in order to deliver the transfer vector to the host cell genome. This process is called lentiviral transduction. Specifically, we used lentiviral vectors to express a short hairpin RNA to induce HERC2 silencing. All this process must be performed in an adequate virus facility. We followed the subsequent steps described below:

1- Seed your target cells in a 6-well plate. Each well should be at approximately 50% of confluence the day of infection (Cells should be dividing until day 7). Since antibiotic selection will be performed, do not forget to seed extra wells that will be used as selection negative controls.

2- The day of infection remove the cell culture medium of the target cells and add fresh medium not supplemented with antibiotics (700 µL/well).
3- Add the lentivirus mix (300 µL/well) to the corresponding conditions. Conversely, add fresh medium (300 µL/well) to the extra wells used as selection negative controls. Infections are performed in a total volume of 1 mL/ well
4- Add polybrene to each well at a final concentration of 5 µg/mL. Polybrene is a small, positively charged molecule that binds to cell surfaces and increases binding between viral particles and the cellular membrane.
5- Next, optionally, you can centrifuge the plates at 400 g for 30 min. This further increases the efficiency of transduction.
6- Incubate the plates overnight at 37 ºC and 5% CO_2 (Infection for 6 hours is also enough. Maximum 24h to avoid toxicity).
7- The next day remove the cell media containing lentiviruses and add fresh medium (2 mL/well). Incubate for 24 hours.
8- Then, proceed to the selection step. Add the selection antibiotic (puromycin), at an adequate concentration (Table 5).
9- During the following days, monitor cell death using the non-infected cells as a selection control. Once all selection control cells are death, you can proceed. Infected cells should be puromycin resistant. Selection typically takes about 2-3 days in presence of puromycin.
10- After selection, change de medium containing puromycin and add fresh medium. Incubate overnight before starting a treatment or proceeding to fixation, cell lysis, visualisation or analysis.

The optimal puromycin concentration for an accurate selection depends on the target cells that are used for the infection. The following table indicates the concentration of puromycin used depending on the cell type (Table 5).

Table 5. Concentration of puromycin required for selection according to cell type.

Cell type	Puromycin concentration
HEK 293T	2 µg/mL
HeLa	2 µg/mL
U2OS	2 µg/mL
A549	1.5 µg/mL
H1299	3 µg/mL
RAW 264.7	5 µg/mL
Mouse embryonic fibroblasts	5 µg/mL
Mouse osteoblasts	5 µg/mL

Cell treatments

Cells were treated with different inhibitors, drugs or compounds depending on the experiment. The company name, reference numbers and assay concentration are indicated below (Table 6):

Table 6. Inhibitors, drugs and compounds.

Compound	Company name	Reference number	Assay concentration
Ammonium Chloride (NH_4Cl)	MERCK	#101145	20 mM
Chloroquine	Selleckchem	#S6999	100 µM
Hydrogen Peroxide (H_2O_2)	PanReac AppliChem	# 141076	500 or 50 µM
LY3009120	Selleckchem	#S7842	1 µM
MG132	MERCK	#C2211	10 µM
Polybrene	Selleckchem	#E1299	5 µg/mL
Puromycin	MERCK	#P8833	1-5 µg/mL
SB203580	Selleckchem	#S1076	10 µM
Sodium Chloride (NaCl)	MERCK	#S9888	100 mM
Sorafenib	Santa Cruz Biotechnology	#sc-220125	1 µM

Protein analysis

For protein analysis, proteins were extracted from cells and separated by electrophoresis. Then, detection of specific bands was performed by Western Blot.

Protein extraction

For protein extraction and determination of specific protein levels, cells were lysed with NP40 lysis buffer (50 mM Tris–HCl, 150 mM NaCl, and 0.5% NP40 detergent, pH 7.5). This buffer was supplemented with protease and phosphatase inhibitors to avoid degradation of proteins and the removing of phosphorylation marks (50 mM β-glicerophosphate, 50 mM sodium fluoride (NaF), 1 mM sodium vanadate, 1 mM phenylmethylsulfonyl fluoride (PMSF), 5 µg/mL leupeptin, 5 µg/mL aprotinin, 1 µg/mL pepstatin A, 100 µg/mL benzamidine, 1 µM E-64). Protein extraction process was performed on ice to minimise protein degradation. In detail, the protocol is described below:

1- Discard the culture medium from the cells and rinse with cold PBS.
2- Add 100 µL of NP40 lysis buffer per well.
3- Detach the cells with a cell scraper and transfer the cell extracts to an 1.5 mL tube.
4- Incubate the samples for 15 minutes on ice with strong agitation to allow total cell lysis.
5- Sonicate samples to ensure total disruption of cellular membranes.
6- Then, centrifuge at 13,000 g for 10 minutes at 4°C. After centrifugation you should visualize a pellet corresponding to the cellular debris.
7- Transfer the supernatants, which contain extracted proteins, to new tubes and discard the pellets.
8- Quantify the protein concentration in the samples with the BCA Pierce protein assay (ThermoFisher #23227), following manufacturer's instructions.
9- Add lithium dodecyl sulphate (LDS) 4X buffer (250 mM Tris-HCl, 2% LDS, 0.4 mM EDTA, 10% glycerol, 0.2 mM phenol red, and 0.2 mM Coomassie Blue, pH 8.5) to the samples. For a volume of cell extract of 100 µL it corresponds to add 33.3 µL of LDS 4X.
10- After this, samples can be prepared for electrophoresis or stored at -20°C.

Protein electrophoresis and Western Blot

Proteins were separated using a Tris-Acetate Polyacrylamide gel electrophoresis (PAGE) system. This system, previously developed in our laboratory, uses a special recipe for a gradient gel that enables simultaneous analysis of high and low molecular weight proteins [143]. The gradient gel is elaborated by the continuous mixing of two different concentrations of polyacrylamide solutions in a two-vase communicating system. For standard gradient gels, concentrations from 3% to 15% acrylamide were used. For the resolution of very low molecular weight proteins, a gradient from 3 to 17.5% was employed. This last one was mainly used for the separation of LC3-I and LC3-II proteins. The recipes for the gels are detailed in Table 7.

Table 7. Recipe for polyacrylamide gels.

Reagent	Standard gel		Low MW resolution gel	
	3% solution	15% solution	3% solution	17.5% solution
MilliQ H_2O	6 mL	2.23 mL	3.44 mL	3.44 mL
40% Acrylamide	0.53 mL	1.5 mL	0.3 mL	3.09 mL
3M Tris-Acetate pH 7	0.47 mL	0.27 mL	0.27 mL	0.47 mL
Ammonium persulfate 10%	33.25 µL	19 µL	19 µL	33.25 µL
TEMED	8.75 µL	5 µL	5 µL	8.75 µL

The PAGE system protocol that was followed is detailed below:

1- Prepare the samples to be loaded into the PAGE system. Typically we took between 20 and 30 µg of protein sample supplemented with 100 mM DTT in a total volume of 30 µL.
2- Incubate the samples for 10 minutes at 100°C, to denaturalise the proteins.
3- Add electrophoresis buffer (50 mM Tricine, 50 mM Tris, 0.1 % SDS and 1.3 mM sodium bisulphite) to the cuvette and the polyacrylamide gel where the electrophoresis will be performed.
4- Load the samples into the wells of the polyacrylamide gel.
5- Run electrophoresis with a constant voltage of 130 V for approximately 1 hour and 30 minutes.

After polyacrylamide gel electrophoresis, the separated proteins were transferred to a polyvinylidene difluoride (PVDF) membrane by electrotransfer. In brief:

1- Equilibrate the gel and PVDF membrane in transfer buffer (20% methanol, 25 mM bicine, 25 mM Bis-Tris, 1 mM EDTA and 1.3 mM sodium bisulphite).
2- Then, place the gel in the "transfer sandwich" (transfer sponge - filter paper - gel - PVDF membrane - filter paper - transfer sponge), pressed together by the support grid.
3- Place the supported transfer sandwich vertically in the tank with the electrodes and put it into the cuvette.
4- Gently fill the cuvette with transfer buffer and run transference during 2 hours at 200 mA at 4°C.

Following transference, we proceeded to Western Blot to detect specific proteins. In detail, the protocol is described below:

1- Block PVDF transferred membranes with 10% skimmed milk in TBS-T for 1 hour.
2- Afterwards, incubate the membrane with primary antibodies against specific proteins at 4°C overnight in agitation. The list of antibodies used during the thesis is listed in Table 8. Primary antibodies were prepared in a solution containing TBS-T with 3% BSA and 0.02% sodium azide.
3- The next day, save primary antibodies for reuse and wash the membrane 3 times with TBS-T.
4- Then, incubate the membrane for 1 hour in agitation with peroxidase-labelled secondary antibodies (Table 9) prepared in blocking solution (10% skimmed milk in TBS-T).
5- Wash the membrane 3 times with TBS-T.
6- Afterwards, incubate the membrane for 1 minute with the Enhanced Chemiluminescence (ECL) reactive to unchain the peroxidase reaction.
7- Visualize bands with a gel documentation system (LAS-3000, Fujifilm). For imaging processing and threshold adjusting we used MultiGauge V3.0 software.

Table 8. List of primary antibodies

Recognised protein	Detected band (Observed M.W)	Source	Dilution to use	Reference
HERC2	528 kDa	Mouse	1:1000	BD Biosciences #610151
CHC	200 kDa	Mouse	1:1000	Santa Cruz Biotechnology #sc12734
P-ERK1/2	42-44 kDa	Mouse	1:5000	MERCK #M8159
ERK1/2	42-44 kDa	Rabbit	1:1000	Cell Signaling #9102
P-p38	38 kDa	Rabbit	1:1000	Cell Signaling #9211
p38	38 kDa	Rabbit	1:1000	Santa Cruz Biotechnology #sc-535
HERC1	532 kDa	Rabbit	1:1000	Produced in the laboratory, antibody #410 [29]
P-MKK3	40 kDa	Rabbit	1:1000	Cell Signaling #9231
MKK3	40 kDa	Rabbit	1:1000	Proteintech #13898-1-AP
A-RAF	68 kDa	Mouse	1:1000	Santa Cruz Biotechnology #sc-166771
B-RAF	84 kDa	Mouse	1:1000	Santa Cruz Biotechnology #sc-5284
C-RAF	75 kDa	Mouse	1:1000	BD Biosciences #610151
MYC-tag	1.2 kDa	Mouse	1:1000	MERCK #11667149001
GFP-tag	27 kDa	Chicken	1:5000	Abcam #ab13970
Flag-tag	1 kDa	Mouse	1:1000	MERCK #F3165
NRF2	97-100 kDa	Rabbit	1:500	Cell Signaling #12721
Ubiquitylated proteins	Smear-like band	Mouse	1:1000	MERCK #04-263
LC3	17 kDa (LC3-I) 16 kDa (LC3-II)	Mouse	1:1000	Santa Cruz Biotechnology #sc-376404
USP20	110-120 kDa	Rabbit	1:1000	Proteintech #17491-1-AP
ULK1	150 kDa	Rabbit	1:1000	Cell Signaling #8054

Table 9. List of peroxidase conjugated secondary antibodies.

Secondary antibody	Dilution to use	Reference
anti-Chicken, HRP	1:10,000	ThermoFisher #A16054
anti-Mouse, HRP	1:10,000	ThermoFisher #62-6520
anti-Rabbit, HRP	1:10,000	ThermoFisher #31460

Gene expression analysis

For the analysis of gene expression in cells, total RNA was isolated from U2OS, retrotranscribed to cDNA and then analysed by quantitative real time PCR (qRT-PCR).

RNA isolation

Total RNA was isolated from U2OS cells using the TRIsure reagent (Bioline #BIO-38033) according to the manufacturer's instructions. All the procedure was performed with autoclaved material and inside a fume hood, since phenols and alcohols were used. The followed protocol proceeds as follows:

1- Lyse the cells directly by adding 500 µL of TRIsure reagent per well of a 6-well plate. At this point, plates can be frozen at -80°C or you can proceed with the RNA isolation.
2- For processing, scrape cells with a 1 mL pipette tip and collect the cell lysate in a 1.5 mL tube.
3- Incubate the samples for 5 minutes at room temperature.
4- Then, add 100 µL of chloroform to each tube.
5- Vortex the samples and incubate 3 minutes at room temperature.
6- Afterwards, centrifuge the samples at 12,000 g for 20 minutes at 4°C. The samples will split in two phases: a lower pale organic phase and an upper colourless aqueous phase that contains the RNA.
7- Transfer the aqueous phase into a new 1.5 mL tube and add 1 µL of glycogen solution (500 µg/µL) and 250 µL of isopropanol to precipitate the RNA.
8- Vortex the samples and incubate 10 minutes at room temperature.
9- Then, centrifuge at 12,000 g for 20 minutes at 4°C. After centrifugation you should visualize a pellet corresponding to the RNA.
10- Discard the supernatant and add 500 µL of ethanol 75% to wash the pellet.

11- Vortex the sample to detach the pellet from the bottom of the tube and centrifuge again at 7,500 g for 5 minutes at 4°C.
12- Discard the supernatant and air-dry the pellet by placing the tubes in a thermoblock at 45°C with the lids opened.
13- Once the pellet is dry dissolve it in DEPC-treated water and incubate 10 minutes at 55°C to facilitate its dissolution.
14- Finally, the samples can be quantified using a Nanodrop. At this point, samples can be stored at -80°C or you can proceed to the retrotranscription step.

Retrotranscription

Total RNA (typically 2 µg) was reverse-transcribed using the high-capacity cDNA Reverse Transcription kit (Applied Biosystems #4368814). Reaction mixes were prepared as indicated in Table 10. Then, samples were introduced in a PCR thermal cycler. Once obtained the cDNA, samples were stored at 4°C.

Table 10. Retrotranscription reaction mix

Reagent	Quantity for 30 µL reaction
RNA	2 µg
10x buffer	3 µL
dNTP Mix	1.2 µL
Random primers	3 µL
Retrotranscriptase	1.5 µL
DEPC-treated water	Up to 15 µL

Quantitative Real Time PCR

Quantitative PCRs were performed with the QuantStudio 7 Pro Real-Time PCR system. Applied Biosystems' TaqMan Gene Expression Assays (ThermoFisher Scientific) (Table 11) and SensiFAST Probe Hi-ROX Mix (Bioline #BIO-82002) were used to quantify the gene expressions. All transcripts were normalized using *GAPDH* as an endogenous control.

Table 11. List of Taqman probes.

Gene	Taqman probe ID (ThermoFisher)
GAPDH	Hs99999905_m1
GPX1	Hs00829989_Gh
GUSB	Hs00939627_m1
NFE2L2	Hs00975960_m1
SOD1	Hs00533490_m1
SOD2	Hs00167309_m1

Reactions were carried out in 384 well plates with technical triplicates if possible. Reaction mixes are detailed in Table 12. For the preparation of master-mixes, from one hand each cDNA sample was mixed with milliQ water, and from the other hand each Taqman probe was mixed with SensiFAST.

Table 12. qRT-PCR reaction mix

Reagent	Volume for 11 µL reaction
cDNA sample	0.5 µL
MilliQ water	4.5 µL
Taqman probe	0.5 µL
SensiFAST	5.5 µL

Confocal fluorescence microscopy

Confocal fluorescence microscopy was used to analyse the subcellular localization of some proteins such as phosphorylated p38 and also to study specific subcellular structures such as autophagosomes using a tandem-tagged mCherry-YFP-LC3 fluorescence reporter.

For the analysis of P-p38 subcellular localization we combined immunofluorescence techniques with other non-antibody fluorescent methods such as DAPI (MERCK #D9542) and Alexa Fluor™ 647 Phalloidin (ThermoFisher #A22287) staining. In brief:

1- Seed U2OS cells on poly-Lys coated glass coverslips. Place each coverslip inside a well of a 12-well plate and then seed the cells on top.

2- Perform cell fixation by incubating cells at room temperature for 20 minutes in 4% paraformaldehyde. At this point, coverslips containing the samples can be stored at 4°C submerged in PBS solution.
3- To proceed, permeabilize cells for 20 minutes with PBS-BS solution (PBS solution containing 0.5% bovine serum albumin and 0.05% saponin).
4- Next, incubate for 1 hour at 37°C with the primary antibody anti-phospho-p38 (Cell Signaling #9211) diluted 1:200 with PBS-B solution (PBS solution containing 0.5% bovine serum albumin).
5- After incubation, wash three times with PBS-B solution.
6- After washing, incubate for 45 minutes at 37°C with Alexa-Fluor 488™ secondary antibody (ThermoFisher #A-11008) diluted 1:500 with PBS-B solution.
7- Wash three times with PBS-B solution.
8- Next, stain actin filaments by incubation for 20 minutes at room temperature with Alexa Fluor™ 647 Phalloidin at a concentration of 100 ng/mL in PBS-B solution.
9- Wash three times with PBS-B solution.
10- Stain nuclei by incubating for 1 minute with DAPI at a concentration of 1 µg/mL in PBS.
11- Mount coverslips on slides with Fluoromount mounting medium (ThermoFisher #00-4958-02).
12- Allow the mounting medium to dry before proceeding to analyse the slides by confocal microscopy.

On the other hand, for the analysis of autophagosomes we used a tandem-tagged mCherry-YFP-LC3 fluorescence reporter. The YFP tag is acid-sensitive, while the mCherry tag is acid-insensitive. Thus, this double tag system enables to monitor the autophagic flux since inside mature autophagosomes, both tags emit fluorescent light (colocalization of yellow and red signals). However, fusion of autophagosomes to lysosomes causes acidification that triggers loss of YFP signal, leaving only mCherry emission. To analyse fluorescence using this reporter proceed as follows:

1- Seed U2OS in a 6-well plate.
2- Transfect the mCherry-YFP-LC3 fluorescence reporter following the LTX transfection protocol.

3- The next day, seed the transfected cells on poly-Lys coated glass coverslips.
4- On the following day you can proceed to the steps of fixation, permeabilization, DAPI staining and mounting in the same way as explained above.

All images were acquired using a confocal laser scanning microscope (LSM 880 spectral, Carl Zeiss Microscopy GmbH, Jena, Germany). For the analysis of P-p38 subcellular localization, the nucleus area was determined by the DAPI staining and the cytoplasm area by the actin labelling. Then, P-p38 fluorescence intensity in the nucleus and the cytoplasm per cell was measured and quantified. Next, the ratio nucleus/cytoplasm was calculated to quantify shifts in the protein localization. Alternatively, the autophagic flux was determined by quantification of the number of red dots, performed by subtracting the number of YFP puncta from total puncta.

Immunoprecipitations and pull-downs

For the analysis of protein interactions we performed immunoprecipitations and pull-down experiments. For this type of assays, cells were lysed with CHAPS buffer (10 mM Tris-HCl, 100 mM NaCl, 0.3% CHAPS, pH 7.5) containing protease and phosphatase inhibitors as described above.

For immunoprecipitation of endogenous HERC2 protein we used an anti-HERC2 polyclonal antibody previously produced in our laboratory (bvg3) and described elsewhere [29]. The followed protocol is indicated below:

1- Seed cells in a 10 cm plate. They should be around 90-100% confluent the day of cell lysis and protein extraction.
2- Lyse cells with 1mL CHAPS buffer per plate. Proceed to protein extraction and quantification as previously indicated. Save a portion of each cell lysate for the inputs. Typically around 50-100 µL is enough.
3- Incubate 1 mg of the protein extract in a total volume of 1 mL of CHAPS buffer with 10 µL of pre-immune serum, used as a negative control, or with 5 µL of anti-HERC2 polyclonal antibody (bvg3), for 2 hours at 4°C with gentle rotation.
4- After incubation, add to the immunoprecipitation mixes 100 µL of protein A-Sepharose (MERCK #GE17-0780-01) and incubate for 1 hour at 4°C with gentle rotation.

5- Then, pellet the Sepharose beads by centrifugation at 2,500 g for 2 minutes.
6- Discard the supernatant and proceed to wash the pellet by resuspending it in cold CHAPS buffer without protease and phosphatase inhibitors.
7- Repeat the centrifugation and washing steps at least 4 extra times.
8- After the last centrifugation, resuspend the pellet with 20 µL of LDS 2X buffer and add 4 µL of DTT 1M. In this way the samples are ready to be analysed by electrophoresis and Western Blot.

For the pull-downs, we used ChromoTek GFP-Trap® Agarose (chromotek #gta-20) and DYKDDDDK Fab-Trap™ Agarose (chromotek #ffa-20). In brief we proceeded as follows:

1- Seed the cells in a 6-well plate and transfect them with a plasmid encoding the protein of interest fused with a GFP or Flag epitope following LTX transfection protocol.
2- Lyse the cells with 500 µL of CHAPS buffer per well. Proceed to protein extraction and quantification as previously indicated. Save a portion of each cell lysate for the inputs.
3- Incubate 0.5-1 mg of protein extract (depending on how much protein you have) in a total volume of 1 mL of CHAPS buffer with 2 µL of GFP-Trap (for GFP-tagged proteins) or 5 µL of DYKDDDDK Fab-Trap (for Flag-tagged proteins) for 2 hours at 4°C with gentle rotation.
4- After incubation, pellet the agarose beads by centrifugation at 2,500 g for 2 minutes.
5- Wash the pellets and resuspend the samples as indicated before to prepare them to be analysed by electrophoresis and immunoblot.

Ubiquitylation assay

Ubiquitylation assays were performed in HEK 293T cells to measure changes in the relative level of ubiquitylation of a specific protein. To do so we transfected cells with a plasmid encoding His-tagged ubiquitin along with the plasmids encoding the proteins we wanted to study. Transfections were performed following LTX transfection protocol. In detail, the ubiquitylation assay proceeds as follows:

1- Seed HEK 293T in a 6-well plate using two wells for each condition.

2- Transfect His-tagged ubiquitin and the other plasmids of interest following LTX transfection protocol.
3- The next day expand the cells of each condition by joining the two wells together and transferring them into a 10 cm culture plate.
4- After 48 hours post-transfection, treat transfected HEK 293T cells for 4 hours with the proteasome inhibitor MG132 at a concentration of 10 µM. This prevents ubiquitylated proteins from being degraded by the proteasome and allows its enrichment and subsequent detection.
5- Next, aspirate the cell medium and add 5 mL of cold PBS at 4°C.
6- Lift cells by gently scraping and retrieve the 5 mL of cell suspension. Transfer 0,5 mL to another tube for the inputs. The assay will be carried out with the remaining 4.5 mL of cell suspension.
7- Centrifuge the tubes at 150 g for 5 minutes at 4°C to obtain a cellular pellet.
8- Resuspend the cellular pellet of the inputs with NP40 lysis buffer and proceed to protein extraction and quantification as indicated above. On the other hand, resuspend the cellular pellet reserved for the assay with the denaturing Buffer #1 (6 M guanidinium, 10 mM Tris-HCl, 100 mM Na_2HPO_4, 100 mM NaH_2PO_4, pH 8). Protein extracts resuspended in Buffer #1 can be stored at -20°C.
9- To proceed, supplement each protein extract with 5 mM imidazole and 10 mM 2-mercaptoethanol.
10- Sonicate samples to reduce viscosity.
11- Centrifuge samples at 13,000 g for 5 minutes at 4°C. After centrifugation you should observe a pellet corresponding to the cellular debris.
12- Transfer the supernatant into a new tube and discard the pellet.
13- Incubate the supernatants with 20 µL of Ni^{2+}-NTA agarose beads (Qiagen, #30210) for 2 hours at 4°C with rotation. Incubation can also be done overnight.
14- After incubation, pull-down agarose beads by centrifugation at 4,400 g for 2 minutes at 4°C.
15- Discard the supernatant and wash the pellet resuspending it with 1 mL Buffer #1 plus 10 mM 2-mercaptoethanol.

16- Repeat the centrifugation and wash the pellet two times with 1 mL Buffer #2 (8 M Urea, 100 mM Na_2HPO_4, 100 mM NaH_2PO_4, 10 mM Tris-HCl, pH 8) plus 10 mM 2-mercaptoetanol.
17- Next, wash one time with 1 mL Buffer #3 (8 M Urea, 100 mM Na_2HPO_4, 100 mM NaH_2PO_4, 10 mM Tris-HCl, pH 6.8) plus 10 mM 2-mercaptoetanol; one time with 1 mL Buffer #3 plus 10 mM 2-mercaptoetanol and 0.2% Triton X-100; and one last time with 1 mL Buffer #3 plus 10 mM 2-mercaptoetanol and 0.1 % Triton X-100.
18- After the last washing, elute the pellet by resuspending it in 30 µL of Elution Buffer (200 mM imidazole, 5% SDS, 0.15 M Tris-HCl, 30% (vol/vol) glycerol, 0.72 M 2-mercaptoethanol, pH 6.7).
19- Incubate the elution for 1 hour at 37ºC under agitation.
20- Finally, add 10 µL of LDS 4X buffer, 4µL of DTT 1M solution and samples are ready to be analysed by electrophoresis and western blot.

MTT assay for cell proliferation and cell viability

Thiazolyl Blue Tetrazolium Blue (MTT) (MERCK #M5655) was used as a colorimetric metabolic activity indicator in cell proliferation and cell viability assays. MTT produces a yellowish solution that is converted to dark blue, water-insoluble crystals by mitochondrial dehydrogenases of living cells. The crystals can be solubilized with isopropanol and the colorimetrically intensity is measured at 570 nm. This assay was performed as indicated below:

1- Seed the cells in a 96-well plate. U2OS cells were seeded at a final concentration of 10,000 cells/well and human skin fibroblasts at 15,000 cells/well.
2- The following day, initiate the treatments of cell viability experiments. If, conversely, you are assessing cell proliferation, just incubate cells for another 24 hours.
3- After treatments in the case of cell viability experiments, or after 48 hours in the case of cell proliferation assays, aspirate the cell culture medium and add MTT diluted in fresh medium at a concentration of 0.5 mg/mL in each well.
4- Incubate cells in presence of MTT for 4h at 37°C in a humidified incubator.
5- Then, discard the media containing MTT and solubilize the formazan crystals with isopropanol.

6- Incubate for 10 minutes at room temperature in agitation to fully solubilize the crystals.
7- Finally, determine the absorbance at a wavelength of 570 nm using a 96-well plate spectrophotometer.

MitoSOX and Mitotracker staining

To determine the levels of oxidative stress we used MitoSOX™ Red reagent (ThermoFisher #M36007). Mitochondrial superoxide are reactive oxygen species generated as a product of oxidative phosphorylation and can be determined by fluorescence probes such as MitoSOX. This live-cell fluorogenic dye selectively targets the mitochondria and is selectively oxidized by superoxide, exhibiting red fluorescence. On the other hand, to determine the morphology of the mitochondria, we stained cells with MitoTracker™ Red CMXRos dye (ThermoFisher #M7512). MitoTracker dyes are cell permeable probes that contain a thiol-reactive chloromethyl moiety for mitochondrial labelling.

In detail, for cellular staining with these live-cell dyes proceed as follows:

1- Seed the cells in a µ-Slide 8 well chambered coverslip. Human skin fibroblasts were seeded at a concentration of 15,000 cells/well.
2- The next day, aspirate the cell culture medium and add fresh medium containing 1 µg/mL of Hoechst 33342 (ThermoFisher #H3570) to stain the nucleus and either 2 µM of MitoSOX or 50 nM MitoTracker.
3- Incubate at 37°C for 15 minutes for MitoSOX or 30 minutes for MitoTracker staining.
4- Proceed to live cell imaging with a fluorescence microscope for analysis.

Cells were examined in a Zeiss LSM 880 laser scanning confocal spectral microscope equipped with an incubation control system (37°C, 5% CO2). For the evaluation of oxidative stress, based on superoxide levels, fluorescence intensity per cell was measured, quantified and expressed as arbitrary units (a.u). Conversely, for the evaluation of mitochondrial morphology, the percentage of fragmented mitochondrial was estimated by counting spherical non-contiguous mitochondrial particles and dividing by the number of total structures comprised in the mitochondrial network.

Quantitative proteomic analysis with the ^{bio}Ub strategy

The quantitative proteomic analysis of ubiquitylated proteins was performed in collaboration with the group of Dr. Ugo Mayor from Euskal Herriko Unibertsitatea (EHU) and Ikerbasque (Basque Foundation for Science). Dr. Juanma Ramírez conducted the experiments.

Biotin pull-downs were performed in triplicates as previously described [71]. In brief, cell lysates were incubated with NeutrAvidin agarose beads. After washing with different buffers to reduce non-specific interactions, the ubiquitylated material was eluted from the beads. Eluted material was resolved by SDS-PAGE system. After the exclusion of avidin monomers and dimer, each lane was subjected to in-gel digestion as described previously [144]. Briefly, digestion of proteins was performed by incubation of the gel slices with trypsin. The resulting peptides were extracted from the gel and subjected to LC-MS/MS analysis. Mass spectrometric analyses were performed on an EASY-nLC 1000 liquid chromatography system interfaced via a nanospray flex ion source with a Q Exactive (ThermoFisher Scientific, Waltham, MA, USA) mass spectrometer. Data were acquired using Xcalibur software (Thermo Fisher Scientific, Waltham, MA, USA).

Bioinformatic tools

Protein bands from Western Blot and immunofluorescence images from confocal microscopy were analysed and quantified using ImageJ software (Rasband, W.S., ImageJ, U. S. National Institutes of Health, Bethesda, Maryland, USA, https://imagej.nih.gov/ij/).

Different bioinformatic tools were employed for different purposes. The public freely accessible database UniProt (https://www.uniprot.org/) was used to consult protein sequences and functional information. The RCSB Protein Data Bank (PDB) (https://www.rcsb.org/) was used to consult 3D structure of proteins and to obtain structure models. Prediction of phosphorylation sites by a determined kinase was performed using the algorithm Group-based Prediction System 5.0 (GPS 5.0) (http://gps.biocuckoo.cn/) [145]. To evaluate functional association between a group of proteins we used the Search Tool for the Retrieval of Interacting Genes/Proteins (STRING) (http://string-db.org/). STRING analysis serves to highlight functional enrichments in user-provided lists of proteins, using a number of functional classification systems such as GO terms.

Statistical analysis

The results displayed in graphs indicate the means and standard error of the mean (± SEM) of, at least, three independent experiments. Individual data points are plotted as single dots. Significance was calculated by Student t-test and indicated as follows: *, **, or *** for p-values of ≤ 0.05, ≤ 0.01, or ≤ 0.001, respectively. Figures were created, and statistical analysis was performed, using GraphPad Prism version 8.4.3 for Windows (GraphPad Software, San Diego, California USA), www.graphpad.com.

CHAPTER IV. Results

HERC2 regulates C-RAF/MKK3/p38 signalling pathway modulating the oxidative stress response

Biallelic pathogenic sequence variants in the *HERC2* gene are associated with HERC2 Angelman-like syndrome. In pathogenic HERC2 variants, complete absence or marked reduction in HERC2 protein levels are observed. The most common pathological variant, c.1781C>T (p.Pro594Leu), encodes an unstable HERC2 protein. A better understanding of how pathologic HERC2 variants affect intracellular signalling may aid definition of potential new therapies for these disorders. For this purpose, we studied patient-derived cells with the HERC2 Pro594Leu variant. We observed alteration of MAPK signalling pathways, reflected by increased levels of C-RAF protein and p38 phosphorylation. HERC2 knockdown experiments reproduced the same effects in other human and mouse cells. Moreover, we demonstrated that HERC2 and RAF proteins form molecular complexes, pull-down experiments showed that HERC2 regulates C-RAF ubiquitylation, and we found out that the p38 activation due to HERC2 depletion occurs in a RAF/MKK3-dependent manner. The displayed cellular response was that patient-derived and other human cells with HERC2 deficiency showed higher resistance to oxidative stress with an increase in the master regulator of the antioxidant response NRF2 and its target genes. This resistance was independent of p53 and abolished by RAF or p38 inhibitors. Altogether these findings identify the activation of C-RAF/MKK3/p38 signalling pathway in HERC2 Angelman-like syndrome and highlight the inhibition of RAF activity as a potential therapeutic option for individuals affected with these rare diseases.

Human HERC2 Pro594Leu cells display MAPK pathway alteration

Several recessive mutations affecting the *HERC2* gene cause developmental delay with Angelman-like features [51, 61]. Knowing how pathologic *HERC2* variants affect intracellular signalling could reveal the underlying pathology and identify possible therapies. Therefore, we studied cells from an individual with the mutant HERC2 P594L variant described in most cases. Because HERC1 had previously been reported to regulate the ERK and p38 MAPK signalling pathways [25, 102], we wondered if HERC2 also had a modulatory role. As expected, cells with the HERC2 P594L mutation showed almost undetectable HERC2 protein levels (Figure 19A-C). Interestingly, although they showed higher protein levels of C-RAF

(Figure 19A), this did not correlate with the canonical activation of the ERK signalling pathway, assessed by ERK phosphorylation (Figure 19B). An increment in p38 phosphorylation was also detected while total p38 protein levels remained stable (Figure 19C).

In order to provide more evidence that these changes in MAPK signalling pathways are a general hallmark of disease in patients with biallelic HERC2 mutations, we analysed samples of two more individuals carrying the mutant HERC2 P594L variant. Consistently, patients with the HERC2 P594L mutation (P1, P2 and P3) showed lower HERC2 protein levels than the wild type controls (C1, C2 and C3). In addition, C-RAF protein levels and p38 phosphorylation were upregulated in all three patients, but no changes were detected in ERK activation (Figure 19D). These results showed that cells with the HERC2 P594L mutation exhibit altered MAPK signalling pathway activation, as reflected by higher C-RAF and phopspho-p38 protein levels.

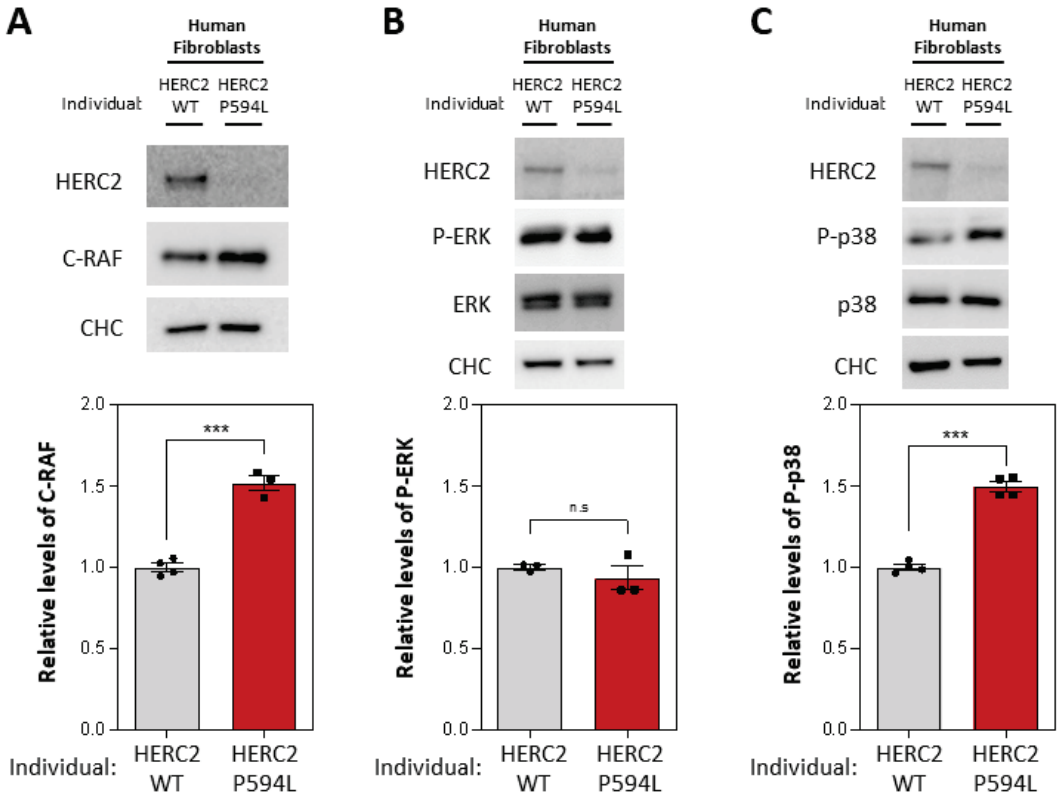

Figure 19. Figure continues on next page ▼

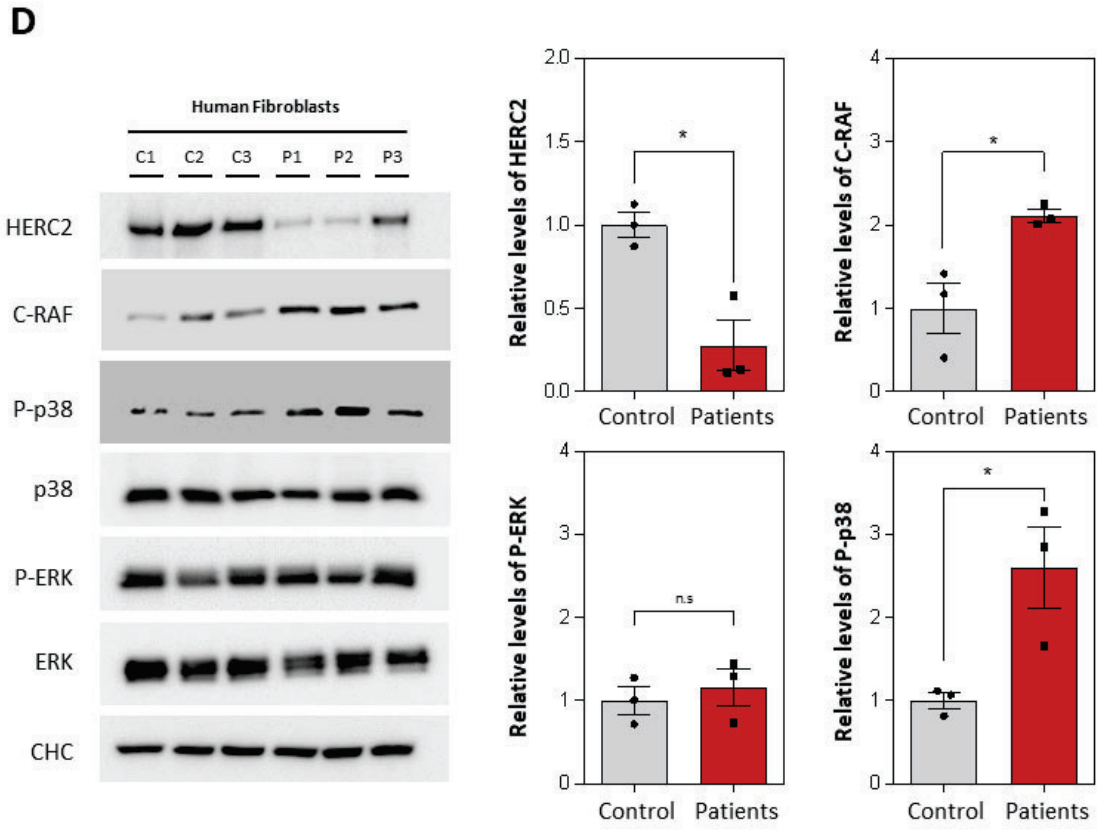

Figure 19. Patient-derived cells with a homozygous mutation in human *HERC2* gene show MAPK pathway alterations. (A-C) We analysed lysates of human skin fibroblasts from an individual with the wild-type HERC2 (HERC2 WT) and the p.Pro594Leu mutant HERC2 variant (HERC2 P594L) by immunoblot, using the indicated antibodies. C-RAF (A), phospho-ERK (P-ERK) (B) or phospho-p38 (P-p38) (C) levels were quantified and normalized based on clathrin heavy chain (CHC), ERK or p38 protein levels, respectively. The results are expressed relative to the control condition. Plots represent mean ± standard error of the mean. Representative results are shown for experiments repeated at least three times and the data points of each experimental repetition are plotted as single dots. **(D)** We analysed lysates of human skin fibroblasts from three different control individuals with the wild-type HERC2 (C1, C2 and C3) and three different patients with the HERC2 P594L mutant variant (P1, P2 and P3) by immunoblot. Levels of HERC2 and C-RAF proteins were quantified as in (A). Levels of P-ERK and P-p38 were quantified as in (B) and (C), respectively. The results are expressed relative to the control condition. Plots represent mean ± standard error of the mean. Representative results are shown for experiments repeated at least three times and the data points of each of the individuals analysed are plotted as single dots. Significance levels: ns = non significance; * $p \leq 0.05$; ** $p \leq 0.01$; *** $p \leq 0.001$.

HERC2 regulates C-RAF protein levels

To delve deeper into the molecular mechanisms involved in the altered MAPK signalling pathway in HERC2 P594L cells, first we wondered whether these alterations also occur in human cell lines such as U2OS cells with knocked-down HERC2 protein levels. If so, we could use this cell line as a study model for further experiments. In knockdown experiments, human U2OS cells were transfected with either a negative control (NC) small-interfering RNA (siRNA), an siRNA against HERC2, or a positive control siRNA against HERC1. The positive control was chosen because previous work had shown that HERC1 controls ERK

and p38 signalling pathways modulating C-RAF protein levels [25, 102]. HERC2 knockdown mimicked the effect observed in HERC2 P594L cells, with depletion of HERC2 correlating with increased C-RAF protein levels. As expected, this was also observed after HERC1 silencing (Figure 20A). These results validated U2OS cells with HERC2 knockdown as an appropriate cellular model to further study the molecular mechanisms behind the HERC2-dependent regulation of MAPK signalling.

Then, we evaluated whether HERC2 depletion affects the other isoforms of RAF. Knockdown of HERC2 modified neither A-RAF nor B-RAF protein levels (Figure 20B and C). These data indicated that RAF regulation by HERC2 is specific for the C-RAF isoform. Subsequently, we analysed the RAF MAPK signalling pathway, in which canonical RAF activation triggers ERK phosphorylation [102]. We noted that C-RAF upregulation observed after HERC1 depletion correlated with increased phosphorylated ERK levels, while total ERK protein levels remained stable. However, we detected no changes in ERK phosphorylation in the HERC2 depleted cells (Figure 20D). These results suggested that C-RAF upregulation caused by HERC2 depletion was not signalled through the canonical MEK/ERK pathway.

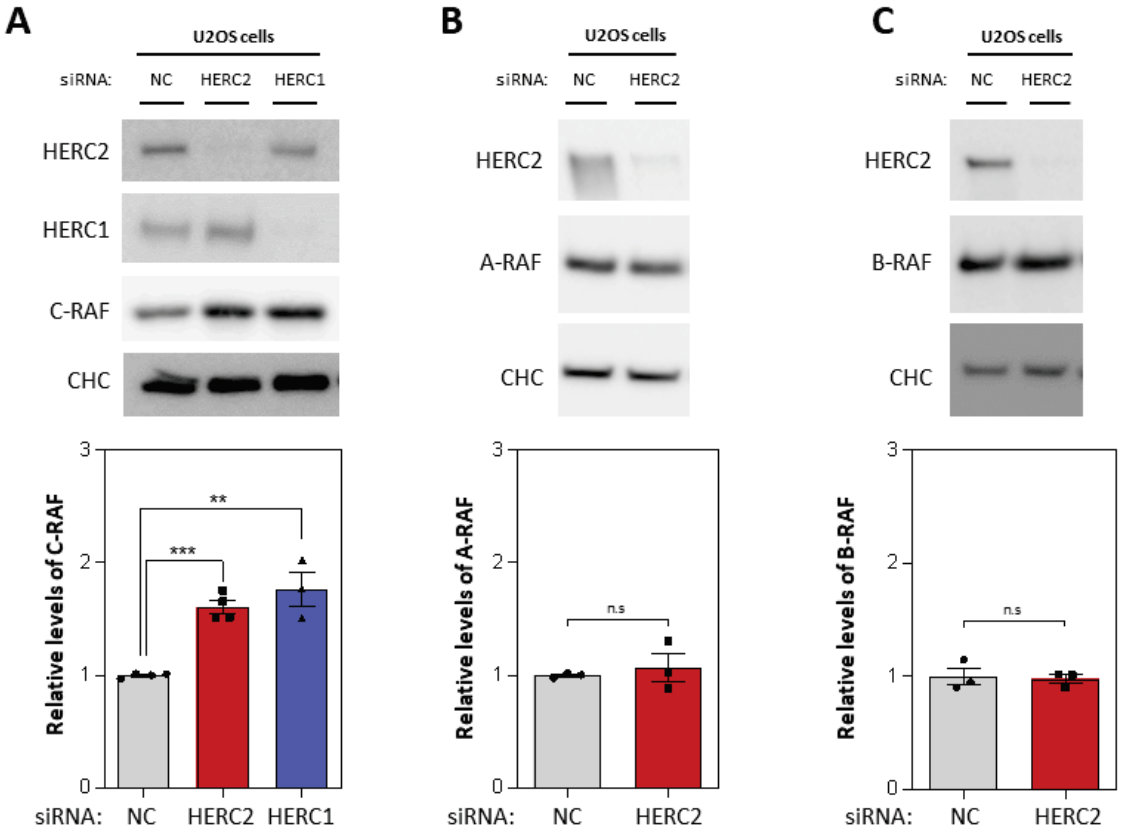

Figure 20. Figure continues on next page ▼

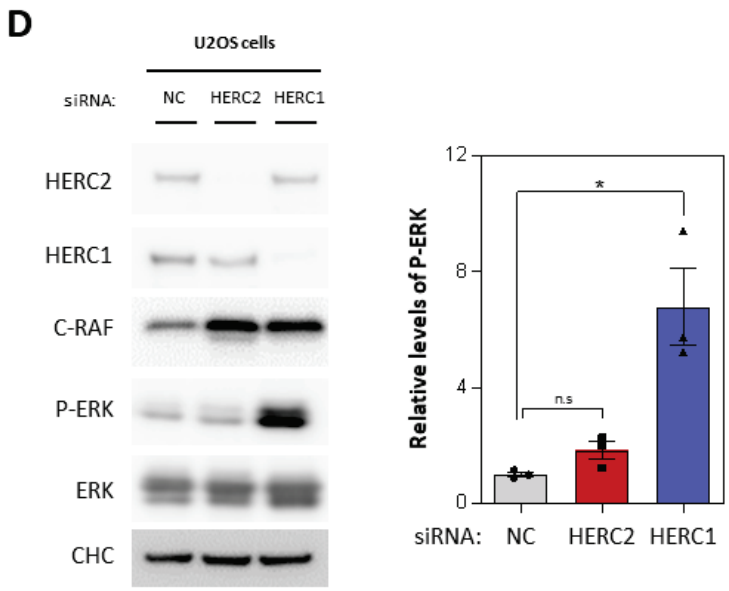

Figure 20. HERC2 regulates C-RAF protein levels. (A) U2OS cells were transfected with an siRNA negative control (NC), an siRNA against HERC2, or an siRNA against HERC1. The indicated protein levels were analysed by immunoblot. Levels of C-RAF proteins were quantified, normalized based on clathrin heavy chain (CHC) protein levels (loading control), and expressed relative to the control condition. **(B-C)** U2OS cells were transfected with a NC siRNA or a siRNA against HERC2. Levels of A-RAF (B) or B-RAF (C) were analysed by immunoblot, quantified, normalized based on CHC protein levels, and expressed relative to the control condition. **(D)** U2OS cells were transfected as in (A), and the indicated protein levels were analysed by immunoblot. Phospho-ERK (P-ERK) levels were quantified, normalized based on ERK protein levels and expressed relative to the control condition. Plots represent the mean ± standard error of the mean. Representative results are shown from experiments repeated at least three times and the individual data points are plotted as single dots. Significance levels: ns = non significance; * $p \leq 0.05$; ** $p \leq 0.01$; *** $p \leq 0.001$.

HERC2 regulates p38 phosphorylation

Given that HERC1 regulates the MKK3/p38 axis through a RAF-dependent mechanism [102], we decided to study if this mechanism was the same for HERC2. We analysed levels of p38 phosphorylation in U2OS cells transfected with a negative control siRNA, an siRNA against HERC2, and a positive control siRNA against HERC1. We observed the induction of p38 phosphorylation in HERC2-depleted cells, though with total p38 protein levels remaining stable, and higher C-RAF protein levels. Analogous behaviour was detected in HERC1-depleted cells (Figure 21A). The same results for p38 phosphorylation were obtained when silencing HERC2 with siRNAs containing different RNA sequences (HERC2 H2.2 and HERC2 H2.4) (Figure 21B).

The phosphorylation of p38 is associated with its activation and nuclear translocation. To check this, we analysed p38 subcellular localization. Immunofluorescence experiments showed increased p38 nuclear localization in HERC2-depleted cells (Figure 21C). This was

quantified assessing the nucleus/cytoplasm ratio, which was higher in HERC2-depleted cells compared with control cells (Figure 21D).

After HERC2 silencing, p38 activation, was replicated in other human cells, such as the p53-lacking human non-small lung carcinoma cell line (H1299) and the non-tumorigenic human kidney 293T cell line (HEK 293T) (Figure 21E). In addition, the same results were obtained in mouse cells and when using a different HERC2 silencing methodology. RAW 264.7 macrophage cell line, primary mouse osteoblasts and mouse embryonic fibroblasts (MEFs) were infected with lentiviral particles carrying either an empty vector as a control (plKO) or a short hairpin RNA (shRNA) against HERC2. All HERC2 knockdown cells presented higher phospho-p38 protein levels compared to controls, while total p38 protein levels remained constant (Figure 21F). In conjunction, these results demonstrated that HERC2 participates in regulating p38 signalling.

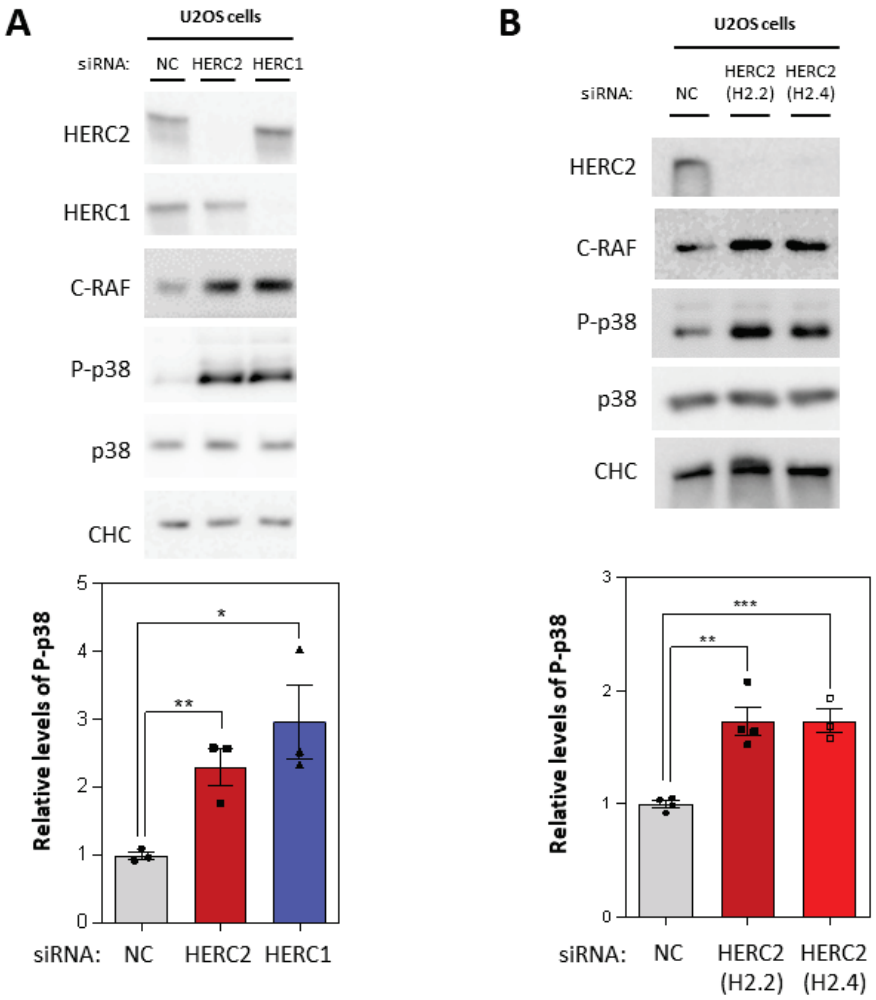

Figure 21. Figure continues on next page ▼

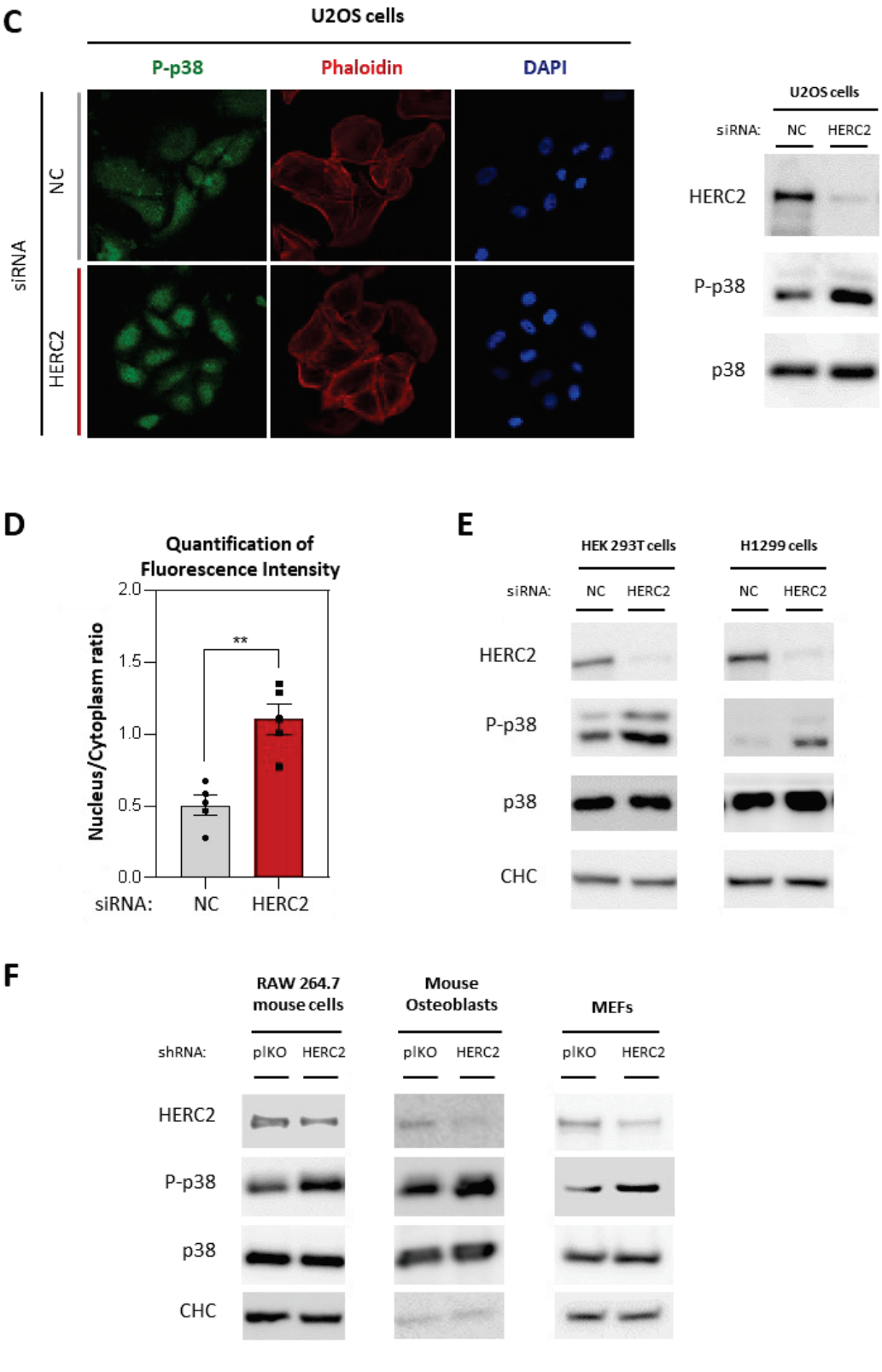

Figure 21. Figure caption on next page ▼

Figure 21 ▲. HERC2 regulates p38 phosphorylation. (A) U2OS cells were transfected with an siRNA negative control (NC), an siRNA against HERC2, or an siRNA against HERC1. The indicated protein levels were analysed by immunoblot. Levels of phospho-p38 (P-p38) were quantified, normalized based on total p38 protein levels, and expressed relative to the control condition. **(B)** U2OS cells were transfected with an siRNA negative control (NC) and two different siRNA sequences against HERC2: H2.2 or H2.4. The indicated protein levels were analysed by immunoblot and phospho-p38 levels were quantified and represented as in (A). **(C)** U2OS cells transfected with NC or HERC2 siRNA were analysed by immunoblot against the indicated proteins and by confocal microscopy. Fixed cells were stained for phospho-p38 (green), F-actin with phalloidin (red), and nuclei with DAPI (blue) and analysed by immunofluorescence. **(D)** Fluorescence intensity in the nucleus and cytoplasm per cell was measured and quantified. The ratio nucleus/cytoplasm was calculated. Each data point represent mean of a different field. **(E)** HEK 293T and H1299 cells were transfected with a NC or HERC2 siRNA. The indicated protein levels were analysed by immunoblot. **(F)** A RAW 264.7 mouse macrophage cell line, mouse primary osteoblasts and mouse embryonic fibroblasts (MEFs) were infected with lentiviral particles carrying either the empty plKO vector as a negative control (plKO) or an shRNA against HERC2. The indicated protein levels were analysed by immunoblot. Plots represent mean ± standard error of the mean. Representative results are shown from experiments repeated at least three times and the individual data points are plotted as single dots. Significance levels: ns = non significance; * $p \leq 0.05$; ** $p \leq 0.01$; *** $p \leq 0.001$.

HERC2 regulates the MKK3/p38 pathway through crosstalk mediated by C-RAF

MAPK kinase (MAPKK or MKK) mediates p38 activation through phosphorylation. MKK3 is the predominant isoform in human U2OS cell lines [102], and its activation has been analysed by measuring its phosphorylation at Ser189 [146]. Thus, we analysed MKK3 activation and its total protein expression in HERC2-depleted U2OS cells, revealing that neither MKK3 phosphorylation at Ser189 nor total MKK3 protein levels were altered compared with control cells (Figure 22A). To confirm whether p38 phosphorylation triggered by HERC2 depletion depends on MKK3, we co-transfected U2OS with an MKK3 siRNA and either the negative control or the HERC2 siRNA. This revealed that MKK3 knockdown significantly abolished the increment in p38 phosphorylation after HERC2 depletion (Figure 22B). These data demonstrated that MKK3 activation caused the increase in phospho-p38 independently of phosphorylation at Ser189.

Given the finding that HERC2 regulates C-RAF and p38 activation, we used two specific RAF kinase inhibitors to identify a potential crosstalk mechanism between the two pathways. LY300912 was used to inhibit all RAF isoforms, and Sorafenib was used to inhibit only B-RAF and C-RAF. In absence of the inhibitors, cells showed an increase in p38 phosphorylation after HERC2 depletion; remarkably, this increase was clearly abrogated after incubation with LY3009120 or Sorafenib inhibitors for 1 hour (Figure 23A). Because RAF isoforms interact by forming different heterodimers [84], sometimes all isoforms must be depleted to rescue the regulatory effects mediated by RAF proteins. Therefore, we co-transfected U2OS cells with

siRNAs against C-RAF or all three RAF isoforms (A-RAF, B-RAF and C-RAF) along with either the negative control siRNA or the siRNA against HERC2 to achieve knockdown. Although silencing C-RAF alone was insufficient to reduce p38 phosphorylation significantly, silencing all three isoforms led to a significant decrease in p38 activation in HERC2-depleted cells (Figure 23B). Unlike pharmacological inhibition of RAF, triple knockdown failed to produce a complete abrogation of p38 phosphorylation after HERC2 depletion, which is probably due to the fact that siRNA silencing did not achieve sufficient RAF isoforms knockdown.

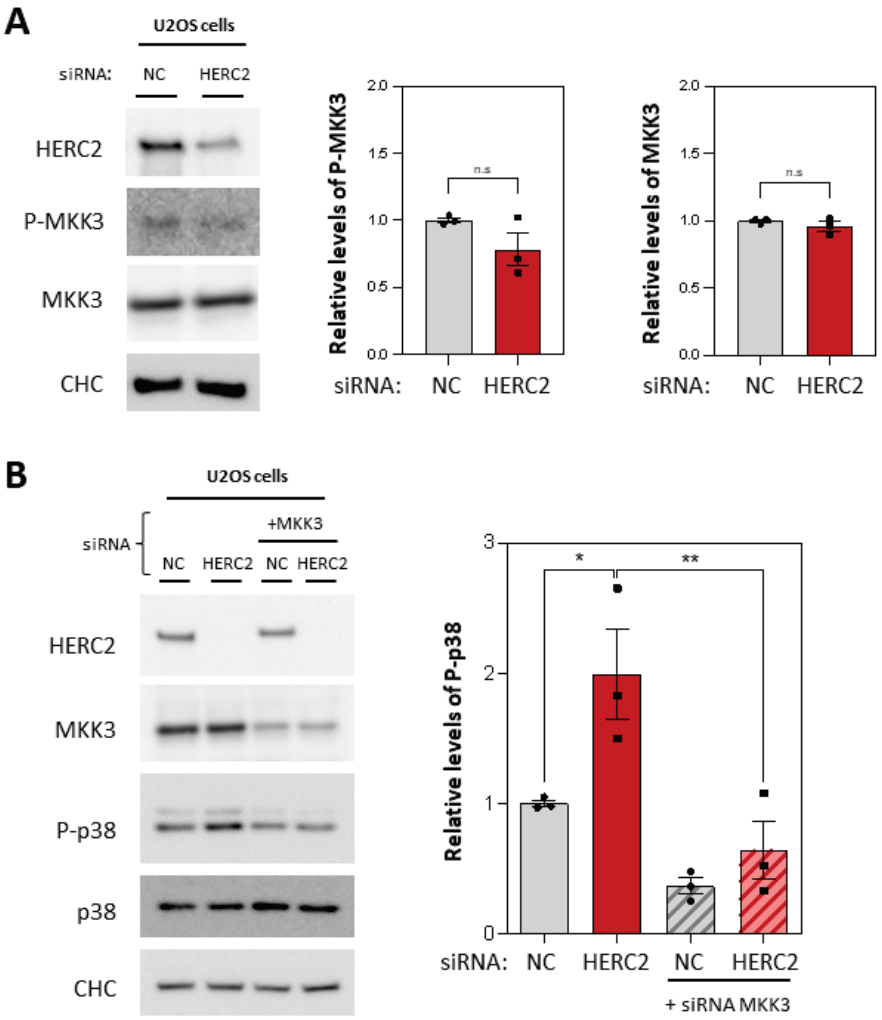

Figure 22. HERC2 regulates the MKK3/p38 pathway. (A) U2OS cells were transfected with an siRNA negative control (NC) or an siRNA against HERC2. The indicated protein levels were analysed by immunoblot. Levels of MKK3 and P-MKK3 were quantified and normalized based on clathrin heavy chain (CHC) protein levels (loading control) and total MKK3 protein levels, respectively, and expressed relative to the control condition. **(B)** U2OS cells were transfected with the NC or HERC2 siRNA. An siRNA against MKK3 was added in the indicated conditions (+MKK3) and the indicated protein levels were analysed by immunoblot. Levels of phospho-p38 (P-p38) were quantified, normalized based on total p38 protein levels and expressed relative to the control condition. Plots represent mean ± standard error of the man. Representative results are shown from experiments repeated at least three times and the individual data points are plotted as single dots. Significance levels: ns = non significance; * $p \leq 0.05$; ** $p \leq 0.01$.

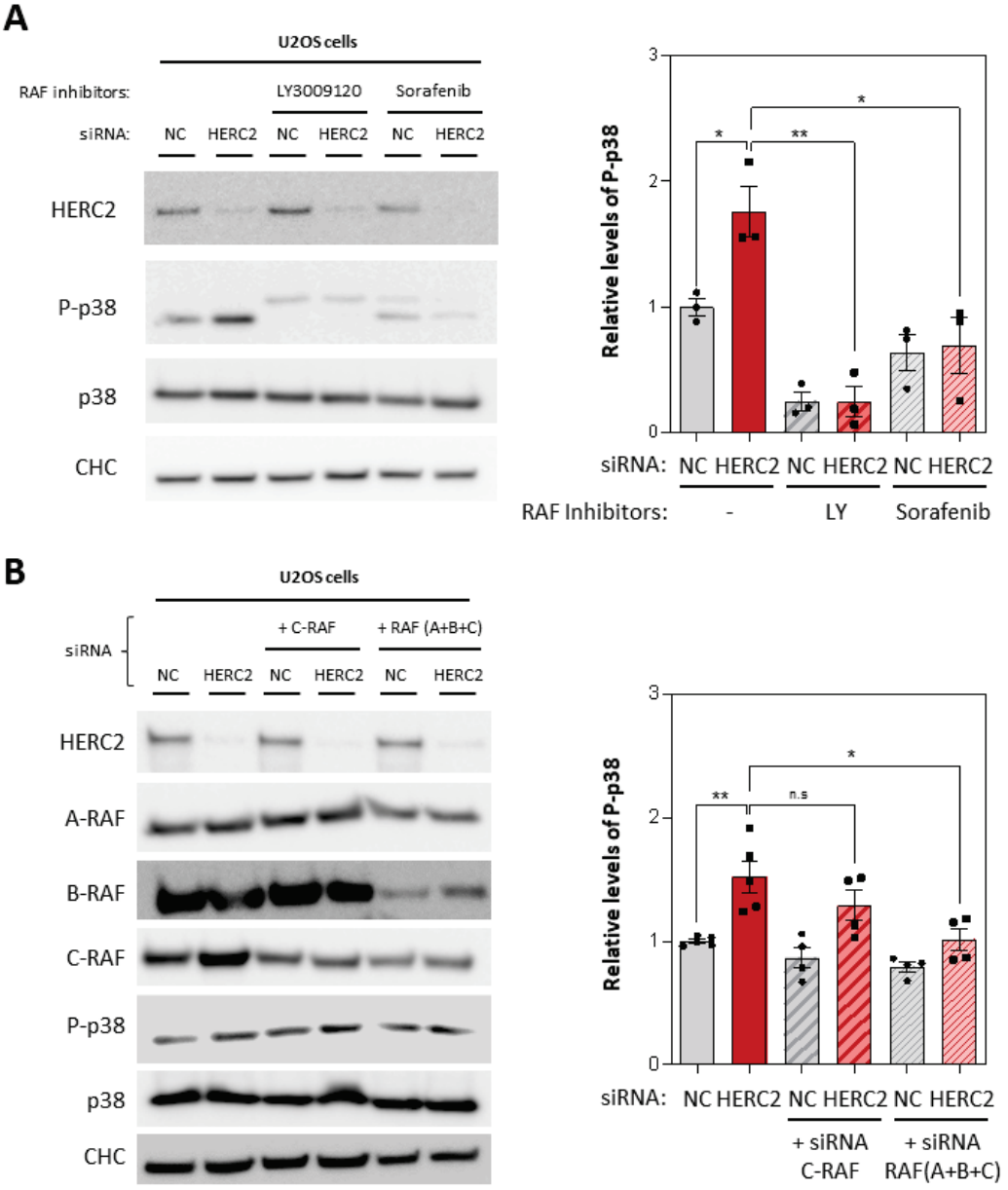

Figure 23. HERC2 regulates the MKK3/p38 pathway through crosstalk mediated by C-RAF. (A) U2OS cells were transfected with NC or HERC2 siRNA. At 72 hours post-transfection, cells were treated with 1 µM of LY3009120 or 1 µM Sorafenib for 1 hour. Untreated cells were incubated with dimethyl sulfoxide (DMSO) as a negative control. Lysates were analysed by immunoblotting and phospho-p38 levels were quantified, normalized by total p38 protein levels and expressed relative to the control condition. **(B)** U2OS cells were transfected with the NC or HERC2 siRNA. C-RAF siRNA alone or a combination of A-, B- and C-RAF siRNAs (A+B+C) was added when indicated. The indicated protein levels were analysed by immunoblot. Phospho-p38 levels were quantified, normalized by total p38 protein levels and expressed relative to control condition. Plots represent mean ± standard error of the mean. Representative results are shown from experiments repeated at least three times and the individual data points are plotted as single dots. Significance levels: ns = non significance; * $p \leq 0.05$; ** $p \leq 0.01$.

Altogether these results confirm the existence of a crosstalk between the RAF and p38 signalling pathways regulated by HERC2.

HERC2 interacts with C-RAF

To further investigate the mechanism behind C-RAF regulation by HERC2, we analysed whether these two proteins can interact. In immunoprecipitation experiments in U2OS cells with a specific anti-HERC2 antibody (bvg3), endogenous HERC2 and C-RAF immunoprecipitated, while HERC1 did not, indicating that the interaction of HERC2 and C-RAF was independent of HERC1 (Figure 24A). RAF hetero-dimerization between its isoforms is a well-reported process [84], and consistent with this, A-RAF and B-RAF were also detected in HERC2 immunoprecipitated complexes (Figure 24B-C). The same results were obtained in the human 293T cell line (Figure 24D-F).

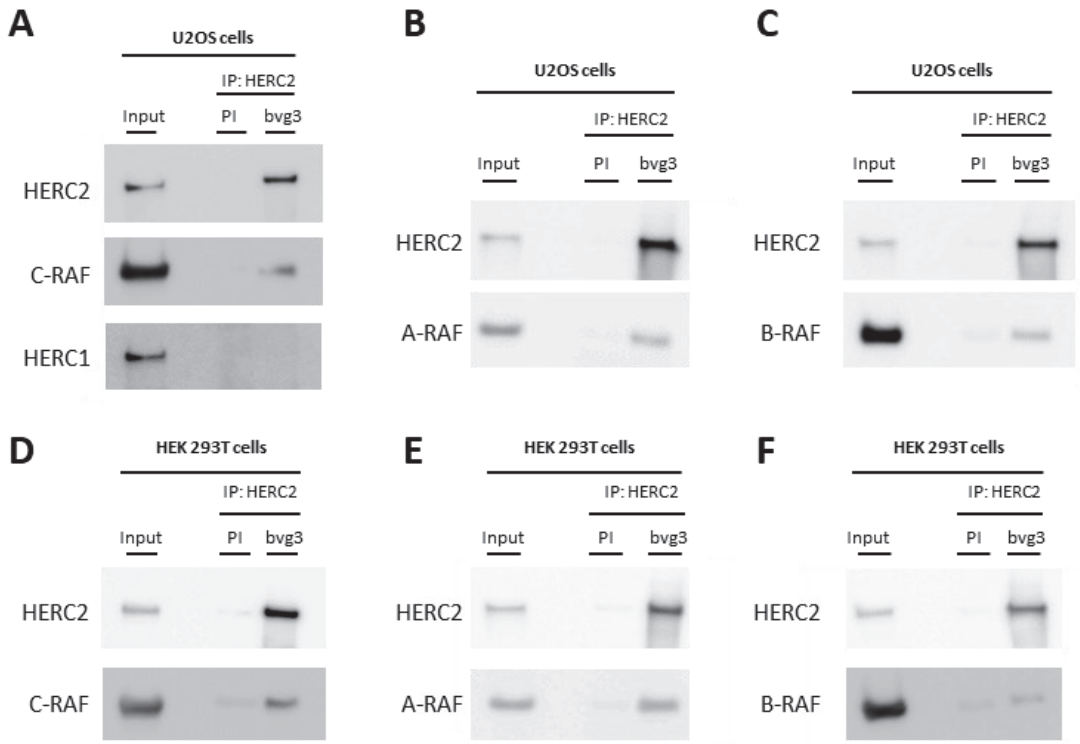

Figure 24. HERC2 interacts with C-RAF. (A-F) Supernatants (Input) of lysates from U2OS (A-C) and HEK 293T cells (D-F) were immunoprecipitated (IP) using anti-HERC2 antibodies (bvg3) and analysed by immunoblotting with antibodies against the indicated proteins. Pre-immune serum (PI) was used as a negative control. Representative results are shown from experiments repeated at least three times.

To identify the region of HERC2 interacting with C-RAF, we co-expressed a GFP-C-RAF fusion protein with a series of Myc-HERC2 fusion proteins in HEK 293T cells (Figure 25A), followed by pull-down assays with GFP-binding beads. Constructs F4, F5, and F5CT coimmunoprecipitated with GFP-C-RAF, indicating that the HERC2 and C-RAF protein interaction occurs mainly in the carboxyl-terminus of HERC2 polypeptide chain. F5CT construct, which contains the HECT domain holding the ubiquitin ligase activity, showed the

highest affinity with C-RAF, suggesting that this is the most relevant interaction site (Figure 25A). HEK 293T cells were then co-transfected with a Flag-HERC2 full-length fusion protein along with GFP (as a negative control) or the GFP-C-RAF fusion constructs (CR1, CR2, CR3 or full-length) to map the C-RAF region involved. In the GFP pull-down, Flag-HERC2 was coimmunoprecipitated with CR1, CR3, and the full-length constructs (Figure 25B). To characterize this interaction further, we co-expressed the F4 Myc-HERC2 construct with GFP-C-RAF fusion constructs and performed a GFP pull-down, which showed preferential co-immunoprecipitation of the F4 construct with CR3 (Figure 25C). In parallel, the same experiment was done but with the F5CT Myc-HERC2 construct instead of F4, and this revealed co-immunoprecipitation of F5CT with CR1 and CR3 (Figure 25D). In conjunction, pull-down experiments confirmed the interaction between HERC2 and C-RAF, and indicated the possible domains involved. The HERC2 HECT domain, contained in the F5CT construct, showed the highest affinity for C-RAF and its catalytic domain (CR3), suggesting that the HECT and CR3 domains could be the most relevant at the physiological level. Subsequent structural studies should confirm this relevance.

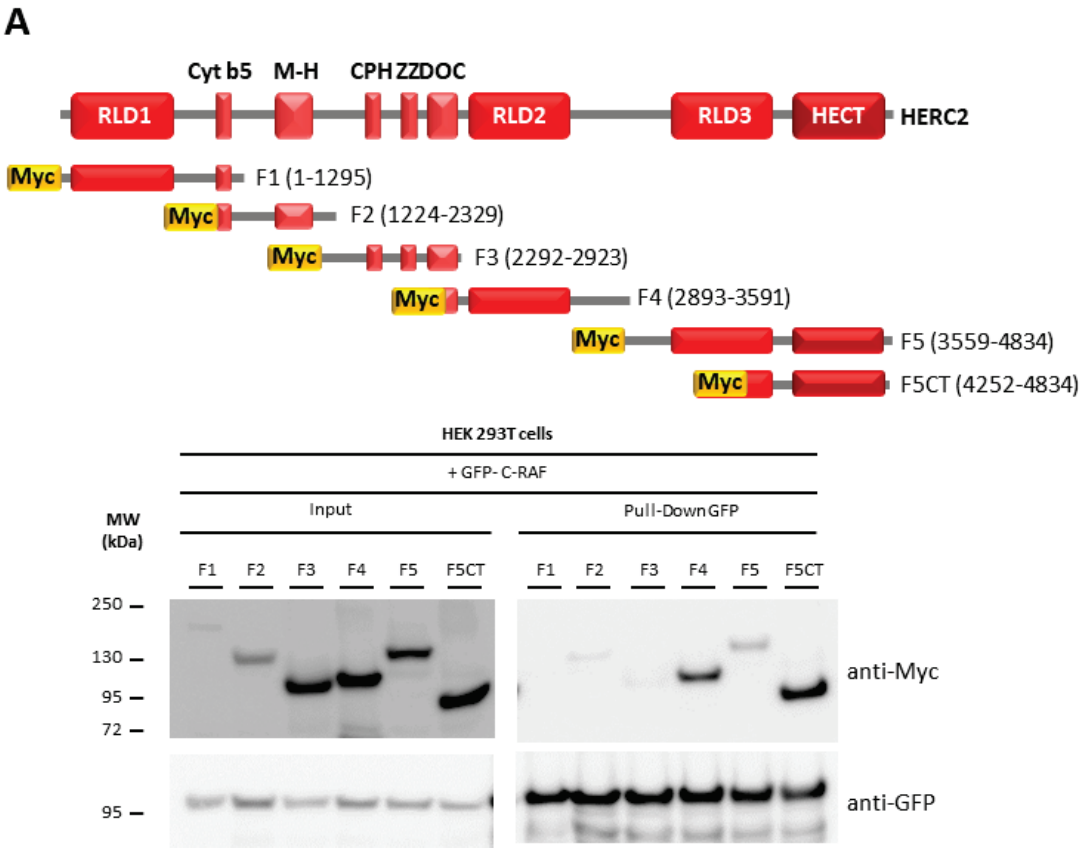

Figure 25. Figure continues on next page ▼

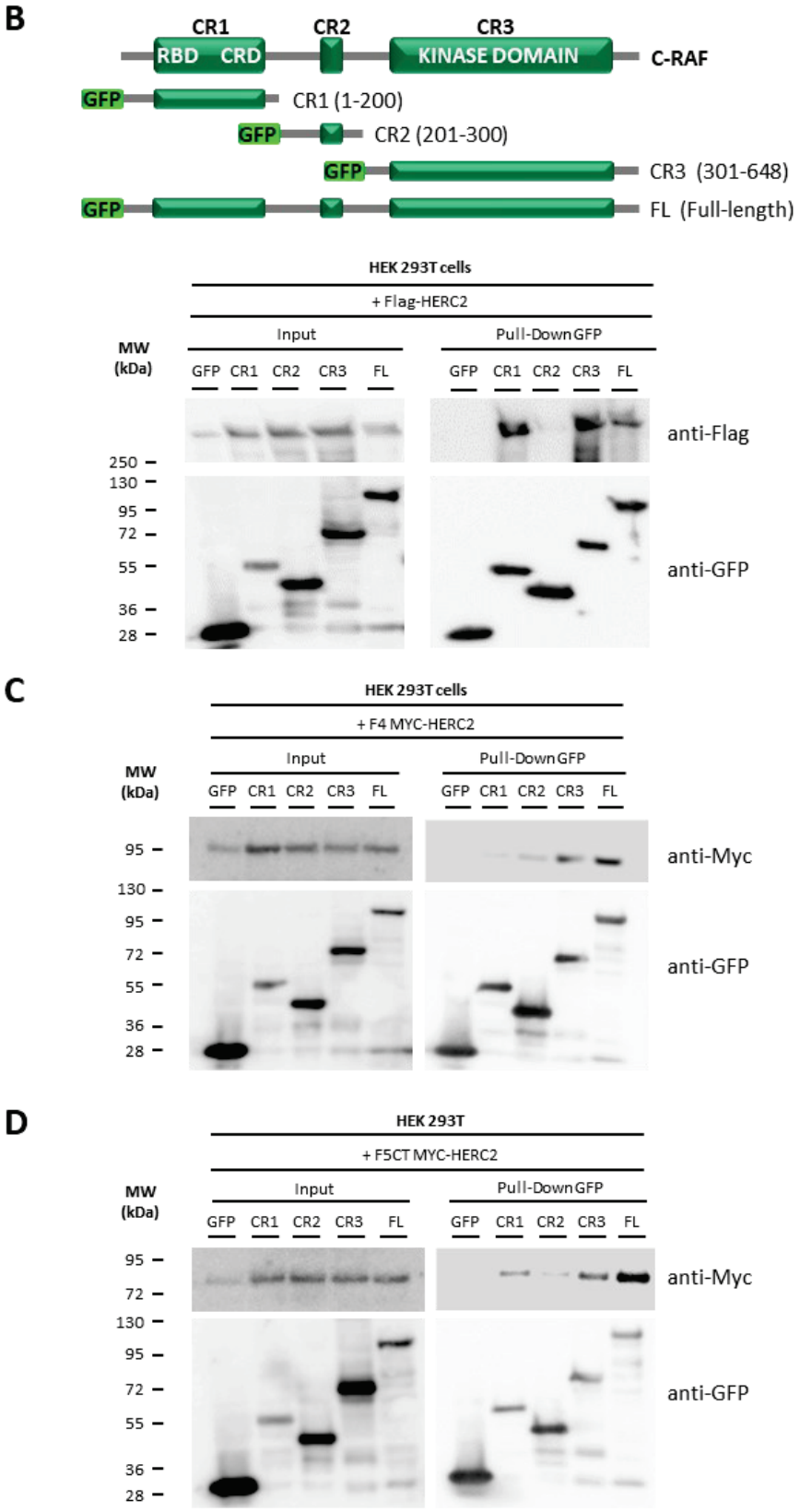

Figure 25. Figure caption on next page ▼

Figure 25 ▲. Domains involved in the interaction between HERC2 and C-RAF protein. (A) Schematic representation of HERC2 structure and its relevant domains is shown. The different Myc-HERC2 protein constructs are indicated. Pull-down experiments were performed in HEK 293T cells co-transfected with GFP-C-RAF and the indicated Myc-HERC2 fusion construct. 48 hours post-transfection, lysates from these cells were incubated with GFP-binding beads as indicated in "Materials and Methods". Proteins retained in the resin were analysed by immunoblotting with antibodies against the indicated proteins. **(B)** Schematic representation of C-RAF structure and its relevant domains is shown. The different GFP-C-RAF protein constructs are indicated. HEK 293T cells were co-transfected with full-length Flag-HERC2 fusion protein and the indicated GFP-C-RAF fusion construct or GFP as a negative control. A pull-down experiment was performed as in (A). **(C-D)** HEK 293T cells were co-transfected with F4 Myc-HERC2 (C) or F5CT Myc-HERC2 (D) fusion constructs and the indicated GFP-C-RAF fusion construct or GFP as a negative control. A pull-down experiment was performed as in (A). Representative results are shown from experiments repeated at least three times.

HERC2 regulates C-RAF ubiquitylation and proteasome-dependent degradation

Having shown that the ubiquitin E3 ligase HERC2 interacts with C-RAF and regulates its protein levels, we wanted to dissect whether HERC2 regulates C-RAF ubiquitylation targeting it to proteasomal degradation. To determine this, we analysed C-RAF ubiquitylation both in control and HERC2-depleted cells in the absence and presence of the proteasome inhibitor MG132. Control and HERC2-depleted HEK 293T cells were transfected with constructs expressing GFP-C-RAF or GFP as a negative control. Forty-eight hours later, cells were incubated for 6 hours in the absence or presence of MG132 (10 μM). Lysates from these cells were pulled down using GFP resin. Inputs and pull-down proteins were analysed by PAGE/SDS and immunoblotted with the anti-ubiquitylated proteins antibody (FK2) or with specific antibodies against the indicated proteins. GFP-C-RAF polyubiquitylation slightly decreased in HERC2-depleted cells compared to control cells under basal conditions (Figure 26A, lane 10 compared with lane 12). Treatment with MG132 efficiently caused accumulation of polyubiquitylated GFP-C-RAF due to proteasome degradation inhibition in control cells (Figure 26A, lane 10 compared with lane 14). Remarkably, under MG132 treatment, GFP-C-RAF polyubiquitylation levels were much lower in HERC2-depleted cells (Figure 26A, lane 14 compared with lane 16). Altogether, these results demonstrated C-RAF proteasome-dependent degradation and its regulation by HERC2 through ubiquitylation.

To confirm the role of HERC2 regulating C-RAF polyubiquitylation we performed an ubiquitylation assay. First, we checked expression of different HERC2 constructs in HEK 293T cells. We transfected either a negative control plasmid (Flag-CTL), a plasmid encoding wild-type HERC2 protein tagged with Flag peptide (Flag-HERC2 WT), or a plasmid encoding a mutant variant lacking ubiquitin ligase activity (Flag-HERC2 C4762S). HERC2 overexpression

occurred in both Flag-HERC2 WT and Flag-HERC2 C4762S transfected cells, being greater with the mutated form (Figure 26B). Next, HEK 293T cells were also transfected with GFP-C-RAF and His-tagged ubiquitin constructs. Cells were lysed after incubation with the proteasome inhibitor MG132 to enrich ubiquitylated proteins degraded by the proteasome, and incubated with Ni-NTA agarose resin to pull-down His-tagged ubiquitin molecules and the proteins to which they were attached (Figure 26C). The results showed a smear of high molecular weight GFP-C-RAF indicating much greater C-RAF ubiquitylation with wild-type HERC2 overexpression. The plasmid construct HERC2 C4762S, which is catalytically inactive, was used to determine if the effect on C-RAF ubiquitylation by HERC2 WT overexpression, was dependent on the ubiquitin ligase activity of HERC2. Despite greater overexpression of the mutated form (HERC2 C4762S), this did not correlate with increased C-RAF ubiquitylation (Figure 26D). These results confirmed that HERC2 regulates C-RAF ubiquitylation.

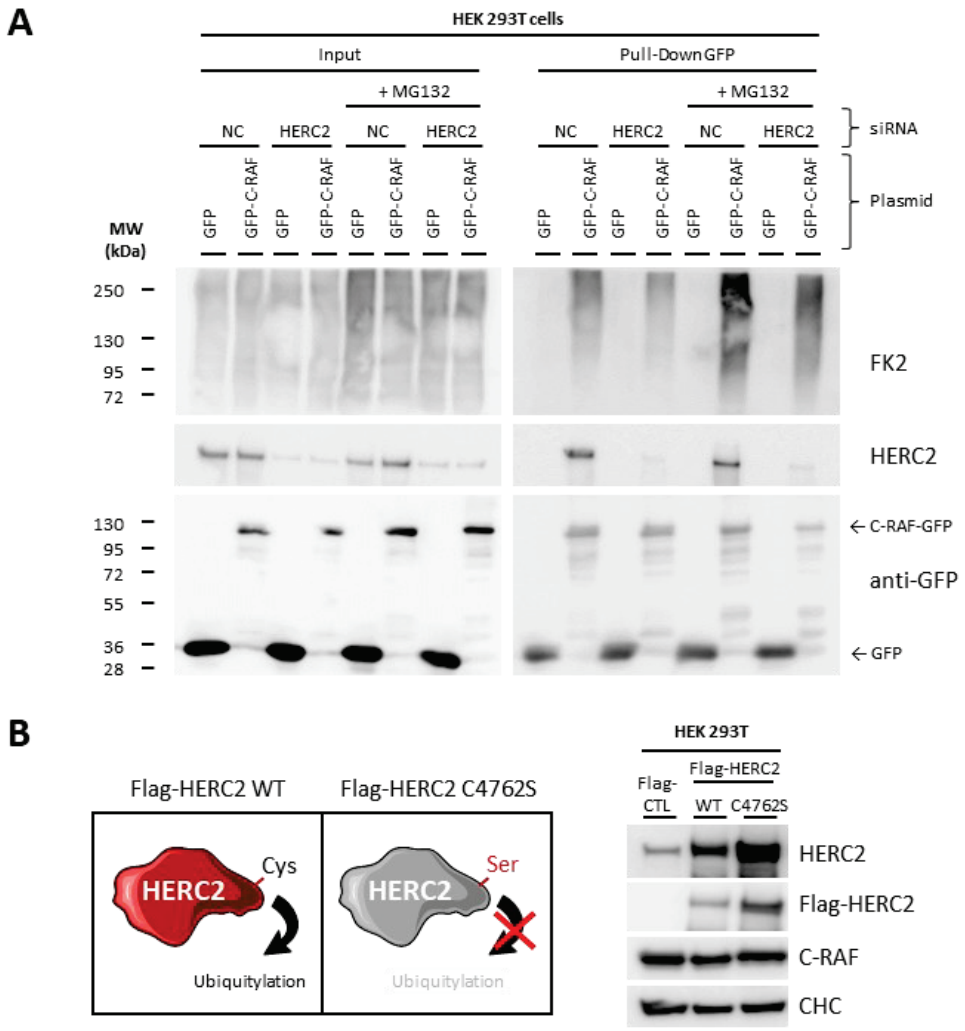

Figure 26. Figure continues on next page ▼

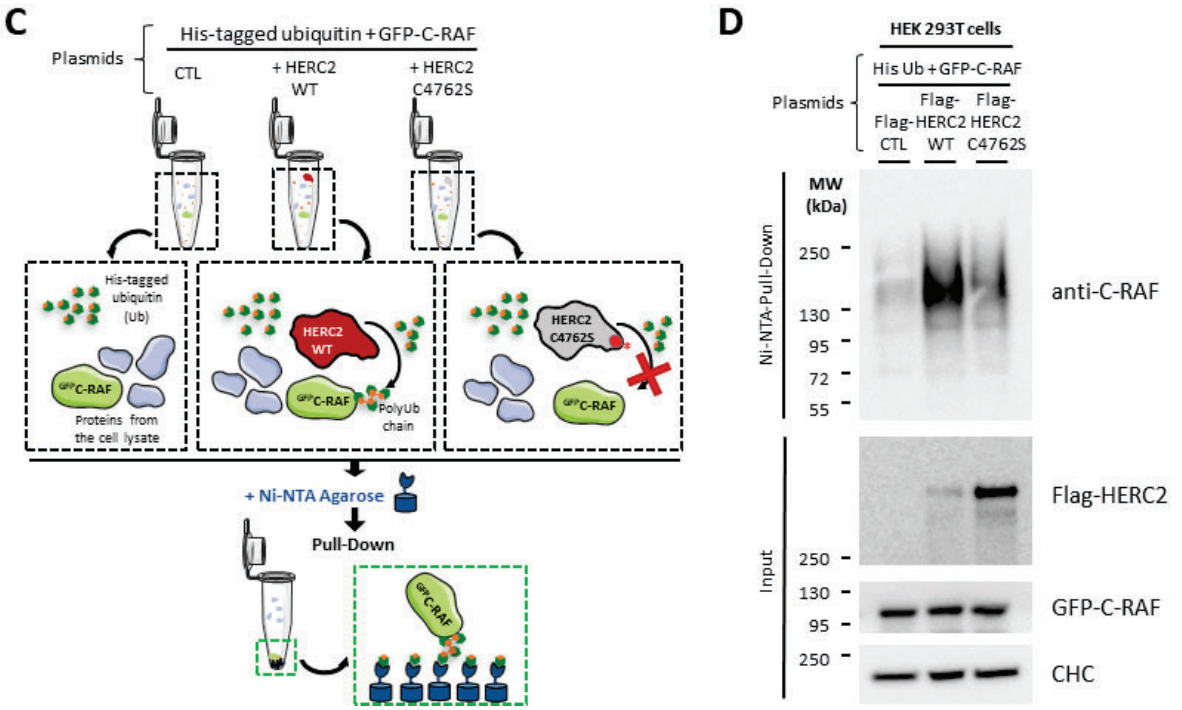

Figure 26. HERC2 regulates C-RAF ubiquitylation and proteasome-dependent degradation. (A) HEK 293T cells were transfected with the NC or HERC2 siRNA. Twenty-four hours later, cells were transfected with GFP or GFP-C-RAF plasmids. Forty-eight hours later, cells were incubated for 6 hours in the absence or presence of MG132 (10 µM). Lysates were pulled down using GFP resin as indicated in "Materials and Methods". Inputs and proteins retained in the resin (Pull-Down GFP) were analysed by immunoblotting with the indicated antibodies. **(B)** HEK 293T cells were transfected with a negative control plasmid (Flag-CTL), a plasmid encoding wild-type HERC2 protein (Flag-HERC2 WT) or a plasmid encoding a mutated form of HERC2 harbouring a substitution of the catalytic cysteine for a serine, which renders it catalytically inactive (Flag-HERC2 C4762S). The indicated proteins were analysed by immunoblot. **(C)** Schematic representation of the ubiquitylation assay. Briefly, cells were transfected with His-tagged ubiquitin plus GFP-C-RAF plasmid. Then we transfected Flag plasmids as in (B). Cell lysates were incubated with Ni-NTA agarose, which binds His-tagged ubiquitin. Pull-Down was performed and ubiquitylated proteins were purified. **(D)** HEK 293T cells were transfected as indicated in (C). After 48 hours, cells were incubated for 6h with MG132 (10 µM). Ubiquitylated proteins were purified using a Ni-NTA-agarose resin as indicated in (C) and in "Materials and Methods". Inputs and pull-downs were analysed by immunoblotting with antibodies against the indicated proteins. Representative results are shown from experiments repeated at least three times.

HERC2 modulates cellular response to H_2O_2-induced oxidative stress

Given that a major function of p38 is to regulate cellular stress, we analysed the cellular response to oxidative stress. U2OS cells were transfected with a negative control siRNA or an siRNA against HERC2, and oxidative stress was induced by treating cells with 500 µM H_2O_2 for different durations. Protein levels of phosphorylated p38 were analysed by immunoblot. As expected, HERC2-depleted cells started from a more phosphorylated basal state (t = 0) (Figure 27A). After 3 hours of H_2O_2 stimulation, both control cells and HERC2-depleted cells clearly showed induced phosphorylation of p38 and reached a maximum peak intensity, which was higher in HERC2-depleted cells. Interestingly, while p38 phosphorylation

levels in control cells were clearly reduced after 6 and 12 hours of treatment, the HERC2-depleted cells maintained significantly higher levels at these times, resulting in a more pronounced and prolonged phosphorylation response curve (Figure 27A).

Consistent with HERC2 having a role in regulating the cellular antioxidant response, mRNA levels of the antioxidant gene nuclear factor erythroid 2-related factor 2 (*NFE2L2)*, superoxide dismutase genes (*SOD1* and *SOD2*) and glutathione peroxidase 1 (*GPX1*), increased in the HERC2-depleted cells compared with control cells. By contrast, mRNA levels of beta-glucuronidase (*GUSB)*, used as a negative control, did not change significantly (Figure 27B). At the level of translational regulation, the protein encoded by the *NFE2L2* gene, which is called NRF2 and is a master regulator of all the beforementioned antioxidant genes, was also up-regulated in HERC2-depleted cells (Figure 27C).

To determine whether the role of HERC2 regulating the cellular response to oxidative stress depends on the activation of the RAF/MKK3/p38 signalling pathway we used inhibitors of p38 (SB203580) and RAF (LY3009120). As previously shown, in absence of the inhibitors, cells showed an increase in NRF2 protein levels after HERC2 depletion; however, this increase was abrogated after incubation with SB203580 or LY3009120 for 1 hour (Figure 27D). These results suggested that p38 acts upstream NRF2 activation and that the cellular response to oxidative stress regulated by HERC2 depends on the RAF/MKK3/p38 pathway.

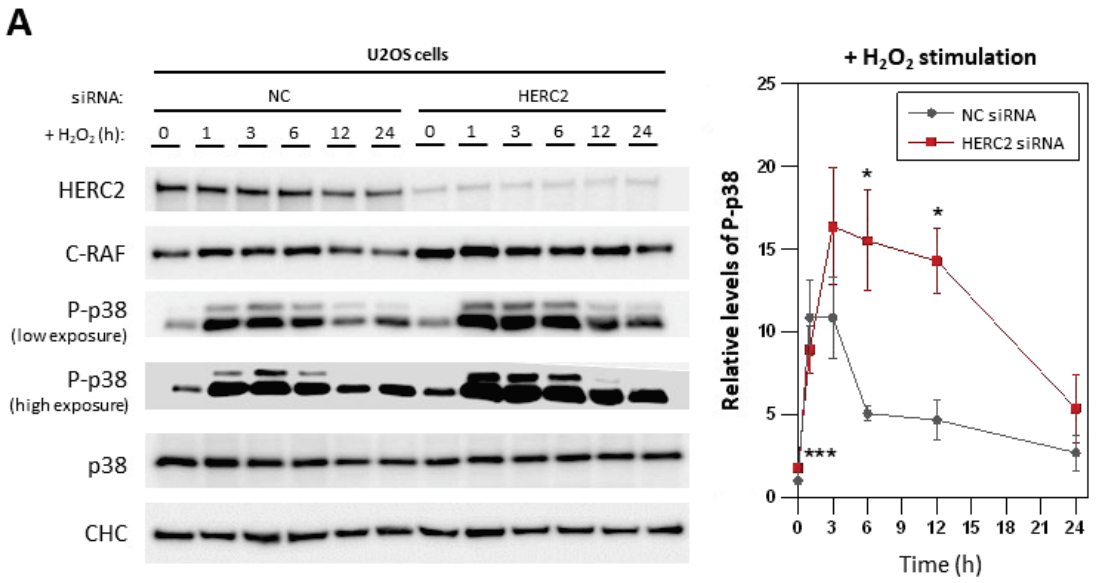

Figure 27. Figure continues on next page ▼

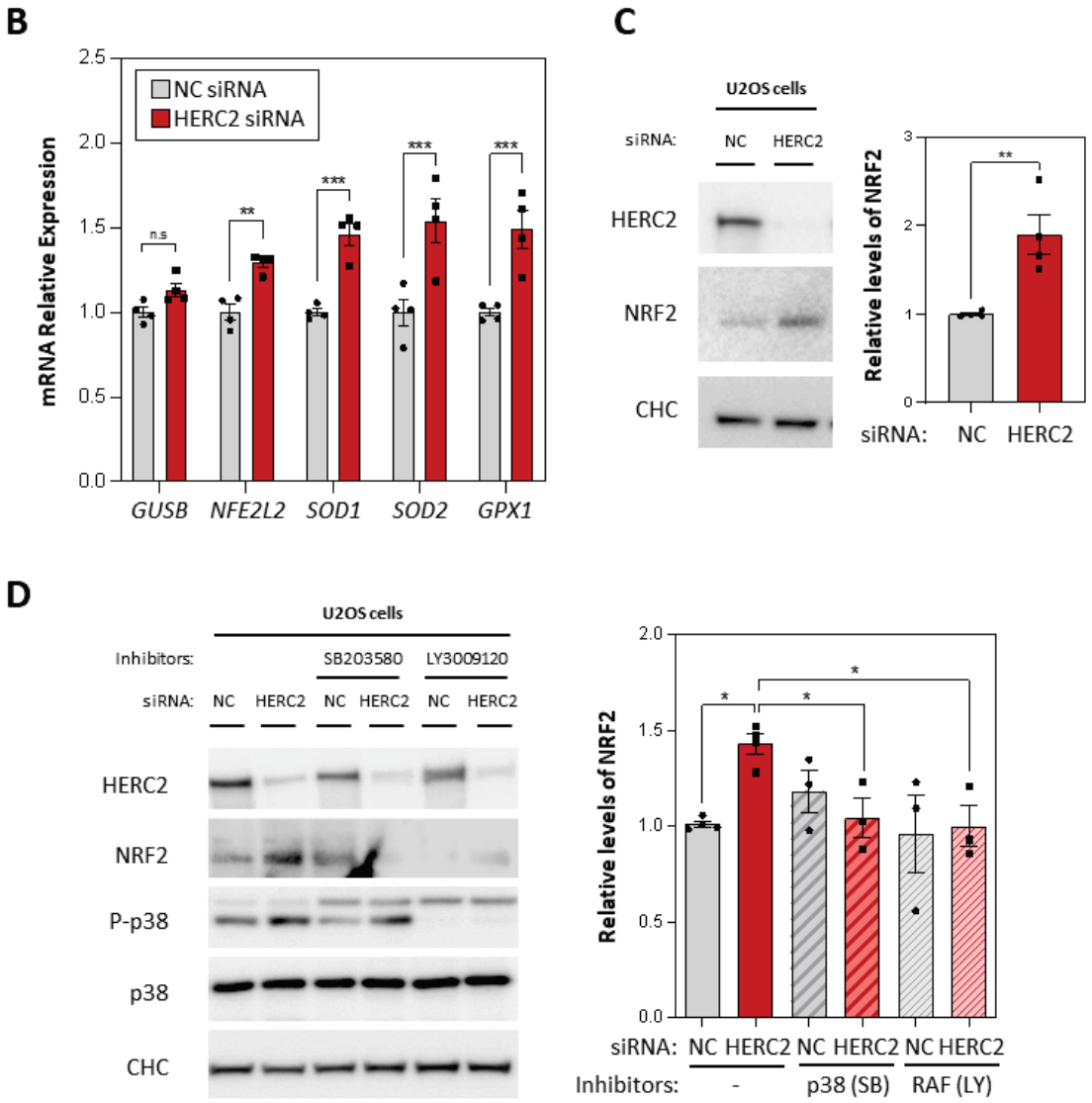

Figure 27. HERC2 modulates cellular response to H_2O_2-induced oxidative stress. (A) U2OS cells were transfected with an siRNA negative control (NC) or an siRNA against HERC2. Subsequently, cells were treated with 500 µM H_2O_2 to induce oxidative stress for the indicated durations. The indicated protein levels were analysed by immunoblot. Pospho-p38 (P-p38) levels were quantified, normalized based on total p38 protein levels, and expressed relative to the non-treated control condition (NC, t = 0). Plots represent mean ± standard error of the mean of 4 independent experiments (n = 4). **(B)** U2OS cells transfected with the NC or HERC2 siRNA were analysed by RT-qPCR. *GUSB*, *NFE2L2*, *SOD1*, *SOD2*, and *GPX1* mRNA expression levels were quantified, and *GAPDH* levels were used to normalize. Each gene quantification is expressed relative to the control condition and individual data points are plotted as single dots. **(C)** U2OS cells were transfected with the NC or HERC2 siRNA. The indicated protein levels were analysed by immunoblot. NRF2 protein levels were quantified, normalized based on Clathrin Heavy Chain (CHC) protein levels (loading control), and expressed relative to the control condition. **(D)** U2OS cells were transfected with the NC or HERC2 siRNA. At 72 hours post-transfection, cells were treated with 10 µM SB203580 or 1 µM of LY3009120 for 1 hour. Untreated cells were incubated with dimethyl sulfoxide (DMSO) as a negative control. Lysates were analysed by immunoblotting and protein levels of NRF2 were quantified, normalized by Clathrin Heavy Chain (CHC) protein levels (loading control), and expressed relative to the control condition. Plots represent mean ± standard error of the mean. Representative results are shown from experiments repeated at least three times and the individual data points are plotted as single dots. Significance levels: ns = non significance; * $p \leq 0.05$; ** $p \leq 0.01$; *** $p \leq 0.001$.

We then evaluated if HERC2 also regulates other stress types modulated by p38. To assess osmotic stress, we treated control cells and HERC2-depleted cells with 100 mM NaCl for different durations. HERC2-depleted cells started from a more phosphorylated basal state in untreated conditions (t = 0). As with H_2O_2 stimulation, both control cells and HERC2-depleted cells showed p38 activation and reached a maximum peak intensity after 3 hours of stimulation. Again, while p38 phosphorylation levels were returning to the basal state in the control cells after 6 and 12 hours of stimulation, the HERC2-depleted cells still maintained significantly higher levels (Figure 28).

Ultimately, these data showed a complex regulation of downstream p38 signalling dependent on HERC2, pointing out HERC2 as a modulator of the cellular response to oxidative and osmotic stresses.

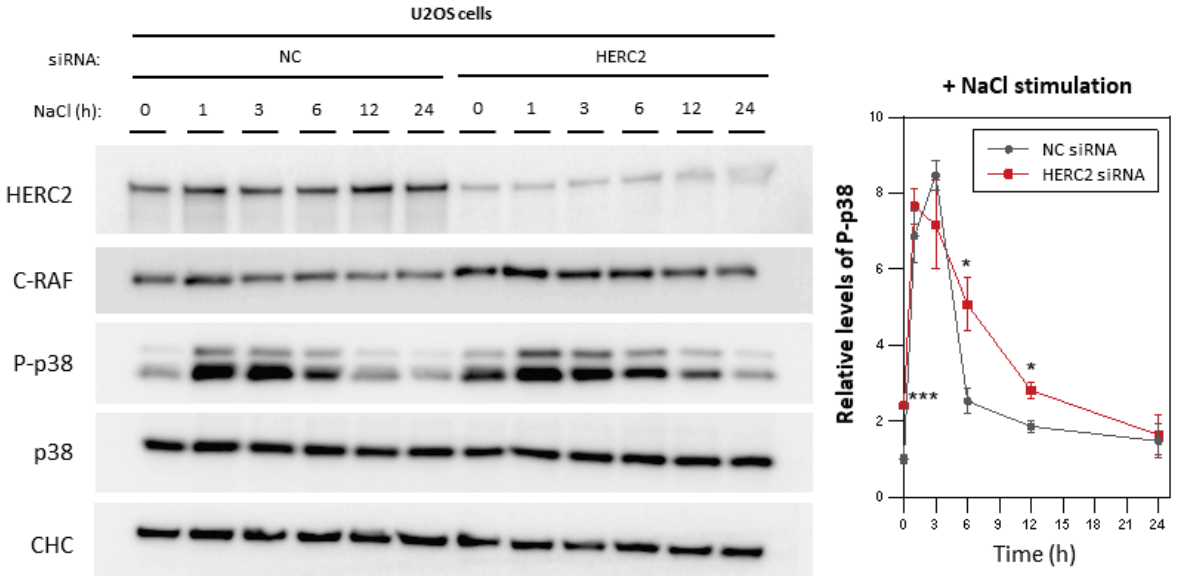

Figure 28. Regulation of the cellular stress response by HERC2. U2OS cells were transfected with an siRNA negative control (NC) or an siRNA against HERC2. Subsequently, cells were treated with 100 mM NaCl for the indicated time periods. The indicated protein levels were analysed by immunoblot. Levels of phospho-p38 (P-p38) were quantified, normalized based on total p38 protein levels and expressed relative to the non-treated control condition (NC, t = 0). Plots represent mean ± standard error of the mean. Representative results are shown from experiments repeated 3 times (n = 3). Significance levels: ns = no significance * $p \leq 0.05$; *** $p \leq 0.001$.

HERC2 deficiency alters cellular resistance to H_2O_2-induced oxidative stress

Finally, to determine whether cells with the HERC2 P594L mutation showed an altered response to H_2O_2-induced oxidative stress, we treated them with 500 µM H_2O_2 for different durations. Both the controls (HERC2 WT) and the fibroblasts carrying the mutation (HERC2

P594L) responded with a strong induction of p38 phosphorylation by 1-3 hours after H_2O_2 treatment. Notably, HERC2 P594L cells maintained higher p38 phosphorylation levels after 6 hours, while levels in control cells had already decreased to baseline (Figure 29A). These differences in p38 signalling correlated with differences in cell morphology spotted by optical microscopy. After 3 hours of treatment with H_2O_2, the HERC2 WT cells had already begun to show a rounder morphology, probably due to the toxic effect of H_2O_2, and after 6 hours, most cells showed this altered morphology. By contrast, the HERC2 P594L cells seemed to be more resistant to H_2O_2 exposure, appearing healthier and more attached to the plate culture surface than controls at both 3 and 6 hours (Figure 29B). To confirm the differences in cell viability and test their dependence on the C-RAF/MKK3/p38 signalling pathway, MTT assays were performed in the presence of a p38 inhibitor (SB203580) or the RAF inhibitors (LY3009120 or Sorafenib). After 6 hours of treatment with 500 µM H_2O_2, cell viability fell to 13.7% and 44.8% in the control cells and the HERC2 P594L cells, respectively. The higher resistance of HERC2 P594L cells to H_2O_2-induced oxidative stress was abrogated by treatment with the inhibitors (Figure 29C). We then evaluated this effect under prolonged but less aggressive exposure to H_2O_2 (50 µM for 24 hours). Again, HERC2 P594L cell viability was higher compared to the controls after stress exposure and, this higher resistance was abrogated by the p38 or RAF inhibitors (Figure 29D).

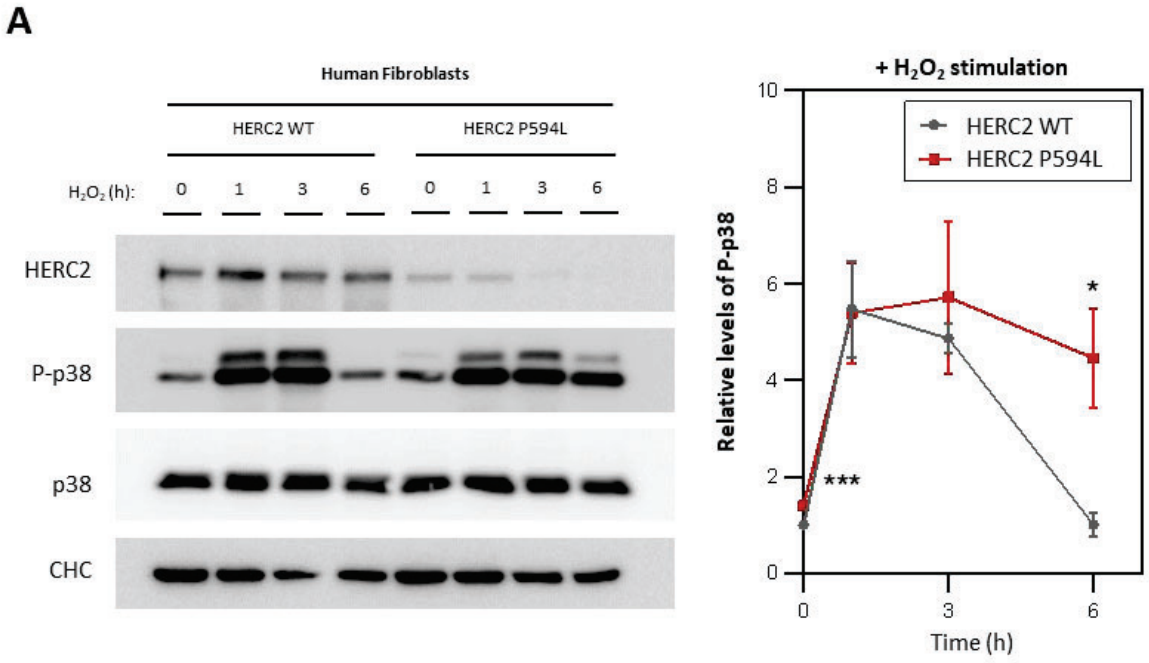

Figure 29. Figure continues on next page ▼

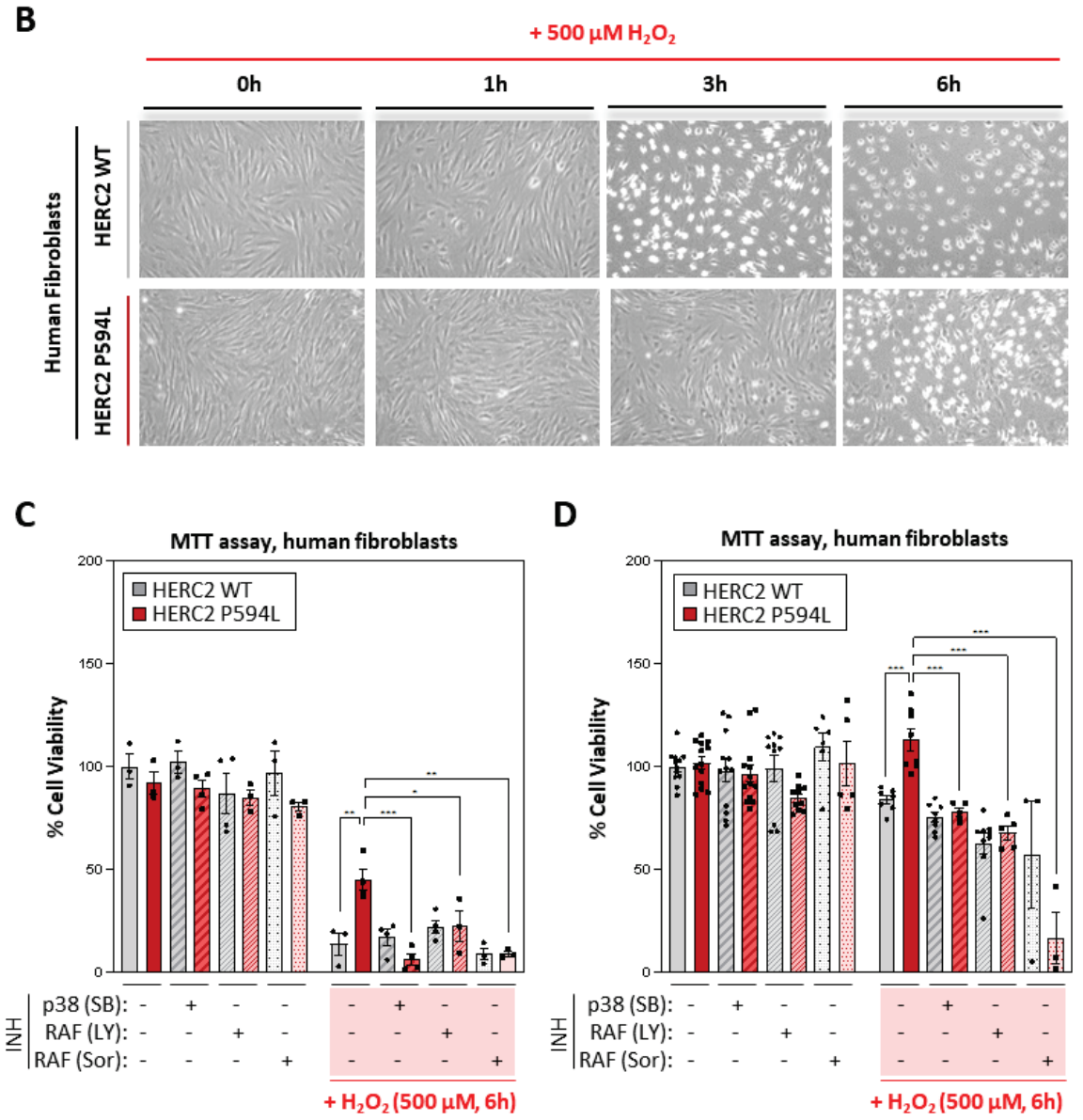

Figure 29. HERC2 deficiency alters cellular resistance to H_2O_2-induced oxidative stress. (A) Human skin fibroblasts derived from an HERC2 wild-type individual (HERC2 WT) and an individual with the p.Pro594Leu HERC2 mutant variant (HERC2 P594L) were treated with 500 µM H_2O_2 to induce oxidative stress for the indicated time points and protein levels were analysed by immunoblot. Phospho-p38 (P-p38) levels were quantified, normalized based on total p38 protein levels and expressed relative to the non-treated control condition (HERC2 WT, t = 0). Plots represent mean ± standard error of the mean of 4 independent experiments (n = 4). **(B)** Human skin fibroblasts were treated as in (A) and images were acquired by optical microscopy after the indicated treatment times, with representative images shown from experiments repeated three times (n = 3). **(C-D)** HERC2 WT and HERC2 P594L human skin fibroblasts were treated with 500 µM H_2O_2 for 6 hours (C) or with 50 µM H_2O_2 for 24 hours (D) as indicated. Cells were treated with the following inhibitors (INH): 1 µM LY3009120, 1 µM Sorafenib or 10 µM SB203580. The inhibitors were added when indicated by the (+) symbol 1 hour before adding H_2O_2. An MTT assay was performed. Data are presented as a percentage relative to the control and untreated condition. Plots represent mean ± standard error of the mean. Representative results are shown from experiments repeated at least three times and the individual data points are plotted as single dots. Significance levels: ns = non significance; * $p \leq 0.05$; ** $p \leq 0.01$; *** $p \leq 0.001$.

Previous studies have reported that HERC2 depletion enhances cell proliferation due to impaired p53 transcriptional activity [29, 48, 49]. Given that HERC2 modulates the activity of p53, we wanted to determine whether the evaluated effects on cell viability also depend, in part, on this tumour suppressor protein. As expected, in U2OS cells with functional p53 (WT p53), depletion of HERC2 resulted in higher cell growth compared to the control cells. These differences in cell growth between both conditions were abolished under p53 knockdown (siRNA p53) (Figure 30A). Thus, we used the p53-knockdown U20S cell model to repeat the cell viability assay after H_2O_2 exposure. In untreated conditions, no significant differences were observed between negative control cells (NC siRNA + p53 siRNA) and HERC2-depleted cells (HERC2 siRNA + p53 siRNA), including after treatment with the inhibitors (Figure 30B). However, after 24 hours of treatment with 50 µM H_2O_2, cell viability reduced to 67,5% in control cells and only to 89.2% in HERC2-depleted cells. Again, the higher cell resistance of HERC2-depleted cells was abrogated by treatment with inhibitors of p38 (SB203580) and RAF (LY3009120) (Figure 30B). Taken together, these results demonstrated that cellular resistance to H_2O_2-induced oxidative stress acquired by HERC2 deficiency is independent of p53, instead being mediated through the C-RAF/MKK3/p38 signalling pathway.

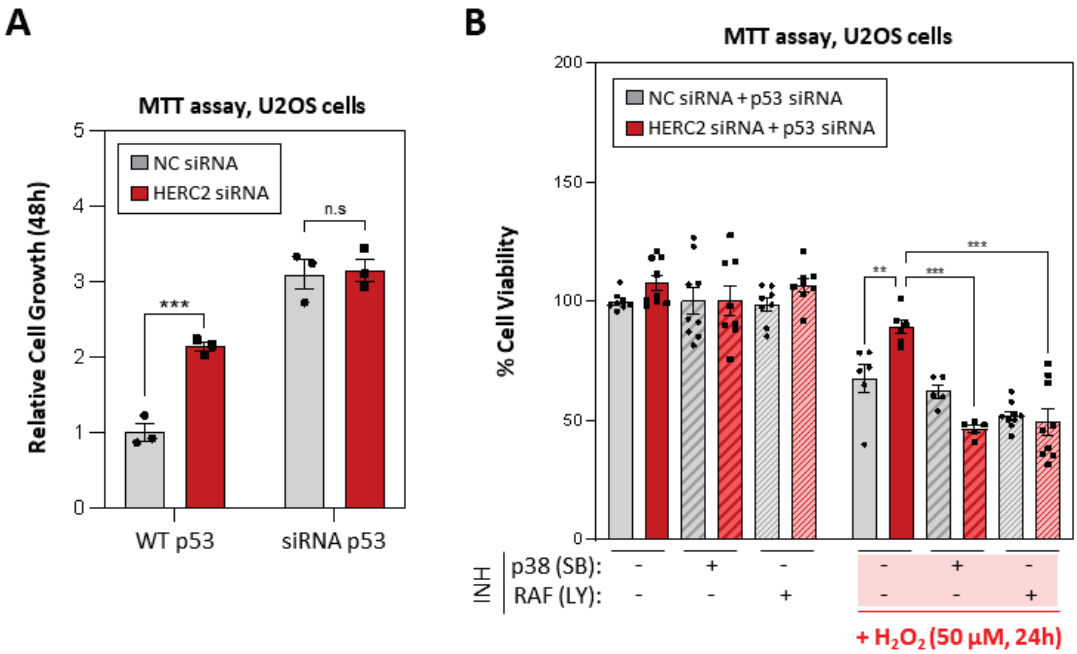

Figure 30. Figure caption on next page ▼

Figure 30 ▲. Cellular resistance to H_2O_2-induced oxidative stress in HERC2-depleted cells is independent of p53 (A) U2OS were transfected with an siRNA negative control (NC) or an siRNA against HERC2. A p53 siRNA was added when indicated (siRNA p53). Subsequently, cells were plated in a 96-well plate and allowed to grow for 48 hours to evaluate cell proliferation and an MTT assay was performed. Data are presented relative to the control condition (NC, WT p53). **(B)** U2OS cells were transfected with the NC or HERC2 siRNA along with p53 siRNA. Cells were treated with 50 µM H_2O_2 for 24 hours as indicated. The following inhibitors (INH) were used: 1 µM LY3009120, 1 µM Sorafenib or 10 µM SB203580. The inhibitors were added when indicated by the (+) symbol 1 hour before adding H_2O_2. Cell viability was assessed by an MTT assay. Data are presented as a percentage relative to the control and untreated condition. Plots represent mean ± standard error of the mean. Representative results are shown from experiments repeated at least three times and the individual data points are plotted as single dots. Significance levels: ns = non significance; * $p \leq 0.05$; ** $p \leq 0.01$; *** $p \leq 0.001$.

These above results suggested that cells with HERC2 deficiency are better equipped against oxidative stress, so we wondered how does increased protection against oxidative stress fits into pathology. Although excessive reactive oxygen species (ROS) cause oxidative stress, ROS also play a physiological role in cell signalling. Thus, appropriate ROS production is essential to maintain redox balance. Overexpression of antioxidant enzymes, such as NRF2, may lead the cell to a more reduced state. This pathophysiological situation is known as reductive stress and can be as harmful as is oxidative stress [140, 147, 148]. To assess this, mitochondrial ROS levels were evaluated with MitoSOX staining. Cells with the HERC2 P594L mutation showed lesser production of mitochondrial ROS than control cells, suggesting a more reduced state in these cells (Figure 31A). In addition, mitochondria were stained using MitoTracker probes. HERC2 P594L cells presented a more fragmented mitochondrial network than control cells, indicating a possible mitochondrial disfunction (Figure 31B). Further experiments should confirm these preliminary observations and deepen how ROS levels and mitochondrial function participate in the neurological syndrome caused by the HERC2 P594L variant.

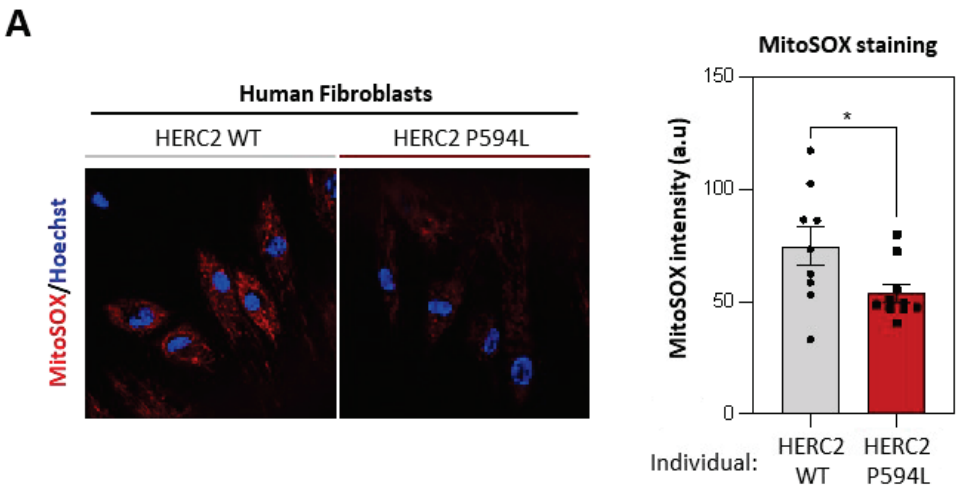

Figure 31. Figure continues on next page ▼

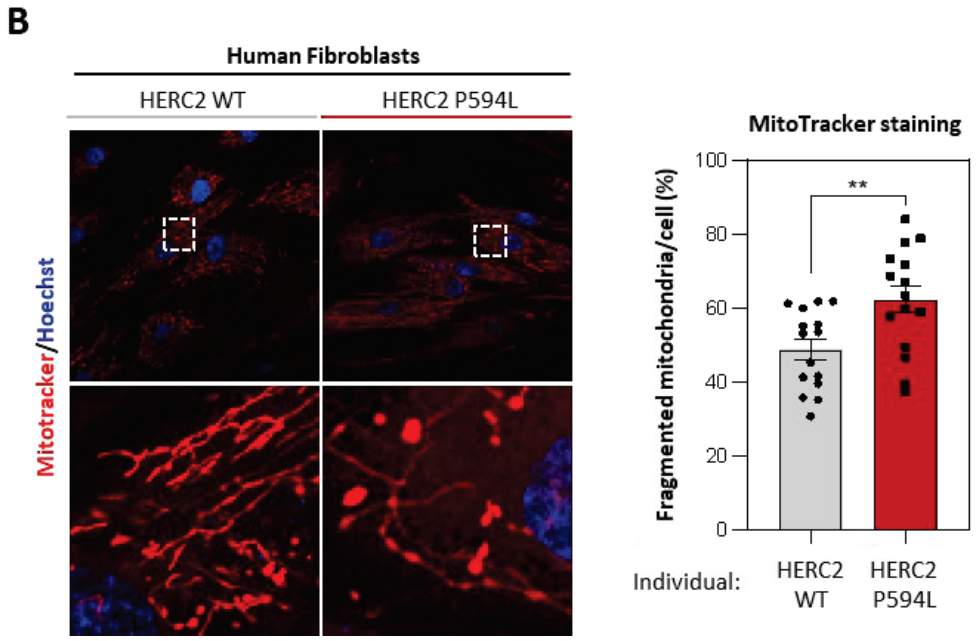

Figure 31. Presence of reductive stress in HERC2 P594L cells. (A) Human skin fibroblasts from an individual with the wild-type HERC2 (HERC2 WT) and the p.Pro594Leu mutant HERC2 variant (HERC2 P594L) were stained for mitochondrial superoxide using MitoSox (red). Nuclei were stained in blue with Hoechst. Red fluorescence intensity per cell was measured, quantified and expressed as arbitrary units (a.u). Each data point represent mean of a different field. **(B)** Mitochondrial morphology was examined in HERC2 WT and HERC2 P594L cells by immunofluorescence microscopy using Mitotracker staining (red). Nuclei were stained in blue with Hoechst. Fragmented mitochondrial percentage per cell was calculated. Each data point represent mean of a different field. Plots represent mean ± standard error of the mean. Representative results are shown from experiments repeated at least three times. Significance levels: ns = no significance * $p \leq 0.05$; ** $p \leq 0.01$.

The role of HERC2 in autophagy and the implication of the USP20-ULK1 axis

Macroautophagy is a catabolic process in which cytoplasmic components are engulfed in autophagosomes and transported to lysosomes for degradation. It is tightly regulated and initiated by the activation of the ULK1 kinase. Then, the cytosolic form of LC3 (LC3-I) is conjugated to phosphatidylethanolamine (PE), forming LC3-II, which is incorporated to the double-membrane structures and aids autophagosome biogenesis. Regarding the implication of HERC2 in autophagy, the HERC2 deficient mouse model *Herc2*$^{+/530}$, showed a specific loss of Purkinje cells with increased number of autophagosomes and lysosomes. On the other hand, the deubiquitinating enzyme USP20, which is targeted to proteasomal degradation by HERC2, has been involved in autophagy initiation through ULK1 stabilisation. Also, sustained p38 activation was reported to enhance the autophagic flux. With all these precedents, we studied patient-derived cells with HERC2 Angelman-like syndrome caused by the HERC2 P594L variant. We observed alteration of LC3-II protein levels, as well as in HERC2 knockdown experiments with other human cells. Experiments with lysosomal inhibitors identified an increased autophagy as the possible cause. Moreover, we demonstrated that HERC2 regulates protein levels of USP20 and ULK1; pull-down experiments showed that HERC2 interacts with USP20; and we observed that p38 activation regulates HERC2-USP20 interaction. Given these evidences, and that autophagy is involved in many neurodegenerative disorders, it is reasonable to think that these mechanisms may be involved in the clinical outcomes of HERC2 Angelman-like syndrome.

HERC2 deficiency dysregulates autophagy

A previous study described a mouse model with targeted inactivation of HERC2 in heterozygosis (*Herc2*$^{+/530}$ mice). Those mice, with approximately one-half lower HERC2 protein levels, showed impaired motor synchronization. Indeed, a specific loss of Purkinje cells was observed and those cells displayed increased number of autophagosomes and lysosomes. This indicated a possible dysregulation of autophagy [54]. However, a direct implication and the precise role of HERC2 in autophagy has not been elucidated to date.

Because previous evidences of the role of HERC2 in autophagy are in a mouse model, we wondered if this regulation also occurs in human cells. Therefore, we studied cells from an individual with the mutant HERC2 P594L variant and analysed protein levels of the standard marker of autophagosomes LC3. Cells with the HERC2 P594L mutation showed

increased protein levels of LC3-I and LC3-II (Figure 32A). This suggested that HERC2 deficiency increases the number of autophagosomes. Since the lipidated form of LC3 (LC3-II) is the one targeted to autophagic membranes, we focused on this form in our further experiments.

Increased protein levels of LC3-II detected by immunoblotting could reflect both an increased or inhibited autophagic flux. Hence, we wondered if the accumulation of LC3-II was due to an upregulation in the formation of autophagosomes (autophagic flux increased) or, contrary, to an impaired autophagolysosome degradation (autophagic flux inhibited). For that, both HERC2 WT and HERC2 P594L fibroblasts were treated with the lysosomal inhibitor ammonium chloride (NH_4Cl) for 4h. As showed before, HERC2 P594L cells showed higher protein levels of LC3-II (Figure 32B, lane 1 compared with lane 2). Treatment with ammonium chloride efficiently inhibited autophagolysosome degradation in HERC2 WT cells, assessed by LC3-II accumulation (Figure 32B, lane 1 compared with lane 3). Interestingly, LC3-II accumulation also occurred in HERC2 P594L cells after incubation with ammonium chloride (Figure 32B, lane 2 compared with lane 4). In addition, the differences in LC3-II protein levels between HERC2 WT and HERC2 P594L were maintained under lysosomal inhibition conditions (Figure 32B, lane 3 compared with lane 4). These data indicated that HERC2 deficiency induces autophagosome formation and subsequently an increase in the autophagic flux.

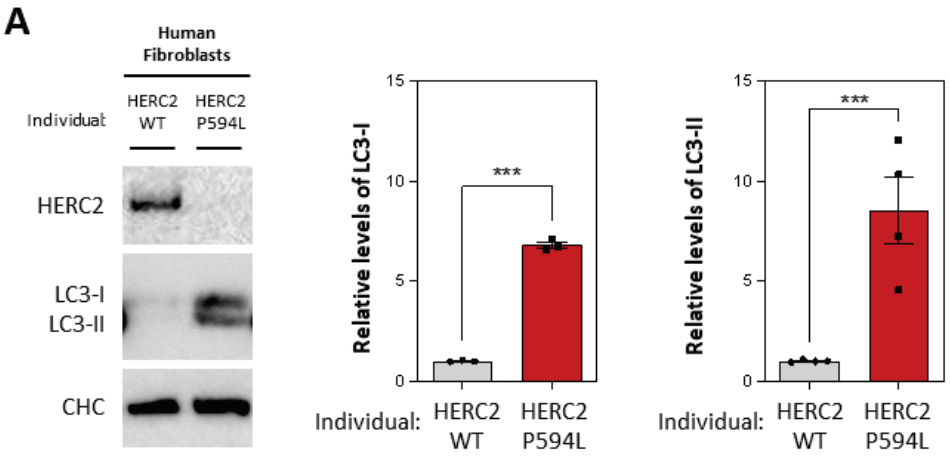

Figure 32. Figure continues on next page ▼

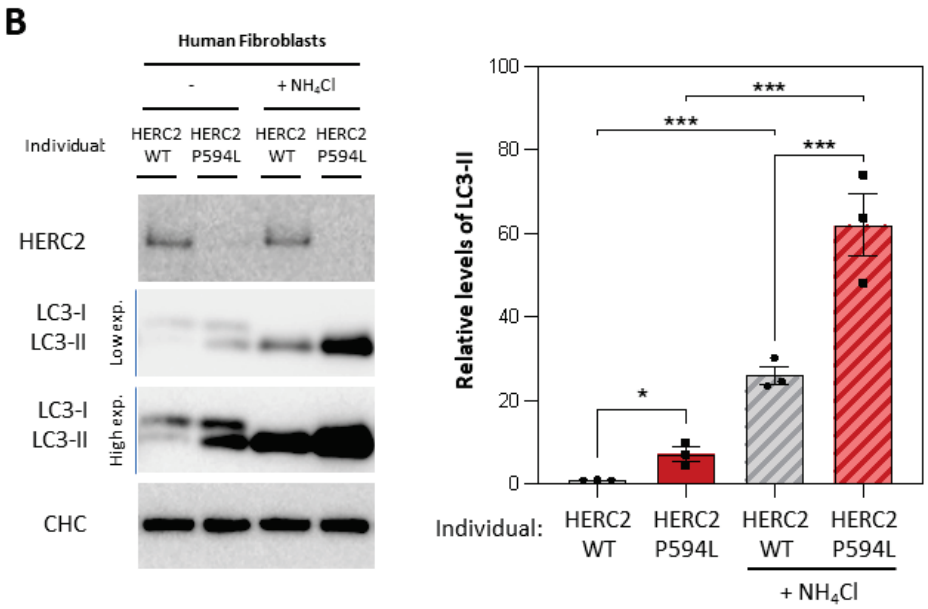

Figure 32. Patient-derived cells with a homozygous mutation in human *HERC2* gene show autophagy dysregulation. (A) We analysed lysates of human skin fibroblasts from an individual with the wild-type HERC2 (HERC2 WT) and the p.Pro594Leu mutant HERC2 variant (HERC2 P594L) by immunoblot, using the indicated antibodies. LC3-I and LC3-II protein levels were quantified and normalized based on clathrin heavy chain (CHC) protein levels. **(B)** HERC2 WT and HERC2 P594L cells were treated with 20 mM NH_4Cl for 4 hours when indicated. Levels of LC3-II were quantified as in (A). The results are expressed relative to the control condition. Plots represent mean ± standard error of the mean. Representative results are shown for experiments repeated at least three times and the data points of each experimental repetition are plotted as single dots. Significance levels: * $p \leq 0.05$; *** $p \leq 0.001$.

Next, to confirm that autophagy dysregulation observed in HERC2 deficient cells was indeed caused by the reduction of HERC2 protein levels, we performed knockdown experiments in HEK 293T cells. Cells were transfected either with a negative control siRNA (NC) or a siRNA against HERC2. Consistently, HERC2 knockdown mimicked the effect observed in HERC2 P594L fibroblasts, with depletion of HERC2 correlating with increased LC3-I and LC3-II protein levels (Figure 33A). Similarly, experiments with ammonium chloride were also replicated and results showed that LC3-II accumulation is due to autophagosome formation upregulation and not to an impaired autophagic flux (Figure 33B).

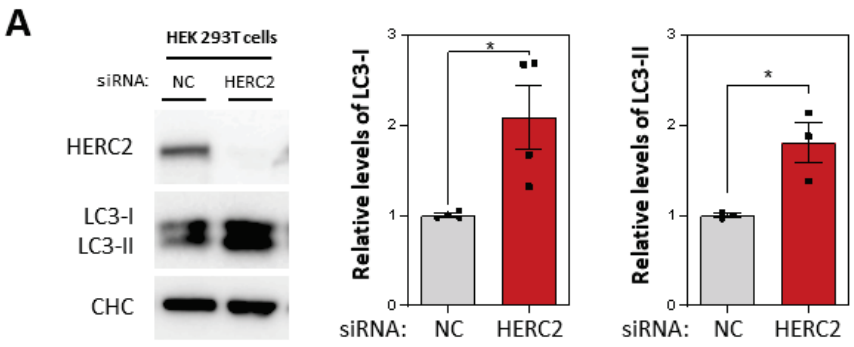

Figure 33. Figure continues on next page ▼

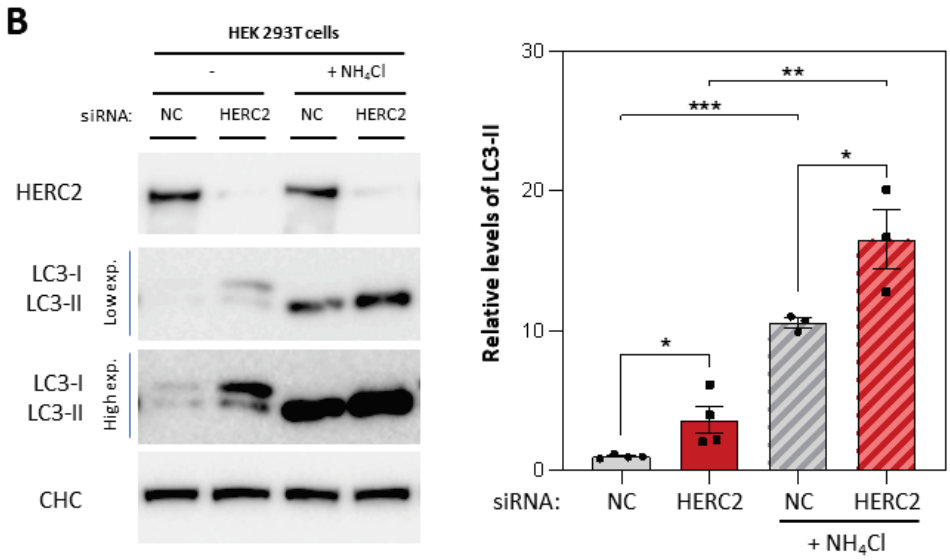

Figure 33. Downregulation of HERC2 induces autophagosome formation. (A) HEK 293T cells were transfected with an siRNA negative control (NC) or an siRNA against HERC2. The indicated protein levels were analysed by immunoblot. Levels of LC3-I and LC3-II proteins were quantified, normalized based on clathrin heavy chain (CHC) protein levels (loading control), and expressed relative to the control condition. **(B)** HEK 293T cells were transfected with a NC siRNA or a siRNA against HERC2. Next, cells were treated with 20 mM NH_4Cl for 4 hours when indicated. Levels of LC3-II were quantified as in (A). Plots represent the mean ± standard error of the mean. Representative results are shown from experiments repeated at least three times and the individual data points are plotted as single dots. Significance levels: * $p \leq 0.05$; ** $p \leq 0.01$; *** $p \leq 0.001$.

HERC2 regulates protein levels of the USP20-ULK1 axis

Previous studies showed that the deubiquitinating enzyme USP20 promotes autophagy initiation through stabilisation of the autophagy-initiation kinase ULK1 [149]. On the other hand, HERC2 was found to regulate the stability of USP20 by promoting its ubiquitylation-mediated proteasomal degradation, with implications on the DNA damage response [43, 44]. However, a direct link between HERC2, USP20 and autophagy has not yet been demonstrated. For this reason, we decided to assess whether the autophagy regulated by HERC2 depends on the USP20-ULK1 axis. First, we studied protein levels of USP20 and ULK1 in HEK 293T cells transfected with the negative control or the HERC2 siRNA. We observed induction of both USP20 and ULK1 protein levels in HERC2-depleted cells (Figure 34A). The same phenomenon was observed in HERC2 P594L cells compared to HERC2 WT cells (Figure 34B). These results support the claim that HERC2 controls USP20 protein levels and indicate a positive correlation between USP20 and its substrate ULK1.

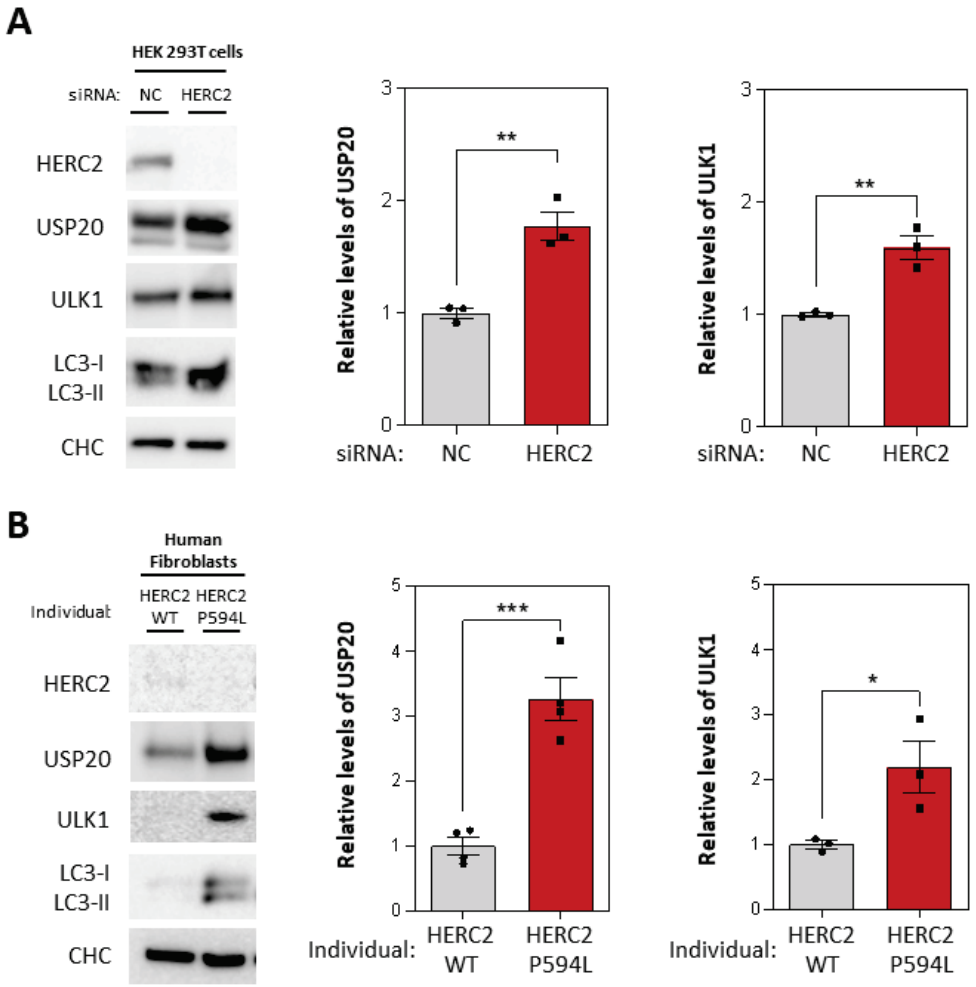

Figure 34. HERC2 depletion correlates with increased protein levels of the deubiquitinating enzyme USP20 and its substrate ULK1. (A) HEK 293T cells were transfected with an siRNA negative control (NC) or an siRNA against HERC2. The indicated protein levels were analysed by immunoblot. USP20 and ULK1 protein levels were quantified and normalized based on CHC protein levels. **(B)** Lysates of HERC2 WT and HERC2 P594L cells were analysed by immunoblot, using the indicated antibodies. USP20 and ULK1 protein levels were quantified as in (A). The results are expressed relative to the control condition. Plots represent mean ± standard error of the mean. Representative results are shown for experiments repeated at least three times and the data points of each experimental repetition are plotted as single dots. Significance levels: * $p \leq 0.05$; ** $p \leq 0.01$; *** $p \leq 0.001$.

Regulation of autophagy dependent on HERC2 differs in tumour-derived cell lines

Subsequently, we wondered if the effect observed in patient-derived fibroblasts and the non-tumorigenic human kidney 293T cell line (HEK 293T), would replicate in human tumour cell lines such as the osteosarcoma U2OS cell line or the cervical cancer HeLa cell line. Results showed increased USP20 protein levels after HERC2 silencing in both U2OS and HeLa cell lines. However, the effect on LC3-II was the opposite of what was previously observed with non-tumorigenic cells. In these cancer cell lines, LC3-II protein levels were reduced after HERC2 depletion (Figure 35A-B). The decrease in LC3-II may indicate a lower autophagosome

production due to an impaired autophagy or an increased autophagic flux, which boosts the fusion with lysosomes and the subsequent autophagosomes degradation. To determine which of the scenarios it was, U2OS were transfected with the NC or the HERC2 siRNA and then were treated with the lysosomal inhibitors chloroquine (CQ) or ammonium chloride (NH_4Cl) for 4 hours. Levels of LC3-II were accumulated after treatment with both inhibitors. Interestingly, in presence of the inhibitors, no differences in LC3-II protein levels were observed between control and HERC2-depleted cells. That is, lysosome inhibition rescued LC3-II protein levels in HERC2 silenced cells (Figure 35C). This indicated that in these cells, downregulation of HERC2, increases the autophagic flux. To confirm these findings, we used an mCherry-YFP-LC3 reporter. The YFP tag is acid-sensitive while the mCherry tag is acid-insensitive. Thus, the double tag enables to monitor the autophagic flux. In autophagosomes both tags emit fluorescent light. However, fusion of autophagosomes to lysosomes causes acidification that triggers loss of YFP signal [128]. Immunofluorescence analysis revealed an increased number of red LC3 puncta (autolysosomes), indicating increased autophagic flux, in HERC2-depleted cells (Figure 35D).

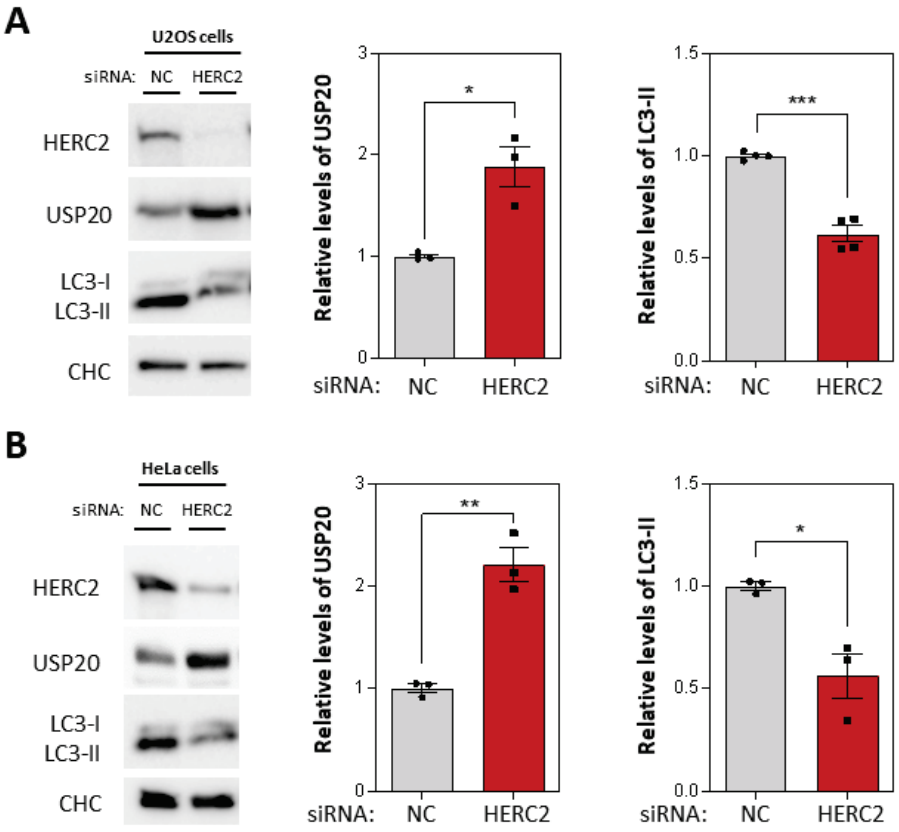

Figure 35. Figure continues on next page ▼

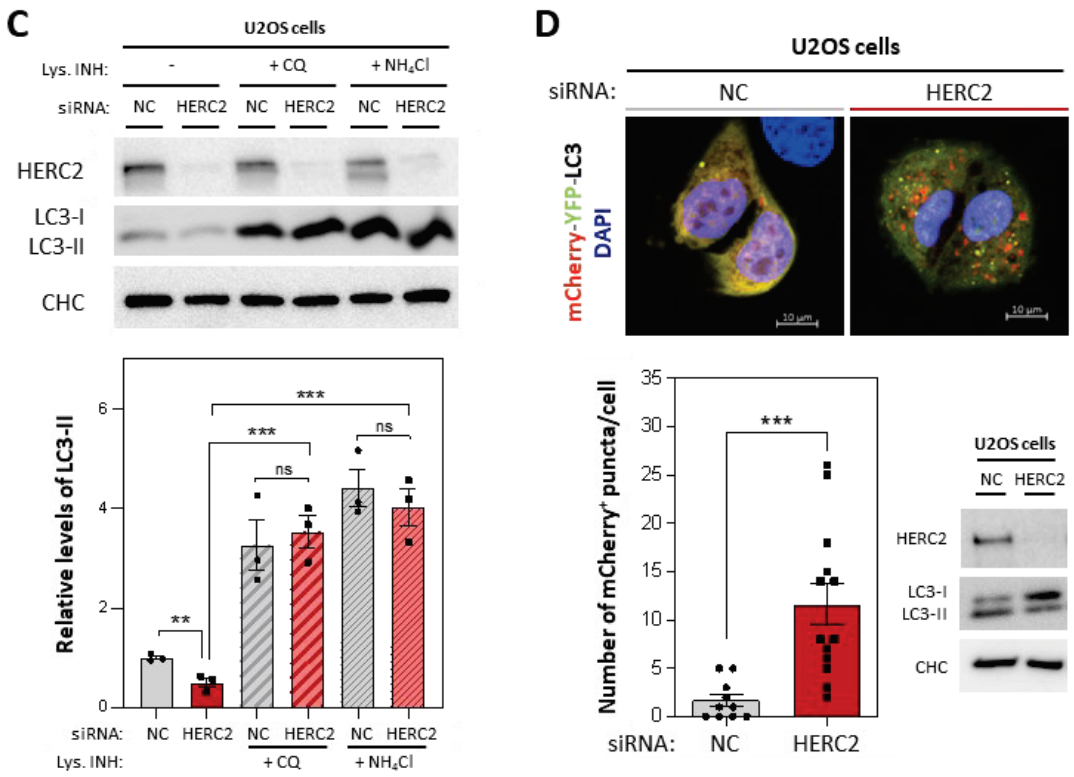

Figure 35. HERC2 depletion in tumour-derived cell lines. (A-B) U2OS (A) and HeLa (B) cells were transfected with an siRNA negative control (NC) or an siRNA against HERC2. The indicated protein levels were analysed by immunoblot. USP20 and LC3-II protein levels were quantified and normalized based on CHC protein levels. **(C)** U2OS cells were transfected as in (A). Then, cells were treated with 100 µM chloroquine (CQ) or 20 mM NH_4Cl for 4 hours when indicated. LC3-II protein levels were quantified as in (A). **(D)** Immunofluorescence analysis of negative control (NC) and HERC2-depleted U2OS cells expressing mCherry-YFP-LC3 reporter. Bar = 10 µm. The autophagic flux was determined by quantification of the number of red dots, performed by subtracting the number of green puncta from red puncta. Each data point represent mean of a different field. The results are expressed relative to the control condition. Plots represent mean ± standard error of the mean. Representative results are shown from experiments repeated at least three times and the individual data points are plotted as single dots. Significance levels: ns = no significance; * $p \leq 0.05$; ** $p \leq 0.01$; *** $p \leq 0.001$.

In conjunction these results suggested that in tumour-derived cell lines such as U2OS and HeLa cells, HERC2 depletion causes an increase in the autophagic flux but not in autophagosome formation, indicating some differences in the molecular mechanisms between tumour and non-tumorigenic cells. Given these differences we decided to focus our study on the non-tumorigenic cells.

Phosphorylation of p38 regulates HERC2-USP20 interaction and modulates autophagy

To delve deeper into the molecular mechanisms involved in the regulation of autophagy dependent on HERC2, first we wanted to dissect whether HERC2 and USP20 proteins interact in our model of study and if LC3 protein is also present in this complex. For

this reason HEK 293T cells were transfected with a control plasmid (Flag-CTL) and a plasmid encoding HERC2 protein fused with the Flag epitope (Flag-HERC2). Then, a pull-down with a Flag-Trap resin was performed. Results confirmed protein interaction between HERC2 and USP20, while no interaction was detected with HERC2 and LC3 (Figure 36A).

Given our previous results showing that HERC2 modulates p38 phosphorylation, and that this kinase has been identified as a positive regulator of autophagosome formation and autophagic flux [128], we wondered whether p38 signalling is involved in the autophagy dependent of HERC2 and if it is related with the USP20-ULK1 axis. In first place, we analysed USP20 protein sequence and performed a computational prediction of phosphorylation sites (p-sites) by p38α kinase. For that, we obtained the amino acid sequence of human USP20 from UniProt (https://www.uniprot.org/) and used the algorithm Group-based Prediction System 5.0 (GPS 5.0) (http://gps.biocuckoo.cn/) [145]. The algorithm identified 16 putative phosphorylation sites by p38α. Of these, 13 were found within the HERC2 interacting region (amino acids 129 to 688) [44] (Figure 36B). These data led us to hypothesize that phosphorylation of USP20 by p38 might affect the interaction between USP20 and HERC2. To answer this, HEK 293T were transfected with Flag-CTL, Flag-HERC2 or with Flag-HERC2 plus MKK6(glu) plasmid. The MKK6(glu) construct encodes a constitutively active MKK6 protein that strongly stimulates p38 phosphorylation. Next, a Flag pull-down was performed. Results showed that HERC2-USP20 interaction was reduced when p38 phosphorylation was induced by MKK6(glu) overexpression (Figure 36C). This indicated that a complex regulation mechanism involving p38 signalling might be modulating HERC2-USP20 interaction.

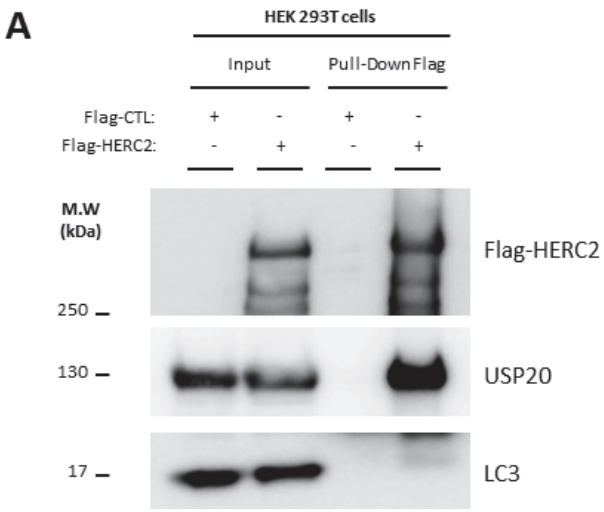

Figure 36. Figure continues on next page ▼

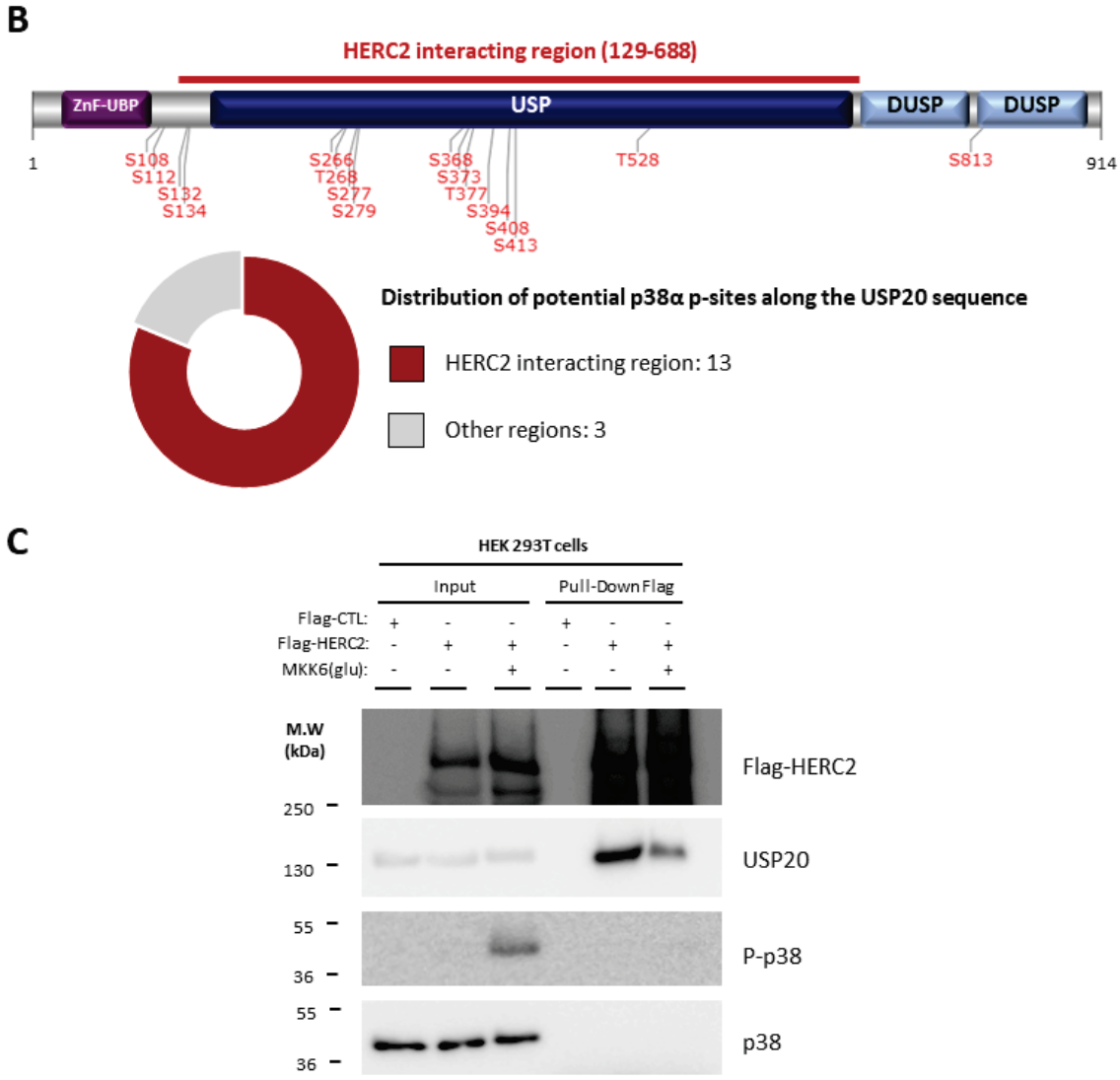

Figure 36. HERC2 interacts with USP20 and this interaction is modulated by p38 phosphorylation. (A) HEK 293T cells were transfected with a control plasmid (Flag-CTL) or a plasmid encoding HERC2 protein tagged with Flag epitope (Flag-HERC2). Cell lysates were pulled-down using Flag resin. Inputs and proteins retained in the resin (Pull-Down Flag) were analysed by immunoblotting with antibodies against the indicated proteins. **(B)** Prediction of USP20 phosphorylation sites (p-sites) by p38α using the algorithm Group-based Prediction System 5.0 (GPS 5.0) (http://gps.biocuckoo.cn/). Predicted p-sites and its position are shown in light red. Different USP20 domains are indicated (ZnF-UBP, USP, DUSP). HERC2 interacting region is indicated in dark red. The graph shows the number of p-sites located within (dark red) or outside (grey) the region of interaction with HERC2 [44]. **(C)** HEK 293T were transfected with Flag-CTL, Flag-HERC2 or Flag-HERC2 plus MKK6(glu) plasmids. Pull-down was performed as in (A). The indicated protein levels were analysed by immunoblot. Representative results are shown from experiments repeated at least three times.

Knowing that HERC2 interacts with USP20 and, according to a previous study, promotes its ubiquitylation-mediated proteasomal degradation [43, 44], we wondered if the decrease in HERC2-USP20 interaction observed after p38 phosphorylation correlates with increased protein levels of USP20. If HERC2 is targeting USP20 to proteasomal degradation, the fact that the interaction of USP20 with its ubiquitin ligase is prevented might be

protecting USP20 from ubiquitylation and subsequent degradation. To check this, HEK 293T cells were transfected with a control plasmid (CTL) or with a MKK6(glu) plasmid. Expression of MKK6(glu) strongly activated p38 assessed by its phosphorylation. Interestingly, protein levels of USP20 were upregulated in MKK6(glu) expressing cells. In addition, LC3-II protein levels were also higher in those cells (Figure 37). These data suggested that p38 phosphorylation might prevent HERC2-USP20 interaction, thus protecting USP20 from its ubiquitination-dependent degradation and stabilizing it. This mechanism seems to be implicated in the regulation of autophagy, since it correlated with increased protein levels of the autophagosome marker LC3-II. However, further research is needed to fully unravel this complex regulatory mechanism.

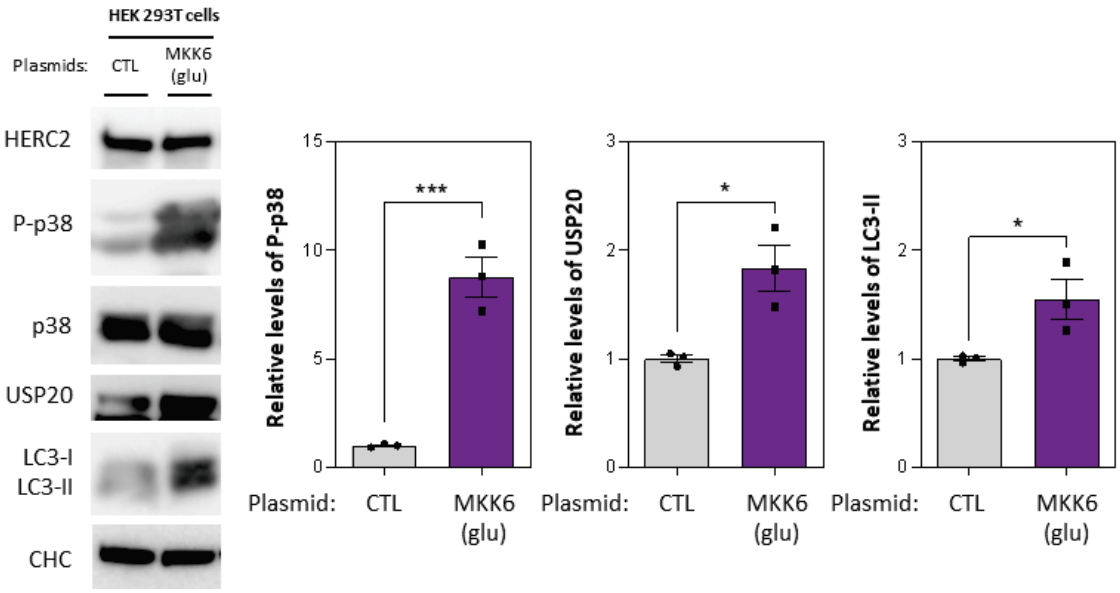

Figure 37. Phosphorylation of p38 regulates USP20 and LC3-II protein levels. HEK 293T were transfected with a control plasmid (CTL) or a plasmid encoding **a** constitutively active MKK6 protein (MKK6(glu)). Cell lysates were analysed by immunoblot, using the indicated antibodies. Levels of phosphor-p38 (P-p38) were quantified, normalized based on total p38 protein levels, and expressed relative to the control condition. Levels of USP20 and ULK1 were also quantified and normalized based on CHC protein levels. The results are expressed relative to the control condition. Plots represent mean ± standard error of the mean. Representative results are shown for experiments repeated at least three times and the data points of each experimental repetition are plotted as single dots. Significance levels: * $p \leq 0.05$; *** $p \leq 0.001$.

Identification of ubiquitylated proteins regulated by HERC2 applying a proteomic approach

Protein ubiquitylation is a highly conserved post-translational modification that regulates different cellular processes such as proteasomal degradation, protein trafficking, cell cycle progression and DNA repair. Ubiquitin E3 ligases are a critical component of the ubiquitylation cascade determining substrate specificity. Therefore, the identification of E3 ligases' substrates is key to infer its physiological functions. Here we applied the ^{bio}Ub approach to identify potential HERC2 ubiquitylation substrates, combining gene overexpression and proteomic analysis. First, cells were provided with a biotinylatable version of ubiquitin (^{bio}Ub). Next, overexpression of HERC2 protein was used to increase its ubiquitin ligase activity, leading to an increase of the ubiquitylation of its substrates. Using avidin beads, we were able to isolate the ubiquitylated proteins, which were then identified and quantified by mass-spectrometry analysis. By determining which ubiquitylated proteins were enriched in cells overexpressing HERC2 we were able to identify possible HERC2 substrates. Results showed that HERC2 regulates ubiquitylation of several proteasomal proteins such as PSMC5 and PAAF1. PSMC5 is one of the proteins that forms the subunit base of the 19S regulatory particle of the proteasome, and PAAF1 is its cognate chaperone, which regulates the correct assembly of PSMC5 with the other subunit components. The other large HERC family member, HERC1, had already been identified as quality-control factor that monitors failures during proteasome assembly by detecting and ubiquitylating unassembled PSMC5. Thus, HERC2 may play a similar role, which points to large HERCs as important regulators of the proteasome assembly pathway.

Overexpression of HERC2 protein in HEK 293T cells for the identification of ubiquitylation substrates

In order to identify HERC2 putative ubiquitylation substrates we performed the ^{bio}Ub approach [71], combining gene overexpression and proteomics analysis. First, we transfected HEK 293T cells with a control plasmid (Flag-CTL), a plasmid encoding wild-type HERC2 protein (HERC2 WT) or a plasmid encoding an HERC2 variant with a mutation in its catalytic cysteine, which impairs its ubiquitin ligase activity (HERC2 C4762S). Lysates were analysed by western blot and results showed a significant overexpression of HERC2 protein in HERC2 WT cells compared to control cells. Interestingly, a greater overexpression was obtained with the transfection of the mutated form, being significantly higher than the one achieved with the

HERC2 WT construct (Figure 38). One possible explanation is that HERC2 regulates its own ubiquitylation-mediated proteasome degradation. Thus, transfection of a catalytically inactive form such as HERC2 C4762S, would exhibit greater stability. In conjunction, these results confirmed that HERC2 overexpression is achieved in HEK 293T cells and validated this model to proceed with the proteomic analysis.

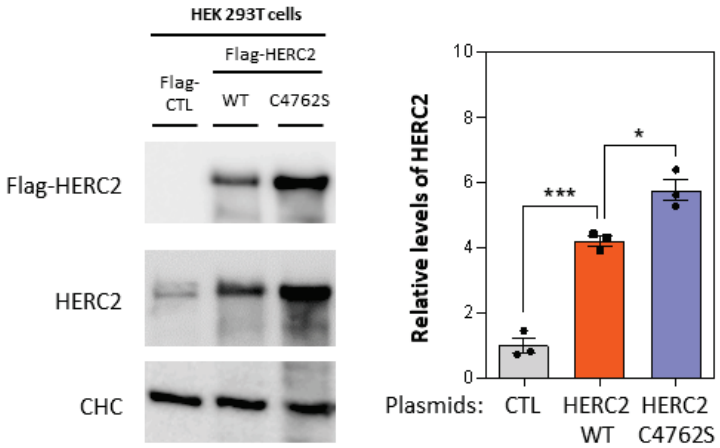

Figure 38. Expression of HERC2 plasmids in HEK 293T cells. HEK 293T cells were transfected with a negative control plasmid (Flag-CTL), a plasmid encoding wild-type HERC2 protein (Flag-HERC2 WT) or a plasmid encoding a catalytically inactive form of HERC2 (Flag-HERC2 C4762S). The indicated proteins were analysed by immunoblot. The results are expressed relative to the control condition. Plots represent mean ± standard error of the mean. Representative results are shown from experiments repeated at least three times and the individual data points are plotted as single dots. Significance levels: * $p \leq 0.05$; *** $p \leq 0.001$.

Identification of ubiquitylated proteins regulated by HERC2 using mass spectrometry analysis

Higher levels of the HERC2 WT ubiquitin ligase in HEK 293T cells should result in an enhanced ubiquitylation of HERC2 substrates. As a negative control condition we used HEK 293T cells overexpressing the HERC2 C4762S mutant variant, in which the increase in ubiquitylation should not occur due to the inactivating mutation. Therefore, quantitative proteomic experiments were carried out to decipher the ubiquitylated proteome from both HERC2 WT- and HERC2 C4762S-overexpressing cells and, hence, detect those proteins whose ubiquitylation is regulated by HERC2.

To do so, cells were transfected with the corresponding HERC2 plasmid and supplied with a biotinylated version of ubiquitin by transfection of the ^{bio}Ub construct, which encodes a precursor polypeptide composed of six biotinylatable versions of ubiquitin and the biotin ligase enzyme of *E. coli*, BirA. Once this precursor is expressed in cells, it is digested by

endogenous DUBs. Then, ubiquitins and BirA are released and the BirA enzyme is able to label each ubiquitin with a biotin molecule. After that, HEK 293T cells were ready for the isolation of the ubiquitylated material, which was analysed by mass spectrometry.

In brief, we subjected triplicate samples of HERC2 WT and HERC2 C4762S-overexpressing cells to biotin pulldown using Avidin-agarose. Then, the pulldowns were analysed by liquid chromatography with tandem mass spectrometry (LC-MS/MS). This allowed us to isolate, detect and quantify ubiquitylated proteins in HEK 293T cells overexpressing HERC2 WT and HERC2 C4762S proteins.

A high reproducibility across the biological replicas of the HERC2 WT samples was observed, as illustrated by the Venn diagrams. Of a total of 3541 identified proteins, 2975 were commonly found in the three replicates. The same high reproducibility occurred with the replicas of the HERC2 C4762S negative control samples since of a total of 3601 identified proteins, 3005 were found in the three replicates. In conjunction, the overlap between the aggregated values of the HERC2 WT and HERC2 C4762S samples was also high. In detail, a total of 3677 proteins were identified in the experiment, of which 3465 were found both in wild-type and C4762S samples (Figure 39A).

Moreover, abundance correlation of the quantified proteins, determined using label-free quantification (LFQ) intensities, also displayed a high correlation across the samples, with Pearson correlation coefficients > 0.95 (Figure 39B).

Altogether, these data showed highly reproducible results and validated our approach, which prompted us to further analyse the results obtained. Thoroughly, the enrichment of ubiquitylated proteins upon HERC2 WT overexpression was determined by Student's t-test. Proteins that showed a significant increase of their LFQ intensity relative to control samples ($\log_2$ HERC2 WT LFQ/HERC2 C4762S LFQ ≥ 1, p-value < 0.05) were considered to be more ubiquitylated. Of these proteins, only those that were identified with at least two unique peptides were taken into account. In addition, we only considered the proteins that were quantified (had an LFQ intensity value) in the three WT samples, or in 2 WT and 2 C4762S samples. Proteins that fulfilled all these criteria were classified as HERC2 ubiquitylation putative substrates. The same criteria were used to classify the less ubiquitylated proteins.

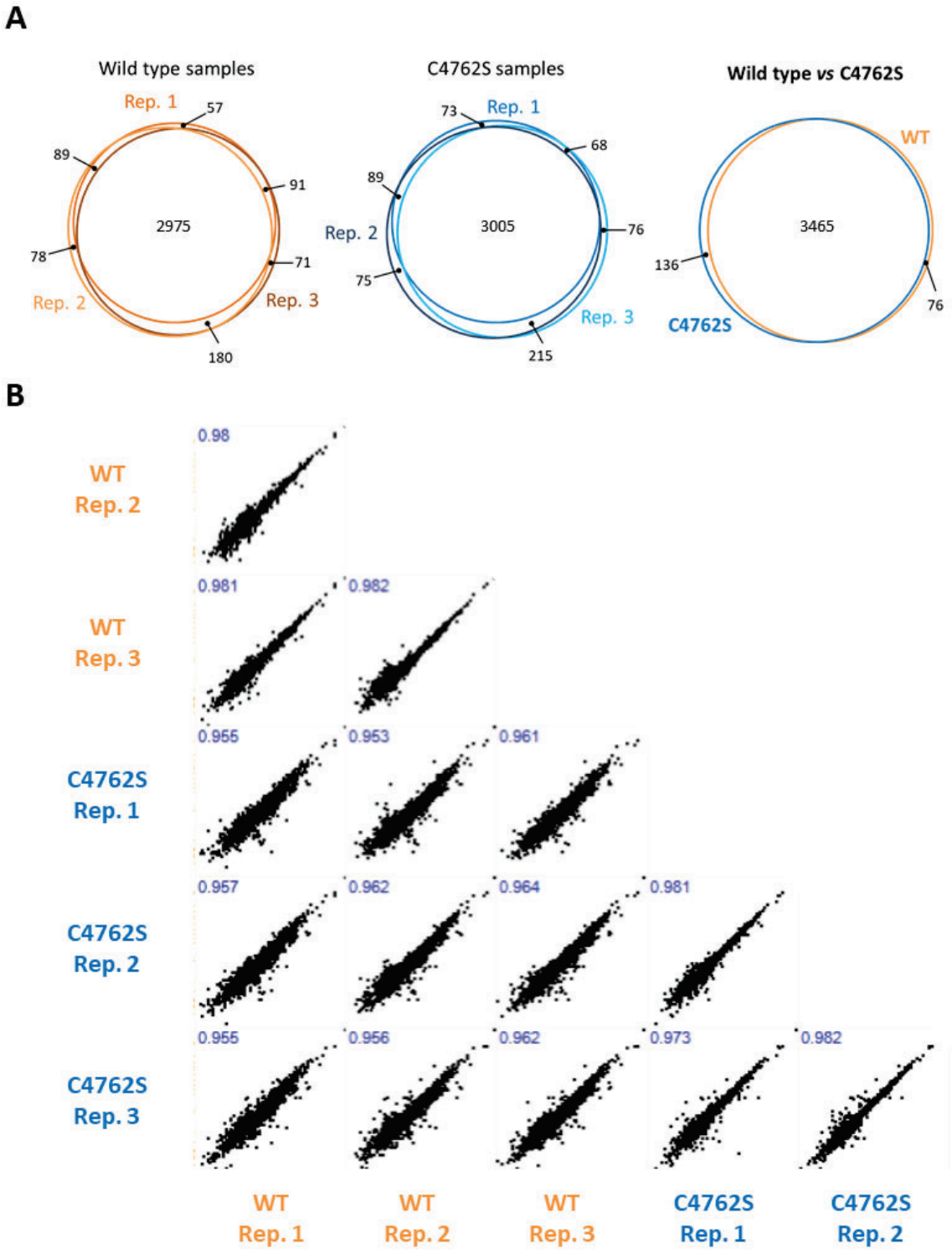

Figure 39. Reproducibility of the mass spectrometry analysis. (A) Overlap between proteins identified in HERC2 wild type (depicted in orange) and HERC2 C4762S samples (depicted in blue). Venn diagrams showing the overlap of the proteins identified among the three replicas of each condition, as well as between both conditions are shown. **(B)** Correlation graphs of label free quantification (LFQ) intensities (in $\log_2$ scale) of proteins identified across the different samples. Pearson's correlation coefficient is shown in blue.

Endogenous ubiquitin (Ub), ^{bio}Ub levels, and the relative abundance of the majority of the proteins quantified did not change significantly. This included avidin and proteins known to be endogenously conjugated with biotin (MCCC1, PCCA, PC, HLCS, ACACA). These act as internal controls to determine the correct processing of the biotin pull-downs (Figure 40A, marked in blue).

Out of 3677 proteins quantified, 139 proteins were found significantly enriched in HERC2 WT cells relative to HERC2 C4762S cells (Figure 40A, marked in green; and Table 13). Some of them had already been identified or suggested as HERC2 substrates, as is the case of NEURL4 [63]. In addition, NEURL4-HERC2 complex was found to participate in the ubiquitin-dependent regulation of centrosome architecture [63], and in agreement with this, we also identified some centrosomal proteins such as CEP41 and CEP170, which could represent novel HERC2 substrates. On the other hand, we also observed some proteins that had previously been identified in other proteomics studies as HERC2-binding partners. These are proteins of the eukaryotic initiation factor complex eIF3 and eIF4 (EIF3A, EIF3J, EIF4E2) [103, 150, 151]. Besides, the previously identified HERC2 substrate BRCA1 [36], and also C-RAF (RAF1), which we identified and described in the first part of the results of this doctoral thesis, also appeared as more ubiquitylated proteins, although did not cross the statistical significance threshold. Altogether, the identification of the mentioned proteins validated our experimental approach (Figure 40A, marked in purple). Interestingly, HERC2 appeared to be more ubiquitylated in HERC2 WT-overexpressing cells (Figure 40A, marked in blue). This indicated a presumed auto-ubiquitylation mechanism.

On the contrary we also found 31 proteins which ubiquitylation levels were reduced in HERC2 WT cells compared to HERC2 C4762S cells (Figure 40A, marked in red; and Table 14). One possible explanation is that HERC2 regulates ubiquitylation of other ubiquitin ligases or deubiquitylating enzymes (DUBs) affecting their activity. In this way, the less ubiquitylated proteins that were detected could be the substrates of these ubiquitin ligases or DUBs.

The proteomic approach we applied does not particularly enrich for ubiquitylation sites, yet we also identified some peptides containing the characteristic GlyGly remnant of ubiquitin. That is, the last two Glycines of ubiquitins that are left covalently attached to the substrates after trypsin digestion of the proteins. This, allowed us to identify the precise

amino acid position of the substrate where ubiquitylation occurred. We included a table indicating the detected ubiquitylation sites of those proteins positively regulated by HERC2 (Table 15).

With the identified putative substrates of HERC2 we performed a STRING analysis (http://string-db.org/) to evaluate functional protein association networks and hence identify functional enrichments of any biological or cellular function. The analysis showed 5 different connectivity groups: proteasome (green), microtubule associated complex (red), t-RNA biosynthesis (blue), AP-membrane coat (yellow) and centrosome (purple), being the proteasome group the most evident (Figure 40B). These results suggested that HERC2 regulates ubiquitylation of several proteins related with the proteasome assembly pathway such as PSMC1, PSMD10, PSMC5 and PAAF1, among others.

Next, we decided to validate some of the results obtained. We decided to focus on validating HERC2 auto-ubiquitylation and the apparent role of HERC2 in proteasome assembly.

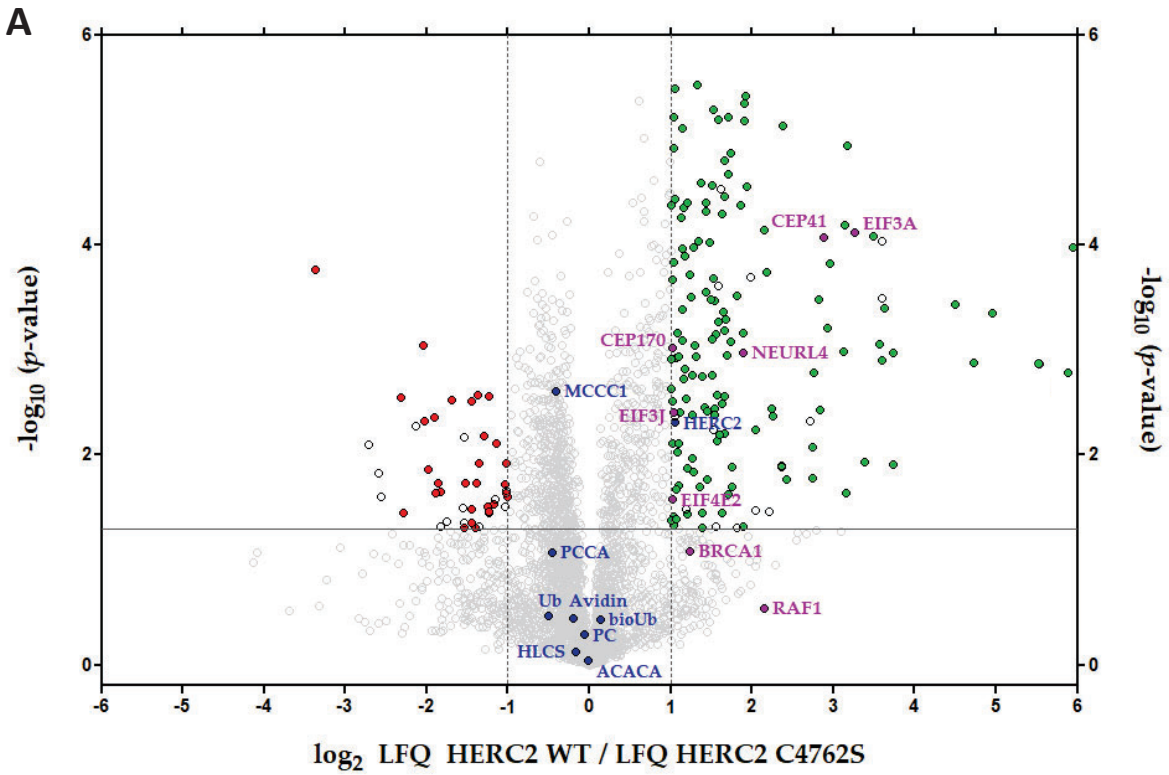

Figure 40. Figure continues on next page ▼

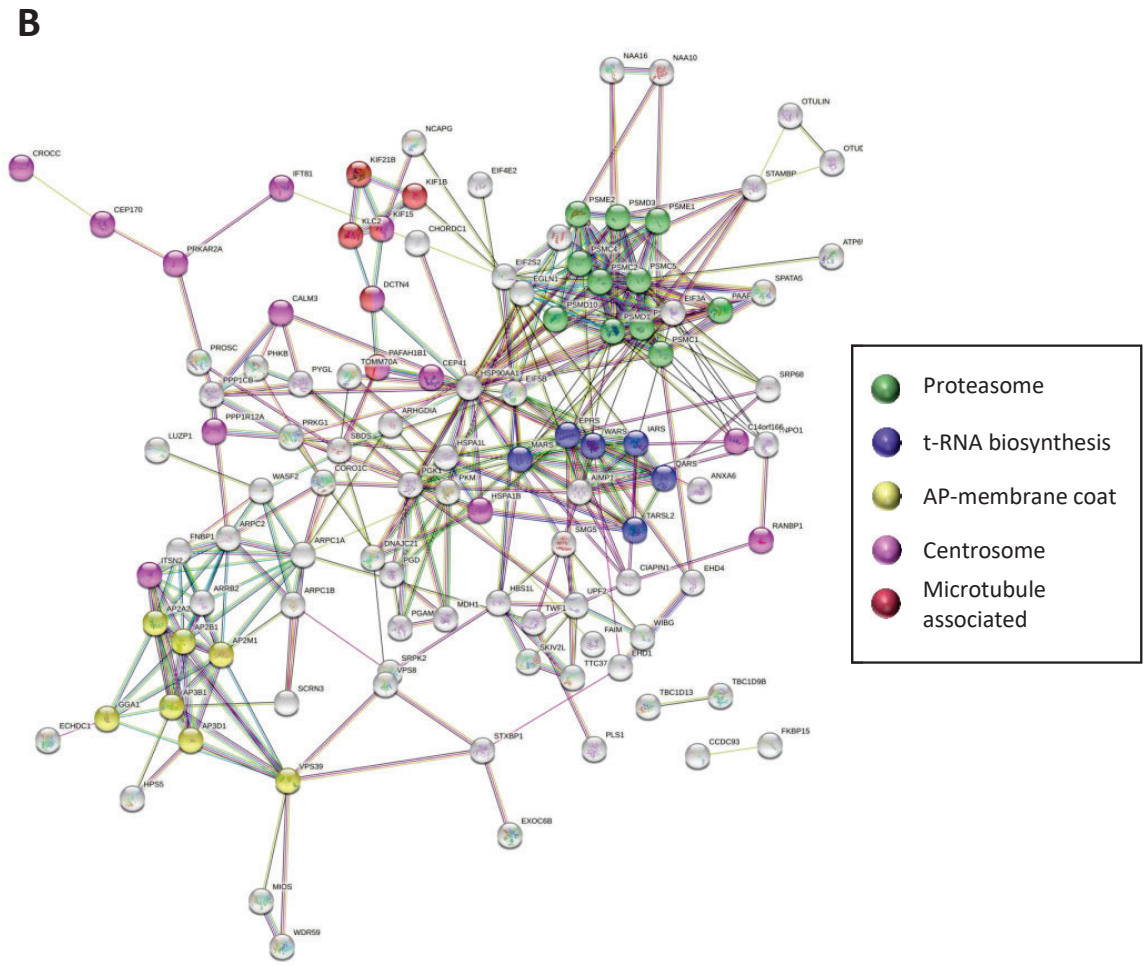

Figure 40. Identification of ubiquitylated proteins regulated by HERC2 using mass spectrometry. (A) Volcano plot shows differentially ubiquitylated proteins upon HERC2 WT overexpression, relative to control samples (HERC2 C4762S). Abundance of each individual protein was determined by their label free quantification (LFQ) intensities. The LFQ WT/C4762S ratios (log_2 scale) and the t-test p-values ($-log_{10}$ scale) are displayed in the X and Y axis, respectively. The threshold for statistical significance (p-value < 0.05) is indicated with a horizontal grey line, while vertical grey lines depict a > 1 fold increase or decrease of the ubiquitylated levels upon HERC2 WT overexpression. Proteins with a two-fold increase or reduction of their ubiquitination levels upon HERC2 WT overexpression are shown in green and red, respectively (log_2 LFQ WT/LFQ C4762S > 1 marked in green; log_2 LFQ WT/LFQ C4762S < -1 marked in red). Previously described or suggested substrates are shown in purple. HERC2, endogenously biotinylated proteins (ACACA, MCCC1, PC, PCCA, HLCS), ubiquitin (Ub) and avidin (AVD) are coloured in blue. **(B)** STRING analysis (http://string-db.org/) shows functional connectivity of the putative substrates of the HERC2 ubiquitin ligase identified by mass spectrometry. Analysis shows 5 different connectivity groups: microtubule associated complex (red), proteasome (green), t-RNA biosynthesis (blue), AP-membrane coat (yellow), centrosome (purple).

HERC2 regulates its own ubiquitylation

As beforementioned, transfection of the HERC2 C4762S construct resulted in a higher protein expression compared with the transfection of the wild type form (Figure 38). This occurred although we transfected equal amounts of plasmid in each condition. Besides, we identified HERC2 protein as more ubiquitylated in HERC2 WT-overexpressing cells in the proteomic analysis (Figure 40A, Table 13 and Table 15). Given these findings, we

hypothesized that HERC2 is able to regulate its own protein levels through an auto-ubiquitylation mechanism. To verify this, we performed an ubiquitylation assay. HEK 293T cells were transfected with negative control (Flag-CTL), HERC2 WT or HERC2 C4762S plasmids. In addition, cells were supplied with His-Tagged ubiquitin. After incubation with the proteasome inhibitor MG132, cells were lysed and incubated with Ni-NTA agarose resin to pull-down His-tagged ubiquitin molecules and the proteins to which they were attached. The results showed a smear of high molecular weight HERC2 indicating much greater HERC2 ubiquitylation with wild-type HERC2 overexpression. These results demonstrated that HERC2 regulates its own ubiquitylation (Figure 41). Further experiments are needed to confirm that this ubiquitylation serves as a proteasome-dependent degradation signal and to fully understand the physiological relevance of this mechanism.

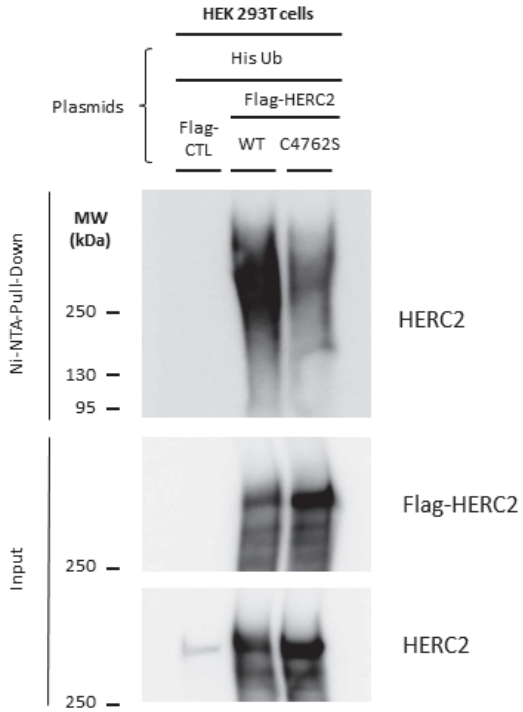

Figure 41. HERC2 regulates its own ubiquitylation. HEK 293T cells were transfected with the indicated plasmids. After 48 hours, cells were incubated for 6h with MG132 (10 µM). Ubiquitylated proteins were purified using a Ni-NTA-agarose resin. Inputs and pull-downs were analysed by immunoblotting with antibodies against the indicated proteins. Representative results are shown from experiments repeated at least three times.

HERC2 interacts with the proteasomal proteins PSMC5 and PAAF1

HERC1, the other large HERC family member, had already been associated with the proteasome assembly pathway in a previous study [26]. Specifically, it was described as a quality-control factor that monitors failures during proteasome assembly by identifying and ubiquitylating unassembled PSMC5 by its cognate assembly chaperone PAAF1 [26]. The 26S

protease regulatory subunit 8 (PSMC5) is one of the essential subunits that form the base sub complex of the 19S regulatory particle of the proteasome complex. PAAF1 is its associated chaperone, which serves as a scaffold and fine-tunes the assembly process with the other subunits [152].

Because of this precedent and the fact that HERC2 was found to regulate ubiquitylation of a bunch of proteasomal proteins, including PSMC5 and PAAF1, we wanted to validate its possible role in the regulation of proteasome assembly. To do so, HEK 293T cells were transfected with a plasmid encoding Flag-tagged PAAF1 protein (Flag-PAAF1). Then, we transfected plasmids encoding either GFP-tagged PSMC5 protein (GFP-PSMC5) or the fluorescent protein GFP as a negative control. Pull-downs with a GFP-Trap resin were performed. Results showed that PSMC5 interacted with PAAF1 and HERC1, confirming previously published data (Figure 42A). Remarkably, we also detected interaction of PSMC5 with HERC2, suggesting that HERC2 also recognises PSMC5-PAAF1 protein complexes (Figure 42B). These data suggested that HERC2 may also act, like HERC1 does, as a quality-control factor of the proteasome assembly pathway. Nevertheless, more experimental evidence is needed to establish this relationship.

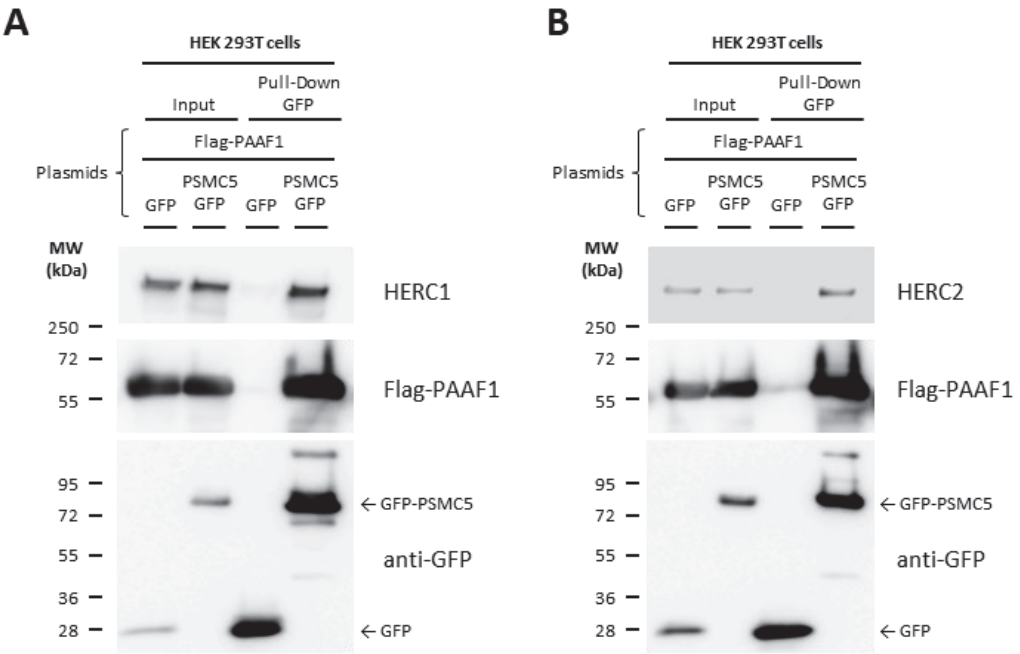

Figure 42. Large HERC proteins interact with PSMC5-PAAF1 complex. HEK 293T cells were transfected with the indicated plasmids. Cell lysates were pulled-down using GFP-Trap resin. Inputs and proteins retained in the resin (Pull-Down GFP) were analysed by immunoblotting with antibodies against the indicated proteins. Representative results are shown from experiments repeated at least three times.

Table 13. Ubiquitylated proteins positively regulated by HERC2.

Gene names	Protein names	[1]FC
PHKB	Phosphorylase b kinase regulatory subunit beta	5.95
VPS8	Vacuolar protein sorting-associated protein 8 homolog	5.89
LUZP1	Leucine zipper protein 1	5.53
PPP1R12A	Protein phosphatase 1 regulatory subunit 12A	4.95
STXBP1	Syntaxin-binding protein 1	4.73
SRPK2	SRSF protein kinase 2;SRSF protein kinase 2 N-terminal;SRSF protein kinase 2 C-terminal	4.50
WASF2	Wiskott-Aldrich syndrome protein family member 2	3.74
CORO1C	Coronin-1C	3.74
TARSL2	Probable threonine--tRNA ligase 2, cytoplasmic	3.63
UPF2	Regulator of nonsense transcripts 2	3.60
GGA1	ADP-ribosylation factor-binding protein GGA1	3.57
SPATA5	Spermatogenesis-associated protein 5	3.49
MTMR3	Myotubularin-related protein 3	3.39
EIF3A	Eukaryotic translation initiation factor 3 subunit A	3.26
PGAM1	Phosphoglycerate mutase 1	3.17
PSME2	Proteasome activator complex subunit 2	3.15
JAM3	Junctional adhesion molecule C	3.14
MAP1A	Microtubule-associated protein 1A;MAP1A heavy chain;MAP1 light chain LC2	3.12
GCC1	GRIP and coiled-coil domain-containing protein 1	2.96
PDLIM1	PDZ and LIM domain protein 1	2.93
CEP41	Centrosomal protein of 41 kDa	2.89
PPP1CB	Serine/threonine-protein phosphatase PP1-beta catalytic subunit	2.84
MIOS	WD repeat-containing protein mio	2.82
CRYZ	Quinone oxidoreductase	2.76
DNAJC21	DnaJ homolog subfamily C member 21	2.75
HIBCH	3-hydroxyisobutyryl-CoA hydrolase, mitochondrial	2.75
CALM	Calmodulin-1	2.42
EPRS	Bifunctional glutamate/proline--tRNA ligase;Glutamate--tRNA ligase;Proline--tRNA ligase	2.38
VPS39	Vam6/Vps39-like protein	2.36
MSTO1	Protein misato homolog 1	2.26
WIBG	Partner of Y14 and mago	2.24
TBC1D13	TBC1 domain family member 13	2.18
PSME1	Proteasome activator complex subunit 1	2.16
OTUD3	OTU domain-containing protein 3	2.05
PSMD10	26S proteasome non-ATPase regulatory subunit 10	1.94
HSP90AA1	Heat shock protein HSP 90-alpha	1.93
PSMC4	26S protease regulatory subunit 6B	1.91
MARS	Methionine--tRNA ligase, cytoplasmic	1.90
NEURL4	Neuralized-like protein 4	1.90
EHD1	EH domain-containing protein 1	1.89
PROSC	Proline synthase co-transcribed bacterial homolog protein	1.89
C14orf166	UPF0568 protein C14orf166	1.86
EHD4	EH domain-containing protein 4	1.82
AK6	Adenylate kinase isoenzyme 6	1.75
FKBP15	FK506-binding protein 15	1.75
QARS	Glutamine--tRNA ligase	1.74
TBC1D9B	TBC1 domain family member 9B	1.74
ARPC1A	Actin-related protein 2/3 complex subunit 1A	1.71
C12orf4	Protein C12orf4	1.71

GNE	Bifunctional UDP-N-acetylglucosamine 2-epimerase/N-acetylmannosamine kinase;UDP-N-acetylglucosamine 2-epimerase (hydrolyzing);N-acetylmannosamine kinase	1.71
IBTK	Inhibitor of Bruton tyrosine kinase	1.69
EIF5B	Eukaryotic translation initiation factor 5B	1.68
NT5DC1	5-nucleotidase domain-containing protein 1	1.67
PSMD2	26S proteasome non-ATPase regulatory subunit 2	1.67
KLC2	Kinesin light chain 2	1.67
PYGL	Glycogen phosphorylase, liver form	1.66
FNBP1	Formin-binding protein 1	1.66
PKM	Pyruvate kinase PKM	1.65
SRPK1	SRSF protein kinase 1	1.64
NAA10	N-alpha-acetyltransferase 10	1.63
IFT81	Intraflagellar transport protein 81 homolog	1.63
RANBP1	Ran-specific GTPase-activating protein	1.60
TNPO1	Transportin-1	1.59
CCDC93	Coiled-coil domain-containing protein 93	1.58
AP2M1	AP-2 complex subunit mu	1.57
ARRB2	Beta-arrestin-2	1.57
HSP90AB4P	Putative heat shock protein HSP 90-beta 4	1.55
PLS1	Plastin-1	1.54
NAA16	N-alpha-acetyltransferase 16, NatA auxiliary subunit	1.54
EIF2S2	Eukaryotic translation initiation factor 2 subunit 2	1.54
IARS	Isoleucine--tRNA ligase, cytoplasmic	1.54
TTC37	Tetratricopeptide repeat protein 37	1.53
PAAF1	Proteasomal ATPase-associated factor 1	1.53
CHORDC1	Cysteine and histidine-rich domain-containing protein 1	1.51
NAP1L1	Nucleosome assembly protein 1-like 1	1.51
RNF214	RING finger protein 214	1.51
PAFAH1B1	Platelet-activating factor acetylhydrolase IB subunit alpha	1.50
ARHGDIA	Rho GDP-dissociation inhibitor 1	1.48
KIF1B	Kinesin-like protein KIF1B	1.46
WDR59	WD repeat-containing protein 59	1.44
RPRD1A	Regulation of nuclear pre-mRNA domain-containing protein 1A	1.44
ATP6V1C1	V-type proton ATPase subunit C 1	1.43
SRP68	Signal recognition particle subunit SRP68	1.43
ARPC1B	Actin-related protein 2/3 complex subunit 1B	1.43
ITSN2	Intersectin-2	1.39
OTULIN	Ubiquitin thioesterase otulin	1.39
HPS5	Hermansky-Pudlak syndrome 5 protein	1.38
PSMD3	26S proteasome non-ATPase regulatory subunit 3	1.37
STAMBP	STAM-binding protein	1.35
ANXA6	Annexin A6	1.34
PSMC2	26S protease regulatory subunit 7	1.33
WARS	Tryptophan--tRNA ligase, cytoplasmic;T1-TrpRS;T2-TrpRS	1.32
PSMC1	26S protease regulatory subunit 4	1.29
HSPA1B;HSPA1A	Heat shock 70 kDa protein 1B;Heat shock 70 kDa protein 1A	1.28
TWF1	Twinfilin-1	1.28
ARPC2	Actin-related protein 2/3 complex subunit 2	1.26
KIF15	Kinesin-like protein KIF15	1.26
ARHGAP5	Rho GTPase-activating protein 5	1.26
PSMD1	26S proteasome non-ATPase regulatory subunit 1	1.25
CPNE3	Copine-3	1.23
HSPA1L	Heat shock 70 kDa protein 1-like	1.20
C11orf54	Ester hydrolase C11orf54	1.20
TAX1BP1	Tax1-binding protein 1	1.20

KIF21B	Kinesin-like protein KIF21B	1.19
SKIV2L	Helicase SKI2W	1.18
SBDS	Ribosome maturation protein SBDS	1.17
AP3B1	AP-3 complex subunit beta-1	1.16
CIAPIN1	Anamorsin	1.16
PSMC5	26S protease regulatory subunit 8	1.15
DCTN4	Dynactin subunit 4	1.14
MDH1	Malate dehydrogenase, cytoplasmic	1.14
AASDHPPT	L-aminoadipate-semialdehyde dehydrogenase-phosphopantetheinyl transferase	1.14
PGD	6-phosphogluconate dehydrogenase, decarboxylating	1.12
SMG5	Protein SMG5	1.12
MAP4K4	Mitogen-activated protein kinase kinase kinase kinase 4	1.10
WDR11	WD repeat-containing protein 11	1.10
TNPO2	Transportin-2	1.09
SEPTIN8	Septin-8	1.09
AP3D1	AP-3 complex subunit delta-1	1.08
PRKG1	cGMP-dependent protein kinase 1	1.07
PBDC1	Protein PBDC1	1.07
SCRN3	Secernin-3	1.06
EXOC6B	Exocyst complex component 6B	1.05
AP2B1	AP-2 complex subunit beta	1.05
HERC2	E3 ubiquitin-protein ligase HERC2	1.05
EIF3J	Eukaryotic translation initiation factor 3 subunit J	1.04
TOMM70A	Mitochondrial import receptor subunit TOM70	1.04
AP2A2	AP-2 complex subunit alpha-2	1.04
EGLN1	Egl nine homolog 1	1.03
PGK1	Phosphoglycerate kinase 1	1.03
CROCC	Rootletin	1.03
ECHDC1	Ethylmalonyl-CoA decarboxylase	1.02
PRKAR2A	cAMP-dependent protein kinase type II-alpha regulatory subunit	1.02
CEP170	Centrosomal protein of 170 kDa	1.02
EIF4E2	Eukaryotic translation initiation factor 4E type 2	1.02
HBS1L	HBS1-like protein	1.02
AIMP1	Aminoacyl tRNA synthase complex-interacting multifunctional protein 1;Endothelial monocyte-activating polypeptide 2	1.01
NCAPG	Condensin complex subunit 3	1.01
ZC3H7B	Zinc finger CCCH domain-containing protein 7B	1.01
FAIM	Fas apoptotic inhibitory molecule 1	1.00

[1] FC: LFQ HERC2 WT/LFQ HERC2 C4762S in $\log_2$ scale.

Table 14. Identified down-ubiquitylated proteins

Gene names	Protein names	[1]FC
P4HA1	Prolyl 4-hydroxylase subunit alpha-1	-3.38
BRD2	Bromodomain-containing protein 2	-2.31
LMAN1	Protein ERGIC-53	-2.29
RER1	Protein RER1	-2.04
WIZ	Protein Wiz	-2.03
SFT2D2	Vesicle transport protein SFT2B	-1.99
YLPM1	YLP motif-containing protein 1	-1.91
TJP2	Tight junction protein ZO-2	-1.89
AATF	Protein AATF	-1.86
LAMB1	Laminin subunit beta-1	-1.82
BRD4	Bromodomain-containing protein 4	-1.69
RNH1	Ribonuclease inhibitor	-1.54
WBP11	WW domain-binding protein 11	-1.52
SPRYD3	SPRY domain-containing protein 3	-1.45
PPP6R2	Serine/threonine-protein phosphatase 6 regulatory subunit 2	-1.45
FLNC	Filamin-C	-1.45
RAB9A;RAB9B	Ras-related protein Rab-9A;Ras-related protein Rab-9B	-1.40
RLIM	E3 ubiquitin-protein ligase RLIM	-1.39
SON	Protein SON	-1.38
RPN2	Dolichyl-diphosphooligosaccharide--protein glycosyltransferase subunit 2	-1.36
CLDN12	Claudin-12	-1.29
NEFL	Neurofilament light polypeptide	-1.25
KIAA0922	Transmembrane protein 131-like	-1.23
DCPS	m7GpppX diphosphatase	-1.23
ZFR	Zinc finger RNA-binding protein	-1.23
KIF20B	Kinesin-like protein KIF20B	-1.17
APLP2	Amyloid-like protein 2	-1.15
RAB39B	Ras-related protein Rab-39B	-1.03
SUN1	SUN domain-containing protein 1	-1.03
NCCRP1	F-box only protein 50	-1.02
ITGAV	Integrin alpha-V;Integrin alpha-V heavy chain;Integrin alpha-V light chain	-1.01

[1] FC: LFQ HERC2 WT/LFQ HERC2 C4762S in $\log_2$ scale.

Table 15. GlyGly peptides of the up-ubiquitylated proteins identified by Mass Spectrometry (MS)

Gene names	GlyGly site position
AASDHPPT	263
ANXA6	135; 478
AP3B1	609
ARHGDIA	43
ARPC1B	308
C14orf166	58
CALM3	31
CHORDC1	144
EHD4	165
EIF3A	105; 420; 775
EPRS	300; 417; 435; 437; 642; 782; 907; 925; 939; 943; 1009; 1109
HERC2	20; 82; 95; 105; 701; 969; 990; 1090; 1212; 1220; 1231; 1178; 2657; 2969; 2976; 3231; 3515; 4133
HSP90AA1	283; 292
HSPA1B	77
IARS	796; 903
MARS	375; 726
MIOS	443; 479
NAP1L1	116
NCAPG	522; 816
PGAM1	106; 100; 113
PGK1	30; 264
PLS1	524
PSMC1	91
PSMD10	23; 30
PSMD2	66; 397
PSMD3	54; 273
PYGL	10
RANBP1	182; 189
SPATA5	887
SRP68	220
TBC1D13	296
TOMM70A	285
VPS8	801
WARS	450

CHAPTER V. Discussion

Molecular mechanisms of HERC2 in cell signalling pathways

This work identifies several signalling pathways that are regulated by the ubiquitin ligase HERC2. Specifically, we demonstrate a role of HERC2 in: 1) p38 signalling, with implications in the cellular response to oxidative stress; 2) Autophagy, through the USP20/ULK1 axis; 3) The proteasome assembly pathway, through the regulation of ubiquitylation of several proteasome subunits and its cognate chaperones. This represents a great advance for the characterization of the physiological function of this ubiquitin ligase. In this chapter, we will discuss the molecular mechanisms involved in the regulation of these pathways, trying to postulate a working model that adds the results we obtained to the knowledge stablished so far in the scientific literature.

Regulation of the p38 MAPK signalling pathway and the cellular response to oxidative stress

This study provides the first evidence that HERC2 controls the p38 signalling pathway through mechanisms dependent on C-RAF. Our results demonstrate that HERC2 forms a complex with RAF proteins, consistent with the results of a previous proteomic analysis, in which C-RAF was identified to interact with the carboxyl-terminus domain of HERC2 [150]. Mechanistically, our data show that HERC2 regulates C-RAF ubiquitylation and proteasome-dependent degradation; thus, in individuals with the HERC2 P594L mutation, the resulting HERC2 deficiency, causes an increase in C-RAF protein levels. However, this increase is not signalled through the canonical MEK/ERK pathway, and instead, seems to affect the MKK3/p38 pathway specifically (Figure 43). Activation of crosstalk between C-RAF and the MKK3/p38 pathway has also been described as a mechanism regulated by HERC1, the other member of the large HERC protein family [102]. This raises the question of whether this signalling mechanism is specific to the Large HERC proteins. In any case, our results demonstrate that the role of HERC2 in the C-RAF/MKK3/p38 signalling pathway is independent of HERC1. Several lines of evidences show this independent role: 1) HERC1 and HERC2 proteins do not interact [102]; 2) HERC1 is not present in the HERC2/C-RAF complex;

and 3) while HERC1 depletion regulates ERK signalling, HERC2 does not. By contrast, activation dependent on HERC2 affects the cellular response to oxidative and osmotic stresses. Although the precise mechanism explaining the differences between HERC1 and HERC2 should be further explored, differences could be explained by the different complexes formed between RAF and Large HERC proteins. In line with this, molecular chaperones such as Heat Shock Protein 70 (HSP70) and Heat Shock Protein 90 (HSP90) may be playing an important role. HSP70 interacts with C-RAF and modulates its biological activity [153, 154]. Likewise, C-RAF assembly with HSP90 is crucial for its stability and activation [155–157]. Notably, HERC1 forms a complex with HSP70 [158] and our proteomic analysis shows that both HSP70 and HSP90 ubiquitylation are regulated by HERC2 (Table 13). These facts reveal that the Large HERCs may act as molecular scaffolds for cell signalling pathways, forming different protein complexes with C-RAF and its cognate chaperones. Thus, the differences in MAPK signalling between HERC1 and HERC2 could be explained by their different binding partners and by their different substrate specificity. That is, each Large HERC member might act fine-tuning C-RAF protein levels, affecting one signalling pathway or another depending on the chaperone to which C-RAF is attached. In this regard, our preliminary results indicate that there is a protein interaction between HERC2 and HSP90, but not between HERC1 and HSP90 (Data not shown). This suggests that the protein complex between C-RAF and HSP90 would be specifically recognised by HERC2 and not by HERC1. If these results are corroborated, HSP90 would be a promising candidate explaining the cell signalling differences between the members of the Large HERC family.

Focusing now on HERC2, our results indicate that the C-RAF/MKK3/p38 signalling pathway regulated by this ubiquitin ligase affects the cellular response to oxidative stress through NRF2 activation. NRF2 is a transcription factor encoded by the *NFE2L2* gene and it is considered the master regulator of the cellular antioxidant response [159]. A critical regulatory step leading to its activation is its dissociation from the complex formed by the E3 ligase Cullin 3 (CUL3) and the ubiquitin ligase Kelch-like ECH-associated protein 1 (KEAP1). CUL3 ubiquitylates NRF2, targeting it to proteasomal degradation, and upon exposure to oxidative stress, the NRF2-KEAP1-CUL3 complex is disrupted and NRF2 is stabilized for translocation to the nucleus. Nevertheless, the precise mechanism by which cellular stress signals end up reaching NRF2 and causing its dissociation of the complex remains unclear

[160]. Indeed, several studies have pointed out that some MAPK pathways are responsible for regulating this signal transduction. The p38 MAPK can regulate NRF2 activity through its activation [161–163] and its repression [164] depending on the context [165]. Our results show that NRF2 protein levels increase after p38 phosphorylation induced by HERC2 depletion, consistent with p38 activating NRF2 by protein stabilisation. Moreover, the mRNA levels of NRF2-regulated antioxidant genes are also upregulated (e.g., *SOD1*, *SOD2* and *GPX1*) (Figure 43). The *NFE2L2* gene contains an antioxidant response element within its promoter region, providing NRF2 the ability to activate its own transcription [166]. This could explain why we observe increased mRNA levels of *NFE2L2* in addition to its protein levels. Moreover, the fact that the inhibition of RAF or p38 activity, abolishes the upregulation of NRF2 protein levels in HERC2-depleted cells, confirms that p38 acts upstream of NRF2 activation. Still, given the variety of p38 substrates we cannot discard that other transcription factors, apart from NRF2, could also be involved in the regulation of the studied antioxidant genes. For instance, the transcription factor ATF-2 is another important mediator of p38 in the induction of *SOD2* expression upon H_2O_2-induced oxidative stress in MEFs [167]. This possible cooperation between NRF2 and ATF-2, or some other transcription factors targeted by p38, requires more experimental evidence (Figure 43).

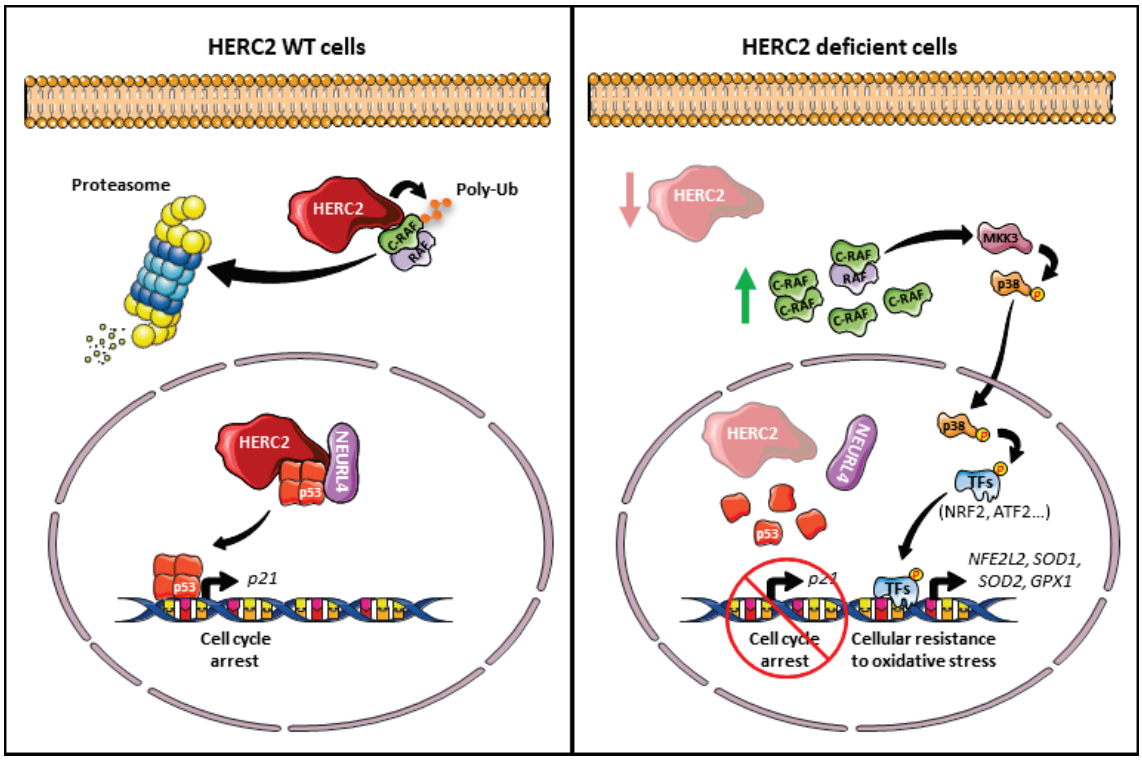

Figure 43. Figure caption on next page ▼

Figure 43 ▲. Working model of HERC2 function in health and disease. Previous studies showed that independently of the ubiquitin ligase activity, HERC2 along with NEURL4, facilitates p53 oligomerization to promote p53 transcriptional program activation. For example, the target gene p21 regulates the cell cycle and promotes cell cycle arrest. Under conditions of HERC2 deficiency or down-regulation, the transcriptional activation of p53 is impaired due to the compromised p53 oligomerization process [29, 48, 49, 54]. Now, with data presented in this study, we complement this working model by adding an important function of HERC2 dependent on its ubiquitin ligase activity. Under normal conditions, HERC2 controls C-RAF protein levels by regulating its ubiquitylation and targeting it to proteasomal degradation. Hence, in HERC2 deficient cells, C-RAF protein levels increase, which activates a crosstalk between the C-RAF and MKK3/p38 signalling pathways. Once p38 is activated by phosphorylation, it translocates to the nucleus and activates its target transcription factors (TFs), such as NRF2. This eventually activates transcription of genes related to the oxidative stress response such as *NFE2L2*, *SOD1*, *SOD2* and *GPX1*, which predisposes cells to an enhanced resistance to oxidative stress. The combination of these effects in the p53/p21 and MKK3/p38 pathways may affect both tumorigenesis and cell homeostasis.

Overall, our findings reveal a pro-survival function of p38 that is regulated by HERC2. The possible relevance of this mechanism in physiological conditions is that HERC2 potentially fine-tunes the cellular response to oxidative stress by controlling protein levels of C-RAF and therefore C-RAF/MKK3/p38 signalling to regulate antioxidant gene expression. One possibility is that some stress signals could trigger disruption of HERC2-C-RAF interaction, thus increasing C-RAF protein levels and activating the crosstalk between C-RAF and MKK3. HERC2 immunoprecipitation experiments under stress conditions could help to verify this hypothesis.

Implication in the regulation mechanisms of autophagy

Autophagy is a tightly regulated intracellular degradation process. Signals that activate the autophagic process typically come from distinct stress conditions such as oxidative stress, hypoxia, starvation, protein aggregation, among others. These upstream pathways commonly converge on ULK1 complex activation, which acts as a node, transducing multiple stress signals into autophagic flux activation [119, 168]. Ubiquitin ligases and ubiquitylation also regulate autophagy in different ways. For instance, by controlling stability of components of the autophagic machinery; and by facilitating recruitment of autophagy adaptors like p62, which acts as a linking factor between ubiquitylated proteins and autophagosome membranes in selective autophagy [169]. For instance, the RBR E3 ligase PARKIN induces mitophagy by generating ubiquitin chains on the mitochondrial outer membrane of damaged mitochondria [170]. In addition, the HECT E3 ligases NEDD4-1 and NEDD4-2 have also been implicated in autophagy. NEDD4-1 interacts with LC3 and polyubiquitylates p62, enabling autophagosome and inclusion body formation [171]. On the

other hand, NEDD4-2, induces ubiquitylation and proteasome-dependent degradation of ULK1 [172].

For now, little is known about the involvement of HERC E3 ligases in autophagy. Small HERC proteins were found to interact with each other and to localize to cellular structures identified as late endosomes and lysosomes [173]. However its precise role in the endocytic pathway remains unknown. Most evidence of the implication of HERC E3 ligases in autophagy comes from the Large HERC family. Two different mice models with inactivating mutations in Large *Herc* genes have enabled the study of these implications: the *tambaleante* mutant for *Herc1* and the *Herc2*$^{+/530}$ mutant for *Herc2*. Both mice display impaired motor coordination, showing a specific loss of Purkinje cells in the cerebellum with clear signs of autophagy dysregulation [51, 54, 174]. The molecular mechanism causing increased autophagy in the *tambaleante* mice seems to be caused by a deregulation of the mTOR pathway [174]. However, other mechanisms cannot be discarded. Regarding the *Herc2*$^{+/530}$ mice, the precise mechanism explaining the autophagy dysregulation remains elusive. With this aim, we studied autophagy regulation in patient-derived cells with the HERC2 P594L mutation, that share with the *Herc2*$^{+/530}$ mice model the reduced levels of HERC2 protein and some phenotypic characteristics such as the movement disturbances [58].

Our results indicate that HERC2 deficient cells show higher levels of LC3-II, which is explained by an increase in the number of autophagosomes. These observations support the idea that HERC2 deficiency stimulates the process of autophagy, as previously suggested in the *Herc2*$^{+/530}$ mice model work. Now, we go a bit further and provide evidence of a possible regulation mechanism. Prior studies showed that HERC2 interacts and controls the protein stability of USP20 by promoting its ubiquitylation-mediated proteasomal degradation, with implications in the DNA damage response pathway [43, 44]. Separately, a study concluded that USP20 stimulates autophagy initiation by promoting ULK1 stabilization. Mechanistically USP20 interacts with and deubiquitylates ULK1, thus preventing its lysosomal degradation [149]. In this study, we demonstrate that HERC2 interacts with USP20 and that in HERC2 deficient cells protein levels of USP20 are incremented. Also, USP20 upregulation correlates with increased ULK1 stability. Therefore, our data fit with a role of HERC2 regulating USP20 stability and point out for the first time that this mechanism might also be important for

autophagy regulation, with HERC2 being the upstream factor that through USP20 regulates ULK1 protein levels and autophagy initiation (Figure 44).

Another factor that appears to be involved in the regulation mechanisms of autophagy by HERC2 is the MAPK p38. Activation of p38 seems to has a dual role in autophagy, both as a positive and negative regulator. Probably, the response might depend on the stimuli and the nature of the specific signalling cascade that is involved in each case [175]. Describing p38 as a positive regulator of autophagy there is a report showing that MK2 and MK3, downstream targets of p38, positively regulate starvation-induced autophagy by phosphorylating Beclin 1 [176]. In addition, another study revealed that sustained p38 activation triggers autophagosome formation and enhances the basal autophagic flux [128]. Given these precedents, and that HERC2 also regulates p38 signalling pathway as previously shown, we wondered how p38 activation may fit in our working model of HERC2 regulating autophagy through the USP20/ULK1 axis. Although some reports already described ULK1 as a p38 phosphorylation target to induce autophagy [128, 177], whether USP20 is also targeted by p38 remains unknown. Our *in silico* results reveal that USP20 possesses 16 potential phosphorylation sites (p-sites) by p38α. According to previous reports, the majority of p38α phosphorylation sites are SP or TP amino acid residues [178]. Intriguingly, USP20 sequence has 8 SP and 2 TP motifs, all of them identified as potential phosphorylation sites by the algorithm used in our study, which validates our approach. In addition, the algorithm also identified 6 extra p-sites, other than SP and TF motifs. Remarkably, 13 of the potential p-sites identified are found within the HERC2 interacting region [44]. Of note, our experiments reveal that upon p38 activation, HERC2 and USP20 interaction is disrupted and this correlates with increased protein levels of USP20 and LC3-II. These observations fit with the hypothesis that p38 phosphorylates USP20, possibly within the HERC2 binding domain. This might trigger the disruption of HERC2-USP20 interaction, preventing USP20 ubiquitylation by HERC2 and hence stabilizing USP20 protein levels. In turn, USP20 would deubiquitylate and stabilize ULK1, consequently promoting autophagy initiation which eventually leads to an increase in LC3-II protein levels due to the autophagosome formation (Figure 44).

In conjunction our findings reveal that HERC2 might act as an autophagy-suppressor like factor, restricting autophagy initiation by controlling protein levels of USP20. This mechanism could be upstream regulated by the p38 signalling pathway.

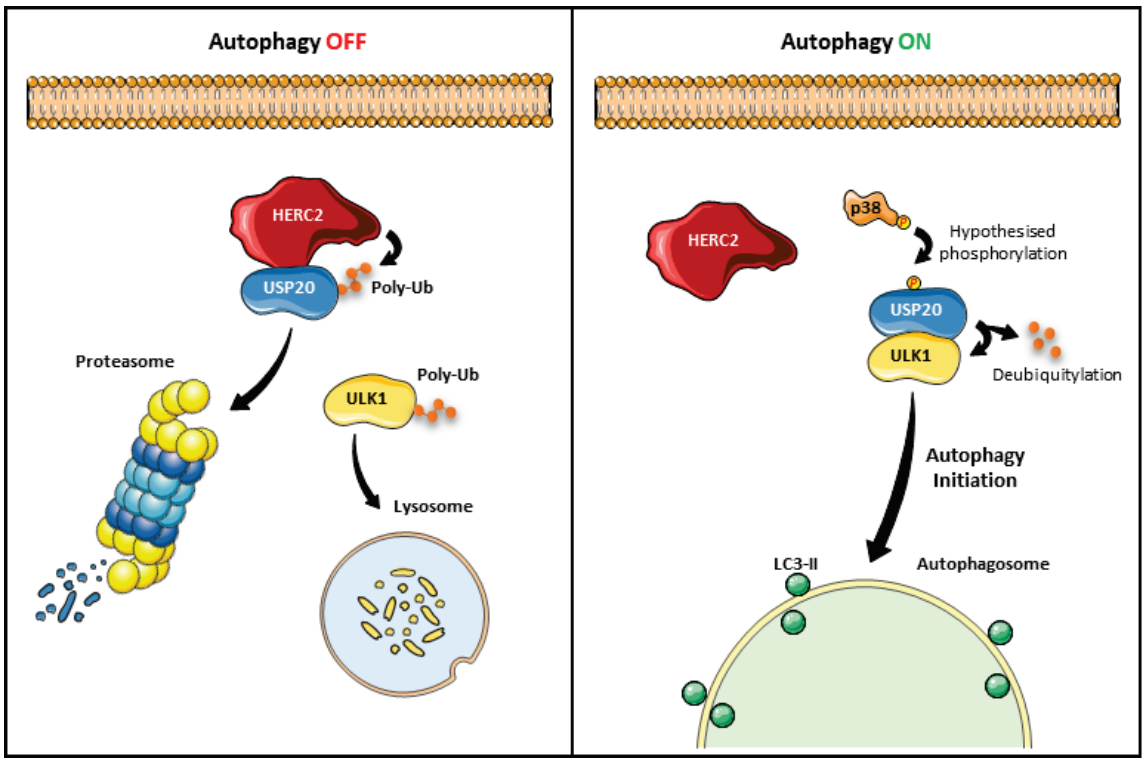

Figure 44. Proposed model of autophagy regulation by HERC2. Under conditions in which autophagy is not activated (Autophagy OFF), HERC2 ubiquitylates and targets USP20 to proteasomal degradation. ULK1 is ubiquitylated and targeted to lysosome-dependent degradation. When autophagy is activated (Autophagy ON), p38 might phosphorylate USP20, disrupting HERC2-USP20 interaction and preventing USP20 proteasome-dependent degradation. Thus, USP20 interacts with and deubiquitylates ULK1, stabilizing its protein levels and enabling autophagy initiation and autophagosome formation.

Quality-control factor of the proteasome assembly pathway

The proteasome is a multiprotein complex that degrades cellular proteins in a strictly coordinated way. Therefore it controls many processes such as cell signalling, protein quality control, cell cycle and transcription, among others. Increasing evidence points to that cells regulate proteasome abundance through the expression of proteasome subunits and assembly chaperones. In addition, the assembly mechanism of the different subunits is a key and highly regulated process [129]. The assembly of multiprotein complexes, such as the proteasome, requires each subunit to be produced at a determined amount relative to its partners. Thus, a correct balance in subunits protein levels is needed. Proportional synthesis as a result of a tightly regulated transcription and translation might be important to control the stoichiometry of the complex. Still, imbalances are inevitable, and the elimination of excess or orphan proteins, derived of unassembled intermediates, also plays an important role [134]. However, how cells detect these stalled orphaned assembly intermediates for selective degradation is not fully elucidated. In this aspect, HERC1 was identified as a quality-

control factor responsible for marking certain unassembled intermediates of the proteasome for degradation. Specifically, HERC1 recognises PSMC5, a subunit of the proteasome base, when it is associated with its cognate assembly chaperone PAAF1. PAAF1 only dissociates from PSMC5 after assembly into the complex, therefore, chaperone association is what allows the identification of this unassembled intermediate as an orphan protein, that will then be degraded [26] (Figure 45).

Given the structural similarity between HERC1 and HERC2 [19], it is reasonable to think that they could share some functions. Our proteomic analysis searching for putative substrates of HERC2 provides the first clue that it might have a similar role as a quality-control factor in the proteasome assembly pathway. According to our data, HERC2 regulates ubiquitylation of a bunch of structural proteins of the 19S regulatory particle of the proteasome. Specifically, it regulates ubiquitylation of PSMC1, PSMC2, PSMC4 and PSMC5. These proteins are AAA^{+}-ATPases that are part of the heterohexameric ring that forms the base of the 19S regulatory particle, which binds directly to the 20S core particle of the proteasome (Figure 45). PSMD1 and PSMD2 are non-ATPases that bind to the heterohexameric ring, also forming the base structure [179]. These last two also have been identified in our proteomic study. As well PSMD3, which is part of the lid of the 19S regulatory particle [152]. Interestingly, two of the identified proteins are base assembly chaperones. This is the case of PSMD10 and PAAF1. These two chaperones are not present in the structure of the fully assembled proteasome but are essential for the regulatory particle assembly pathway. Each chaperone binds to the carboxy-terminal domain of a specific PSMC protein aiding and accompanying its assembly. Specifically, PSMD10 binds PSMC4 and PAAF1 binds PSMC5 [180] (Figure 45). Since HERC2 regulates ubiquitylation of both these chaperones and also their particular substrates, one possibility is that HERC2 marks PSMC5-PAAF1 and PSMC4-PSMD10 unassembled intermediates for degradation. Another possibility is that HERC2-dependent ubiquitylation promotes subunits stability and their correct assembly. Further research is needed to decipher the biological outcome of these ubiquitylations. Still, HERC2 might be acting as a quality-control factor, orchestrating the correct assembly of the different proteasome subunits, with a greater implication in the assembly of the regulatory particle. Reinforcing the idea of HERC2 regulating the correct assembly of the regulatory particle of the proteasome, our proteomic analysis also identified as putative HERC2

substrates the Proteasome activator complex subunit PSME1 and PSME2, also known as PA28α and PA28ß, respectively. These two are structural proteins of the so called immunoproteasome, which main function is the processing of class I MHC peptides. The immunoproteasome contains an alternative regulatory particle, the 11S. This 11S regulatory particle is formed by PA28αß heterooligomers and their expression is inducible by interferon-γ [133].

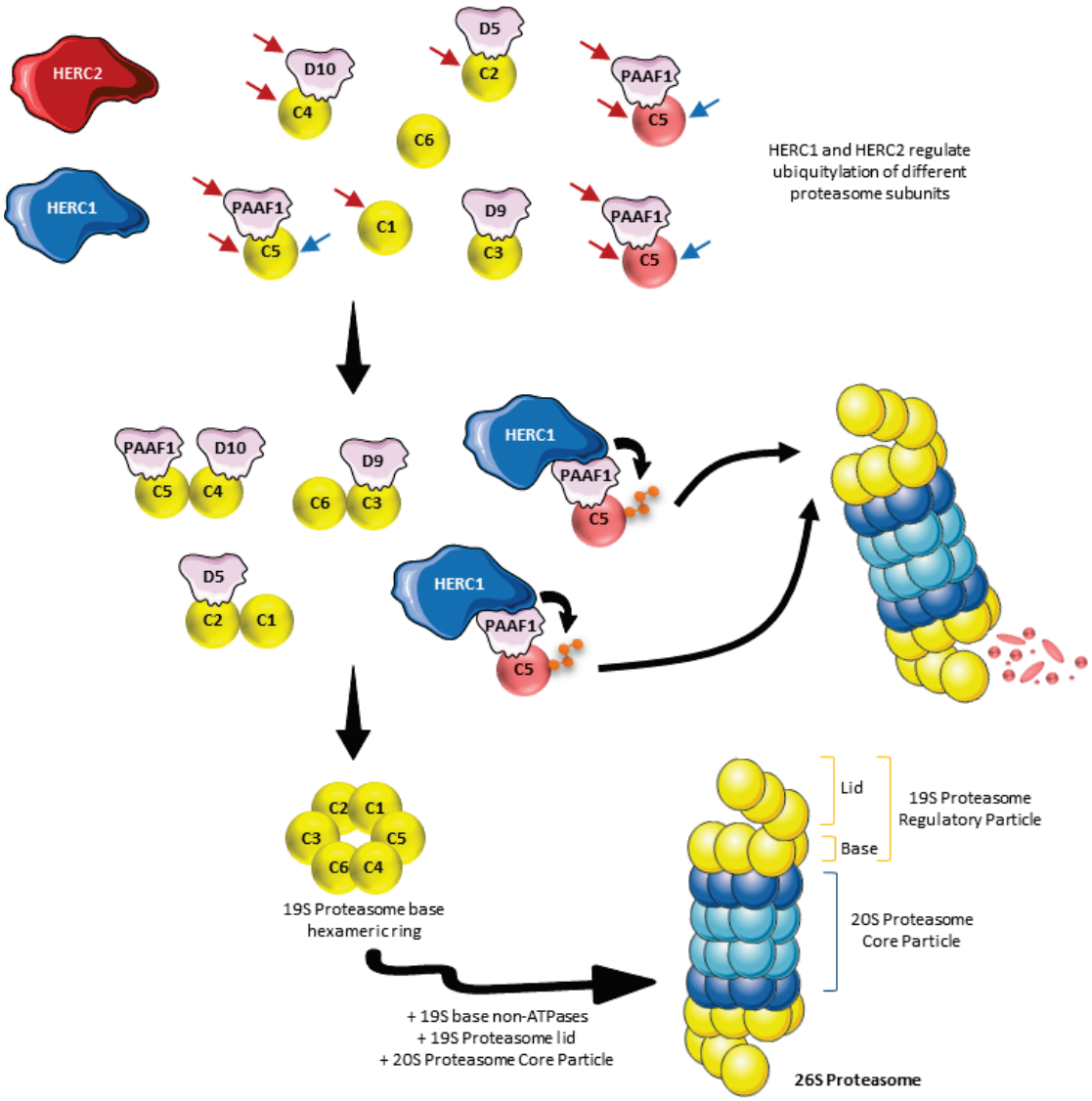

Figure 45. Working model of the role of Large HERCs in the proteasome assembly pathway. HERC1 and HERC2 regulate ubiquitylation of different proteasome subunits. Blue arrows indicate HERC1 putative substrates and red arrows indicate HERC2 putative substrates. During the assembly of the 19S Regulatory Particle of the proteasome, the AAA-ATPases (PSMC1-6; C1-C6) assemble forming dimers. Base assembly chaperones PSMD10 (D10), PAAF1, PSMD5 (D5), PSMD9 (D9) bind to their specific PSMC protein and assist their correct assembly. A correct balance in the different subunits protein levels is needed. HERC1 recognises excess of PSMC5 intermediates (in red) bound to PAAF1 and promotes their ubiquitylation and proteasome-dependent degradation. In the following stages of base assembly, PSMC1-6 proteins form the heterohexameric ring. To this, other base proteins non-ATPases will add. Then, the lid will assemble to the base, completing the 19S Regulatory Particle structure. Finally, along with the 20S Core Particle, the complete 26S proteasome will be assembled.

On the whole, our results indicate that large HERCs might act as important quality-control factors of the proteasome assembly pathway, in particular regulating assembly of the regulatory particle through its ubiquitin ligase activity. Although more experiments will be required to validate these results, these preliminary data have opened a new and promising line of research.

New insights in HERC2 functions

The proteomic analysis presented here identifies a large number of putative substrates of HERC2. In addition to the role in the proteasome assembly pathway discussed above, we reveal a functional enrichment of ubiquitylated proteins regulated by HERC2 related with other cellular functions such as centrosomal proteins, membrane associated proteins, t-RNA biosynthesis factors and microtubule associated proteins.

Regarding the involvement of HERC2 in centrosome function, our observations fit with previously published data. HERC2, along with NEURL4, localize to the centrosome and interact with CP110, a centrosome component implicated in centrosome biogenesis. NEURL4 presumably acts as a substrate adaptor for HERC2 and the NEURL4-HERC2 complex participates in the ubiquitin-dependent regulation of centrosome architecture [63]. In addition, HERC2 was found to regulate centriole duplication through regulating ubiquitylation-mediated proteasome degradation of USP33 [64]. Now, we identify additional HERC2 putative substrates such as CEP170, required for centriole assembly [181]; and CEP41 and Rootletin (CROCC), important factors involved in ciliogenesis [182, 183].

Another new insight in HERC2 function described here is the fact that HERC2 is self-ubiquitylated. Some self-ubiquitylating E3 ligases have been described such as the RING ligases MDM2, SIAH1 and TRAF6. Also the HECT ligases RSP5, ITCH, NEDD4-1, NEDD4-2, SMURF and WWP1 [184]. Nevertheless, to our knowledge, HERC2 is the first HERC subfamily E3 ligase implicated in self-ubiquitylating mechanisms. The proposed biological role of self-ubiquitylation is that it serves as a negative feedback loop, targeting the ligase itself to degradation. However, non-proteolytic functions have also been described. For instance, regulation of ligases' activity and the recruitment of substrates [184]. Therefore, another line of research that opens up is to decipher the biological significance of HERC2 self-ubiquitylation.

Pathophysiological implications

HERC2 is involved in a wide range of cellular functions including neurodevelopment, cell response to DNA damage, cell proliferation, cell migration and immune responses. In addition, results provided here show a novel role of HERC2 in the cellular response to oxidative stress, autophagy and proteasome assembly. These functions are very important for the maintenance of cellular homeostasis. Indeed, alterations in these processes have been linked with pathology. Accordingly, HERC2 mutations are associated with several diseases such as cancer and the HERC2 Angelman-like neurodevelopmental disorder. In this chapter, we will discuss how the molecular mechanisms of HERC2 described here fit with the pathophysiology of these diseases.

HERC2 and cancer

Implication of Large HERC family members in tumorigenesis is well documented. As such, mutations in both *HERC1* and *HERC2* are associated with different types of cancers [19, 23, 185, 186], such as leukaemia [187–191] and breast cancer [192, 193]. Frameshift mutations in *HERC2* have been found in both gastric and colorectal carcinomas with microsatellite instability [194]. The *HERC2* locus has also been associated with both cutaneous melanoma and uveal melanoma, whereas the *HERC1* locus has been found to be mutated in non-melanoma skin cancer [195–198].

Regarding the clinical outcomes of Large *HERC* genes mutations in different types of tumours, higher expression levels of the Large HERCs are associated with better patient prognosis in kidney, head and neck, and pancreatic cancers when *HERC1* expression levels are elevated; and in patients with renal cancer when *HERC2* expression levels are elevated [199]. In addition, in osteosarcoma, upregulation of HERC2-binding protein SOX18 enhances cell proliferation. This is associated with a reduction in both Large and Small HERCs mRNA levels [200]. Hence, in this case there is a correlation between low expression of both Small and Large *HERC* genes and a greater malignancy of the osteosarcoma.

Focusing on HERC2, a list of cancers associated with this E3 ligase is provided in Table 16. A brief description of the related molecular mechanism and the corresponding references are indicated.

Table 16. Cancers associated with HERC2 and its related molecular mechanisms.

Associated cancers	Related molecular mechanisms	References
Pheochromocytoma and paraganglioma	*HERC2* mutations	[201]
T-cell prolymphocytic leukemia	*HERC2* mutations	[189]
Chronic Myeloid Leukemia	*HERC2* Downregulation	[191]
Cutaneous melanoma	SNPs in *HERC2* gene increase susceptibility	[195, 196, 202, 203]
	Gene-gene interactions between *HERC2* gene and *IL31RA* and *DDX4* genes	[204]
	Epistatic effects between *HERC2* and *VDR* genes	[197]
Squamous cell carcinoma	SNPs in *HERC2* gene impact on time to develop the tumor in organ transplant recipients	[205]
	HERC2 mutations	[206]
	Prognostic signature based on the mRNA expression of DNA Damage Response genes (including *HERC* expression)	[207]
Uveal melanoma	SNPs in *HERC2* gene increase susceptibility	[198, 208]
	High expression of HERC2 protein	[209]
Non-small-cell lung cancer	Worse prognosis in patients expressing high *HERC2* mRNA levels	[210]
Breast cancer	Enhanced BRCA1 degradation	[36, 38]
Gastric and colorectal carcinomas	*HERC2* mutations	[194]
	High HERC2 expression	[211]
	HERC2-mediated p53 regulation	[50]
Osteosarcoma	Negative correlation of *SOX18* overexpression and *HERC2* mRNA levels	[200]
Pancreatic cancer	*HERC2* mutation	[212, 213]
De-differentiated liposarcoma	*HERC2* mutations	[214]

These precedents associating different types of tumours with *HERC2* mutations, suggest that HERC2 may act as a tumour suppressor in some contexts, its deficit correlating with greater tumorigenicity [186, 199]. In this line, HERC2-NEURL4 complex, regulate the transcriptional activity of the tumour suppressor p53, facilitating its oligomerization. Accordingly, HERC2 knockdown increases cell proliferation due to the impaired capability to arrest the cell cycle through p53 [29, 48, 49]. Now, our results of HERC2 regulating the oxidative stress response through the p38 MAPK signalling pathway reveal a new mechanism by which HERC2 deficiency might be contributing to malignancy. Although the precise mechanism remains elusive, it is well established that the production of reactive oxygen species in tumour cells increases due to the higher metabolic rate, with the resulting excess being countered by an increased antioxidant cellular response [215]. Supporting this, in mice, oncogenic alleles of *Kras*, *Braf* and *Myc*, associated with increased *Nfe2l2* expression. This appear to stably enhance NRF2 antioxidant program and lower intracellular reactive oxygen species [216]. Furthermore, in p53 mutated cancer cells, the NRF2-dependent antioxidant response was selectively modulated to enhance cancer cell survival [217]. Taking all of this into account, HERC2 deficiency may contribute to tumorigenesis first by impairing p53 transcriptional activity and then by activating C-RAF/MKK3/p38 signalling pathway, which result in increased NRF2 transcriptional activity. The activation of this C-RAF/MKK3/p38/NRF2 axis would boost the cellular antioxidant response, making cancer cells more resistant to oxidative stress and promoting cancer cell survival (Figure 43). In this context, combination treatments with drugs causing non-genotoxic activation of p53 oligomerization and FDA-approved RAF inhibitors, such as Sorafenib, represent potential therapeutic candidates for tumours associated with HERC2 deficiency.

On the other hand, our results also reveal a role of HERC2 in autophagy. Autophagy plays opposites roles in tumorigenesis. It is well stablished that in early stages autophagy acts as a tumour suppressor mechanism, via degradation of potentially oncogenic molecules and maintaining cellular homeostasis. However, once the tumour is fully stablished, autophagy becomes a tumour-promoting mechanism that increases survival of cancer cells [218]. This dual role of autophagy in cancer, fits with the fact that HERC2 acts either as a tumour suppressor or an oncogene depending on the context. Considering this, for tumours that rely on autophagy for survival, autophagy inhibition would be beneficial. Instead, for tumours

with defective autophagy, treatment with autophagy inducers might be a good therapeutic option. So far, the autophagy inhibitors chloroquine and hydroxychloroquine have become the only FDA (Food and Drug Administration)-approved agents. Its use to treat cancer is being evaluated in several ongoing clinical trials. Despite this, these drugs have limited cellular uptake in acidic tumour microenvironments, which represents its major weakness [219]. This *in vivo* limitation generates a need for the production of more potent and specific autophagy inhibitors. In the case of tumours associated with mutations in HERC2, since the regulation of autophagy seems to occur through the USP20-ULK1 axis, it would be logical to focus on these two therapeutic targets. SBI-0206965 is a small molecule inhibitor of ULK1 that inhibits tumour-protective autophagy and enhances apoptosis in cancer cells [220, 221]. Therefore, it represents a good therapeutic option. On the other hand, USP20 is now emerging as a potential therapeutic target in cancer since it is implicated in the regulation of tumour growth and metastasis by participating in multiple signalling pathways [222]. However the impact of USP20-dependent autophagy regulation in cancer has been poorly studied. Besides, to date, only one USP20 inhibitor has been identified, the so called GSK2643943A. It showed anti-tumour efficacy in combination with an oncolytic virotherapy in mice bearing squamous cell carcinoma SCC9 tumours [223]. Still, more research is needed and novel USP20 inhibitors may provide further treatment options. Nevertheless here we propose that USP20 inhibitors could be employed in autophagic-dependent tumours bearing HERC2 loss-of-function mutations.

Regarding the novel putative HERC2 substrates identified in this study, and focusing on those related with the proteasome, the PSMD10 protein stands out due to its known implication in cancer. PSMD10 (also called Gankyrin) is an oncoprotein upregulated in many cancers. It binds to different proteins and promotes degradation of several tumour suppressors such as RB, p53, C/EBPα, TSC2, HNF4α, and CUGBP1. For this reason it was described as a tumour suppressor killer [224]. Concerning PSMC5, which interaction with HERC2 is confirmed with our pull-down experiments, its overexpression has been associated with some cancers such as colorectal, lung and breast cancer [225–227]. Of note, the problem of proteasome subunit imbalance and excess of orphan stalled intermediates is enhanced in cancer cells [26]. Thus, HERC2 might act in these contexts as a tumour suppressor, ensuring a correct subunit assembly and preventing the accumulation of these

stalled intermediates, which overexpression is associated with tumorigenesis. Though, this hypothesis should be further investigated.

The neurodevelopmental disorder HERC2 Angelman-like syndrome

Hereditary neurodevelopmental disorders arise from alterations in central nervous system development and manifest perinatally or during infancy and childhood. Despite showing wide genetic and clinical heterogeneity, most share some common phenotypic features, such as developmental delay, impaired motor function and intellectual disability. The identification of genes responsible for these disorders has enabled genetic diagnosis, accurate genetic counselling, and better management [228].

HERC2 is highly expressed in the nervous system and has been linked with hereditary neurodegenerative disorders [51]. Specifically, *HERC2* mutations cause a type of neurodevelopmental disorder called HERC2 Angelman-like syndrome (autosomal recessive mental retardation type 38; OMIM # 615516). It is caused by missense and frameshift mutations that result in a loss of function. In all cases, these mutations are associated with a complete loss or markedly reduced levels of HERC2 protein [57–61]. The condition was first described in Amish/Mennonite communities, associated with homozygosity for a *HERC2* (c.1781C>T, p.Pro594Leu) founder gene variant at increased frequency in the population. Despite the progress made so far, the molecular mechanisms underlying HERC2-related disorders remain elusive, impeding efforts to find potential treatments for these rare diseases. Further investigation of their molecular basis could reveal not only the underlying pathology but also potential therapeutic targets.

To this end, proteomic studies of peripheral blood-derived lymphoblasts from individuals with HERC2-Angelman like syndrome revealed derangements of multiple cellular pathways probably involving disparate pathogenic mechanisms. Intriguingly, an enrichment of the NRF2-mediated oxidative stress response in *HERC2* mutants compared to the control group was identified. In addition, protein-protein interaction networks containing signal transduction proteins and MAPKs were found to be differentially expressed in *HERC2* mutants [229]. Our study and identification of the HERC2-dependent antioxidant response regulated by the C-RAF/MKK3/p38/NRF2 signalling pathway add to these observations and, importantly, provide a potential molecular mechanism.

Moreover, alterations in p38 MAPK signalling in neurons have been linked to neurodegenerative diseases including Parkinson's disease, Alzheimer's disease and amyotrophic lateral sclerosis (ALS) [230]. Therefore, we cannot discount the possibility that alterations in this pathway could be associated with clinical outcomes in HERC2 Angelman-like syndrome. Consistent with this, previous studies have shown that SOD1 overexpression, in which gene variants are associated with ALS and whose mRNA levels are increased following HERC2 depletion, is associated with defects in the cerebellar architecture [231, 232].

In addition, while excessive ROS elicit oxidative stress, their persistent depletion, as observed in HERC2 deficient cells, leads to an opposite condition called reductive stress. Persistent activation of antioxidant signalling can cause reductive stress and lead to pathology [148]. In HERC2 P594L cells, the overactivation of NRF2 signalling could be one of the causes. In fact, NRF2 sustained activation has already been linked to reductive stress [233]. Highlighting the importance of reductive stress on pathology, mutations in key components of the cellular reductive stress response can cause developmental diseases. For instance, FEM1B gain-of-function mutation, which cause a persistent activation of the reductive stress response, elicit developmental syndromes with some similarities to the HERC2 Angelman-like syndrome [147, 148]. An example of the damage that reductive stress can exert on cells is that it can induce mitochondrial dysfunction and impact on the correct cell function [234, 235]. In addition, mitochondrial fragmentation is a common feature observed in neurodegeneration [236]. Accordingly, cells with the HERC2 P594L mutation show increased number of fragmented mitochondria. This fragmentation of the mitochondrial network was also observed in fibroblasts of another patient holding a distinct loss-of-function mutation in *HERC2* in a different study [60]. In conjunction, our results uncover a possible molecular mechanism to explain the pathophysiology of HERC2 Angelman-like syndrome. Consequently, the findings in this study identify p38 and RAF inhibitors as potential therapeutic options for individuals who present with such rare disease, for the capacity of these inhibitors to counteract the NRF2-mediated antioxidant program dependent on HERC2 and thereby alleviating the possible reductive stress that is being caused.

Another point to be considered is that deregulation of autophagy, whether up or downregulated, has been linked with neurodegenerative disorders such as Alzheimer, Huntington and Parkinson diseases. Accumulation of autophagosomes, autolysosomes, inclusion bodies and protein aggregates are hallmarks of most of these pathologies [237]. In addition, recent genetic studies have demonstrated a significant involvement of autophagy in human brain development and so in a wide range of neurodevelopmental disorders [238]. Neurons are post-mitotic and long lived cells. Therefore, they rely on a correct control of the autophagic flux to correctly eliminate dysfunctional organelles and protein aggregates. Consequently, basal autophagy in healthy neurons appears to be relatively active. A correct balance between autophagosome formation and autophagic degradation is crucial. If the rate of autophagosome formation exceeds the rate of autophagic degradation or if late stages of the autophagic process are impaired, an accumulation of autophagic vesicles is triggered, which would inevitably lead to neurodegeneration [239, 240]. For instance, loss-of-function mutations in *TBCK* gene, which encodes a putative Rab GTPase-activating protein, result in mTORC1 inhibition that leads to uncontrolled autophagy induction. These mutations cause a neurodevelopmental disorder with intellectual disability and, interestingly, patient-derived fibroblasts exhibit increased number of autophagosomes and increased autophagic flux [241]. Similarly, individuals with HERC2 Angelman-like syndrome show intellectual disability, autism and gait movement disturbance. Although few data are available on brain imaging of these patients, studies made so far show brain and cerebellar morphological defects. Remarkably, in patient-derived fibroblasts, an increased number of protein aggregates is observed [57–60]. As in *TBCK* loss-of-function mutations, in HERC2 Angelman-like syndrome, an uncontrolled autophagy induction might be contributing to the accumulation of aggregates and autophagic vesicles. This may be caused by the USP20-ULK1 axis upregulation. Consequently, the increased autophagic flux might impair neuronal homeostasis, affecting neuronal correct development and triggering neurodegeneration. Consistent with this hypothesis, in the *Herc2*$^{+/530}$ mice model, with reduced protein levels of HERC2, an increased number of autophagosomes and lysosomes is observed in their Purkinje cells, correlating with cerebellar neurodegeneration [54].

Another mechanism possibly contributing to the neurological phenotype observed in individuals with HERC2-Angelman like syndrome and in *Herc2*$^{+/530}$ mice could be a deficiency

in the HERC2-mediated quality control for proteasome assembly. As mentioned above, protein aggregation is a common feature in neurodegeneration. Moreover, neuronal cells and Purkinje cells are specifically sensitive to disturbed proteostasis [242, 243]. Therefore, HERC2 deficiency might disrupt correct proteasome assembly, enhancing accumulation of orphan protein intermediates, leading to protein aggregation and eventually toxicity and neuronal death. Though, biological consequences of HERC2 depletion in the proteasome assembly pathway have not yet been explored.

CHAPTER VI. Conclusions

Throughout this work we revealed previously unexplored functions of the ubiquitin ligase HERC2 in cell signalling and provided the potential molecular mechanism behind them. In particular, several conclusions can be drawn from the results presented here:

1. HERC2 forms a complex with RAF proteins and regulates C-RAF ubiquitylation targeting it for proteasomal-dependent degradation.
2. HERC2 deficiency increases C-RAF protein levels, which triggers overactivation of a crosstalk between C-RAF and MKK3/p38 MAPK signalling pathways.
3. The C-RAF/MKK3/p38 signalling pathway regulated by HERC2 modulates the oxidative stress response through NRF2 and the expression of antioxidant genes.
4. RAF and p38 inhibitors abrogate the altered cellular response to oxidative stress upon HERC2 deficiency.
5. HERC2 deficiency enhances the autophagy-lysosome pathway.
6. HERC2 interacts with USP20 and regulates its protein levels.
7. Activation of p38 disrupts HERC2-USP20 interaction, correlating with increased protein levels of USP20, ULK1 and LC3-II.
8. The ^{bio}Ub strategy can be used to identify ubiquitylated proteins regulated by HERC2.
9. An important number of the ubiquitylated proteins regulated by HERC2 identified in this study are related to the assembly and structure of the proteasome, revealing a previously unexplored role of HERC2 in this pathway.
10. HERC2 forms a complex with the proteasome subunit PSMC5 and its cognate chaperone PAAF1.

The importance of these findings lies in the fact that a better understanding of the molecular mechanisms behind HERC2-dependent cell signalling allows the identification of novel therapeutic targets. This may be relevant for cases with pathologic HERC2 variants, such as the neurodevelopmental disorder HERC2 Angelman-like syndrome, and for tumours harbouring HERC2 mutations.

That being said, in this world so focused on productivity and immediate applicability, we must not forget that basic research also provides immediate value. This value goes beyond material products and economic profitability and is called *knowledge*. It may seem simple, but we should still give it the importance it deserves.

Bibliography

1. Goldstein G, Scheid M, Hammerling U, et al (1975) Isolation of a polypeptide that has lymphocyte differentiating properties and is probably represented universally in living cells. Proc Natl Acad Sci USA 72:11–15. https://doi.org/10.1073/pnas.72.1.11

2. Hershko A, Ciechanover A, Heller H, et al (1980) Proposed role of ATP in protein breakdown: conjugation of protein with multiple chains of the polypeptide of ATP-dependent proteolysis. Proc Natl Acad Sci USA 77:1783–1786. https://doi.org/10.1073/pnas.77.4.1783

3. Ciechanover A, Heller H, Katz-Etzion R, Hershko A (1981) Activation of the heat-stable polypeptide of the ATP-dependent proteolytic system. Proc Natl Acad Sci USA 78:761–765. https://doi.org/10.1073/pnas.78.2.761

4. Ciechanover A, Elias S, Heller H, Hershko A (1982) "Covalent affinity" purification of ubiquitin-activating enzyme. J Biol Chem 257:2537–2542. https://doi.org/10.1016/s0021-9258(18)34957-3

5. Kresge N, Simoni RD, Hill RL (2006) The Discovery of Ubiquitin-mediated Proteolysis by Aaron Ciechanover, Avram Hershko, and Irwin Rose. J Biol Chem 281:32–36. https://doi.org/10.1016/s0021-9258(19)33845-1

6. Komander D, Rape M (2012) The Ubiquitin Code. Annu Rev Biochem 81:203–229. https://doi.org/10.1146/annurev-biochem-060310-170328

7. Kliza K, Husnjak K (2020) Resolving the Complexity of Ubiquitin Networks. Front Mol Biosci 7:21. https://doi.org/10.3389/fmolb.2020.00021

8. Buetow L, Huang DT (2016) Structural insights into the catalysis and regulation of E3 ubiquitin ligases. Nat Rev Mol Cell Biol 17:626–642. https://doi.org/10.1038/nrm.2016.91

9. Mevissen TET, Komander D (2017) Mechanisms of deubiquitinase specificity and regulation. Annu Rev Biochem 86:159–192. https://doi.org/10.1146/annurev-biochem-061516-044916

10. Swatek KN, Komander D (2016) Ubiquitin modifications. Cell Res 26:399–422. https://doi.org/10.1038/cr.2016.39

11. Chen BB, Mallampalli RK (2009) Masking of a Nuclear Signal Motif by Monoubiquitination Leads to Mislocalization and Degradation of the Regulatory Enzyme Cytidylyltransferase. Mol Cell Biol 29:3062–3075. https://doi.org/10.1128/MCB.01824-08

12. Braten O, Livneh I, Ziv T, et al (2016) Numerous proteins with unique characteristics are degraded by the 26S proteasome following monoubiquitination. Proc Natl Acad Sci USA 113:4639–4647. https://doi.org/10.1073/pnas.1608644113

13. Kim W, Bennett EJ, Huttlin EL, et al (2011) Systematic and quantitative assessment of the ubiquitin-modified proteome. Mol Cell 44:325–340. https://doi.org/10.1016/j.molcel.2011.08.025

14. Mattern M, Sutherland J, Kadimisetty K, et al (2019) Using Ubiquitin Binders to Decipher the Ubiquitin Code. Trends Biochem Sci 44:599–615. https://doi.org/10.1016/j.tibs.2019.01.011

15. Huang Q, Zhang X (2020) Emerging Roles and Research Tools of Atypical Ubiquitination. Proteomics 20:e1900100. https://doi.org/10.1002/pmic.201900100

16. Akutsu M, Dikic I, Bremm A (2016) Ubiquitin chain diversity at a glance. J Cell Sci 129:875–880. https://doi.org/10.1242/jcs.183954

17. Morreale FE, Walden H (2016) Types of Ubiquitin Ligases. Cell 165:248-248.e1. https://doi.org/10.1016/j.cell.2016.03.003

18. Dove KK, Klevit RE (2017) RING-Between-RING E3 Ligases: Emerging Themes amid the Variations. J Mol Biol 429:3363–3375. https://doi.org/10.1016/j.jmb.2017.08.008

19. García-Cano J, Martinez-Martinez A, Sala-Gaston J, et al (2019) HERCing: Structural and Functional Relevance of the Large HERC Ubiquitin Ligases. Front Physiol 10:1014. https://doi.org/10.3389/fphys.2019.01014

20. Scheffner M, Kumar S (2014) Mammalian HECT ubiquitin-protein ligases: Biological and pathophysiological aspects. Biochim Biophys Acta 1843:61–74. https://doi.org/10.1016/j.bbamcr.2013.03.024

21. Sluimer J, Distel B (2018) Regulating the human HECT E3 ligases. Cell Mol Life Sci 75:3121–3141. https://doi.org/10.1007/s00018-018-2848-2

22. Marin I (2010) Animal HECT ubiquitin ligases: Evolution and functional implications. BMC Evol Biol 10:56. https://doi.org/10.1186/1471-2148-10-56

23. Sánchez-Tena S, Cubillos-Rojas M, Schneider T, Rosa JL (2016) Functional and pathological relevance of HERC family proteins: A decade later. Cell Mol Life Sci 73:1955–1968. https://doi.org/10.1007/s00018-016-2139-8

24. Hadjebi O, Casas-Terradellas E, Garcia-Gonzalo FR, Rosa JL (2008) The RCC1 superfamily: From genes, to function, to disease. Biochim Biophys Acta 1783:1467–79. https://doi.org/10.1016/j.bbamcr.2008.03.015

25. Schneider T, Martinez-Martinez A, Cubillos-Rojas M, et al (2018) The E3 ubiquitin ligase HERC1 controls the ERK signaling pathway targeting C-RAF for degradation. Oncotarget 9:31531–31548. https://doi.org/10.18632/oncotarget.25847

26. Zavodszky E, Peak-Chew SY, Juszkiewicz S, et al (2021) Identification of a quality-control factor that monitors failures during proteasome assembly. Science 373:998–1004. https://doi.org/10.1126/science.abc6500

27. Grossberger R, Gieffers C, Zachariae W, et al (1999) Characterization of the DOC1/APC10 subunit of the yeast and the human anaphase-promoting complex. J Biol Chem 274:14500–14507. https://doi.org/10.1074/jbc.274.20.14500

28. Itoh M, Kim CH, Palardy G, et al (2003) Mind bomb is a ubiquitin ligase that is essential for efficient activation of notch signaling by delta. Dev Cell 4:67–82. https://doi.org/10.1016/S1534-5807(02)00409-4

29. Cubillos-Rojas M, Amair-Pinedo F, Peiró-Jordán R, et al (2014) The E3 ubiquitin protein ligase HERC2 modulates the activity of tumor protein p53 by regulating its oligomerization. J Biol Chem 289:14782–14795. https://doi.org/10.1074/jbc.M113.527978

30. Danielsen JR, Povlsen LK, Villumsen BH, et al (2012) DNA damage-inducible SUMOylation of HERC2 promotes RNF8 binding via a novel SUMO-binding Zinc finger. J Cell Biol 197:179–187. https://doi.org/10.1083/jcb.201106152

31. Liu J, Xue Z, Zhang Y, et al (2020) Structural Insight into Binding of the ZZ Domain of HERC2 to Histone H3 and SUMO1. Structure 28:1225–1230. https://doi.org/10.1016/j.str.2020.07.003

32. Tencer AH, Liu J, Zhu J, et al (2022) The ZZ domain of HERC2 is a receptor of arginylated substrates. Sci Rep 12:6063. https://doi.org/10.1038/s41598-022-10119-w

33. Martinez-Noel G, Galligan JT, Sowa ME, et al (2012) Identification and Proteomic Analysis of Distinct UBE3A/E6AP Protein Complexes. Mol Cell Biol 32:3095–3106. https://doi.org/10.1128/mcb.00201-12

34. Kang TH, Lindsey-Boltz LA, Reardon JT, Sancar A (2010) Circadian control of XPA and excision repair of cisplatin-DNA damage by cryptochrome and HERC2 ubiquitin ligase. Proc Natl Acad Sci USA 107:4890–4895. https://doi.org/10.1073/pnas.0915085107

35. Lee TH, Park JM, Leem SH, Kang TH (2014) Coordinated regulation of XPA stability by ATR and HERC2 during nucleotide excision repair. Oncogene 33:19–25. https://doi.org/10.1038/onc.2012.539

36. Wu W, Sato K, Koike A, et al (2010) HERC2 is an E3 ligase that targets BRCA1 for degradation. Cancer Res 70:6384–6392. https://doi.org/10.1158/0008-5472.CAN-10-1304

37. Jiang Q, Greenberg RA (2015) Deciphering the BRCA1 tumor suppressor network. J Biol Chem 290:17724–17732. https://doi.org/10.1074/jbc.R115.667931

38. Peng Y, Dai H, Wang E, et al (2015) TUSC4 functions as a tumor suppressor by regulating BRCA1 stability. Cancer Res 75:378–386. https://doi.org/10.1158/0008-5472.CAN-14-2315

39. Xu S, Wu X, Wang P, Cao S (2021) ASPM promotes homologous recombination-mediated DNA repair by safeguarding BRCA1 stability. iScience 24:102534. https://doi.org/10.1016/j.isci.2021.102534

40. Bekker-Jensen S, Danielsen JR, Fugger K, et al (2010) HERC2 coordinates ubiquitin-dependent assembly of DNA repair factors on damaged chromosomes. Nat Cell Biol 12:80–86. https://doi.org/10.1038/ncb2008

41. Zhang Z, Yang H, Wang H (2014) The histone H2A deubiquitinase USP16 interacts with HERC2 and fine-tunes cellular response to DNA damage. J Biol Chem 289:32883–32894. https://doi.org/10.1074/jbc.M114.599605

42. Izawa N, Wu W, Sato K, et al (2011) HERC2 interacts with claspin and regulates DNA origin firing and replication fork progression. Cancer Res 71:5621–5625. https://doi.org/10.1158/0008-5472.CAN-11-0385

43. Zhu M, Zhao H, Liao J, Xu X (2014) HERC2/USP20 coordinates CHK1 activation by modulating CLASPIN stability. Nucleic Acids Res 42:13074–13081. https://doi.org/10.1093/nar/gku978

44. Yuan J, Luo K, Deng M, et al (2014) HERC2-USP20 axis regulates DNA damage checkpoint through Claspin. Nucleic Acids Res 42:13110–13121. https://doi.org/10.1093/nar/gku1034

45. Wu W, Rokutanda N, Takeuchi J, et al (2018) HERC2 facilitates BLM and WRN helicase complex interaction with RPA to suppress G-quadruplex DNA. Cancer Res 78:6371–6385. https://doi.org/10.1158/0008-5472.CAN-18-1877

46. Lai Y, Zhu M, Wu W, et al (2019) HERC2 regulates RPA2 by mediating ATR-induced Ser33 phosphorylation and ubiquitin-dependent degradation. Sci Rep 9:14257. https://doi.org/10.1038/s41598-019-50812-x

47. Zhu M, Wu W, Togashi Y, et al (2021) HERC2 inactivation abrogates nucleolar localization of RecQ helicases BLM and WRN. Sci Rep 11:360. https://doi.org/10.1038/s41598-020-79715-y

48. Cubillos-Rojas M, Schneider T, Bartrons R, et al (2017) NEURL4 regulates the transcriptional activity of tumor suppressor protein p53 by modulating its oligomerization. Oncotarget 8:61824. https://doi.org/10.18632/oncotarget.18699

49. García-Cano J, Sánchez-Tena S, Sala-Gaston J, et al (2020) Regulation of the MDM2-p53 pathway by the ubiquitin ligase HERC2. Mol Oncol 14:69–86. https://doi.org/10.1002/1878-0261.12592

50. Wang H, Xing J, Wang W, et al (2021) Molecular Characterization of the Oncogene BTF3 and Its Targets in Colorectal Cancer. Front Cell Dev Biol 8:601502. https://doi.org/10.3389/fcell.2020.601502

51. Pérez-Villegas EM, Ruiz R, Bachiller S, et al (2022) The HERC proteins and the nervous system. Semin Cell Dev Biol 132:5. https://doi.org/10.1016/j.semcdb.2021.11.017

52. Lehman AL, Nakatsu Y, Ching A, et al (1998) A very large protein with diverse functional motifs is deficient in rjs (runty, jerky, sterile) mice. Proc Natl Acad Sci USA 95:9436–9441. https://doi.org/10.1073/pnas.95.16.9436

53. Walkowicz M, Yonggang J, Xiaojia R, et al (1999) Molecular characterization of radiation- and chemically induced mutations associated with neuromuscular tremors, runting, juvenile lethality, and sperm defects in jdf2 mice. Mamm Genome 10:870–878. https://doi.org/10.1007/s003359901106

54. Cubillos-Rojas M, Schneider T, Hadjebi O, et al (2016) The HERC2 ubiquitin ligase is essential for embryonic development and regulates motor coordination. Oncotarget 7:56083–56106. https://doi.org/10.18632/oncotarget.11270

55. Ji Y, Rebert NA, Joslin JM, et al (2000) Structure of the highly conserved HERC2 gene and of multiple partially duplicated paralogs in human. Genome Res 10:319–329. https://doi.org/10.1101/gr.10.3.319

56. Dimitropoulos A, Schultz RT (2007) Autistic-like symptomatology in Prader-Willi syndrome: A review of recent findings. Curr Psychiatry Rep 9:159–164. https://doi.org/10.1007/s11920-007-0086-7

57. Puffenberger EG, Jinks RN, Wang H, et al (2012) A homozygous missense mutation in HERC2 associated with global developmental delay and autism spectrum disorder. Hum Mutat 33:1639–1646. https://doi.org/10.1002/humu.22237

58. Harlalka G V., Baple EL, Cross H, et al (2013) Mutation of HERC2 causes developmental delay with angelman-like features. J Med Genet 50:65–73. https://doi.org/10.1136/jmedgenet-2012-101367

59. Morice-Picard F, Benard G, Rezvani HR, et al (2016) Complete loss of function of the ubiquitin ligase HERC2 causes a severe neurodevelopmental phenotype. Eur J Hum Genet 25:52–58. https://doi.org/10.1038/ejhg.2016.139

60. Elpidorou M, Best S, Poulter JA, et al (2021) Novel loss-of-function mutation in HERC2 is associated with severe developmental delay and paediatric lethality. J Med Genet 58:334–341. https://doi.org/10.1136/jmedgenet-2020-106873

61. Vincent KM, Eaton A, Yassaee VR, et al (2021) Delineating the expanding phenotype of HERC2-related disorders: The impact of biallelic loss of function versus missense variation. Clin Genet 100:637–640. https://doi.org/10.1111/cge.14039

62. Imai Y, Kobayashi Y, Inoshita T, et al (2015) The Parkinson's Disease-Associated Protein Kinase LRRK2 Modulates Notch Signaling through the Endosomal Pathway. PLoS Genet 11:e1005503. https://doi.org/10.1371/journal.pgen.1005503

63. Al-Hakim AK, Bashkurov M, Gingras AC, et al (2012) Interaction proteomics identify NEURL4 and the HECT E3 ligase HERC2 as novel modulators of centrosome architecture. Mol Cell Proteomics 11:M111.014233. https://doi.org/10.1074/mcp.M111.014233

64. Li M, Xu X, Zhang J, et al (2019) NudC-like protein 2 restrains centriole amplification by stabilizing HERC2. Cell Death Dis 10:628. https://doi.org/10.1038/s41419-019-1843-3

65. Moroishi T, Yamauchi T, Nishiyama M, Nakayama KI (2014) HERC2 targets the iron regulator FBXL5 for degradation and modulates iron metabolism. J Biol Chem 289:16430–16441. https://doi.org/10.1074/jbc.M113.541490

66. Mancias JD, Vaites LP, Nissim S, et al (2015) Ferritinophagy via NCOA4 is required for erythropoiesis and is regulated by iron dependent HERC2-mediated proteolysis. Elife 4:e10308. https://doi.org/10.7554/eLife.10308

67. Wang LQ, Zheng YY, Zhou HJ, et al (2021) LncRNA-Fendrr protects against the ubiquitination and degradation of NLRC4 protein through HERC2 to regulate the pyroptosis of microglia. Mol Med 27:39. https://doi.org/10.1186/s10020-021-00299-y

68. Suarez P, Baumer K, Hall D (2021) Further insight into the global variability of the OCA2-HERC2 locus for human pigmentation from multiallelic markers. Sci Rep 11:22530. https://doi.org/10.1038/s41598-021-01940-w

69. Peng J, Schwartz D, Elias JE, et al (2003) A proteomics approach to understanding protein ubiquitination. Nat Biotechnol 21:921–926. https://doi.org/10.1038/nbt849

70. Xu G, Paige JS, Jaffrey SR (2010) Global analysis of lysine ubiquitination by ubiquitin remnant immunoaffinity profiling. Nat Biotechnol 28:868–873. https://doi.org/10.1038/nbt.1654

71. Ramirez J, Prieto G, Olazabal-Herrero A, et al (2021) A proteomic approach for systematic mapping of substrates of human deubiquitinating enzymes. Int J Mol Sci 22:4851. https://doi.org/10.3390/ijms22094851

72. Martinez A, Lectez B, Ramirez J, et al (2017) Quantitative proteomic analysis of Parkin substrates in Drosophila neurons. 12:29. https://doi.org/10.1186/s13024-017-0170-3

73. Ramirez J, Lectez B, Osinalde N, et al (2018) Quantitative proteomics reveals neuronal ubiquitination of Rngo/Ddi1 and several proteasomal subunits by Ube3a , accounting for the complexity of Angelman syndrome. Hum Mol Genet 27:1955–1971. https://doi.org/10.1093/hmg/ddy103

74. Ramírez J, Morales M, Osinalde N, et al (2021) The ubiquitin ligase Ariadne-1 regulates neurotransmitter release via ubiquitination of NSF. J Biol Chem 296:100408. https://doi.org/10.1016/j.jbc.2021.100408

75. Cargnello M, Roux PP (2011) Activation and Function of the MAPKs and Their Substrates, the MAPK-Activated Protein Kinases. Microbiol Mol Biol Rev 75:50–83. https://doi.org/10.1128/mmbr.00031-10

76. Plotnikov A, Zehorai E, Procaccia S, Seger R (2011) The MAPK cascades: Signaling components, nuclear roles and mechanisms of nuclear translocation. Biochim Biophys Acta 1813:1619–1633. https://doi.org/10.1016/j.bbamcr.2010.12.012

77. Coulombe P, Meloche S (2007) Atypical mitogen-activated protein kinases: Structure, regulation and functions. Biochim Biophys Acta 1773:1376–1387. https://doi.org/10.1016/j.bbamcr.2006.11.001

78. Molina JR, Adjei AA (2006) The Ras/Raf/MAPK Pathway. J Thorac Oncol 1:7–9. https://doi.org/10.1016/s1556-0864(15)31506-9

79. Samson SC, Khan AM, Mendoza MC (2022) ERK signaling for cell migration and invasion. Front Mol Biosci 9:998475. https://doi.org/10.3389/fmolb.2022.998475

80. Lavoie H, Gagnon J, Therrien M (2020) ERK signalling: a master regulator of cell behaviour, life and fate. Nat Rev Mol Cell Biol 21:607–632. https://doi.org/10.1038/s41580-020-0255-7

81. Martinez-Lopez N, Athonvarangkul D, Mishall P, et al (2013) Autophagy proteins regulate ERK phosphorylation. Nat Commun 4:2799. https://doi.org/10.1038/ncomms3799

82. Casar B, Crespo P (2016) ERK Signals: Scaffolding scaffolds? Front Cell Dev Biol 4:49. https://doi.org/10.3389/fcell.2016.00049

83. Desideri E, Cavallo AL, Baccarini M (2015) Alike but Different : RAF Paralogs and Their Signaling Outputs. Cell 161:967–970. https://doi.org/10.1016/j.cell.2015.04.045

84. Brummer T, McInnes C (2020) RAF kinase dimerization: implications for drug discovery and clinical outcomes. Oncogene 39:4155–4169. https://doi.org/10.1038/s41388-020-1263-y

85. Maloney R, Nussinov R (2021) The mechanism of Raf activation through dimerization. Chem Sci 12:15609–15619. https://doi.org/10.1039/d1sc03444h

86. Kostenko S, Dumitriu G, Jenssen Lægreid K, Moens U (2011) Physiological roles of mitogen-activated-protein-kinase-activated p38-regulated/activated protein kinase. World J Biol Chem 2:73–89. https://doi.org/10.4331/wjbc.v2.i5.73

87. Cuevas BD, Abell AN, Johnson GL (2007) Role of mitogen-activated protein kinase kinase kinases in signal integration. Oncogene 26:3159–3171. https://doi.org/10.1038/sj.onc.1210409

88. Sakauchi C, Wakatsuki H, Ichijo H, Hattori K (2017) Pleiotropic properties of ASK1. Biochim Biophys Acta 1861:3030–38. https://doi.org/10.1016/j.bbagen.2016.09.028

89. Matsushita M, Nakamura T, Moriizumi H, et al (2020) Stress-responsive MTK1 SAPKKK serves as a redox sensor that mediates delayed and sustained activation of SAPKs by oxidative stress. Sci Adv 6:eaay9778. https://doi.org/10.1126/sciadv.aay9778

90. Canovas B, Nebreda AR (2021) Diversity and versatility of p38 kinase signalling in health and disease. Nat Rev Mol Cell Biol 22:346–366. https://doi.org/10.1038/s41580-020-00322-w

91. Bouhaddou M, Memon D, Meyer B, et al (2020) The Global Phosphorylation Landscape of SARS-CoV-2 Infection. Cell 182:685–712. https://doi.org/10.1016/j.cell.2020.06.034

92. Maik-Rachline G, Lifshits L, Seger R (2020) Nuclear p38: Roles in physiological and pathological processes and regulation of nuclear translocation. Int J Mol Sci 21:6102. https://doi.org/10.3390/ijms21176102

93. Cuadrado A, Nebreda AR (2010) Mechanisms and functions of p38 MAPK signalling. Biochem J 429:403–417. https://doi.org/10.1042/BJ20100323

94. Han J, Wu J, Silke J (2020) An overview of mammalian p38 mitogen-activated protein kinases, central regulators of cell stress and receptor signaling. F1000 Res 9:F1000 Faculty Rev-653. https://doi.org/10.12688/f1000research.22092.1

95. Coulthard LR, White DE, Jones DL, et al (2009) p38MAPK: stress responses from molecular mechanisms to therapeutics. Trends Mol Med 15:369–379. https://doi.org/10.1016/j.molmed.2009.06.005

96. Sun A, Liu M, Nguyen X V., Bing G (2003) p38 MAP kinase is activated at early stages in Alzheimer's disease brain. Exp Neurol 183:394–405. https://doi.org/10.1016/S0014-4886(03)00180-8

97. Bendotti C, Atzori C, Piva R, et al (2004) Activated p38MAPK Is a Novel Component of the Intracellular Inclusions Found in Human Amyotrophic Lateral Sclerosis and Mutant SOD1 Transgenic Mice. J Neuropathol Exp Neurol 63:113–119. https://doi.org/10.1093/jnen/63.2.113

98. Chen J, Ren Y, Gui C, et al (2018) Phosphorylation of Parkin at serine 131 by p38 MAPK promotes mitochondrial dysfunction and neuronal death in mutant A53T α-synuclein model of Parkinson's disease. Cell Death Dis 9:700. https://doi.org/10.1038/s41419-018-0722-7

99. Robson MJ, Quinlan MA, Margolis KG, et al (2018) p38α MAPK signaling drives pharmacologically reversible brain and gastrointestinal phenotypes in the SERT Ala56 mouse. Proc Natl Acad Sci USA 115:E10245–E10254. https://doi.org/10.1073/pnas.1809137115

100. Igea A, Nebreda AR (2015) The stress kinase p38α as a target for cancer therapy. Cancer Res 75:3997–4002. https://doi.org/10.1158/0008-5472.CAN-15-0173

101. Park H, Baek K (2022) E3 ligases and deubiquitinating enzymes regulating the MAPK signaling pathway in cancers. Biochim Biophys Acta 1877:188736. https://doi.org/10.1016/j.bbcan.2022.188736

102. Pedrazza L, Schneider T, Bartrons R, et al (2020) The ubiquitin ligase HERC1 regulates cell migration via RAF-dependent regulation of MKK3/p38 signaling. Sci Rep 10:824. https://doi.org/10.1038/s41598-020-57756-7

103. Martínez-Noël G, Luck K, Kühnle S, et al (2018) Network Analysis of UBE3A/E6AP-Associated Proteins Provides Connections to Several Distinct Cellular Processes. J Mol Biol 430:1024–1050. https://doi.org/10.1016/j.jmb.2018.01.021

104. Cullinan SB, Diehl JA (2006) Coordination of ER and oxidative stress signaling: The PERK/Nrf2 signaling pathway. Int J Biochem Cell Biol 38:317–332. https://doi.org/10.1016/j.biocel.2005.09.018

105. Abdal Dayem A, Choi HY, Kim JH, Cho SG (2010) Role of oxidative stress in stem, cancer, and cancer stem cells. Cancers (Basel) 2:859–884. https://doi.org/10.3390/cancers2020859

106. Sies H, Berndt C, P. Jones D (2010) Oxidative stress. Annu Rev Biochem 86:715–748. https://doi.org/10.1007/978-3-540-69361-1_27

107. McCubrey JA, LaHair MM, Franklin RA (2006) Reactive Oxygen Species-Induced Activation of the MAP Kinase Signaling Pathways. Antioxid Redox Signal 8:1775–1789. https://doi.org/10.1089/ars.2006.8.1775

108. Yong S, Sangduck K, Hun-Taeg C, Hyun-Ock P (2013) Reactive oxygen species in the activation of MAP kinases. Methods Enzymol 528:27–48. https://doi.org/10.1016/B978-0-12-405881-1.00002-1

109. Vomund S, Schäfer A, Parnham MJ, et al (2017) Nrf2, the master regulator of anti-oxidative responses. Int J Mol Sci 18:2772. https://doi.org/10.3390/ijms18122772

110. Cullinan SB, Gordan JD, Jin J, et al (2004) The Keap1-BTB Protein Is an Adaptor That Bridges Nrf2 to a Cul3-Based E3 Ligase: Oxidative Stress Sensing by a Cul3-Keap1 Ligase. Mol Cell Biol 24:8477–8486. https://doi.org/10.1128/mcb.24.19.8477-8486.2004

111. Li Y, Li S, Wu H (2022) Ubiquitination-Proteasome System (UPS) and Autophagy Two Main Protein Degradation Machineries in Response to Cell Stress. Cells 11:851. https://doi.org/10.3390/cells11050851

112. Dikic I (2017) Proteasomal and autophagic degradation systems. Annu Rev Biochem 86:193–224. https://doi.org/10.1146/annurev-biochem-061516-044908

113. Lamb CA, Yoshimori T, Tooze SA (2013) The autophagosome: Origins unknown, biogenesis complex. Nat Rev Mol Cell Biol 14:759–774. https://doi.org/10.1038/nrm3696

114. Wang L, Klionsky DJ, Shen HM (2022) The emerging mechanisms and functions of microautophagy. Nat Rev Mol Cell Biol. https://doi.org/10.1038/s41580-022-00529-z

115. Kaushik S, Cuervo AM (2018) The coming of age of chaperone-mediated autophagy. Nat Rev Mol Cell Biol 19:365–381. https://doi.org/10.1038/s41580-018-0001-6

116. Lamark T, Johansen T (2021) Mechanisms of Selective Autophagy. Annu Rev Cell Dev Biol 37:143–169. https://doi.org/10.1146/annurev-cellbio-120219-035530

117. Nishimura T, Tooze SA (2020) Emerging roles of ATG proteins and membrane lipids in autophagosome formation. Cell Discov 6:32. https://doi.org/10.1038/s41421-020-0161-3

118. Nakatogawa H (2020) Mechanisms governing autophagosome biogenesis. Nat Rev Mol Cell Biol 21:439–458. https://doi.org/10.1038/s41580-020-0241-0

119. Dikic I, Elazar Z (2018) Mechanism and medical implications of mammalian autophagy. Nat Rev Mol Cell Biol 19:349–364. https://doi.org/10.1038/s41580-018-0003-4

120. Saxton RA, Sabatini DM (2017) mTOR Signaling in Growth, Metabolism, and Disease. Cell 168:960–976. https://doi.org/10.1016/j.cell.2017.02.004

121. Martina JA, Chen Y, Gucek M, Puertollano R (2012) MTORC1 functions as a transcriptional regulator of autophagy by preventing nuclear transport of TFEB. Autophagy 8:903–914. https://doi.org/10.4161/auto.19653

122. Gwinn DM, Shackelford DB, Egan DF, et al (2008) AMPK Phosphorylation of Raptor Mediates a Metabolic Checkpoint. Mol Cell 30:214–226. https://doi.org/10.1016/j.molcel.2008.03.003

123. Zaffagnini G, Martens S (2016) Mechanisms of Selective Autophagy. J Mol Biol 428:1714–1724. https://doi.org/10.1016/j.jmb.2016.02.004

124. Aman Y, Schmauck-medina T, Hansen M, et al (2021) Autophagy in healthy aging and disease. Nat Aging 1:634–650. https://doi.org/10.1038/s43587-021-00098-4

125. Vargas JNS, Wang C, Bunker E, et al (2019) Spatiotemporal Control of ULK1 Activation by NDP52 and TBK1 during Selective Autophagy. Mol Cell 74:347–362. https://doi.org/10.1016/j.molcel.2019.02.010

126. Richter B, Sliter DA, Herhaus L, et al (2016) Phosphorylation of OPTN by TBK1 enhances its binding to Ub chains and promotes selective autophagy of damaged mitochondria. Proc Natl Acad Sci USA 113:4039–4044. https://doi.org/10.1073/pnas.1523926113

127. Ravenhill BJ, Boyle KB, Foeglein A, et al (2019) The Cargo Receptor NDP52 Initiates Selective Autophagy by Recruiting the ULK Complex to Cytosol-Invading Bacteria. Mol Cell 74:320–329. https://doi.org/10.1016/j.molcel.2019.01.041

128. Slobodnyuk K, Radic N, Llado A, et al (2019) Autophagy-induced senescence is regulated by p38α signaling. Cell Death Dis 10:376. https://doi.org/10.1038/s41419-019-1607-0

129. Rousseau A, Bertolotti A (2018) Regulation of proteasome assembly and activity in health and disease. Nat Rev Mol Cell Biol 19:697–712. https://doi.org/10.1038/s41580-018-0040-z

130. Inobe T, Matouschek A (2014) Paradigms of protein degradation by the proteasome. Curr Opin Struct Biol 24:156–164. https://doi.org/10.1016/j.sbi.2014.02.002

131. Kamber Kaya HE, Radhakrishnan SK (2021) Trash Talk: Mammalian Proteasome Regulation at the Transcriptional Level. Trends Genet 37:160–173. https://doi.org/10.1016/j.tig.2020.09.005

132. McCarthy MK, Weinberg JB (2015) The immunoproteasome and viral infection: A complex regulator of inflammation. Front Microbiol 6:21. https://doi.org/10.3389/fmicb.2015.00021

133. Basler M, Groettrup M (2021) On the Role of the Immunoproteasome in Protein Homeostasis. Cells 10:3216. https://doi.org/10.3390/cells10113216

134. Harper JW, Bennett EJ (2016) Proteome complexity and the forces that drive proteome imbalance. Nature 537:328–338. https://doi.org/10.1038/nature19947

135. Marshall RS, Vierstra RD (2019) Dynamic regulation of the 26S proteasome: From synthesis to degradation. Front Mol Biosci 6:40. https://doi.org/10.3389/fmolb.2019.00040

136. Hirano Y, Hendil KB, Yashiroda H, et al (2005) A heterodimeric complex that promotes the assembly of mammalian 20S proteasomes. Nature 437:1381–1385. https://doi.org/10.1038/nature04106

137. Wani PS, Rowland MA, Ondracek A, et al (2015) Maturation of the proteasome core particle induces an affinity switch that controls regulatory particle association. Nat Commun 6:6384. https://doi.org/10.1038/ncomms7384

138. Fricke B, Heink S, Steffen J, et al (2007) The proteasome maturation protein POMP facilitates major steps of 20S proteasome formation at the endoplasmic reticulum. EMBO Rep 8:1170–1175. https://doi.org/10.1038/sj.embor.7401091

139. Finley D (2009) Recognition and Processing of Ubiquitin-Protein Conjugates by the Proteasome. Annu Rev Biochem 78:477–513. https://doi.org/10.1146/annurev.biochem.78.081507.101607

140. Bellezza I, Giambanco I, Minelli A, Donato R (2018) Nrf2-Keap1 signaling in oxidative and reductive stress. Biochim Biophys Acta 1865:721–733. https://doi.org/10.1016/j.bbamcr.2018.02.010

141. Antonioli M, Albiero F, Nazio F, et al (2014) AMBRA1 Interplay with Cullin E3 Ubiquitin Ligases Regulates Autophagy Dynamics. Dev Cell 31:734–746. https://doi.org/10.1016/j.devcel.2014.11.013

142. Moffat J, Grueneberg DA, Yang X, et al (2006) A Lentiviral RNAi Library for Human and Mouse Genes Applied to an Arrayed Viral High-Content Screen. Cell 124:1283–1298. https://doi.org/10.1016/j.cell.2006.01.040

143. Cubillos-Rojas M, Amair-Pinedo F, Tato I, et al (2010) Simultaneous electrophoretic analysis of proteins of very high and low molecular mass using Tris-acetate polyacrylamide gels. Electrophoresis 31:1318–1321. https://doi.org/10.1002/elps.200900657

144. Osinalde N, Sánchez-Quiles V, Akimov V, et al (2015) SILAC-based quantification of changes in protein tyrosine phosphorylation induced by Interleukin-2 (IL-2) and IL-15 in T-lymphocytes. Data Brief 5:53–58. https://doi.org/10.1016/j.dib.2015.08.007

145. Wang C, Xu H, Lin S, et al (2020) GPS 5.0: An Update on the Prediction of Kinase-specific Phosphorylation Sites in Proteins. Genomics Proteomics Bioinformatics 18:72–80. https://doi.org/10.1016/j.gpb.2020.01.001

146. Raingeaud J, Gupta S, Rogers JS, et al (1995) Pro-inflammatory cytokines and environmental stress cause p38 mitogen- activated protein kinase activation by dual phosphorylation on tyrosine and threonine. J Biol Chem 270:7420–7426. https://doi.org/10.1074/jbc.270.13.7420

147. Manford AG, Rodríguez-Pérez F, Shih KY, et al (2020) A Cellular Mechanism to Detect and Alleviate Reductive Stress. Cell 183:46-61.e21. https://doi.org/10.1016/j.cell.2020.08.034

148. Manford AG, Mena EL, Shih KY, et al (2021) Structural basis and regulation of the reductive stress response. Cell 184:5375-5390.e16. https://doi.org/10.1016/j.cell.2021.09.002

149. Kim JH, Seo D, Kim S, et al (2018) The deubiquitinating enzyme USP20 stabilizes ULK1 and promotes autophagy initiation. EMBO Rep 19:e44378. https://doi.org/10.15252/embr.201744378

150. Galligan T, Martinez-noe G, Arndt V, et al (2015) Proteomic Analysis and Identification of Cellular Interactors of the Giant Ubiquitin Ligase HERC2. J Proteome Res 14:953−966. https://doi.org/doi:10.1021/pr501005v

151. Saez I, Koyuncu S, Gutierrez-Garcia R, et al (2018) Insights into the ubiquitin-proteasome system of human embryonic stem cells. Sci Rep. https://doi.org/10.1038/s41598-018-22384-9

152. Gu ZC, Enenkel C (2014) Proteasome assembly. Cell Mol Life Sci 71:4729–4745. https://doi.org/10.1007/s00018-014-1699-8

153. Sato S, Trackman PC, Mäki JM, et al (2011) The Ras Signaling Inhibitor LOX-PP Interacts with Hsp70 and c-Raf To Reduce Erk Activation and Transformed Phenotype of Breast Cancer Cells. Mol Cell Biol 31:2683–2695. https://doi.org/10.1128/mcb.01148-10

154. Guo Z, Song T, Wang Z, et al (2020) The chaperone Hsp70 is a BH3 receptor activated by the pro-apoptotic Bim to stabilize anti-apoptotic clients. J Biol Chem 295:12900–12909. https://doi.org/10.1074/jbc.ra120.013364

155. Grammatikakis N, Lin J-H, Grammatikakis A, et al (1999) p50 cdc37 Acting in Concert with Hsp90 Is Required for Raf-1 Function . Mol Cell Biol 19:1661–1672. https://doi.org/10.1128/mcb.19.3.1661

156. Mitra S, Ghosh B, Gayen N, et al (2016) Bipartite role of heat shock protein 90 (Hsp90) keeps CRAF kinase poised for activation. J Biol Chem 291:24579–24593. https://doi.org/10.1074/jbc.M116.746420

157. García-Alonso S, Mesa P, Ovejero L de la P, et al (2022) Structure of the RAF1-HSP90-CDC37 complex reveals the basis of RAF1 regulation. Mol Cell 82:3438-3452.e8. https://doi.org/10.1016/j.molcel.2022.08.012

158. Rosa JL, Barbacid M (1997) A giant protein that stimulates guanine nucleotide exchange on ARF1 and Rab proteins forms a cytosolic ternary complex with clathrin and Hsp70. Oncogene 15:1–6. https://doi.org/10.1038/sj.onc.1201170

159. Rojo de la Vega M, Chapman E, Zhang DD (2018) NRF2 and the Hallmarks of Cancer. Cancer Cell 34:21–43. https://doi.org/10.1016/j.ccell.2018.03.022

160. Suzuki T, Yamamoto M (2015) Molecular basis of the Keap1-Nrf2 system. Free Radic Biol Med 88:93–100. https://doi.org/10.1016/j.freeradbiomed.2015.06.006

161. Kang KW, Ryu JIH, Kim SG (2000) The essential role of phosphatidylinositol 3-kinase and of p38 mitogen-activated protein kinase activation in the antioxidant response element-mediated rGSTA2 induction by decreased glutathione in H4IIE hepatoma cells. Mol Pharmacol 58:1017–1025. https://doi.org/10.1124/mol.58.5.1017

162. Alam J, Wicks C, Stewart D, et al (2000) Mechanism of heme oxygenase-1 gene activation by cadmium in MCF-7 mammary epithelial cells: Role of p38 kinase and Nrf2 transcription factor. J Biol Chem 275:27694–27702. https://doi.org/10.1074/jbc.M004729200

163. Zipper LM, Mulcahy RT (2000) Inhibition of ERK and p38 MAP Kinases inhibits binding of Nrf2 and induction of GCS genes. Biochem Biophys Res Commun 278:484–492. https://doi.org/10.1006/bbrc.2000.3830

164. Yu R, Chen C, Mo YY, et al (2000) Activation of mitogen-activated protein kinase pathways induces antioxidant response element-mediated gene expression via a Nrf2-dependent mechanism. J Biol Chem 275:39907–39913. https://doi.org/10.1074/jbc.M004037200

165. Huang HC, Nguyen T, Pickett CB (2002) Phosphorylation of Nrf2 at Ser-40 by protein kinase C regulates antioxidant response element-mediated transcription. J Biol Chem 277:42769–42774. https://doi.org/10.1074/jbc.M206911200

166. He F, Ru X, Wen T (2020) NRF2, a transcription factor for stress response and beyond. Int J Mol Sci 21:1–23. https://doi.org/10.3390/ijms21134777

167. Gutiérrez-Uzquiza Á, Arechederra M, Bragado P, et al (2012) p38α mediates cell survival in response to oxidative stress via induction of antioxidant genes: Effect on the p70S6K pathway. J Biol Chem 287:2632–2642. https://doi.org/10.1074/jbc.M111.323709

168. Zachari M, Ganley IG (2017) The mammalian ULK1 complex and autophagy initiation. Essays Biochem 61:585–596. https://doi.org/10.1042/EBC20170021

169. Kuang E, Qi J, Ronai Z (2013) Emerging roles of E3 ubiquitin ligases in autophagy. Trends Biochem Sci 38:453–460. https://doi.org/10.1016/j.tibs.2013.06.008

170. Wade Harper J, Ordureau A, Heo JM (2018) Building and decoding ubiquitin hains for mitophagy. Nat Rev Mol Cell Biol 19:93–108. https://doi.org/10.1038/nrm.2017.129

171. Lin Q, Dai Q, Meng H, et al (2017) The HECT E3 ubiquitin ligase NEDD4 interacts with and ubiquitylates SQSTM1 for inclusion body autophagy. J Cell Sci 130:3839–3850. https://doi.org/10.1242/jcs.207068

172. Nazio F, Carinci M, Cecconi F (2017) ULK1 ubiquitylation is regulated by phosphorylation on its carboxy terminus. Cell Cycle 16:1744–1747. https://doi.org/10.1080/15384101.2017.1361063

173. Hochrainer K, Kroismayr R, Baranyi U, et al (2008) Highly homologous HERC proteins localize to endosomes and exhibit specific interactions with hPLIC and Nm23B. Cell Mol Life Sci 65:2105–2117. https://doi.org/10.1007/s00018-008-8148-5

174. Mashimo T, Hadjebi O, Amair-Pinedo F, et al (2009) Progressive Purkinje cell degeneration in tambaleante mutant mice is a consequence of a missense mutation in HERC1 E3 ubiquitin ligase. PLoS Genet 5:e1000784. https://doi.org/10.1371/journal.pgen.1000784

175. Webber JL (2010) Regulation of autophagy by p38α MAPK. Autophagy 6:292–293. https://doi.org/10.4161/auto.6.2.11128

176. Wei Y, An Z, Zou Z, et al (2015) The stress-responsive kinases MAPKAPK2/MAPKAPK3 activate starvation-induced autophagy through Beclin 1 phosphorylation. Elife 4:e05289. https://doi.org/10.7554/eLife.05289

177. Liu Z, Sin KWT, Ding H, et al (2018) P38β MAPK mediates ULK1-dependent induction of autophagy in skeletal muscle of tumor-bearing mice. Cell Stress 2:311–324. https://doi.org/10.15698/cst2018.11.163

178. Trempolec N, Dave-Coll N, Nebreda AR (2013) SnapShot: p38 MAPK substrates. Cell 152:924-924.e1. https://doi.org/10.1016/j.cell.2013.01.047

179. Budenholzer L, Cheng CL, Li Y, Hochstrasser M (2017) Proteasome Structure and Assembly. J Mol Biol 429:3500–3524. https://doi.org/10.1016/j.jmb.2017.05.027

180. Roelofs J, Park S, Haas W, et al (2009) Chaperone-mediated pathway of proteasome regulatory particle assembly. Nature 459:861–865. https://doi.org/10.1038/nature08063

181. Huang N, Xia Y, Zhang D, et al (2017) Hierarchical assembly of centriole subdistal appendages via centrosome binding proteins CCDC120 and CCDC68. Nat Commun 8:15057. https://doi.org/10.1038/ncomms15057

182. Nechipurenko I V., Olivier-Mason A, Kazatskaya A, et al (2016) A Conserved Role for Girdin in Basal Body Positioning and Ciliogenesis. Dev Cell 38:493–506. https://doi.org/10.1016/j.devcel.2016.07.013

183. Lee JE, Silhavy JL, Zaki MS, et al (2012) CEP41 is mutated in Joubert syndrome and is required for tubulin glutamylation at the cilium. Nat Genet 44:193–199. https://doi.org/10.1038/ng.1078

184. De Bie P, Ciechanover A (2011) Ubiquitination of E3 ligases: Self-regulation of the ubiquitin system via proteolytic and non-proteolytic mechanisms. Cell Death Differ 18:1393–1402. https://doi.org/10.1038/cdd.2011.16

185. Mao X, Sethi G, Zhang Z, Wang Q (2018) The Emerging Roles of the HERC Ubiquitin Ligases in Cancer. Curr Pharm Des 24:1676–1681. https://doi.org/10.2174/1381612824666180528081024

186. Sala-Gaston J, Martinez-Martinez A, Pedrazza L, et al (2020) Herc ubiquitin ligases in cancer. Cancers (Basel) 12:1653. https://doi.org/10.3390/cancers12061653

187. Diouf B, Pei D, Fan Y, et al (2011) Somatic deletions of genes regulating MSH2 protein stability cause DNA mismatch repair deficiency and drug resistance in human leukemia cells. Nat Med 17:1298–1303. https://doi.org/10.1038/nm.2430.Somatic

188. Neumann M, Vosberg S, Schlee C, et al (2015) Mutational spectrum of adult T-ALL. Oncotarget 6:2754–2766. https://doi.org/10.18632/oncotarget.2218

189. Johansson P, Klein-Hitpass L, Choidas A, et al (2018) SAMHD1 is recurrently mutated in T-cell prolymphocytic leukemia. Blood Cancer J 8:11. https://doi.org/10.1038/s41408-017-0036-5

190. Opatz S, Bamopoulos SA, Metzeler KH, et al (2020) The clinical mutatome of core binding factor leukemia. Leukemia 34:1553–1562. https://doi.org/10.1038/s41375-019-0697-0

191. Ali MS, Magnati S, Panuzzo C, et al (2022) The Downregulation of Both Giant HERCs, HERC1 and HERC2, Is an Unambiguous Feature of Chronic Myeloid Leukemia, and HERC1 Levels Are Associated with Leukemic Cell Differentiation. J Clin Med 11:324. https://doi.org/10.3390/jcm11020324

192. Craig DW, O'Shaughnessy JA, Kiefer JA, et al (2013) Genome and transcriptome sequencing in prospective metastatic triple-negative breast cancer uncovers therapeutic vulnerabilities. Mol Cancer Ther 12:104–116. https://doi.org/10.1158/1535-7163.MCT-12-0781

193. Ping Z, Siegal GP, Harada S, et al (2016) ERBB2 mutation is associated with a worse prognosis in patients with CDH1 altered invasive lobular cancer of the breast. Oncotarget 7:80655–80663. https://doi.org/10.18632/oncotarget.13019

194. Yoo NJ, Park SW, Lee SH (2011) Frameshift mutations of ubiquitinationrelated genes HERC2, HERC3, TRIP12, UBE2Q1 and UBE4B in gastric and colorectal carcinomas with microsatellite instability. Pathology 43:753–755. https://doi.org/10.1097/PAT.0b013e32834c7e78

195. Ibarrola-Villava M, Fernandez LP, Pita G, et al (2010) Genetic analysis of three important genes in pigmentation and melanoma susceptibility: CDKN2A, MC1R and HERC2/OCA2. Exp Dermatol 19:836–844. https://doi.org/10.1111/j.1600-0625.2010.01115.x

196. Amos CI, Wang LE, Lee JE, et al (2011) Genome-wide association study identifies novel loci predisposing to cutaneous melanoma. Hum Mol Genet 20:5012–5023. https://doi.org/10.1093/hmg/ddr415

197. Kosiniak-Kamysz A, Marczakiewicz-Lustig A, Marcińska M, et al (2014) Increased risk of developing cutaneous malignant melanoma is associated with variation in pigmentation genes and VDR, and may involve epistatic effects. Melanoma Res 24:388–396. https://doi.org/10.1097/CMR.0000000000000095

198. Ferguson R, Vogelsang M, Ucisik-Akkaya E, et al (2016) Genetic markers of pigmentation are novel risk loci for uveal melanoma. Sci Rep 6:31191. https://doi.org/10.1038/srep31191

199. Schneider T, Martinez-Martinez A, Cubillos-Rojas M, et al (2019) Large HERCs function as tumor suppressors. Front Oncol 9:524. https://doi.org/10.3389/fonc.2019.00524

200. Zhu D, Yang D, Li X, Feng F (2018) Heterogeneous expression and biological function of SOX18 in osteosaroma. J Cell Biochem 119:4184–4192. https://doi.org/10.1002/jcb.26635

201. Suh YJ, Choe JY, Park HJ (2017) Malignancy in Pheochromocytoma or Paraganglioma: Integrative Analysis of 176 Cases in TCGA. Endocr Pathol 28:159–164. https://doi.org/10.1007/s12022-017-9479-2

202. Fesenko DO, Chudinov A V., Surzhikov SA, Zasedatelev AS (2016) Biochip-Based Genotyping Assay for Detection of Polymorphisms in Pigmentation Genes Associated with Cutaneous Melanoma. Genet Test Mol Biomarkers 20:208–212. https://doi.org/10.1089/gtmb.2015.0272

203. Laino AM, Berry EG, Jagirdar K, et al (2018) Iris pigmented lesions as a marker of cutaneous melanoma risk: an Australian case–control study. Br J Dermatol 178:1119–1127. https://doi.org/10.1111/bjd.16323

204. Xiao F, Ma J, Cai G, et al (2014) Natural and orthogonal model for estimating gene-gene interactions applied to cutaneous melanoma. Hum Genet 133:559–574. https://doi.org/10.1007/s00439-013-1392-2

205. Wei L, Allain DC, Bernhardt MN, et al (2017) Variants at the OCA2/HERC2 locus affect time to first cutaneous squamous cell carcinoma in solid organ transplant recipients collected using two different study designs. Br J Dermatol 177:1066–1073. https://doi.org/10.1111/bjd.15618

206. Lin LH, Chou CH, Cheng HW, et al (2021) Precise Identification of Recurrent Somatic Mutations in Oral Cancer Through Whole-Exome Sequencing Using Multiple Mutation Calling Pipelines. Front Oncol 11:741626. https://doi.org/10.3389/fonc.2021.741626

207. Zhuang W, Ben X, Zhou Z, et al (2021) Identification of a Ten-Gene Signature of DNA Damage Response Pathways with Prognostic Value in Esophageal Squamous Cell Carcinoma. J Oncol 2021:3726058. https://doi.org/10.1155/2021/3726058

208. Mobuchon L, Derrien AC, Houy A, et al (2022) Different Pigmentation Risk Loci for High-Risk Monosomy 3 and Low-Risk Disomy 3 Uveal Melanomas. J Natl Cancer Inst 114:302–309. https://doi.org/10.1093/jnci/djab167

209. Kashyap S, Kumar M, Jayanti S, et al (2020) Prognostic impact of HERC2 protein and pink - eyed dilution protein in uveal melanoma. Hum Cell 33:1264–1272. https://doi.org/10.1007/s13577-020-00397-9

210. Bonanno L, Costa C, Majem M, et al (2016) Combinatory effect of BRCA1 and HERC2 expression on outcome in advanced non-small-cell lung cancer. BMC Cancer 16:312. https://doi.org/10.1186/s12885-016-2339-5

211. Yang Y, He W, Wang ZR, et al (2021) Immune Cell Landscape in Gastric Cancer. Biomed Res Int 2021:1930706. https://doi.org/10.1155/2021/1930706

212. Sanchez P, Espinosa M, Maldonado V, et al (2020) Pancreatic ductal adenocarcinomas from Mexican patients present a distinct genomic mutational pattern. Mol Biol Rep 47:5175–5184. https://doi.org/10.1007/s11033-020-05592-3

213. Lou X, Ye Z, Xu X, et al (2022) Establishment and characterization of the third non-functional human pancreatic neuroendocrine tumor cell line. Hum Cell 35:1248–1261. https://doi.org/10.1007/s13577-022-00696-3

214. Liu W, Tong H, Zhang C, et al (2020) Integrated genomic and transcriptomic analysis revealed mutation patterns of de-differentiated liposarcoma and leiomyosarcoma. BMC Cancer 20:1035. https://doi.org/10.1186/s12885-020-07456-2

215. Perillo B, Donato M Di, Pezone A, et al (2020) ROS in cancer therapy : the bright side of the moon. Exp Mol Med 52:192–203. https://doi.org/10.1038/s12276-020-0384-2

216. Denicola GM, Karreth FA, Humpton TJ, et al (2011) Oncogene-induced Nrf2 transcriptionpromotes ROS detoxification and tumorigenesis. Nature 475:106–109. https://doi.org/10.1038/nature10189

217. Lisek K, Campaner E, Ciani Y, et al (2018) Mutant p53 tunes the NRF2-dependent antioxidant response to support survival of cancer cells. 9:20508–20523. https://doi.org/10.18632/oncotarget.24974

218. Mulcahy Levy JM, Thorburn A (2020) Autophagy in cancer: moving from understanding mechanism to improving therapy responses in patients. Cell Death Differ 27:843–857. https://doi.org/10.1038/s41418-019-0474-7

219. Mohsen S, Sobash PT, Algwaiz GF, et al (2022) Autophagy Agents in Clinical Trials for Cancer Therapy: A Brief Review. Curr Oncol 29:1695–1708. https://doi.org/10.3390/curroncol29030141

220. Egan DF, Chun MGH, Vamos M, et al (2015) Small Molecule Inhibition of the Autophagy Kinase ULK1 and Identification of ULK1 Substrates. Mol Cell 59:285–297. https://doi.org/10.1016/j.molcel.2015.05.031

221. Tang F, Hu P, Yang Z, et al (2017) SBI0206965, a novel inhibitor of Ulk1, suppresses non-small cell lung cancer cell growth by modulating both autophagy and apoptosis pathways. Oncol Rep 37:3449–3458. https://doi.org/10.3892/or.2017.5635

222. Li Q, Ye C, Tian T, et al (2022) The emerging role of ubiquitin-specific protease 20 in tumorigenesis and cancer therapeutics. Cell Death Dis 13:434. https://doi.org/10.1038/s41419-022-04853-2

223. Lu R, Wu G, Chen M, et al (2021) USP18 and USP20 restrict oHSV-1 replication in resistant human oral squamous carcinoma cell line SCC9 and affect the viability of SCC9 cells. Mol Ther Oncolytics 23:477–487. https://doi.org/10.1016/j.omto.2021.11.004

224. Fujita J, Sakurai T (2019) The Oncoprotein Gankyrin/PSMD10 as a Target of Cancer Therapy. Adv Exp Med Biol 1164:63–71. https://doi.org/10.1007/978-3-030-22254-3_5

225. He Z, Yang X, Huang L, et al (2021) PSMC5 Promotes Proliferation and Metastasis of Colorectal Cancer by Activating Epithelial–Mesenchymal Transition Signaling and Modulating Immune Infiltrating Cells. Front Cell Dev Biol 9:657917. https://doi.org/10.3389/fcell.2021.657917

226. Kao TJ, Wu CC, Phan NN, et al (2021) Prognoses and genomic analyses of proteasome 26S subunit, ATPase (PSMC) family genes in clinical breast cancer. Aging 13:18946–18977. https://doi.org/10.18632/aging.203345

227. Ullah MA, Islam NN, Moin AT, et al (2022) Evaluating the Prognostic and Therapeutic Potentials of the Proteasome 26S Subunit, ATPase (PSMC) Family of Genes in Lung Adenocarcinoma: A Database Mining Approach. Front Genet 13:935286. https://doi.org/10.3389/fgene.2022.935286

228. Parenti I, Rabaneda LG, Schoen H, Novarino G (2020) Neurodevelopmental Disorders: From Genetics to Functional Pathways. Trends Neurosci 43:608–621. https://doi.org/10.1016/j.tins.2020.05.004

229. Abraham JR, Barnard J, Wang H, et al (2019) Proteomic investigations of human HERC2 mutants: Insights into the pathobiology of a neurodevelopmental disorder. Biochem Biophys Res Commun 512:421–427. https://doi.org/10.1016/j.bbrc.2019.02.149

230. Sonia A. L. Correa and Katherine L. Eales (2012) The Role of p38 MAPK and Its Substrates in Neuronal Plasticity and Neurodegenerative Disease. J Signal Transduct 2012:649079. https://doi.org/10.1155/2012/649079

231. Jaarsma D, Haasdijk ED, Grashorn JAC, et al (2000) Human Cu / Zn Superoxide Dismutase (SOD1) Overexpression in Mice Causes Mitochondrial Vacuolization , Axonal Degeneration , and Premature Motoneuron Death and Accelerates Motoneuron Disease in Mice Expressing a Familial Amyotrophic Lateral Sclerosis Mut. Neurobiol Dis 7:623–643. https://doi.org/10.1006/nbdi.2000.0299

232. Afshar P, Ashtari N, Jiao X, et al (2017) Overexpression of Human SOD1 Leads to Discrete Defects in the Cerebellar Architecture in the Mouse. Front Neuroanat 11:22. https://doi.org/10.3389/fnana.2017.00022

233. Rajasekaran NS, Varadharaj S, Khanderao GD, et al (2011) Sustained activation of nuclear erythroid 2-related factor 2/antioxidant response element signaling promotes reductive stress in the human mutant protein aggregation cardiomyopathy in mice. Antioxidants Redox Signal 14:957–971. https://doi.org/10.1089/ars.2010.3587

234. Ma WX, Li CY, Tao R, et al (2020) Reductive Stress-Induced Mitochondrial Dysfunction and Cardiomyopathy. Oxid Med Cell Longev 2020:5136957. https://doi.org/10.1155/2020/5136957

235. Xiao W, Loscalzo J (2020) Metabolic Responses to Reductive Stress. Antioxidants Redox Signal 32:1330–1347. https://doi.org/10.1089/ars.2019.7803

236. Knott AB, Perkins G, Schwarzenbacher R, Bossy-Wetzel E (2008) Mitochondrial fragmentation in neurodegeneration. Nat Rev Neurosci 9:505–518. https://doi.org/10.1038/nrn2417

237. Bar-yosef T, Damri O, Agam G (2019) Dual Role of Autophagy in Diseases of the Central Nervous System. Front Cell Neurosci 13:196. https://doi.org/10.3389/fncel.2019.00196

238. Marsh D, Dragich JM (2019) Autophagy in mammalian neurodevelopment and implications for childhood neurological disorders. Neurosci Lett 697:29–33. https://doi.org/10.1016/j.neulet.2018.04.017

239. Stavoe AKH, Holzbaur ELF (2019) Autophagy in Neurons. Annu Rev Cell Dev Biol 35:477–500. https://doi.org/10.1146/annurev-cellbio-100818-125242

240. Lee J-A (2012) Neuronal Autophagy: A Housekeeper or a Fighter in Neuronal Cell Survival? Exp Neurobiol 21:1–8. https://doi.org/10.5607/en.2012.21.1.1

241. Tintos-hern JA, Keller K, Li X, et al (2018) Homozygous Boricua TBCK Mutation Causes Neurodegeneration and Aberrant Autophagy. Ann Neurol 83:153–165. https://doi.org/10.1002/ana.25130

242. Zhao L, Longo-guess C, Harris BS, et al (2005) Protein accumulation and neurodegeneration in the woozy mutant mouse is caused by disruption of SIL1 , a cochaperone of BiP. Nat Genet 37:974–979. https://doi.org/10.1038/ng1620

243. Lee JW, Beebe K, Nangle LA, et al (2006) Editing-defective tRNA synthetase causes protein misfolding and neurodegeneration. Nature 443:50–55. https://doi.org/10.1038/nature05096

Publications

The articles annexed in this doctoral thesis are listed below:

- **Joan Sala-Gaston**, Arturo Martinez-Martinez, Leonardo Pedrazza, L. Francisco Lorenzo-Martín, Rubén Caloto, Xosé R. Bustelo, Francesc Ventura and Jose Luis Rosa (2020) HERC Ubiquitin Ligases in Cancer. Cancers 12 (6):1653. https://doi.org/10.3390/cancers12061653

- **Joan Sala-Gaston**, Leonardo Pedrazza, Juanma Ramirez, Arturo Martinez-Martinez, Lettie E. Rawlins, Emma L. Baple, Andrew H. Crosby, Ugo Mayor, Francesc Ventura and Jose Luis Rosa (2022) HERC2 deficiency activates C-RAF/MKK3/p38 signalling pathway altering the cellular response to oxidative stress. Cellular and Molecular Life Sciences 79:548. https://doi.org/10.1007/s00018-022-04586-7

cancers

MDPI

Review

HERC Ubiquitin Ligases in Cancer

Joan Sala-Gaston [1,†], Arturo Martinez-Martinez [1,†], Leonardo Pedrazza [1], L. Francisco Lorenzo-Martín [2], Rubén Caloto [2], Xosé R. Bustelo [2], Francesc Ventura [1] and Jose Luis Rosa [1,*]

1 Departament de Ciències Fisiològiques, Institut d'Investigació de Bellvitge (IDIBELL), Universitat de Barcelona, L'Hospitalet de Llobregat, 08907 Barcelona, Spain; joansala@ub.edu (J.S.-G.); arturomartinez@ub.edu (A.M.-M.); leopedrazza@gmail.com (L.P.); fventura@ub.edu (F.V.)

2 Centro de Investigación del Cáncer, Instituto de Biología Molecular y Celular del Cáncer and CIBERONC, Consejo Superior de Investigaciones Científicas (CSIC)-University of Salamanca, 37007 Salamanca, Spain; luis.lorenzomartin@epfl.ch (L.F.L.-M.); ruben.fdez.caloto@usal.es (R.C.); xbustelo@usal.es (X.R.B.)

* Correspondence: joseluisrosa@ub.edu

† These authors contributed equally to this work.

Received: 24 April 2020; Accepted: 19 June 2020; Published: 22 June 2020

Abstract: HERC proteins are ubiquitin E3 ligases of the HECT family. The HERC subfamily is composed of six members classified by size into large (HERC1 and HERC2) and small (HERC3–HERC6). HERC family ubiquitin ligases regulate important cellular processes, such as neurodevelopment, DNA damage response, cell proliferation, cell migration, and immune responses. Accumulating evidence also shows that this family plays critical roles in cancer. In this review, we provide an integrated view of the role of these ligases in cancer, highlighting their bivalent functions as either oncogenes or tumor suppressors, depending on the tumor type. We include a discussion of both the molecular mechanisms involved and the potential therapeutic strategies.

Keywords: HECT; E3; oncogene; tumor suppressor; genome stability; p53; MAPK; RAF; ERK; p38

1. Introduction

Ubiquitin E3 ligases take part in protein ubiquitylation. These enzymes catalyze the last step of a cascade where ubiquitin is initially incorporated to a ubiquitin-activating enzyme (E1), which in turn is transferred to a ubiquitin-conjugating enzyme (E2), and finally, to a target protein through a process defined by a ubiquitin E3 ligase that interacts with the substrate protein (Figure 1). The ubiquitin-like proteins SUMO, NEDD8, and ISG15 are also covalently attached to the target protein via an E1/E2/E3 cascade. Specifically, the E3 ligases can be classified into three groups, of which one is homologous to the E6AP carboxyl terminus (HECT) protein. All HECT ligases have a catalytic domain in their carboxyl terminus that contains a conserved cysteine residue that is involved in forming a transiently thioester bond to ubiquitin before transferring it to the lysine residue of the substrate protein (Figure 1) [1]. HECT ligases containing one or more regulator of chromosome condensation 1 (RCC1)-like domains in their amino-terminal domain form a HERC subgroup [2]. HERC1 and HERC2 are the largest HECT ligases, having molecular weights exceeding 500 kDa, and constitute the large HERC protein subfamily [3]. By contrast, HERC3 to HERC6 have molecular weights around 100–120 kDa and constitute the small HERC protein subfamily. Despite the structural similarity between large and small HERC proteins (Figure 1), they are evolutionarily very distant. In fact, they are the result of convergence phenomena rather than being phylogenetic paralogs [3–5]. Moreover, the small HERC proteins HERC5 and HERC6 may also function as ISG15 E3 ligases [6,7].

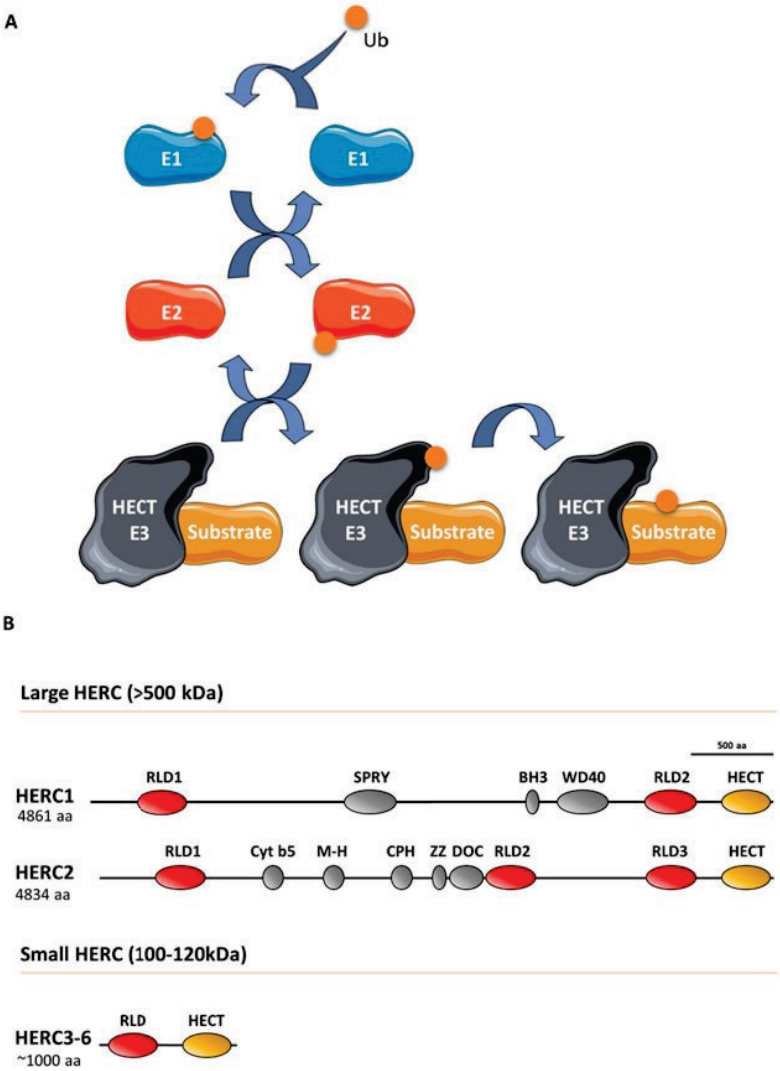

Figure 1. The ubiquitin-conjugating system in HERC E3 ligases: (**A**) Ubiquitin (Ub) is conjugated to a target substrate via a cascade that comprises an E1 activating enzyme, an E2 conjugating enzyme, and an E3 ligase enzyme. The HERC proteins belong to the HECT family of E3 ligases, which form a thioester bond with Ub via a conserved cysteine residue. Once formed, Ub is transferred to the substrate's lysine residue (see text for details). Ub-like proteins, such as ISG15, are also covalently attached to the substrate protein via an E1/E2/E3 cascade; (**B**) structural features of large and small HERC proteins are also shown. HERC5 and HERC6 may also function as ISG15 E3 ligases.

2. The Role of HERCs in Cancer

HERCs play roles in a wide range of cellular functions, including neurodevelopment, cell response to replication stress and DNA damage, cell proliferation, cell migration, and immune responses. As such, mutations in HERCs are associated with severe pathologies [3,6,8], with a notable impact in cancer. An extensive list of the different cancers associated with the specific large and small HERCs is provided in Table 1.

Table 1. Cancers associated with HERCs and related molecular mechanisms.

Genes	Associated Cancers	Related Molecular Mechanisms	Reference
HERC1	Acute promyelocytic leukemia	*HERC1-PML* genomic fusion	[9]
	Acute Myeloid Leukemia	*HERC1* mutations	[10]
	Acute lymphoblastic leukemia	Decreased MSH2 protein levels and *HERC1* deletions	[11]
	Adult T-cell acute lymphoblastic leukemia	*HERC1* mutations	[12]
	T-cell prolymphocytic leukemia	*HERC1* mutations	[13]
	Non-melanoma skin cancer	Enhanced BAK protein degradation	[14]
	Pulmonary sclerosing pneumocytoma	*HERC1* mutations	[15]
	Invasive lobular breast cancer	*HERC1* mutations	[16]
	Metastatic triple-negative breast cancer	*HERC1* mutations	[17]
	Sporadic colorectal cancer	Decreased MSH2 protein levels and *HERC1* deletions	[11]
	Osteosarcoma	Negative correlation of *SOX18* overexpression and *HERC1* mRNA levels	[18]
HERC2	Pheochromocytoma and paraganglioma	*HERC2* mutations	[19]
	T-cell prolymphocytic leukemia	*HERC2* mutations	[13]
	Cutaneous melanoma	SNPs in *HERC2* gene increase susceptibility	[20–23]
		Gene-gene interactions between *HERC2* gene and *IL31RA* and *DDX4* genes	[24]
		Epistatic effects between *HERC2* and *VDR* genes	[25]
	Cutaneous squamous cell carcinoma	SNPs in *HERC2* gene impact on time to develop the tumor in organ transplant recipients	[26]
	Uveal melanoma	SNPs in *HERC2* gene increase susceptibility	[27]
	Non-small-cell lung cancer	Worse prognosis in patients expressing high *HERC2* mRNA levels	[28]
	Breast cancer	Enhanced BRCA1 degradation	[29,30]
	Gastric and colorectal carcinomas	*HERC2* mutations	[31]
	Osteosarcoma	Negative correlation of *SOX18* overexpression and *HERC2* mRNA levels	[18]
HERC3	Glioblastoma	Degradation of SMAD7 and activation of the TGFβ signaling	[32]
	Gastric and colorectal carcinomas	*HERC3* mutations	[31]
	Osteosarcoma	Negative correlation of *SOX18* overexpression and *HERC3* mRNA levels	[18]
HERC4	Multiple myeloma	Decreased c-Maf degradation	[33]
	Lung cancer	*HERC4* overexpression	[34]
	Non-small cell lung cancer	Increased Smo protein stability and Hh pathway activation	[35,36]
	Breast cancer	*HERC4* upregulation	[37]
		Decreased expression of miRNAs targeting *HERC4* expression and enhanced LATS1 degradation	[38]
	Hepatocellular carcinoma	*HERC4* overexpression	[39]
	Osteosarcoma	Negative correlation of *SOX18* overexpression and *HERC4* mRNA levels	[18]

Table 1. *Cont.*

Genes	Associated Cancers	Related Molecular Mechanisms	Reference
HERC5	Pediatric germ cell tumors	Chromosome copy number variations (CNVs) at a region encompassing *HERC5* gene	[40]
	Glioblastoma	*HERC5* upregulation	[41]
	Acute myeloid leukemia	*HERC5* downregulation	[42]
	Oropharyngeal cancer	*HERC5* gene expression is associated with overall survival	[43]
	Non-small cell lung cancer	*HERC5* promoter hypermethylation	[44]
	Breast cancer	*HERC5* upregulation	[45]
	Hepatocellular carcinoma	Negative correlation of *CCL20* overexpression and *HERC5* mRNA levels	[46]
		Reduced p53, p21 and Bax/Bcl-2 pathway activation	[47]
	Ovarian cancer	*HERC5* upregulation is associated with drug resistance	[48,49]
	Osteosarcoma	Negative correlation of *SOX18* overexpression and *HERC5* mRNA levels	[18]
HERC6	Osteosarcoma	Negative correlation of *SOX18* overexpression and *HERC6* mRNA levels	[18]

Mutations in large HERCs have been found in leukemia [10–13] and breast cancer [16,17]. Frameshift mutations in *HERC2* have been found in both gastric and colorectal carcinomas with microsatellite instability [31]. The *HERC2* locus has also been associated with both cutaneous melanoma and uveal melanoma, whereas the *HERC1* locus has been found to be mutated in non-melanoma skin cancer [20,21,25,27]. Higher expression levels of HERCs are associated with better patient prognosis in kidney, head and neck, and pancreatic cancers when *HERC1* expression levels are elevated, and in patients with renal cancer when *HERC2* expression levels are elevated [50]. By contrast, the expression levels of HERC2 have been found to negatively correlate with patient survival in non-small-cell lung cancer [28]. In osteosarcoma, upregulation of the HERC2-binding protein SOX18 enhances cell proliferation, and it correlates with a reduction in both large and small HERC mRNA levels (Table 1) [18].

Several studies using gene expression analyses of different tumor tissues have showed differential expression patterns of small HERCs between healthy and tumor samples as well as between tumors at different stages. This raises the possibility of using small HERCs as diagnostic or prognostic biomarkers for different cancer types. For instance, *HERC4* and *HERC5* expressions have been shown to correlate with tumor progression in breast cancer [37,45] and have been implicated in both lung [34–36,44] and hepatocellular [39,46,47,51] carcinomas. In addition, high levels of *HERC3* expression correlate with poor prognosis in glioblastomas [32], while *HERC5* appears to be differentially expressed and associated with progression in acute myeloid leukemia (Table 1) [42].

3. Signaling Pathways Regulated by HERCs

Gene expression and survival studies suggest that HERCs have different roles in cancer. Gaining a better understanding of HERCs can be facilitated by understanding the intracellular signaling pathways where HERCs operate. HERCs appear to have bivalent functions, acting as either oncogenes or as tumor suppressors depending on the tumor type. In turn, this complicates research into the relevant signaling pathways where HERCs participate. In recent years, several studies have contributed to our understanding of the tumor suppressor function of large HERCs, with three major regulatory mechanisms emerging: regulation of genomic stability, regulation of p53 transcriptional programming, and regulation of mitogen-activated protein kinase (MAPK) signaling.

3.1. Regulation of Genomic Stability

Genomic instability is a hallmark of cancer that is observed in the early stages of tumorigenesis [52,53]. HERC2 participates in the modulation of genomic stability through degradation of key regulators of DNA repair pathways. Xeroderma pigmentosa A (XPA) is critical to the nucleotide excision repair machinery. It is ubiquitylated by HERC2, which targets it for proteasomal degradation in a circadian-dependent manner (Figure 2A) [54]. The regulation of this process depends on the phosphorylation state of XPA. Its phosphorylation by serine/threonine-protein kinase ATR prevents ubiquitylation by HERC2, and its dephosphorylation by protein phosphatase 1D (also known as WIP1) enhances its ubiquitylation by HERC2 [54,55].

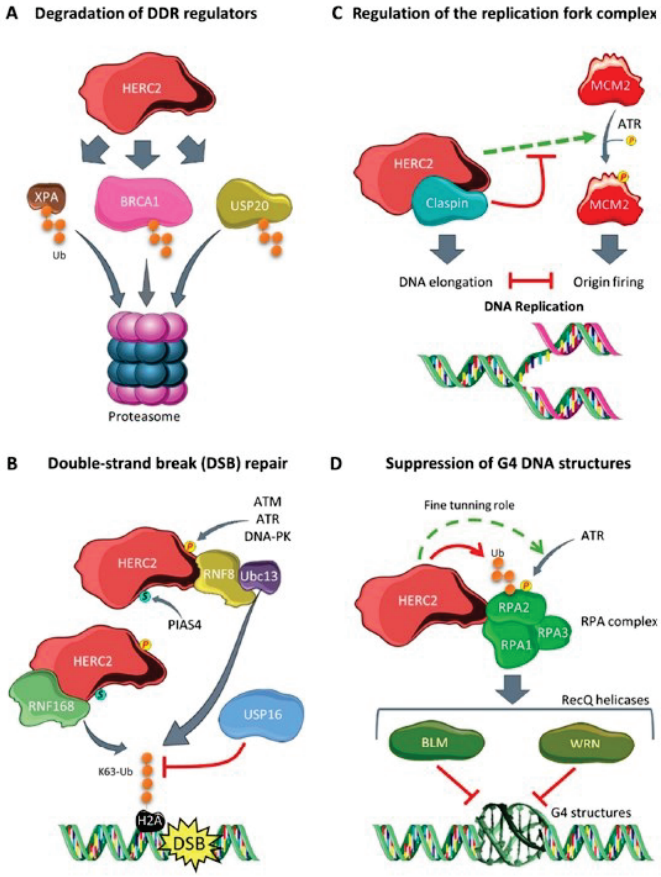

Figure 2. Involvement of HERC2 in the regulation of genomic stability: (**A**) HERC2 catalyzes the polyubiquitylation of different DNA damage response (DDR) regulators, such as XPA, BRCA1, and USP20, targeting them for proteasomal degradation; (**B**) upon double-strand break in the DNA, HERC2 is phosphorylated (by ATM, ATR, or DNA-PK) and SUMOylated (by PIAS4). These posttranslational modifications allow HERC2 to bind to RNF8, promoting the specific assembly of RNF8 with the E2 enzyme Ubc13. This allows the formation of K63 polyubiquitin chains in H2A-type histones flanking the double-strand break site. HERC2 interacts with and stabilizes RNF168, and this amplifies the ubiquitin chain formation in histones. By contrast, USP16 levels increase in a HERC2-dependent manner and negatively regulate H2A histone ubiquitylation to fine-tune chain formation; (**C**) HERC2 is present in the replication fork complex that regulates the balance between DNA elongation and origin firing. HERC2 facilitates ATR-dependent MCM2 phosphorylation, which enhances origin firing, and this is inhibited by Claspin, another HERC2-interacting protein. (**D**) G4 structures cause replication stress, and this leads to HERC2 promoting RPA2 phosphorylation via ATR. Then, HERC2 polyubiquitylates the phosphorylated form of RPA2, targeting it for proteasomal degradation, and thereby fine-tuning the total levels of phospho-RPA2. This mechanism is essential for assembling the BLM and WRN RecQ helicases to the RPA complex and for its later role in suppressing G4 structures.

Another HERC2 degradation target is breast cancer suppressor 1 (BRCA1) (Figure 2A) [29]. BRCA1 maintains genome stability by repairing double-strand breaks [56]. The HERC2-dependent degradation of BRCA1 is regulated by the binding of different protein interactors to HERC2 or BRCA1; for example, BARD1 binds BRCA1, forming a heterodimer that prevents BRCA1 ubiquitylation by HERC2. Similarly, TUSC4 binds to HERC2 and prevents BRCA1 degradation, with its knockdown consistently shown to enhance BRCA1 degradation through the proteasome pathway [29,30].

Further, also concerning the response to DNA damage, HERC2 is required for the retention of DNA repair factors such as 53BP1, RAP80, RNF168, and BRCA1 at sites of DNA damage in response to double-strand breaks [57]. Upon double-strand breaks, HERC2 is phosphorylated on T4827 by serine-protein kinase ATM or other DNA damage-related kinases like ATR or DNA-PK. In addition, it can be SUMOylated in its ZZ domain by the E3 SUMO ligase PIAS4 [58]. These posttranslational modifications allow the binding of HERC2 to RNF8, another ubiquitin E3 ligase involved in the DNA damage response. In these conditions, HERC2 promotes the specific assembly of RNF8 with one of its E2 enzymes, Ubc13, which catalyzes the formation of K63 polyubiquitin chains formed in H2A-type histones flanking the double-strand break site. HERC2 therefore mediates the specificity of the interaction between the E2 enzyme Ubc13 and the E3 ligase RNF8, safeguarding the formation of K63 ubiquitin chains that are essential for recruiting repair factors to the damaged chromosomes. In parallel, HERC2 can interact with, and stabilize, the E3 ligase RNF168 that is responsible for amplifying the ubiquitin chain formation initiated in histones by RNF8 [57,58]. Levels of the deubiquitinase USP16 then increase in a HERC2-dependent manner during DNA damage, and this negatively regulates H2A histone ubiquitylation to fine-tune polyubiquitin chain formation. Ultimately, USP16 triggers the ubiquitylation signal termination once the damage is repaired. These findings suggest that HERC2 has a central role in regulating and fine-tuning the DNA damage response pathway (Figure 2B) [59].

HERC2 also regulates the levels of Claspin, a protein essential for both G_2-M checkpoint activation and replication fork stability. HERC2 interacts with Claspin in the presence of BRCA1 [60]. Upon DNA damage, ATR phosphorylates USP20, a deubiquitinating enzyme which is a degradation target of HERC2 (Figure 2A). USP20 detaches from HERC2, leading to its stabilization, and in turn deubiquitylates and stabilizes Claspin levels. The Claspin can then interact with the serine/threonine-protein kinase CHK1, promoting ATR-dependent phosphorylation, checkpoint activation, and genome stability [61,62]. Moreover, HERC2 has been described as a component of the DNA replication fork complex that regulates origin firing and fork progression. During DNA replication, origin firing and elongation must be correctly balanced. Claspin and CHK1 enhance elongation but restrict origin firing. When faced with replication stress that impairs DNA elongation, HERC2 facilitates the phosphorylation and activation of the DNA replication licensing factor MCM2 (Figure 2C). Thus, origin firing is upregulated as a compensatory mechanism [60]. Dysregulation of these replication mechanisms can lead to DNA damage and genome instability [63].

Some guanine-rich DNA sequences can fold into a secondary structure known as G-quadruplex (G4). These structures are involved in transcriptional initiation and termination, replication initiation, and telomere maintenance. However, the deregulation of G4 can cause fork stalling during DNA replication that promotes DNA damage and genome instability. HERC2 interacts with replication protein A (RPA), a heterotrimeric complex formed by RPA1, RPA2, and RPA3 and that binds to single-stranded DNA and protects it from spontaneous annealing and G4 formation. RPA assembly to the RecQ DNA helicases BLM and WRN is essential for suppressing the formation of G4 DNA structures. Under conditions of replication stress, ATR phosphorylates RPA2 at Ser33 in an HERC2-dependent mechanism. Then, HERC2 ubiquitylates the phosphorylated form of RPA2, targeting it to proteasomal degradation [64]. Although the specific effects of RPA2 phosphorylation and its later degradation by HERC2 are not fully understood, both mechanisms are essential for HERC2 to function correctly in suppressing G4 structures. HERC2 may fine-tune the levels of phosphorylated RPA2 by promoting its ATR-dependent phosphorylation and targeting it for proteasomal degradation through polyubiquitylation. This precise balance might be needed for the correct assembly of the BLM

and WRN helicases to the RPA complex, as well as for the subsequent suppression of G4 structures and the maintenance of genomic stability (Figure 2D) [65].

HERC1 has also been associated with the DNA damage response through its regulation of MSH2, which forms heterodimers with MSH6 and MSH3. Both these dimers are responsible for the DNA mismatch repair mechanism, and loss of function impairs DNA repair. Depleting HERC1 has been linked to reduced protein MSH2 levels in human leukemia cells, leading to increased genomic instability and chemotherapy resistance [11].

3.2. Regulation of p53 Transcriptional Programming

Large HERCs may also function as tumor suppressors by regulating gene expression. For example, HERC2 controls the transcriptional activity of the tumor suppressor protein p53 [66]. Tetramerization of p53 is a key step in its activation, and this oligomerization process is modulated by a complex formed by NEURL4 and HERC2 [67]. Recently, it has been reported that MDM2 is present in this complex. In non-stressed cells, this ubiquitin E3 ligase promotes lower levels of p53 by targeting it for proteasome degradation. Upon DNA damage induced by bleomycin, MDM2 is dissociated from the p53/HERC2/NEURL4 complex, and phosphorylation and acetylation of oligomeric p53 increases. Activated p53 then binds to the p53 response elements in the promoters of its target genes. *MDM2* is one such gene whose promoter competes with HERC2 for binding of oligomeric, phosphorylated, and acetylated p53. As its gene expression increases MDM2 protein levels, these can bind p53 and restart the regulatory loop (Figure 3) [68]. These findings highlight the importance of HERC2 in regulating the transcriptional program of the tumor suppressor protein p53.

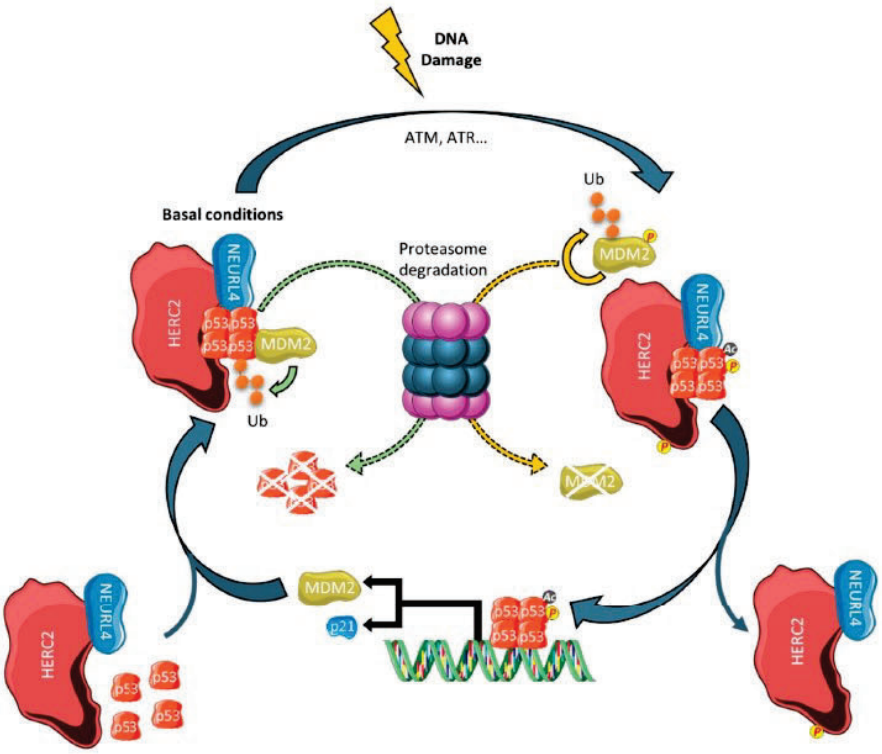

Figure 3. Regulation of the p53/MDM2 pathway by HERC2. In basal conditions, HERC2 and NEURL4 regulate p53 transcriptional activity by promoting its oligomerization. MDM2 maintains low levels of p53 by targeting it for proteasomal degradation. Upon DNA damage, associated kinases phosphorylate MDM2 and HERC2. In addition, p53 is activated by acetylation and phosphorylation. The phosphorylated MDM2 is detached from the complex and is autopolyubiquitylated and subsequently degraded. Activated p53 binds to the promoters of its target genes, such as p21 or MDM2, and a negative feedback loop is established in the latter case.

3.3. Regulation of MAPK Signaling

MAPKs are organized in three-tiered cascades regulated by phosphorylation: MAPKK kinases (MAPKKKs) are serine/threonine-protein kinases that phosphorylate and activate MAPKKs, which in turn phosphorylate the MAPKs that mediate the cellular response by phosphorylating effector proteins. This signaling has therefore been shown to be key for cell differentiation, growth, proliferation, and survival. The classic MAPK cascades include Jun N-terminal kinase (JNK), p38, and extracellular signal-regulated protein kinase (ERK) pathways. Dysregulation of these cascades has been linked extensively to oncogenesis [69–71].

HERC1 and HERC2 each have roles in MAPK signaling. For example, HERC2 has been reported to be part of a high-molecular weight complex formed by UBE3A, NEURL4, and MAPK6/ERK3 [72]. Some cellular functions that might be regulated by this complex involve transcription, protein translation, formation and transport of vesicles, as well as metabolism [73]. To date, the precise molecular mechanism remains to be elucidated, necessitating further research. By contrast, our knowledge of the regulation of MAPK by HERC1 has evolved and grown in recent years. HERC1 controls cell proliferation through the regulation of ERK signaling by targeting the proto-oncogene C-RAF, an MAPKKK, for proteasomal degradation (Figure 4A) [74]. The HERC1 ligase also regulates the p38 pathway and cell migration. Research indicates that HERC1 knockdown increases p38 activity by increasing the levels of MKK3, an MAPKK of the p38 pathway, in a manner dependent on C-RAF. Thus, HERC1 regulates a previously unknown crosstalk between these two MAPK signaling pathways [75]. In this context, it is postulated that HERC1 functions as a tumor suppressor protein, given that its depletion leads to the dysregulation of two essential cascades for tumorigenesis (Figure 4B).

4. Perspective and Therapeutic Implications

The ubiquitin proteasome system has been targeted for cancer therapy through proteasome inhibitors such as bortezomib, and these are achieving promising results in ongoing clinical trials. However, given that the treatments lack specificity, they can induce clinically relevant side effects [76]. Hence, the possibility of targeting E3 ligases, which display high substrate specificity, may help achieve more specific and efficient therapies. Given the possible tumor suppressor role of large HERCs in some cancers, a potential therapeutic approach would be to rely on enhancing their tumor suppressor activities. Following this theory, both HERC1 and HERC2 could be potential drug candidates. On the one hand, promoting the capacity of HERC2 to oligomerize p53 using the CPH domain of HERC2 [66] could boost the p53 transcriptional program and potentially alleviate tumor progression in tumors with non-mutated p53. On the other hand, a growing body of evidence suggests that targeting C-RAF could be a promising therapeutic strategy based on its efficiency in K-Ras and Trp53 mutant mice models of lung [77] and pancreatic ductal [78] adenocarcinomas. Enhancing HERC1 ubiquitin ligase activity in this context could be an interesting approach to stop tumor progression in MAPK-dependent cancers. These approaches could also be combined with other therapeutic strategies that target the inhibition of MDM2 with Nutlins in the case of HERC2, and epidermal growth factor receptor activity with monoclonal antibodies or tyrosine kinase inhibitors in the case of HERC1.

Given the role of large HERCs in DNA damage response, inhibitors for these proteins could be designed to exploit synthetic lethality as a therapeutic strategy in some cancers. Deficiencies in the DNA repair mechanisms of tumor cells can be exploited by inhibiting the remnant mechanisms and triggering tumor cell death [79]. Many genes involved in DNA repair mechanisms are mutated in tumors [80]. Synthetic lethality also benefits from the fact that cancer cells present higher replication stress due to their aberrant proliferation [81]. The viability of synthetic lethality strategies has been demonstrated with the use of poly [ADP-ribose] polymerase (PARP) inhibitors, since tumor cells harboring BRCA1/2 mutations are 1000 times more sensitive to PARP inhibition than wild-type counterparts [82]. Given this evidence, large HERC inhibitors, especially those for HERC2, could eventually be of use in this setting.

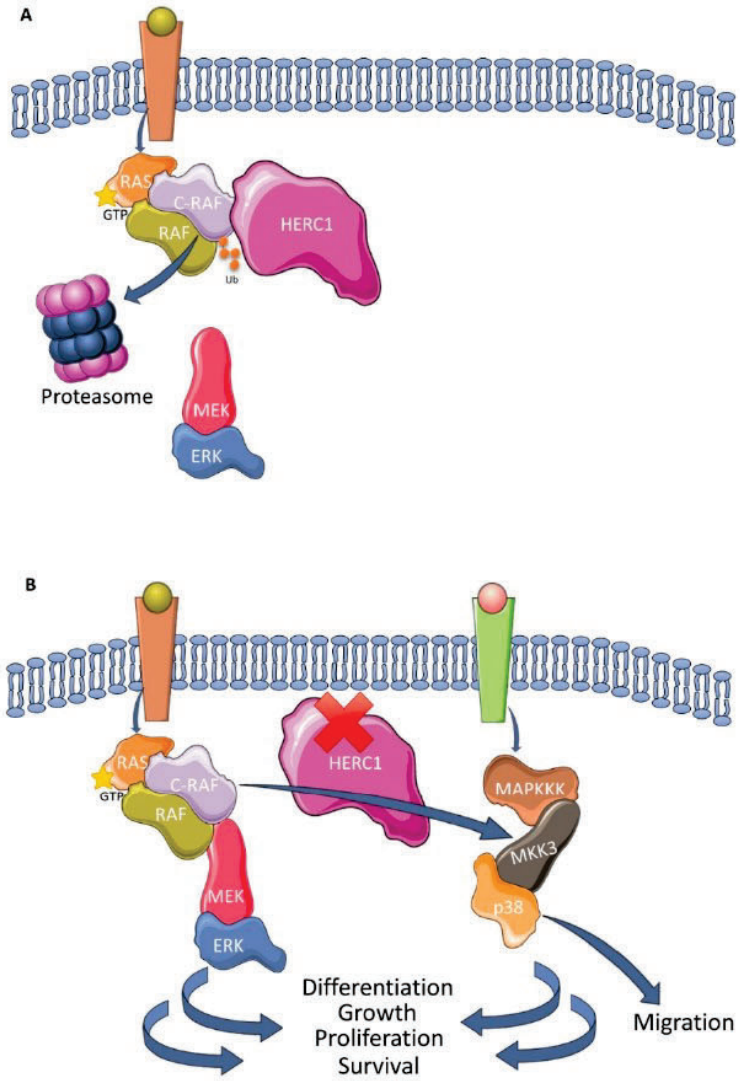

Figure 4. Regulation of MAPK signaling pathways by HERC1: (**A**) HERC1 polyubiquitylates C-RAF with a lysine 48-linked chain that causes its degradation by the proteasome and downregulates ERK activity; (**B**) in the absence of HERC1, the levels of C-RAF increase and upregulate the RAF/MEK/ERK signaling pathway. The levels of MKK3 also increase, which in turn phosphorylates and activates p38. In summary, therefore, the absence of HERC1 may enhance cell responses regulated by these MAPKs, including the migration, differentiation, growth, proliferation, and survival of cells.

5. Conclusions

HERCs can function as either oncogenes or tumor suppressors depending on the cancer type. This bivalent activity hinders the study and understanding of the regulatory mechanisms where they operate. Although important cellular processes such as genome stability, gene expression, and MAPK signaling are regulated by HERCs proteins, future in vivo and in vitro studies are required to elucidate the molecular mechanisms where HERCs participate and to identify new substrates specific for each cancer type. Screenings for activator and inhibitor molecules for their ubiquitin ligase activities could also be useful when developing novel therapeutic strategies.

Funding: J.L.R. is supported by the Spanish Ministry of Science and Innovation (BFU2016-80295-R, SAF2017-90900-REDT, and UBIRed). X.R.B. is supported by grants from the Castilla-León Government (CSI252P18, CLC-2017-01), the Spanish Ministry of Science and Innovation (SAF2015-64556-R, RTI2018-096481-B-100) and the Spanish Association against Cancer (GC16173472GARC). X.R.B.'s institution is supported by the Programa de

Apoyo a Planes Estratégicos de Investigación de Estructuras de Investigación de Excelencia of the Castilla-León autonomous government (CLC-2017-01). Both Spanish and Castilla-León government-associated funding is partially supported by the European Regional Development Fund. J.S.-G. and A.M.-M. received FPU Fellowships (FPU17/02413 and FPU18/06325, respectively) from the Spanish Ministry of Science, Innovation and Universities.

Conflicts of Interest: The authors declare no conflict of interest.

References

1. Ciechanover, A. The unravelling of the ubiquitin system. *Nat. Rev. Mol. Cell Biol.* **2015**, *16*, 322–324. [CrossRef] [PubMed]
2. Garcia-Gonzalo, F.R.; Rosa, J.L. The HERC proteins: Functional and evolutionary insights. *Cell. Mol. Life Sci.* **2005**, *62*, 1826–1838. [CrossRef] [PubMed]
3. García-Cano, J.; Martinez-Martinez, A.; Sala-Gaston, J.; Pedrazza, L.; Rosa, J.L. HERCing: Structural and Functional Relevance of the Large HERC Ubiquitin Ligases. *Front. Physiol.* **2019**, *10*, 1014. [CrossRef] [PubMed]
4. Hadjebi, O.; Casas-Terradellas, E.; Garcia-Gonzalo, F.R.; Rosa, J.L. The RCC1 superfamily: From genes, to function, to disease. *Biochim. Biophys. Acta Mol. Cell Res.* **2008**, *1783*, 1467–1479. [CrossRef]
5. Marin, I. Animal HECT ubiquitin ligases: Evolution and functional implications. *BMC Evol. Biol.* **2010**, *10*, 56. [CrossRef]
6. Sánchez-Tena, S.; Cubillos-Rojas, M.; Schneider, T.; Rosa, J.L. Functional and pathological relevance of HERC family proteins: A decade later. *Cell. Mol. Life Sci.* **2016**, *73*, 1955–1968. [CrossRef]
7. Villarroya-Beltri, C.; Guerra, S.; Sánchez-Madrid, F. ISGylation—A key to lock the cell gates for preventing the spread of threats. *J. Cell Sci.* **2017**, *130*, 2961–2969. [CrossRef]
8. Mao, X.; Sethi, G.; Zhang, Z.; Wang, Q. The Emerging Roles of the HERC Ubiquitin Ligases in Cancer. *Curr. Pharm. Des.* **2018**, *24*, 1676–1681. [CrossRef]
9. Walz, C.; Grimwade, D.; Saussele, S.; Lengfelder, E.; Haferlach, C.; Schnittger, S.; Lafage-Pochitaloff, M.; Hochhaus, A.; Cross, N.C.P.; Reiter, A. Atypical mRNA fusions in PML-RARA positive, RARA-PML negative acute promyelocytic leukemia. *Genes Chromosom. Cancer* **2010**, *49*, 471–479.
10. Opatz, S.; Bamopoulos, S.A.; Metzeler, K.H.; Herold, T.; Ksienzyk, B.; Bräundl, K.; Tschuri, S.; Vosberg, S.; Konstandin, N.P.; Wang, C.; et al. The clinical mutatome of core binding factor leukemia. *Leukemia* **2020**, *34*, 1553–1562. [CrossRef]
11. Diouf, B.; Pei, D.; Fan, Y.; Cheng, C.; Krynetskiy, E.Y.; Geng, H.; Chen, S.; Thierfelder, W.E.; Mullighan, C.G.; Downing, J.R.; et al. Somatic deletions of genes regulating MSH2 protein stability cause DNA mismatch repair deficiency and drug resistance in human leukemia cells. *Nat. Med.* **2012**, *17*, 1298–1303. [CrossRef] [PubMed]
12. Neumann, M.; Vosberg, S.; Schlee, C.; Heesch, S.; Schwartz, S.; Gökbuget, N.; Hoelzer, D.; Graf, A.; Krebs, S.; Bartram, I.; et al. Mutational spectrum of adult T-ALL. *Oncotarget* **2015**, *6*, 2754–2766. [CrossRef] [PubMed]
13. Johansson, P.; Klein-Hitpass, L.; Choidas, A.; Habenberger, P.; Mahboubi, B.; Kim, B.; Bergmann, A.; Scholtysik, R.; Brauser, M.; Lollies, A.; et al. SAMHD1 is recurrently mutated in T-cell prolymphocytic leukemia. *Blood Cancer J.* **2018**, *8*, 11. [CrossRef] [PubMed]
14. Holloway, A.; Simmonds, M.; Azad, A.; Fox, J.L.; Storey, A. Resistance to UV-induced apoptosis by β-HPV5 E6 involves targeting of activated BAK for proteolysis by recruitment of the HERC1 ubiquitin ligase. *Int. J. Cancer* **2015**, *136*, 2831–2843. [CrossRef]
15. Fan, X.; Lin, L.; Wang, J.; Wang, Y.; Feng, A.; Nie, L.; Wu, H.; Meng, F.; Xu, H. Genome profile in a extremely rare case of pulmonary sclerosing pneumocytoma presenting with diffusely-scattered nodules in the right lung. *Cancer Biol. Ther.* **2018**, *19*, 13–19. [CrossRef]
16. Ping, Z.; Siegal, G.P.; Harada, S.; Eltoum, I.E.; Youssef, M.; Shen, T.; He, J.; Huang, Y.; Chen, D.; Li, Y.; et al. ERBB2 mutation is associated with a worse prognosis in patients with CDH1 altered invasive lobular cancer of the breast. *Oncotarget* **2016**, *7*, 80655–80663. [CrossRef]
17. Craig, D.W.; O'Shaughnessy, J.A.; Kiefer, J.A.; Aldrich, J.; Sinari, S.; Moses, T.M.; Wong, S.; Dinh, J.; Christoforides, A.; Blum, J.L.; et al. Genome and transcriptome sequencing in prospective metastatic triple-negative breast cancer uncovers therapeutic vulnerabilities. *Mol. Cancer Ther.* **2013**, *12*, 104–116. [CrossRef]

18. Zhu, D.; Yang, D.; Li, X.; Feng, F. Heterogeneous expression and biological function of SOX18 in osteosaroma. *J. Cell. Biochem.* **2018**, *119*, 4184–4192. [CrossRef]
19. Suh, Y.J.; Choe, J.Y.; Park, H.J. Malignancy in Pheochromocytoma or Paraganglioma: Integrative Analysis of 176 Cases in TCGA. *Endocr. Pathol.* **2017**, *28*, 159–164. [CrossRef]
20. Ibarrola-Villava, M.; Fernandez, L.P.; Pita, G.; Bravo, J.; Floristan, U.; Sendagorta, E.; Feito, M.; Avilés, J.A.; Martin-Gonzalez, M.; Lázaro, P.; et al. Genetic analysis of three important genes in pigmentation and melanoma susceptibility: CDKN2A, MC1R and HERC2/OCA2. *Exp. Dermatol.* **2010**, *19*, 836–844. [CrossRef]
21. Amos, C.I.; Wang, L.E.; Lee, J.E.; Gershenwald, J.E.; Chen, W.V.; Fang, S.; Kosoy, R.; Zhang, M.; Qureshi, A.A.; Vattathil, S.; et al. Genome-wide association study identifies novel loci predisposing to cutaneous melanoma. *Hum. Mol. Genet.* **2011**, *20*, 5012–5023. [CrossRef] [PubMed]
22. Fesenko, D.O.; Chudinov, A.V.; Surzhikov, S.A.; Zasedatelev, A.S. Biochip-Based Genotyping Assay for Detection of Polymorphisms in Pigmentation Genes Associated with Cutaneous Melanoma. *Genet. Test. Mol. Biomarkers* **2016**, *20*, 208–212. [CrossRef] [PubMed]
23. Laino, A.M.; Berry, E.G.; Jagirdar, K.; Lee, K.J.; Duffy, D.L.; Soyer, H.P.; Sturm, R.A. Iris pigmented lesions as a marker of cutaneous melanoma risk: An Australian case–control study. *Br. J. Dermatol.* **2018**, *178*, 1119–1127. [CrossRef] [PubMed]
24. Xiao, F.; Ma, J.; Cai, G.; Fang, S.; Lee, J.E.; Wei, Q.; Amos, C.I. Natural and orthogonal model for estimating gene-gene interactions applied to cutaneous melanoma. *Hum. Genet.* **2014**, *133*, 559–574. [CrossRef]
25. Kosiniak-Kamysz, A.; Marczakiewicz-Lustig, A.; Marcińska, M.; Skowron, M.; Wojas-Pelc, A.; Pośpiech, E.; Branicki, W. Increased risk of developing cutaneous malignant melanoma is associated with variation in pigmentation genes and VDR, and may involve epistatic effects. *Melanoma Res.* **2014**, *24*, 388–396. [CrossRef]
26. Wei, L.; Allain, D.C.; Bernhardt, M.N.; Gillespie, J.L.; Peters, S.B.; Iwenofu, O.H.; Nelson, H.H.; Arron, S.T.; Toland, A.E. Variants at the OCA2/HERC2 locus affect time to first cutaneous squamous cell carcinoma in solid organ transplant recipients collected using two different study designs. *Br. J. Dermatol.* **2017**, *177*, 1066–1073. [CrossRef]
27. Ferguson, R.; Vogelsang, M.; Ucisik-Akkaya, E.; Rai, K.; Pilarski, R.; Martinez, C.N.; Rendleman, J.; Kazlow, E.; Nagdimov, K.; Osman, I.; et al. Genetic markers of pigmentation are novel risk loci for uveal melanoma. *Sci. Rep.* **2016**, *6*, 31191. [CrossRef]
28. Bonanno, L.; Costa, C.; Majem, M.; Sanchez, J.J.; Rodriguez, I.; Gimenez-Capitan, A.; Molina-Vila, M.A.; Vergnenegre, A.; Massuti, B.; Favaretto, A.; et al. Combinatory effect of BRCA1 and HERC2 expression on outcome in advanced non-small-cell lung cancer. *BMC Cancer* **2016**, *16*, 312. [CrossRef]
29. Wu, W.; Sato, K.; Koike, A.; Nishikawa, H.; Koizumi, H.; Venkitaraman, A.R.; Ohta, T. HERC2 is an E3 ligase that targets BRCA1 for degradation. *Cancer Res.* **2010**, *70*, 6384–6392. [CrossRef]
30. Peng, Y.; Dai, H.; Wang, E.; Lin, C.C.J.; Mo, W.; Peng, G.; Lin, S.Y. TUSC4 functions as a tumor suppressor by regulating BRCA1 stability. *Cancer Res.* **2015**, *75*, 378–386. [CrossRef]
31. Yoo, N.J.; Park, S.W.; Lee, S.H. Frameshift mutations of ubiquitinationrelated genes HERC2, HERC3, TRIP12, UBE2Q1 and UBE4B in gastric and colorectal carcinomas with microsatellite instability. *Pathology* **2011**, *43*, 753–755. [CrossRef] [PubMed]
32. Li, H.; Li, J.; Chen, L.; Qi, S.; Yu, S.; Weng, Z.; Hu, Z.; Zhou, Q.; Xin, Z.; Shi, L.; et al. HERC3-Mediated SMAD7 ubiquitination degradation promotes autophagy-induced EMT and chemoresistance in Glioblastoma. *Clin. Cancer Res.* **2019**, *25*, 3602–3616. [CrossRef] [PubMed]
33. Zhang, Z.; Tong, J.; Tang, X.; Juan, J.; Cao, B.; Hurren, R.; Chen, G.; Taylor, P.; Xu, X.; Shi, C.X.; et al. The ubiquitin ligase HERC4 mediates c-Maf ubiquitination and delays the growth of multiple myeloma xenografts in nude mice. *Blood* **2016**, *127*, 1676–1686. [CrossRef] [PubMed]
34. Zeng, W.L.; Chen, Y.W.; Zhou, H.; Zhou, J.Y.; Wei, M.; Shi, R. Expression of HERC4 in lung cancer and its correlation with clinicopathological parameters. *Asian Pac. J. Cancer Prev.* **2015**, *16*, 513–517. [CrossRef] [PubMed]
35. Jiang, W.; Yao, X.; Shan, Z.; Li, W.; Gao, Y.; Zhang, Q. E3 ligase Herc4 regulates Hedgehog signalling through promoting Smoothened degradation. *J. Mol. Cell Biol.* **2019**, *11*, 791–803. [CrossRef]
36. Sun, X.; Sun, B.; Cui, M.; Zhou, Z. HERC4 exerts an anti-tumor role through destabilizing the oncoprotein Smo. *Biochem. Biophys. Res. Commun.* **2019**, *513*, 1013–1018. [CrossRef]
37. Zhou, H.; Shi, R.; Wei, M.; Zheng, W.L.; Zhou, J.Y.; Ma, W.L. The expression and clinical significance of HERC4 in breast cancer. *Cancer Cell Int.* **2013**, *13*, 113. [CrossRef]

38. Xu, Y.; Ji, K.; Wu, M.; Hao, B.; Yao, K.T.; Xu, Y. A miRNA-HERC4 pathway promotes breast tumorigenesis by inactivating tumor suppressor LATS1. *Protein Cell* **2019**, *10*, 595–605. [CrossRef]
39. Zheng, Y.; Li, J.; Pan, C.; Zhou, G.; Zhuge, L.; Jin, L.; Fang, P. HERC4 Is Overexpressed in Hepatocellular Carcinoma and Contributes to the Proliferation and Migration of Hepatocellular Carcinoma Cells. *DNA Cell Biol.* **2017**, *36*, 490–500. [CrossRef]
40. Wang, H.W.; Wu, Y.H.; Hsieh, J.Y.; Liang, M.L.; Chao, M.E.; Liu, D.J.; Hsu, M.T.; Wong, T.T. Pediatric primary central nervous system germ cell tumors of different prognosis groups show characteristic miRNome traits and chromosome copy number variations. *BMC Genom.* **2010**, *11*, 132. [CrossRef]
41. Bhargava, S.; Patil, V.; Mahalingam, K.; Somasundaram, K. Elucidation of the genetic and epigenetic landscape alterations in RNA binding proteins in glioblastoma. *Oncotarget* **2017**, *8*, 16650–16668. [CrossRef] [PubMed]
42. Niu, P.; Yao, B.; Wei, L.; Zhu, H.; Fang, C.; Zhao, Y. Construction of prognostic risk prediction model based on high-throughput sequencing expression profile data in childhood acute myeloid leukemia. *Blood Cells Mol. Dis.* **2019**, *77*, 43–50. [CrossRef] [PubMed]
43. Reddy, R.B.; Khora, S.S.; Suresh, A. Molecular prognosticators in clinically and pathologically distinct cohorts of head and neck squamous cell carcinoma—A meta-analysis approach. *PLoS ONE* **2019**, *14*, e0218989. [CrossRef] [PubMed]
44. Wrage, M.; Hagmann, W.; Kemming, D.; Uzunoglu, F.G.; Riethdorf, S.; Effenberger, K.; Westphal, M.; Lamszus, K.; Kim, S.Z.; Becker, N.; et al. Identification of HERC5 and its potential role in NSCLC progression. *Int. J. Cancer* **2015**, *136*, 2264–2272. [CrossRef]
45. Tang, J.; Yang, Q.; Cui, Q.; Zhang, D.; Kong, D.; Liao, X.; Ren, J.; Gong, Y.; Wu, G. Weighted gene correlation network analysis identifies RSAD2, HERC5, and CCL8 as prognostic candidates for breast cancer. *J. Cell. Physiol.* **2020**, *235*, 394–407. [CrossRef]
46. Xue, F.; Higgs, B.W.; Huang, J.; Morehouse, C.; Zhu, W.; Yao, X.; Brohawn, P.; Xiao, Z.; Sebastian, Y.; Liu, Z.; et al. HERC5 is a prognostic biomarker for post-liver transplant recurrent human hepatocellular carcinoma. *J. Transl. Med.* **2015**, *13*, 379. [CrossRef]
47. Wang, Y.; Ding, Q.; Xu, T.; Li, C.Y.; Zhou, D.D.; Zhang, L. HZ-6d targeted HERC5 to regulate p53 ISGylation in human hepatocellular carcinoma. *Toxicol. Appl. Pharmacol.* **2017**, *334*, 180–191. [CrossRef]
48. Januchowski, R.; Sterzyńska, K.; Zawierucha, P.; Ruciński, M.; Świerczewska, M.; Partyka, M.; Bednarek-Rajewska, K.; Brazert, M.; Nowicki, M.; Zabel, M.; et al. Microarray-based detection and expression analysis of new genes associated with drug resistance in ovarian cancer cell lines. *Oncotarget* **2017**, *8*, 49944–49958. [CrossRef]
49. Swierczewska, M.; Klejewski, A.; Wojtowicz, K.; Brazert, M.; Izycki, D.; Nowicki, M.; Zabel, M.; Januchowski, R. New and old genes associated with primary and established responses to cisplatin and topotecan treatment in ovarian cancer cell lines. *Molecules* **2017**, *22*, 1717. [CrossRef]
50. Schneider, T.; Martinez-Martinez, A.; Cubillos-Rojas, M.; Bartrons, R.; Ventura, F.; Rosa, J.L. Large HERCS function as tumor suppressors. *Front. Oncol.* **2019**, *9*, 524. [CrossRef]
51. Tong, H.V.; Hoan, N.X.; Binh, M.T.; Quyen, D.T.; Meyer, C.G.; Hang, D.T.T.; Hang, D.T.D.; Son, H.A.; Luong, H.V.; Thuan, N.D.; et al. Upregulation of enzymes involved in isgylation and ubiquitination in patients with hepatocellular carcinoma. *Int. J. Med. Sci.* **2020**, *17*, 347–353. [CrossRef] [PubMed]
52. Negrini, S.; Gorgoulis, V.G.; Halazonetis, T.D. Genomic instability an evolving hallmark of cancer. *Nat. Rev. Mol. Cell Biol.* **2010**, *11*, 220–228. [CrossRef] [PubMed]
53. Hanahan, D.; Weinberg, R.A. Hallmarks of cancer: The next generation. *Cell* **2011**, *144*, 646–674. [CrossRef] [PubMed]
54. Kang, T.H.; Lindsey-Boltz, L.A.; Reardon, J.T.; Sancar, A. Circadian control of XPA and excision repair of cisplatin-DNA damage by cryptochrome and HERC2 ubiquitin ligase. *Proc. Natl. Acad. Sci. USA* **2010**, *107*, 4890–4895. [CrossRef] [PubMed]
55. Lee, T.H.; Park, J.M.; Leem, S.H.; Kang, T.H. Coordinated regulation of XPA stability by ATR and HERC2 during nucleotide excision repair. *Oncogene* **2014**, *33*, 19–25. [CrossRef] [PubMed]
56. Jiang, Q.; Greenberg, R.A. Deciphering the BRCA1 tumor suppressor network. *J. Biol. Chem.* **2015**, *290*, 17724–17732. [CrossRef]

57. Bekker-Jensen, S.; Danielsen, J.R.; Fugger, K.; Gromova, I.; Nerstedt, A.; Bartek, J.; Lukas, J.; Mailand, N. HERC2 coordinates ubiquitin-dependent assembly of DNA repair factors on damaged chromosomes. *Nat. Cell Biol.* **2010**, *12*, 80–86. [CrossRef]
58. Danielsen, J.R.; Povlsen, L.K.; Villumsen, B.H.; Streicher, W.; Nilsson, J.; Wikström, M.; Bekker-Jensen, S.; Mailand, N. DNA damage-inducible SUMOylation of HERC2 promotes RNF8 binding via a novel SUMO-binding Zinc finger. *J. Cell Biol.* **2012**, *197*, 179–187. [CrossRef]
59. Zhang, Z.; Yang, H.; Wang, H. The histone H2A deubiquitinase USP16 interacts with HERC2 and fine-tunes cellular response to DNA damage. *J. Biol. Chem.* **2014**, *289*, 32883–32894. [CrossRef]
60. Izawa, N.; Wu, W.; Sato, K.; Nishikawa, H.; Kato, A.; Boku, N.; Itoh, F.; Ohta, T. HERC2 interacts with claspin and regulates DNA origin firing and replication fork progression. *Cancer Res.* **2011**, *71*, 5621–5625. [CrossRef]
61. Zhu, M.; Zhao, H.; Liao, J.; Xu, X. HERC2/USP20 coordinates CHK1 activation by modulating CLASPIN stability. *Nucleic Acids Res.* **2014**, *42*, 13074–13081. [CrossRef] [PubMed]
62. Yuan, J.; Luo, K.; Deng, M.; Li, Y.; Yin, P.; Gao, B.; Fang, Y.; Wu, P.; Liu, T.; Lou, Z. HERC2-USP20 axis regulates DNA damage checkpoint through Claspin. *Nucleic Acids Res.* **2014**, *42*, 13110–13121. [CrossRef] [PubMed]
63. Macheret, M.; Halazonetis, T.D. DNA Replication Stress as a Hallmark of Cancer. *Annu. Rev. Pathol. Mech. Dis.* **2015**, *10*, 425–448. [CrossRef] [PubMed]
64. Wu, W.; Rokutanda, N.; Takeuchi, J.; Lai, Y.; Maruyama, R.; Togashi, Y.; Nishikawa, H.; Arai, N.; Miyoshi, Y.; Suzuki, N.; et al. HERC2 facilitates BLM and WRN helicase complex interaction with RPA to suppress G-quadruplex DNA. *Cancer Res.* **2018**, *78*, 6371–6385. [CrossRef]
65. Lai, Y.; Zhu, M.; Wu, W.; Rokutanda, N.; Togashi, Y.; Liang, W.; Ohta, T. HERC2 regulates RPA2 by mediating ATR-induced Ser33 phosphorylation and ubiquitin-dependent degradation. *Sci. Rep.* **2019**, *9*, 14257. [CrossRef]
66. Cubillos-Rojas, M.; Amair-Pinedo, F.; Peiró-Jordán, R.; Bartrons, R.; Ventura, F.; Rosa, J.L. The E3 ubiquitin protein ligase HERC2 modulates the activity of tumor protein p53 by regulating its oligomerization. *J. Biol. Chem.* **2014**, *289*, 14782–14795. [CrossRef]
67. Cubillos-Rojas, M.; Schneider, T.; Bartrons, R.; Ventura, F.; Rosa, J.L. NEURL4 regulates the transcriptional activity of tumor suppressor protein p53 by modulating its oligomerization. *Oncotarget* **2017**, *8*, 61824–61836. [CrossRef]
68. García-Cano, J.; Sánchez-Tena, S.; Sala-Gaston, J.; Figueras, A.; Viñals, F.; Bartrons, R.; Ventura, F.; Rosa, J.L. Regulation of the MDM2-p53 pathway by the ubiquitin ligase HERC2. *Mol. Oncol.* **2020**, *14*, 69–86. [CrossRef]
69. Chang, L.; Karin, M. Mammalian MAP kinase signalling cascades. *Nature* **2001**, *410*, 37–40. [CrossRef]
70. Wagner, E.F.; Nebreda, Á.R. Signal integration by JNK and p38 MAPK pathways in cancer development. *Nat. Rev. Cancer* **2009**, *9*, 537–549. [CrossRef]
71. Montagut, C.; Settleman, J. Targeting the RAF-MEK-ERK pathway in cancer therapy. *Cancer Lett.* **2009**, *283*, 125–134. [CrossRef] [PubMed]
72. Martinez-Noel, G.; Galligan, J.T.; Sowa, M.E.; Arndt, V.; Overton, T.M.; Harper, J.W.; Howley, P.M. Identification and Proteomic Analysis of Distinct UBE3A/E6AP Protein Complexes. *Mol. Cell. Biol.* **2012**, *32*, 3095–3106. [CrossRef] [PubMed]
73. Martínez-Noël, G.; Luck, K.; Kühnle, S.; Desbuleux, A.; Szajner, P.; Galligan, J.T.; Rodriguez, D.; Zheng, L.; Boyland, K.; Leclere, F.; et al. Network Analysis of UBE3A/E6AP-Associated Proteins Provides Connections to Several Distinct Cellular Processes. *J. Mol. Biol.* **2018**, *430*, 1024–1050. [CrossRef] [PubMed]
74. Schneider, T.; Martinez-Martinez, A.; Cubillos-Rojas, M.; Bartrons, R.; Ventura, F.; Rosa, J.L. The E3 ubiquitin ligase HERC1 controls the ERK signaling pathway targeting C-RAF for degradation. *Oncotarget* **2018**, *9*, 31531–31548. [CrossRef]
75. Pedrazza, L.; Schneider, T.; Bartrons, R.; Ventura, F.; Rosa, J.L. The ubiquitin ligase HERC1 regulates cell migration via RAF-dependent regulation of MKK3/p38 signaling. *Sci. Rep.* **2020**, *10*, 824. [CrossRef]
76. Manasanch, E.E.; Orlowski, R.Z. Proteasome inhibitors in cancer therapy. *Nat. Rev. Clin. Oncol.* **2017**, *14*, 417–433. [CrossRef]
77. Sanclemente, M.; Francoz, S.; Esteban-Burgos, L.; Bousquet-Mur, E.; Djurec, M.; Lopez-Casas, P.P.; Hidalgo, M.; Guerra, C.; Drosten, M.; Musteanu, M.; et al. c-RAF Ablation Induces Regression of Advanced Kras/Trp53 Mutant Lung Adenocarcinomas by a Mechanism Independent of MAPK Signaling. *Cancer Cell* **2018**, *33*, 217–228. [CrossRef]

78. Blasco, M.T.; Navas, C.; Martín-Serrano, G.; Graña-Castro, O.; Lechuga, C.G.; Martín-Díaz, L.; Djurec, M.; Li, J.; Morales-Cacho, L.; Esteban-Burgos, L.; et al. Complete Regression of Advanced Pancreatic Ductal Adenocarcinomas upon Combined Inhibition of EGFR and C-RAF. *Cancer Cell* **2019**, *35*, 573–587. [CrossRef]
79. Ashworth, A.; Lord, C.J.; Reis-Filho, J.S. Genetic interactions in cancer progression and treatment. *Cell* **2011**, *145*, 30–38. [CrossRef]
80. Bhattacharjee, S.; Nandi, S. Synthetic lethality in DNA repair network: A novel avenue in targeted cancer therapy and combination therapeutics. *IUBMB Life* **2017**, *69*, 929–937. [CrossRef]
81. Ubhi, T.; Brown, G.W. Exploiting DNA replication stress for cancer treatment. *Cancer Res.* **2019**, *79*, 1730–1739. [CrossRef] [PubMed]
82. Farmer, H.; McCabe, H.; Lord, C.J.; Tutt, A.H.J.; Johnson, D.A.; Richardson, T.B.; Santarosa, M.; Dillon, K.J.; Hickson, I.; Knights, C.; et al. Targeting the DNA repair defect in BRCA mutant cells as a therapeutic strategy. *Nature* **2005**, *434*, 917–921. [CrossRef] [PubMed]

Cellular and Molecular Life Sciences (2022) 79:548
https://doi.org/10.1007/s00018-022-04586-7

Cellular and Molecular Life Sciences

ORIGINAL ARTICLE

HERC2 deficiency activates C-RAF/MKK3/p38 signalling pathway altering the cellular response to oxidative stress

Joan Sala-Gaston[1] · Leonardo Pedrazza[1] · Juanma Ramirez[2] · Arturo Martinez-Martinez[1] · Lettie E. Rawlins[3,4] · Emma L. Baple[3,4] · Andrew H. Crosby[3] · Ugo Mayor[2,5] · Francesc Ventura[1] · Jose Luis Rosa[1]

Received: 27 April 2022 / Revised: 3 October 2022 / Accepted: 3 October 2022 / Published online: 14 October 2022

Abstract

HERC2 gene encodes an E3 ubiquitin ligase involved in several cellular processes by regulating the ubiquitylation of different protein substrates. Biallelic pathogenic sequence variants in the *HERC2* gene are associated with HERC2 Angelman-like syndrome. In pathogenic *HERC2* variants, complete absence or marked reduction in HERC2 protein levels are observed. The most common pathological variant, c.1781C > T (p.Pro594Leu), encodes an unstable HERC2 protein. A better understanding of how pathologic *HERC2* variants affect intracellular signalling may aid definition of potential new therapies for these disorders. For this purpose, we studied patient-derived cells with the HERC2 Pro594Leu variant. We observed alteration of mitogen-activated protein kinase signalling pathways, reflected by increased levels of C-RAF protein and p38 phosphorylation. HERC2 knockdown experiments reproduced the same effects in other human and mouse cells. Moreover, we demonstrated that HERC2 and RAF proteins form molecular complexes, pull-down and proteomic experiments showed that HERC2 regulates C-RAF ubiquitylation and we found out that the p38 activation due to HERC2 depletion occurs in a RAF/MKK3-dependent manner. The displayed cellular response was that patient-derived and other human cells with HERC2 deficiency showed higher resistance to oxidative stress with an increase in the master regulator of the antioxidant response NRF2 and its target genes. This resistance was independent of p53 and abolished by RAF or p38 inhibitors. Altogether, these findings identify the activation of C-RAF/MKK3/p38 signalling pathway in HERC2 Angelman-like syndrome and highlight the inhibition of RAF activity as a potential therapeutic option for individuals affected with these rare diseases.

Keywords Neurodevelopmental disorder · Angelman · Ubiquitin · MAPK · Cell stress

Introduction

Hereditary neurodevelopmental disorders arise from alterations in central nervous system development and manifest perinatally or during infancy and childhood. Despite showing wide genetic and clinical heterogeneity, most share some common phenotypic features, such as developmental delay, impaired motor function and intellectual disability. The identification of genes responsible for these disorders has enabled genetic diagnosis, accurate genetic counselling, and better management [1].

The *HECT and RCC1-like domain 2 (HERC2)* gene encodes an unusually large protein with 4834 amino acid residues. The HERC2 protein is an E3 ubiquitin ligase that functions in ubiquitylation by accepting ubiquitin from ubiquitin-conjugating enzymes (E2) and transferring it to a target protein [2]. Ubiquitylation affects proteins in many ways, variously marking them for proteasome degradation

✉ Jose Luis Rosa
joseluisrosa@ub.edu

1 Department of Physiological Sciences, Bellvitge Biomedical Research Institute (IDIBELL), University of Barcelona (UB), C/ Feixa Llarga s/n, 08907 L'Hospitalet de Llobregat, Spain

2 Department of Biochemistry and Molecular Biology, Faculty of Science and Technology, UPV/EHU, Leioa, Bizkaia, Spain

3 RILD Wellcome Wolfson Medical Research Centre, RD&E (Wonford) NHS Foundation Trust, University of Exeter Medical School, Exeter, UK

4 Peninsula Clinical Genetics Service, Royal Devon & Exeter Hospital (Heavitree), Exeter, UK

5 Ikerbasque, Basque Foundation for Science, 48013 Bilbao, Spain

or, affecting their activity, localisation or interactions with other proteins. Therefore, ubiquitin ligases are key regulators of many cellular processes, with their dysregulation being common in numerous cancers and neurodegenerative diseases [3]. For example, *HERC2* mutations are associated with breast, skin (melanoma), gastric, colorectal, and haematological (leukaemia) cancers [4]. The underlying molecular mechanism could be that HERC2 regulates BRCA1, XPA, USP20 or RPA2 protein ubiquitylation, involved in regulating DNA repair and genomic stability [5–9]. HERC2 also regulates p53 transcriptional program by promoting p53 tetramerisation and subsequent activation, independent of its ubiquitin ligase activity [10–12].

Besides, HERC2 is essential during embryonic development and plays an important role in regulating motor coordination [13]. Moreover, it is highly expressed in the nervous system and has been linked with hereditary neurodegenerative disorders [14]. Biallelic *HERC2* variants associated with HERC2 Angelman-like syndrome include missense and frameshift mutations with a premature stop codon that result in a loss of function. These cases are associated with a complete loss or markedly reduced levels of HERC2 protein [15–19]. The condition was first described in Amish/Mennonite communities, associated with homozygosity for a *HERC2* (c.1781C > T, p.Pro594Leu) founder gene variant at increased frequency in the population (autosomal recessive mental retardation type 38; OMIM # 615516) [15, 16]. Proteomic studies of peripheral blood-derived lymphoblasts from individuals with this condition suggest derangements of multiple cellular pathways probably involving disparate pathogenic mechanisms [20]. Despite these efforts, the molecular mechanisms underlying HERC2-related disorders remain elusive, impeding efforts to find potential treatments for these rare diseases. Further investigation of their molecular basis could reveal not only the underlying pathology but also potential therapeutic targets.

In this study, we analysed intracellular signalling pathways in skin fibroblasts from individuals with the pathological variant HERC2 Pro594Leu (HERC2 P594L). They displayed altered mitogen-activated protein kinase (MAPK) signalling that affected the oxidative stress response, with increases in C-RAF protein levels and MAPK p38 activation. These effects were reproduced in other human and mouse cells with HERC2 protein knockdown. Furthermore, we showed that HERC2 regulates C-RAF ubiquitylation and that HERC2 deficiency triggers MKK3/p38 pathway activation in a RAF-dependent manner. In line with this, cells with the HERC2 P594L variant had increased resistance to H_2O_2-induced oxidative stress, dependent on the activities of RAF and p38. Finally, we discuss both the implications of these findings for neurodevelopmental disorders caused by HERC2 variants and the potential therapeutic use of RAF inhibitors.

Materials and methods

Human cell sample, cell lines and culture conditions

Samples of human skin fibroblasts were obtained with approved informed consent as previously described elsewhere [16].

U2OS, HEK 293T, H1299, RAW 264.7, mouse embryonic fibroblasts (MEFs) and human skin fibroblasts were cultured in Dulbecco's modified Eagle's medium supplemented with 10% fetal bovine serum, 2 mM L-glutamine, 100 U/mL penicillin, and 0.1 mg/mL streptomycin sulphate. Mouse primary osteoblasts were cultured in Minimum Essential Medium α with 10% FBS, 2 mM L-glutamine, 1 mM pyruvate, 100 U/ml penicillin, and 0.1 mg/ml streptomycin with 50 µg/ml ascorbic acid and 4 mM β-glycerophosphate. All cells were maintained in a humidified incubator at 37 °C and 5% CO_2 atmosphere.

Cell treatments and induction of cellular stress

Cells were treated with one of three inhibitors, as indicated: 1 µM LY3009120 (Selleckchem), 1 µM Sorafenib (Santa Cruz Biotechnology) or 10 µM SB203580 (Selleckchem). Different cellular stress types were induced using different stressors: oxidative stress by 500 µM or 50 µM hydrogen peroxide (H_2O_2) (Panreac), depending on the experiment; saline stress by 100 mM NaCl.

Plasmid and siRNAs transfections

Plasmid transfection was performed using the Lipofectamine LTX method (15338; Invitrogen, Carlsbad, CA, USA), according to the manufacturer's instructions. Myc-tagged fragments of HERC2 (F1, F2, F3, F4, F5 and F5CT) were kindly provided by Dr. Ohta [21]. Green fluorescent protein (GFP) and C-RAF fusion constructs (CR1, CR2, CR3 and full-length) were generated, sub-cloned and tested elsewhere [22]. Plasmids expressing HERC2 full-length protein pcDNA5 FRT/TO SF-HERC2 (ShB-R) (Addgene plasmid # 55613; http://n2t.net/addgene:55613; RRID:Addgene_55613) and pcDNA5 FRT/TO SF-HERC2 C4762S (ShB-R) (Addgene plasmid # 55614; http://n2t.net/addgene:55614; RRID:Addgene_55614) were a gift from David Chan [23]. His-Ubiquitin constructs were kindly provided by Dr. Erazo [24]. The plasmid expressing a biotinylatable version of ubiquitin had been previously described elsewhere [25].

For gene interference, siRNAs were transfected using the calcium phosphate method described elsewhere [10]. Custom double-stranded siRNA oligonucleotides were

obtained from GeneCust (Boynes, France). The forward sequences were as follows: negative control (NC) = 5′-UUC UCCGAACGUGUCACGU**TT**; HERC2 (H2.2) = GAC UGUAGCCAGAUUGAAA**TT**; HERC2 (H2.4) = GGA AAGCACUGGAUUCGUU**TT**; HERC1 = CGGCAU GGAUGAACAAAUU**TT**; MKK3 = GGAAGAAGG AUCUACGGAU**TT**; C-RAF = UAGUUCAGCAGUUUG GCUA**TT**; A-RAF = AACAACAUCUUCCUACAUGAG **TT**; B-RAF = AAAGAAUUGGAUCUGGAUCAU**TT**; p53 = GACUCCAGUGGUAAUCUAC**TT**.

Lentiviral particle production and target cell infection

Lentiviral vectors were produced in HEK 293 T cells. Cells were transfected with 7 µg pMD2.G, 7 µg psPAX2 (VSV-G) and 7 µg of either empty pLKO.1-Puro or pLKO.1-shHERC2 by the calcium phosphate method. Media containing lentiviral particles were collected, filtered using polyvinyl difluoride filters (Millex-HV filter 0.45 µm, Millipore SLHV033RB) and stored in aliquots at − 80 °C. Target cells were seeded at a confluence of 50–60% in a 6-well plate before adding 300 µL of the medium containing the lentiviral vectors to each well. Fresh medium, supplemented with 5 µg/mL polybrene, was added to make a total volume of 1 mL. Media with lentiviral vectors were removed the next day and after 24 h, 5 µg/mL puromycin was added for selection. MISSION shRNA clone of mouse HERC2 (TRCN0000039444) was purchased from Sigma-Aldrich. The plasmid vector pLKO.1—TRC control was a gift from David Root (Addgene plasmid #10879; http://n2t.net/addgene:10879; RRID:Addgene_10879) [26], and the VSV-G envelope expressing plasmid pMD2.G (Addgene plasmid #12259; http://n2t.net/addgene:12259; RRID:Addgene_12259) and the lentivirus packaging plasmid psPAX2 (Addgene plasmid #12260; http://n2t.net/addgene:12260; RRID:Addgene_12260) were a gift from Didier Trono.

Protein extraction, PAGE, and immunoblotting

For protein extraction, cells were washed twice in ice-cold phosphate-buffer saline after discarding the media. Cell lysis was performed by scrapping after adding of NP40 lysis buffer (50 mM Tris–HCl, pH 7.5, 150 mM NaCl, 50 mM NaF, 0.5% NP40) containing protease and phosphatase inhibitors as previously described [27]. Lysates were maintained on ice under agitation for 20 min, and then centrifuged at 13,000×*g* at 4 °C for 10 min. Supernatants were collected before analysis using the Tris–Acetate PAGE system [28]. Band intensities were detected using a gel documentation system (LAS-3000, Fujifilm) and quantified with ImageJ software (Rasband, W.S., ImageJ, U. S. National Institutes of Health, Bethesda, Maryland, USA, https://imagej.nih.gov/ij/).

We used the following antibodies: anti-HERC2 monoclonal (BD Biosciences #612366); anti-C-RAF (BD Biosciences #610151); anti-Clathrin Heavy Chain (TD.1) (Santa Cruz Biotechnology #sc12734); anti-P-ERK1/2 (Sigma-Aldrich #M 8159); anti-p44/42 MAPK (ERK1/2) (Cell signalling #9102); anti-phospho-p38 (Cell signalling #9211); anti-p38 (Santa Cruz Biotechnology #sc-535); anti-HERC1 (410) [10]; anti-P-MKK3 (Cell signalling #9231); anti-MKK3 (Proteintech #13898–1-AP); anti-A-RAF (A-5) (Santa Cruz #sc-166771); anti-B-RAF (F-7) (Santa Cruz Biotechnology #sc-5284); anti-HERC2 polyclonal (bvg3) [10]; anti-c-myc (clone 9E10) (Roche #1 667 149); anti-GFP (Abcam #ab13970); anti-Flag M2 (Sigma-Aldrich #F 3165); anti-p-HSP27 (Enzo Life Sciences #ADI-SPA-523); anti-HSP27 (Santa Cruz Biotechnology #sc-1049); anti-NRF2 (Cell signalling #12721); anti-ubiquitylated proteins (clone FK2; Biomol); and peroxidase-conjugated secondary antibodies (Invitrogen).

Confocal microscopy

We seeded U2OS cells on glass coverslips and performed fixation by incubating cells at room temperature for 20 min in 4% paraformaldehyde. Then, cells were permeabilised for 20 min with 0.05% saponin in phosphate-buffered saline containing 0.5% bovine serum albumin. The primary antibody, anti-phospho-p38 (Cell signalling #9211) (1:200), was incubated at 37 °C for 1 h. After washing, Alexa-Fluor 488 secondary antibody (Invitrogen) (1:500) was incubated at 37 °C for 45 min. Actin filaments were stained by incubation with phalloidin-Alexa 647 (BioProbes) (100 ng/mL) for 20 min at room temperature. Nuclei were stained with DAPI (Sigma-Aldrich) (1 µg/mL). All images were acquired using a confocal laser scanning microscope (LSM 880 spectral, Carl Zeiss Microscopy GmbH, Jena, Germany).

Immunoprecipitation and pull-downs

For immunoprecipitation, cells were lysed with CHAPS buffer (10 mM Tris–HCl, pH 7.5, 100 mM NaCl, 0.3% CHAPS) containing protease and phosphatase inhibitors as described above. Cell lysates (input) were incubated with pre-immune serum or anti-HERC2 polyclonal antibody (bvg3) for 2 h at 4 °C with gentle rotation and immunoprecipitated with protein A-Sepharose (GE Healthcare) for 1 h at 4 °C. Beads were pelleted by centrifugation at 2500×*g*, washed five times with CHAPS buffer, and analysed by electrophoresis and immunoblot.

For the GFP pull-downs, supernatants were incubated with 2 µL GFP-TrapA (ChromoTek) for 2 h at 4 °C. Pellets were washed five times with CHAPS buffer and analysed by electrophoresis and immunoblot.

For ubiquitome proteomic experiments, biotin-pull-downs were performed in triplicates as previously described [25], in order to compare proteins more ubiquitinated in Flag-HERC2 WT-overexpressing cells, relative to Flag-HERC2 C4762S-overexpressing cells.

Ubiquitylation assay

HEK 293 T cells were transfected with the indicated plasmids for 48 h. Before the ubiquitylation assay, the cells were treated for 4 h with 10 µM of the proteasome inhibitor MG132 (Sigma-Aldrich/Merck #C2211). Then, cells were lysed with denaturing buffer #1 (6 M guanidinium-HCl, 10 mM Tris, 100 mM Na_2HPO_4–NaH_2PO_4 buffer, pH 8) and the cells extracts were incubated with the nickel beads (Ni^{2+}-NTA agarose; Qiagen) for 2 h at 4 °C under rotation. Beads were successively washed as follows: twice with 1 ml of denaturing buffer #1 plus 10 mM 2-mercaptoethanol; three times with 1 ml of buffer #2 (8 M urea, 10 mM Tris, 10 mM 2-mercaptoethanol, 100 mM Na_2HPO_4–NaH_2PO_4 buffer, pH 8); twice with 1 ml of buffer #3 (8 M urea, 10 mM Tris, 100 mM Na_2HPO_4–NaH_2PO_4 buffer, pH 6.3) containing 0.2% Triton X-100; once with 1 ml of buffer #3 containing 0.1% Triton X-100 and 0.5 M NaCl; and three times with 1 ml of buffer #3. Finally, proteins were eluted by incubating the beads with 200 mM imidazole in 5% SDS, 0.15 M Tris–HCl, pH 6.7, 30% (vol/vol) glycerol, 0.72 M 2-mercaptoethanol for 1 h at 37 °C with mixing. The samples were analysed by immunoblotting as indicated above.

Reverse transcription and quantitative PCR

Total RNA was isolated from U2OS cells using the TRIsure reagent according to the manufacturer's protocol (Bioline). Total RNA (2 µg) was reverse-transcribed using the high-capacity cDNA Reverse Transcription kit (Applied Biosystems). PCR amplification reactions were performed with the ABI Prism 7900 HT Fast Real-Time PCR System. Applied Biosystems' TaqMan Gene Expression Assays (ThermoFisher Scientific) were used to quantify the gene expressions of the following: *GUSB* (Hs00939627_m1), *NFE2L2* (Hs00975960_m1), *SOD1* (Hs00533490_m1), *SOD2* (Hs00167309_m1), *GPX1* (Hs00829989_Gh), and the housekeeping gene *GAPDH* (Hs99999905_m1), which was used to normalise.

MTT assay for cell viability and cell proliferation

Using 96-well plates, U2OS cells and human skin fibroblasts were seeded to final concentration of 10,000 cells/well or 15,000 cells/well, respectively. After incubation at 37 °C for 24 h in the cell incubator, we initiated treatments, as indicated and performed the MTT assay (M5655; Sigma/Merck) according to manufacturer's instructions. Briefly, we added MTT at a final concentration of 0.5 mg/mL to each well, incubated the cells for 4 h in a humidified incubator, then discarded the media and solubilised the formazan crystals with isopropanol. Finally, absorbance at a wavelength of 570 nm was determined using a 96-well plate spectrophotometer.

MitoSox staining

To evaluate mitochondrial reactive oxygen species (ROS), human skin fibroblasts were seeded in a µ-Slide 8 well-chambered coverslip at a concentration of 15,000 cells/well. The next day, cells were stained with 1 µg/mL of Hoechst 33,342 (H3570, ThermoFisher, USA) for 30 min at 37 °C and with 2 µM MitoSOX Red (Invitrogen) for 15 min at 37 °C. Cells were examined in a Zeiss LSM 880 laser scanning confocal spectral microscope equipped with an incubation control system (37 °C, 5% CO_2). Fluorescence intensity per cell was measured, quantified and expressed as arbitrary units (a.u). Images were analysed using ImageJ software (Rasband, W.S., ImageJ, U.S. National Institutes of Health, Bethesda, Maryland, USA, https://imagej.nih.gov/ij/).

Mitotracker staining

For mitochondria staining, human skin fibroblasts were seeded in a µ-Slide 8 well-chambered coverslip at a concentration of 15,000 cells/well. The next day, cells were stained with 1 µg/mL of Hoechst 33,342 (H3570, ThermoFisher, USA) and 50 nM Mitotracker Red CMXRos (M7512, ThermoFisher, USA) for 30 min at 37 °C. Images were taken using a Zeiss LSM 880 laser scanning confocal spectral microscope equipped with an incubation control system (37 °C, 5% CO_2). Fragmented mitochondrial percentage was calculated by counting spherical non-contiguous mitochondrial particles and dividing by the number of total structures comprised in the mitochondrial network. Images were analysed using ImageJ software (Rasband, W.S., ImageJ, U.S. National Institutes of Health, Bethesda, Maryland, USA, https://imagej.nih.gov/ij/).

Statistical analysis

The results indicate the means and standard error of the mean (± SEM) of, at least, three independent experiments. Individual data points are plotted as single dots. Significance was calculated by Student t-test and indicated as follows: *, **, or *** for p values of ≤ 0.05, ≤ 0.01, or ≤ 0.001, respectively. Figures were created, and statistical analysis was performed, using GraphPad Prism version 8.4.3 for Windows (GraphPad Software, San Diego, California USA), www.graphpad.com.

Results

Human HERC2 Pro594Leu cells display MAPK pathway alteration

Several recessive mutations affecting the *HERC2* gene cause developmental delay with Angelman-like features [14, 19]. Knowing how pathologic *HERC2* variants affect intracellular signalling could reveal the underlying pathology and identify possible therapies. Therefore, we studied cells from an individual with the mutant HERC2 P594L variant described in most cases. Since HERC1 had previously been reported to regulate the ERK and p38 MAPK signalling pathways [22, 29], we wondered if HERC2 also had a modulatory role. As expected, cells with the HERC2 P594L mutation showed almost undetectable HERC2 protein levels (Fig. 1A–C). Interestingly, although they showed higher protein levels of C-RAF (Fig. 1A), this did not correlate with the canonical activation of the ERK signalling pathway, assessed by ERK phosphorylation (Fig. 1B). An increment in p38 phosphorylation was also detected while total p38 protein levels remained stable (Fig. 1C).

In order to provide more evidence that these changes in MAPK signalling pathways are a general hallmark of disease in patients with biallelic HERC2 mutations, we analysed samples of two more individuals carrying the mutant HERC2 P594L variant. Consistently, patients with the HERC2 P594L mutation (P1, P2 and P3) showed lower HERC2 protein levels than the wild-type controls (C1, C2 and C3). In addition, C-RAF protein levels and p38 phosphorylation were upregulated in all three patients, but no changes were detected in ERK activation (Fig. 1D). These results showed that cells with the HERC2 P594L mutation exhibit altered MAPK signalling pathway activation, as reflected by higher C-RAF and phospho-p38 protein levels.

HERC2 regulates C-RAF protein levels

To delve deeper into the molecular mechanisms involved in the altered MAPK signalling pathway in HERC2 P594L cells, we considered human cells with low levels of HERC2 protein shared this alteration. In knockdown experiments performed in human U2OS cells, cells were transfected with either a negative control (NC) small-interfering RNA (siRNA), an siRNA against HERC2, or a positive control siRNA against HERC1. The positive control was chosen because previous work had shown that HERC1 controls ERK and p38 signalling pathways modulating C-RAF protein levels [22, 29]. HERC2 knockdown mimicked the effect observed in HERC2 P594L cells, with depletion of HERC2 correlating with increased C-RAF protein levels. As expected, this was also observed after HERC1 silencing (Fig. 2A). HERC2 depletion modified neither A-RAF nor B-RAF protein levels (Fig. 2B, C). These data indicated that RAF regulation by HERC2 is specific for the C-RAF isoform.

Next, we analysed the RAF MAPK signalling pathway, in which canonical RAF activation triggers ERK phosphorylation [29]. We noted that C-RAF upregulation observed after HERC1 depletion correlated with increased phosphorylated ERK levels, while total ERK protein levels remained stable. However, we detected no changes in ERK phosphorylation in the HERC2-depleted cells (Fig. 2D). These results suggested that C-RAF upregulation caused by HERC2 depletion was not signalled through the canonical MEK/ERK pathway.

HERC2 regulates p38 phosphorylation

Given that HERC1 regulates the MKK3/p38 axis through a RAF-dependent mechanism [29], we decided to study if this mechanism was the same for HERC2. We analysed levels of p38 phosphorylation in U2OS cells transfected with a negative control siRNA, an siRNA against HERC2, and a positive control siRNA against HERC1. We observed the induction of p38 phosphorylation in HERC2-depleted cells, though with total p38 protein levels remaining stable and higher C-RAF protein levels (Fig. 3A). Analogous behaviour was detected in HERC1-depleted cells (Fig. 3A). The same results for p38 phosphorylation were obtained when silencing HERC2 with siRNAs containing different RNA sequences (HERC2 H2.2 and HERC2 H2.4) (Fig. 3B).

The phosphorylation of p38 is associated with its activation and nuclear translocation. To check this, we analysed p38 subcellular localisation. Immunofluorescence

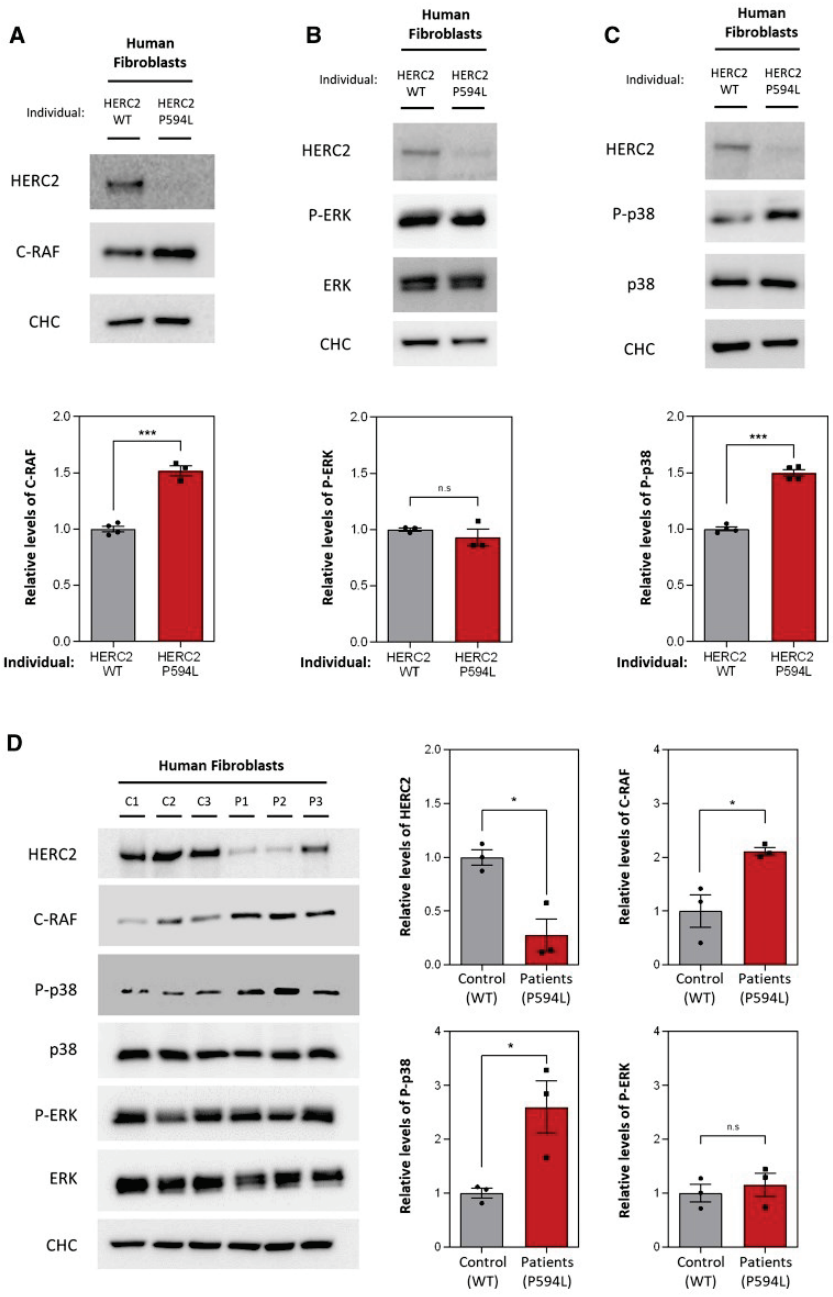

Fig. 1 Patient-derived cells with a homozygous mutation in human *HERC2* gene show MAPK pathway alterations. **A–C** We analysed lysates of human skin fibroblasts from an individual with the wild-type HERC2 (HERC2 WT) and the p.Pro594Leu mutant HERC2 variant (HERC2 P594L) by immunoblot, using the indicated antibodies. C-RAF (**A**), phospho-ERK (P-ERK) (**B**) or phospho-p38 (P-p38) (**C**) levels were quantified and normalised based on clathrin heavy chain (CHC), ERK or p38 protein levels, respectively. The results are expressed relative to the control condition. Plots represent mean ± standard error of the mean. Representative results are shown for experiments repeated at least three times and the data points of each experimental repetition are plotted as single dots. (**D**) We analysed lysates of human skin fibroblasts from three different control individuals with the wild-type HERC2 (C1, C2 and C3) and three different patients with the HERC2 P594L mutant variant (P1, P2 and P3) by immunoblot. Levels of HERC2 and C-RAF proteins were quantified as in **A**. Levels of P-ERK and P-p38 were quantified as in **B**, **C**, respectively. The results are expressed relative to the control condition. Plots represent mean ± standard error of the mean. Representative results are shown for experiments repeated at least three times and the data points of each of the individuals analysed are plotted as single dots. Significance levels: ns = non-significance; $*p \leq 0.05$; $**p \leq 0.01$; $***p \leq 0.001$

experiments showed increased p38 nuclear localisation in HERC2-depleted cells (Fig. 3C). This was quantified assessing the nucleus:cytoplasm ratio, which was higher in HERC2-depleted cells compared with control cells (Fig. 3D).

After HERC2 silencing, p38 activation, was replicated in other human cells, such as the p53-lacking human non-small lung carcinoma cell line (H1299) and the non-tumorigenic human kidney 293 T cell line (HEK 293 T) (Fig. 3E). In addition, the same results were obtained in mouse cells and

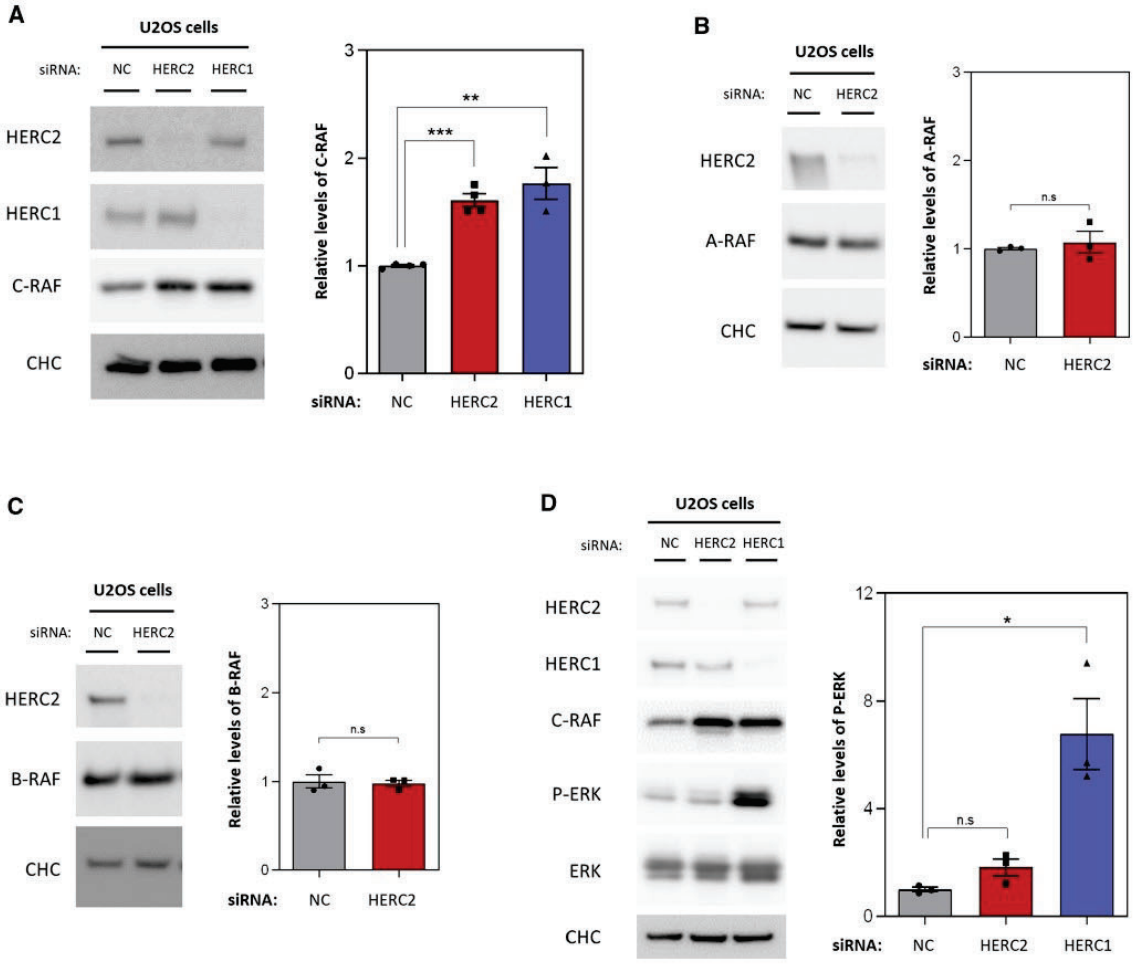

Fig. 2 HERC2 regulates C-RAF protein levels. **A** U2OS cells were transfected with an siRNA negative control (NC), an siRNA against HERC2, or an siRNA against HERC1. The indicated protein levels were analysed by immunoblot. Levels of C-RAF proteins were quantified, normalised based on clathrin heavy chain (CHC) protein levels (loading control), and expressed relative to the control condition. **B**, **C** U2OS cells were transfected with a NC siRNA or an siRNA against HERC2. Levels of A-RAF (**B**) or B-RAF (**C**) were analysed by immunoblot, quantified, normalised based on CHC protein levels, and expressed relative to the control condition. (**D**) U2OS cells were transfected as in **A**, and the indicated protein levels were analysed by immunoblot. Phospho-ERK (P-ERK) levels were quantified, normalised based on ERK protein levels and expressed relative to the control condition. Plots represent the mean ± standard error of the mean. Representative results are shown from experiments repeated at least three times and the individual data points are plotted as single dots. Significance levels: ns = non-significance; $*p \leq 0.05$; $**p \leq 0.01$; $***p \leq 0.001$

when using a different HERC2 silencing method. RAW 264.7 macrophage cell line, primary mouse osteoblasts and MEFs were infected with lentiviral particles carrying either an empty vector as a control (plKO) or a short hairpin RNA (shRNA) against HERC2. All HERC2 knockdown cells presented higher phospho-p38 protein levels compared to controls, while total p38 protein levels remained constant (Fig. 3F). In conjunction, these results demonstrated that HERC2 participates in regulating p38 signalling.

HERC2 regulates the MKK3/p38 pathway through crosstalk mediated by C-RAF

MAPK kinase (MAPKK or MKK) mediates p38 activation through phosphorylation. MKK3 is the dominant isoform

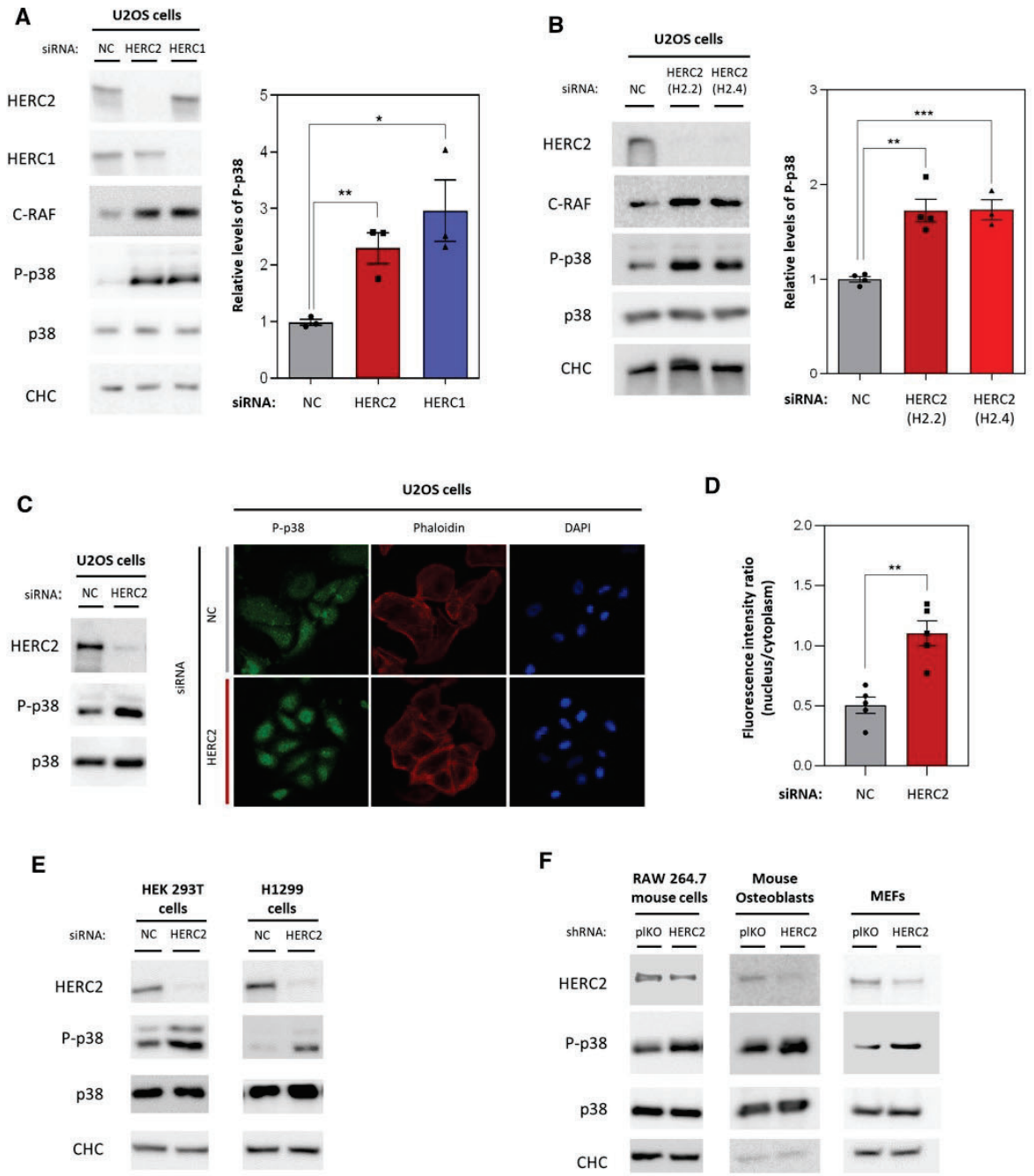

in human U2OS cell lines [29], and its activation has been analysed by measuring its phosphorylation at Ser189 [30]. Thus, we analysed MKK3 activation and its total protein expression in HERC2-depleted U2OS cells, revealing that neither MKK3 phosphorylation at Ser189 nor total MKK3 protein levels were altered compared with control cells (Fig. 4A). To confirm whether p38 phosphorylation triggered by HERC2 depletion depends on MKK3, we co-transfected U2OS with an MKK3 siRNA and either the negative control or the HERC2 siRNA. This revealed that MKK3 knockdown significantly abolished the increment in p38 phosphorylation after HERC2 depletion (Fig. 4B).

◂**Fig. 3** HERC2 regulates p38 phosphorylation. **A** U2OS cells were transfected with an siRNA negative control (NC), an siRNA against HERC2, or an siRNA against HERC1. The indicated protein levels were analysed by immunoblot. Levels of phospho-p38 (P-p38) were quantified, normalised based on total p38 protein levels, and expressed relative to the control condition. **B** U2OS cells were transfected with an siRNA negative control (NC) and two different siRNA sequences against HERC2: H2.2 or H2.4. The indicated protein levels were analysed by immunoblot and phospho-p38 levels were quantified and represented as in (A). **C** U2OS cells transfected with NC or HERC2 siRNA were analysed by immunoblot against the indicated proteins and by confocal microscopy. Fixed cells were stained for phospho-p38 (green), F-actin with phalloidin (red), and nuclei with DAPI (blue) and analysed by immunofluorescence. **D** Fluorescence intensity in the nucleus and cytoplasm per cell was measured and quantified. The ratio nucleus/cytoplasm was calculated. Each data point represent mean of a different field. **E** HEK 293T and H1299 cells were transfected with a NC or HERC2 siRNA. The indicated protein levels were analysed by immunoblot. **F** A RAW 264.7 mouse macrophage cell line, mouse primary osteoblasts and mouse embryonic fibroblasts (MEFs) were infected with lentiviral particles carrying either the empty plKO vector as a negative control (plKO) or an shRNA against HERC2. The indicated protein levels were analysed by immunoblot. Plots represent mean ± standard error of the mean. Representative results are shown from experiments repeated at least three times and the individual data points are plotted as single dots. Significance levels: ns = non-significance; $*p \leq 0.05$; $**p \leq 0.01$; $***p \leq 0.001$

These data suggested that MKK3 activation caused the increase in phospho-p38 independent of phosphorylation at Ser189.

Given the finding that HERC2 regulates C-RAF and p38 activation, we used two specific RAF kinase inhibitors to identify a potential crosstalk mechanism between the two pathways. LY300912 was used to inhibit all RAF isoforms, and Sorafenib was used to inhibit only B-RAF and C-RAF. In absence of the inhibitors, cells showed an increase in p38 phosphorylation after HERC2 depletion; remarkably, however, this increase was clearly abrogated after incubation with LY3009120 or Sorafenib inhibitors for 1 h (Fig. 4C). Since RAF isoforms interact by forming different heterodimers [31], sometimes all isoforms must be depleted to rescue the regulatory effects mediated by RAF proteins. Therefore, we co-transfected U2OS cells with siRNAs against C-RAF or all three RAF isoforms (A-RAF, B-RAF and C-RAF) along with either the negative control siRNA or the siRNA against HERC2 to achieve knockdown (Fig. 4D). Although silencing C-RAF alone was insufficient to reduce p38 phosphorylation significantly, silencing all three isoforms led to a significant decrease in p38 activation in HERC2-depleted cells (Fig. 4D). Unlike pharmacological inhibition of RAF, triple knockdown failed to produce a complete abrogation of p38 phosphorylation after HERC2 depletion, which is probably due to the fact that siRNA silencing did not achieve sufficient RAF isoforms knockdown. Altogether these results confirm the existence of a crosstalk between the RAF and p38 signalling pathways regulated by HERC2.

HERC2 interacts with C-RAF

To further investigate the mechanism behind C-RAF regulation by HERC2, we analysed whether these two proteins can interact. In immunoprecipitation experiments in U2OS cells with a specific anti-HERC2 antibody (bvg3), endogenous HERC2 and C-RAF immunoprecipitated, while HERC1 did not, indicating that the interaction of HERC2 and C-RAF was independent of HERC1 (Fig. 5A). RAF hetero-dimerisation between its isoforms is a well-reported process [31], and consistent with this, A-RAF and B-RAF were also detected in HERC2 immunoprecipitated complexes (Fig. 5B, C). The same results were obtained in the human 293 T cell line (Fig. 5D–F).

To identify the region of HERC2 interacting with C-RAF, we co-expressed a GFP-C-RAF fusion protein with a series of Myc-HERC2 fusion proteins in HEK 293 T cells (Supplementary Fig. 1A), followed by pull-down assays with GFP-binding beads. Constructs F4, F5, and F5CT coimmunoprecipitated with GFP-C-RAF, indicating that the HERC2 and C-RAF protein interaction occurs mainly in the carboxyl-terminus of HERC2 polypeptide chain. F5CT construct, which contains the HECT domain holding the ubiquitin ligase activity, showed the highest affinity with C-RAF, suggesting that this is the most relevant interaction site (Supplementary Fig. 1A). HEK 293 T cells were then co-transfected with a Flag-HERC2 full-length fusion protein along with GFP (as a negative control) or the GFP-C-RAF fusion constructs (CR1, CR2, CR3 or full-length) to map the C-RAF region involved. In the GFP pull-down, Flag-HERC2 was coimmunoprecipitated with CR1, CR3, and the full-length constructs (Supplementary Fig. 1B). To characterise this interaction further, we co-expressed the F4 Myc-HERC2 construct with GFP-C-RAF fusion constructs and performed a GFP pull-down, which showed preferential co-immunoprecipitation of the F4 construct with CR3 (Supplementary Fig. 1C). In parallel, the same experiment was done but with the F5CT Myc-HERC2 construct instead of F4, and this revealed co-immunoprecipitation of F5CT with CR1 and CR3 (Supplementary Fig. 1D). In conjunction, pull-down experiments confirmed the interaction between HERC2 and C-RAF, and indicated the possible domains involved. The HERC2 HECT domain, contained in the F5CT construct, showed the highest affinity for C-RAF and its catalytic domain (CR3), suggesting that the HECT and CR3 domains could be the most relevant at the physiological level. Subsequent structural studies should confirm this relevance.

HERC2 regulates C-RAF ubiquitylation

Having shown that the ubiquitin E3 ligase HERC2 interacts with C-RAF and regulates its protein levels, we wanted

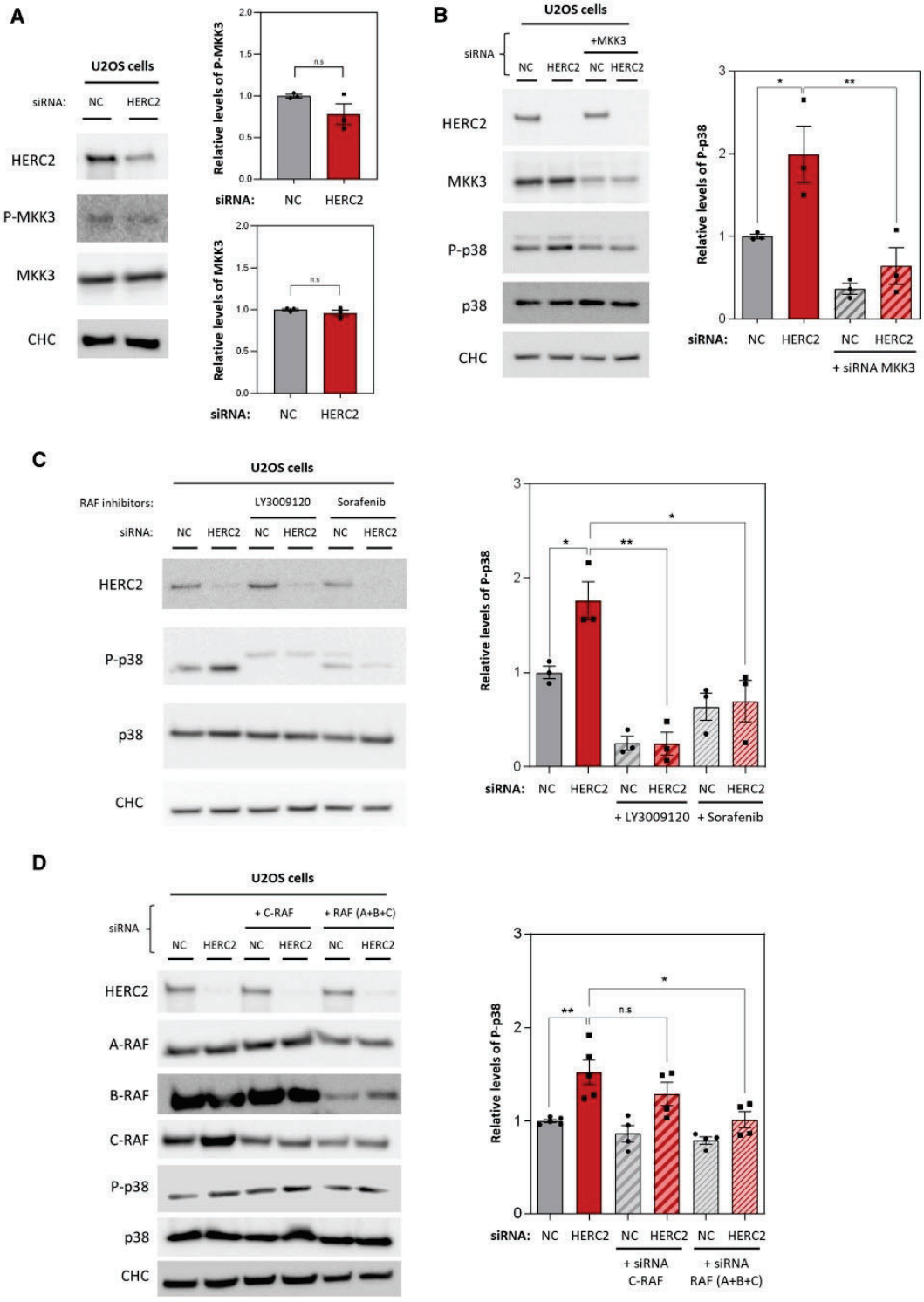
A
U2OS cells
siRNA: NC HERC2
HERC2
P-MKK3
MKK3
CHC
Relative levels of P-MKK3
n.s
siRNA: NC HERC2
Relative levels of MKK3
n.s
siRNA: NC HERC2
B
U2OS cells
siRNA
+MKK3
NC HERC2 NC HERC2
HERC2
MKK3
P-p38
p38
CHC
Relative levels of P-p38
siRNA: NC HERC2 NC HERC2
+ siRNA MKK3
C
U2OS cells
RAF inhibitors: LY3009120 Sorafenib
siRNA: NC HERC2 NC HERC2 NC HERC2
HERC2
P-p38
p38
CHC
Relative levels of P-p38
siRNA: NC HERC2 NC HERC2 NC HERC2
+ LY3009120 + Sorafenib
D
U2OS cells
siRNA
+ C-RAF + RAF (A+B+C)
NC HERC2 NC HERC2 NC HERC2
HERC2
A-RAF
B-RAF
C-RAF
P-p38
p38
CHC
Relative levels of P-p38
n.s
siRNA: NC HERC2 NC HERC2 NC HERC2
+ siRNA C-RAF
+ siRNA RAF (A+B+C)

◂**Fig. 4** HERC2 regulates the MKK3/p38 pathway through crosstalk mediated by C-RAF. **A** U2OS cells were transfected with an siRNA negative control (NC) or an siRNA against HERC2. The indicated protein levels were analysed by immunoblot. Levels of MKK3 and P-MKK3 were quantified and normalised based on clathrin heavy chain (CHC) protein levels (loading control) and total MKK3 protein levels, respectively, and expressed relative to the control condition. **B** U2OS cells were transfected with the NC or HERC2 siRNA. An siRNA against MKK3 was added in the indicated conditions (+MKK3) and the indicated protein levels were analysed by immunoblot. Levels of phospho-p38 (P-p38) were quantified, normalised based on total p38 protein levels and expressed relative to the control condition. **C** U2OS cells were transfected with NC or HERC2 siRNA. At 72 h post-transfection, cells were treated with 1 μM of LY3009120 or 1 μM Sorafenib for 1 h. Untreated cells were incubated with dimethyl sulfoxide (DMSO) as a negative control. Lysates were analysed by immunoblotting and phospho-p38 levels were quantified, normalised by total p38 protein levels and expressed relative to the control condition. **D** U2OS cells were transfected with the NC or HERC2 siRNA. C-RAF siRNA alone or a combination of A-, B- and C-RAF siRNAs (A + B + C) was added when indicated. The indicated protein levels were analysed by immunoblot. Phospho-p38 levels were quantified, normalised by total p38 protein levels and expressed relative to control condition. Plots represent mean ± standard error of the man. Representative results are shown from experiments repeated at least three times and the individual data points are plotted as single dots. Significance levels: ns = non-significance; $*p \leq 0.05$; $**p \leq 0.01$; $***p \leq 0.001$

to dissect whether HERC2 regulates C-RAF ubiquitylation targeting it to proteasomal degradation. To determine this, we analysed C-RAF ubiquitylation both in control and HERC2-depleted cells in the absence and presence of the proteasome inhibitor MG132. Control and HERC2-depleted HEK 293 T cells were transfected with constructs expressing GFP-C-RAF or GFP as a negative control. Forty-eight hours later, cells were incubated for 6 h in the absence or presence of MG132 (10 μM). Lysates from these cells were pulled down using GFP resin. Inputs and pull-down proteins were analysed by PAGE/SDS and immunoblotted with the anti-ubiquitylated proteins antibody (FK2) or with specific antibodies against the indicated proteins. GFP-C-RAF polyubiquitylation slightly decreased in HERC2-depleted cells compared to control cells under basal conditions (Fig. 5G, lane 10 compared with lane 12). Treatment with MG132 efficiently caused accumulation of polyubiquitylated GFP-C-RAF due to proteasome degradation inhibition in control cells (Fig. 5G, lane 10 compared with lane 14). Remarkably, under MG132 treatment, GFP-C-RAF polyubiquitylation levels were much lower in HERC2-depleted cells (Fig. 5G, lane 14 compared with lane 16). Altogether, these results demonstrated C-RAF proteasome-dependent degradation and its regulation by HERC2.

To confirm the role of HERC2 regulating C-RAF polyubiquitylation we performed an ubiquitylation assay. First, we checked expression of different HERC2 constructs in HEK 293 T cells. We transfected either a negative control plasmid (Flag-CTL), a plasmid encoding wild-type HERC2 protein tagged with Flag peptide (Flag-HERC2 WT), or a plasmid encoding a mutant variant lacking ubiquitin ligase activity (Flag-HERC2 C4762S). HERC2 overexpression occurred in both Flag-HERC2 WT and Flag-HERC2 C4762S transfected cells, being greater with the mutated form (Supplementary Fig. 2A). Next, HEK 293 T cells were also transfected with GFP-C-RAF and His-tagged ubiquitin constructs. Cells were lysed after incubation with the proteasome inhibitor MG132 to enrich ubiquitylated proteins degraded by the proteasome, and incubated with Ni–NTA agarose resin to pull-down His-tagged ubiquitin molecules and the proteins to which they were attached (Fig. 5H). The results showed a smear of high molecular weight GFP-C-RAF indicating much greater C-RAF ubiquitylation with wild-type HERC2 overexpression. The plasmid construct HERC2 C4762S, which is catalytically inactive, was used to determine if the effect on C-RAF ubiquitylation by HERC2 WT overexpression, was dependent on the ubiquitin ligase activity of HERC2. Despite greater overexpression of the mutated form (HERC2 C4762S), this did not correlate with increased C-RAF ubiquitylation (Fig. 5H). Ubiquitin proteomic analysis further supported these results. In short, HEK 293 T cells were transiently transfected with a biotinylatable version of ubiquitin, along with either Flag-HERC2 WT or Flag-HERC2 C4762S plasmids. Ubiquitylated proteome from each condition was then isolated by a biotin-based pull-down approach [25] and analysed by mass spectrometry. C-RAF protein appeared in Flag-HERC2 WT-overexpressing cells, but not in Flag-HERC2 C4762S-overexpressing cells (Supplementary Fig. 2B, C). These results confirmed that HERC2 regulates C-RAF ubiquitylation.

HERC2 modulates cellular response to H_2O_2-induced oxidative stress

Given that a major function of p38 is to regulate cellular stress, we analysed the cellular response to oxidative stress. U2OS cells were transfected with a negative control siRNA or an siRNA against HERC2, and oxidative stress was induced by treating cells with 500 μM H_2O_2 for different durations. Protein levels of phosphorylated p38 were analysed by immunoblot. As expected, HERC2-depleted cells started from a more phosphorylated basal state (t = 0) (Fig. 6A). After 3 h of H_2O_2 stimulation, both control cells and HERC2-depleted cells clearly showed induced phosphorylation of p38 and reached a maximum peak intensity, which is higher in HERC2-depleted cells. Interestingly, while p38 phosphorylation levels in control cells were clearly reduced after 6 and 12 h of treatment, the HERC2-depleted cells maintained significantly higher levels at these times, resulting in a more pronounced and prolonged phosphorylation response curve (Fig. 6A).

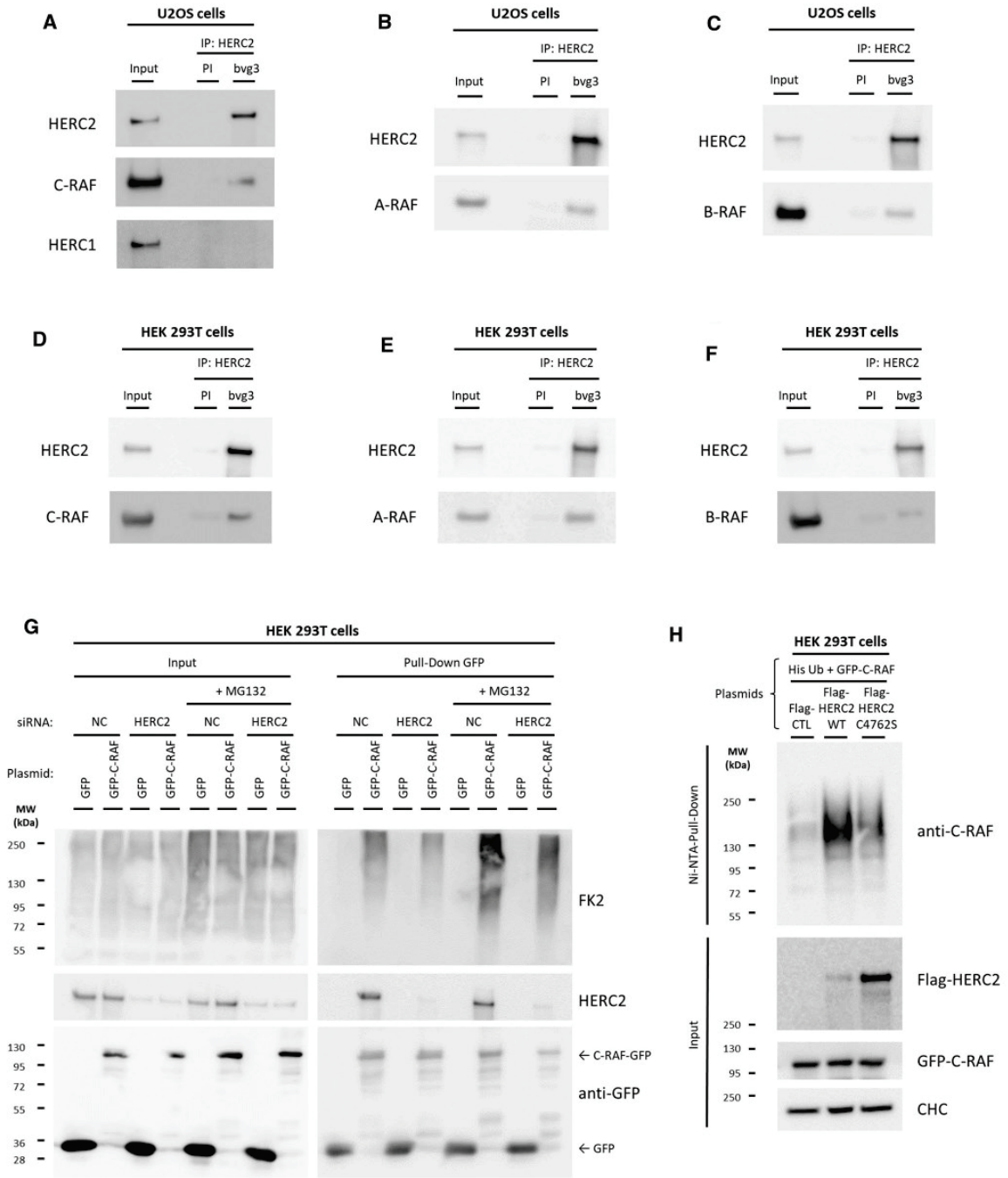

Consistent with HERC2 having a role in regulating the cellular antioxidant response, mRNA levels of the antioxidant genes *NFE2L2*, *SOD1*, *SOD2*, and *GPX1* increased in the HERC2-depleted cells compared with control cells. By contrast, mRNA levels of *GUSB*, used as a negative control, did not change significantly (Fig. 6B). Protein levels of the

◂**Fig. 5** HERC2 interacts with C-RAF and regulates its ubiquitylation. **A–F** Supernatants (Input) of lysates from U2OS (**A–C**) and HEK 293 T cells (**D–F**) were immunoprecipitated (IP) using anti-HERC2 antibodies (bvg3) and analysed by immunoblotting with antibodies against the indicated proteins. Pre-immune serum (PI) was used as a negative control. **G** HEK 293 T cells were transfected with the NC or HERC2 siRNA. Twenty-four hours later, cells were transfected with GFP or GFP-C-RAF plasmids. Forty-eight hours later, cells were incubated for 6 h in the absence or presence of MG132 (10 μM). Lysates were pulled down using GFP resin as indicated in "Materials and methods". Inputs and proteins retained in the resin (Pull-Down GFP) were analysed by immunoblotting with the indicated antibodies. **H** HEK 293 T cells were transfected with His-Ubiquitin (His-Ub) along with GFP-C-RAF plasmids, as well as a Flag-pcDNA control plasmid (Flag-CTL), an HERC2 WT plasmid (Flag-HERC2 WT), or a catalytically inactive form of HERC2 (Flag-HERC2 C4762S). After 48 h, cells were incubated for 6 h with MG132 (10 μM). Ubiquitylated proteins were purified using a Ni–NTA-agarose resin as indicated in "Materials and methods". Inputs and pull-downs were analysed by immunoblotting with antibodies against the indicated proteins. Representative results are shown from experiments repeated at least three times

nuclear factor erythroid 2-related factor 2 (NRF2), a master regulator of all these antioxidants genes, were also upregulated in HERC2-depleted cells (Fig. 6C).

To determine whether the role of HERC2 regulating the cellular response to oxidative stress depends on the activation of the RAF/MKK3/p38 signalling pathway we used p38 (SB203580) and RAF inhibitors (LY3009120). As previously shown, in absence of the inhibitors, cells showed an increase in NRF2 protein levels after HERC2 depletion; however, this increase was abrogated after incubation with SB203580 or LY3009120 for 1 h (Fig. 6D). These results suggested that p38 acts upstream NRF2 activation and that the cellular response to oxidative stress regulated by HERC2 depends on the RAF/MKK3/p38 signalling pathway.

We then evaluated if HERC2 also regulates other stress types modulated by p38. To assess osmotic stress, we treated control cells and HERC2-depleted cells with 100 mM NaCl for different durations; as with H_2O_2, the HERC2-depleted cells maintained higher levels of p38 phosphorylation after 6 and 12 h (Supplementary Fig. 3).

Ultimately, these data showed a complex regulation of downstream p38 signalling dependent on HERC2, pointing out HERC2 as a modulator of the cellular response to oxidative and saline stresses.

HERC2 deficiency alters cellular resistance to H_2O_2-induced oxidative stress

Finally, to determine whether cells with the HERC2 P594L mutation showed an altered response to H_2O_2-induced oxidative stress, we treated them with 500 μM H_2O_2 for different durations. Both the controls (HERC2 WT) and the fibroblasts carrying the mutation (HERC2 P594L) responded with a strong induction of p38 phosphorylation by 1–3 h after H_2O_2 treatment. Notably, HERC2 P594L cells maintained higher p38 phosphorylation levels after 6 h, while levels in control cells had already decreased to baseline (Fig. 7A). These differences in p38 signalling correlated with differences in cell morphology spotted by optical microscopy. After 3 h of treatment with H_2O_2, the HERC2 WT cells had already begun to show a rounder morphology, probably due to the toxic effect of H_2O_2, and after 6 h, most cells showed this altered morphology. By contrast, the HERC2 P594L cells seemed to be more resistant to H_2O_2 exposure, appearing healthier and more attached to the plate culture surface than controls at both 3 and 6 h (Fig. 7B). To confirm the differences in cell viability and test their dependence on the C-RAF/MKK3/p38 signalling pathway, MTT assays were performed in the presence of a p38 inhibitor (SB203580) or the RAF inhibitors (LY3009120 or Sorafenib). After 6 h of treatment with 500 μM H_2O_2, cell viability fell to 13.7% and 44.8% in the control cells and the HERC2 P594L cells, respectively. The higher resistance of HERC2 P594L cells to H_2O_2-induced oxidative stress was abrogated by treatment with the inhibitors (Fig. 7C). We then evaluated this effect under prolonged but less aggressive exposure to H_2O_2 (50 μM for 24 h). Again, HERC2 P594L cell viability was higher compared to the controls after stress exposure and, this higher resistance was abrogated by the p38 or RAF inhibitors (Fig. 7D).

Previous studies have reported that HERC2 depletion enhances cell proliferation due to impaired p53 transcriptional activity [10–12]. Given that HERC2 modulates the activity of p53, we wanted to determine whether the evaluated effects on cell viability also depend, in part, on this tumour suppressor protein. As expected, HERC2-depleted cells with functional p53 (WT p53), presented higher cell growth compared to the control cells (Fig. 7E). The differences in cell growth between the control and HERC2-depleted cells were abolished under p53 knockdown (siRNA p53) (Fig. 7E), so we used this model (p53-knockdown U20S cells) to repeat the cell viability assay after H_2O_2 exposure. In untreated conditions, no significant differences were observed between negative control cells (NC + p53) and HERC2-depleted cells (HERC2 + p53) (Fig. 7F), including after treatment with the inhibitors. However, after 24 h of treatment with 50 μM H_2O_2, cell viability reduced to 67.5% in control cells and only to 89.2% in HERC2-depleted cells. Again, the higher cell resistance of HERC2-depleted cells was abrogated by treatment with p38 (SB203580) and RAF (LY3009120) inhibitors (Fig. 7F). Taken together, these results demonstrated that cellular resistance to H_2O_2-induced oxidative stress acquired by HERC2 deficiency is

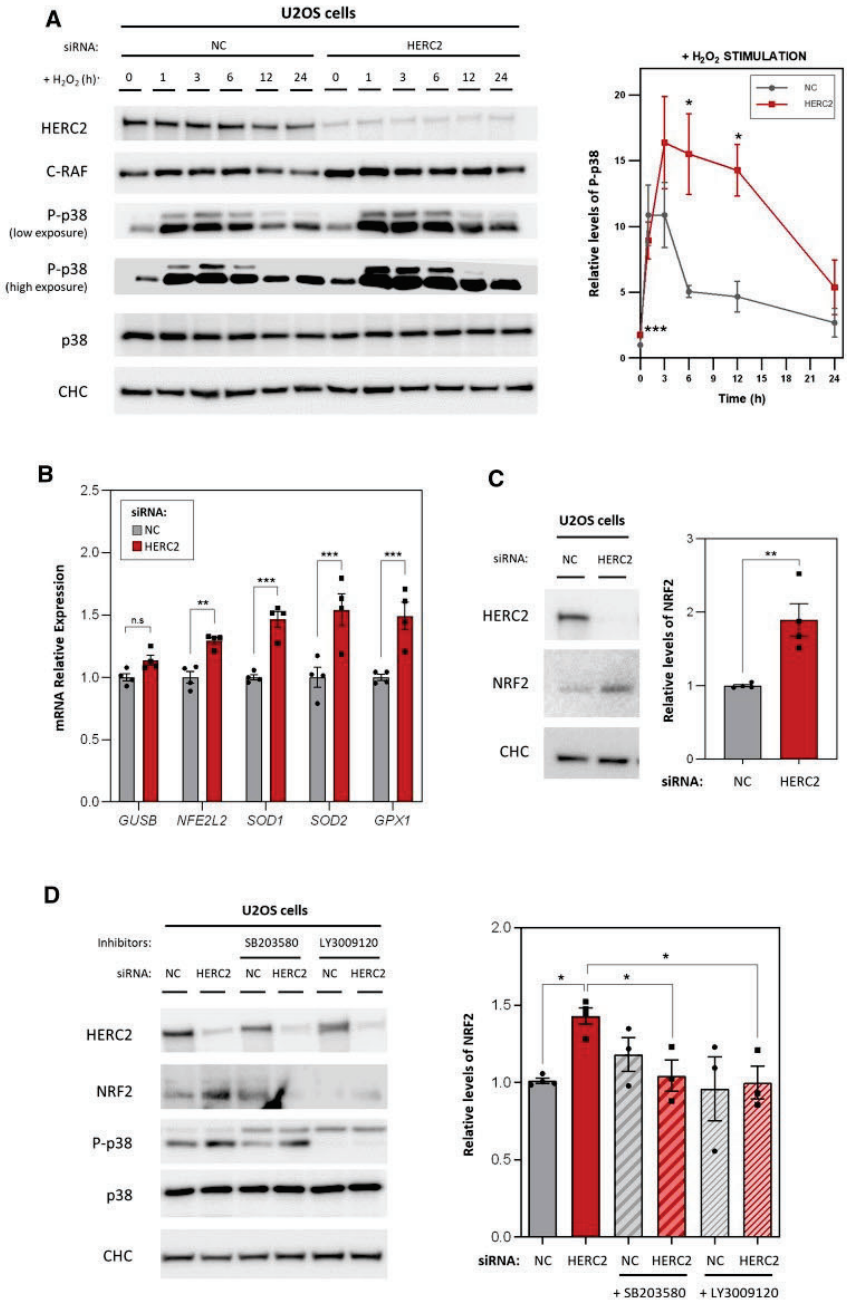

independent of p53, instead being mediated through the C-RAF/MKK3/p38 signalling pathway.

These above results suggested that cells with HERC2 deficiency are better equipped against oxidative stress, so we wondered how does increased protection against oxidative stress fits into pathology. Excessive reactive oxygen species (ROS) cause oxidative stress. However, ROS also play a physiological role in cell signalling. Thus, appropriate ROS production is essential to maintain redox balance. Overexpression of antioxidant enzymes, such as NRF2, may lead

◂**Fig. 6** HERC2 modulates cellular response to H_2O_2-induced oxidative stress. **A** U2OS cells were transfected with an siRNA negative control (NC) or an siRNA against HERC2. Subsequently, cells were treated with 500 µM H_2O_2 to induce oxidative stress for the indicated durations. The indicated protein levels were analysed by immunoblot. Phospho-p38 (P-p38) levels were quantified, normalised based on total p38 protein levels, and expressed relative to the non-treated control condition (NC, $t=0$). Plots represent mean ± standard error of the mean of 4 independent experiments ($n=4$). **B** U2OS cells transfected with the NC or HERC2 siRNA were analysed by RT-qPCR. *GUSB*, *NFE2L2*, *SOD1*, *SOD2*, and *GPX1* mRNA expression levels were quantified, and *GAPDH* levels were used to normalise. Each gene quantification is expressed relative to the control condition and individual data points are plotted as single dots. **C** U2OS cells were transfected with the NC or HERC2 siRNA. The indicated protein levels were analysed by immunoblot. NRF2 protein levels were quantified, normalised based on Clathrin Heavy Chain (CHC) protein levels (loading control), and expressed relative to the control condition. **D** U2OS cells were transfected with the NC or HERC2 siRNA. At 72 h post-transfection, cells were treated with 10 µM SB203580 or 1 µM of LY3009120 for 1 h. Untreated cells were incubated with dimethyl sulfoxide (DMSO) as a negative control. Lysates were analysed by immunoblotting and protein levels of NRF2 were quantified, normalised by Clathrin Heavy Chain (CHC) protein levels (loading control), and expressed relative to the control condition. Plots represent mean ± standard error of the mean. Representative results are shown from experiments repeated at least three times and the individual data points are plotted as single dots. Significance levels: ns = non-significance; $*p \leq 0.05$; $**p \leq 0.01$; $***p \leq 0.001$

the cell to a more reduced state. This pathophysiological situation is known as reductive stress and can be as harmful as is oxidative stress [32–34]. To assess this, mitochondrial ROS levels were evaluated with MitoSOX staining. Cells with the HERC2 P594L mutation showed lesser production of mitochondrial ROS than control cells, suggesting a more reduced state in these cells (Supplementary Fig. 4A). In addition, mitochondria were stained using MitoTracker probes. HERC2 P594L cells presented a more fragmented mitochondrial network than control cells, indicating a possible mitochondrial disfunction (Supplementary Fig. 4B). Further experiments should confirm these preliminary observations and deepen how ROS levels and mitochondrial function participate in the neurological syndrome caused by the HERC2 P594L variant.

Discussion

This study provides the first evidence that HERC2 controls the cellular response to oxidative stress through the p38 signalling pathway dependent on RAF. Our results demonstrate that HERC2 forms a complex with RAF proteins, consistent with the results of a previous proteomic analysis, in which C-RAF was identified to interact with the carboxyl-terminus domain of HERC2 [35]. Mechanistically, our data show that HERC2 regulates C-RAF ubiquitylation and protein degradation; thus, in individuals with the HERC2 P594L mutation, the resulting HERC2 deficiency, causes an increase in C-RAF protein levels. However, this increase is not signalled through the canonical MEK/ERK pathway, and instead, seems to affect the MKK3/p38 pathway specifically (Fig. 8). Activation of crosstalk between C-RAF and the MKK3/p38 pathway has also been described as a mechanism regulated by HERC1, the other member of the large HERC protein family [29]. This raises the question of whether this signalling mechanism is specific to large HERC proteins. In any case, our results demonstrated that the role of HERC2 in the C-RAF/MKK3/p38 signalling pathway is independent of HERC1. Several lines of evidences show this independent role: (1) HERC1 and HERC2 proteins do not interact [29]; (2) HERC1 is not present in the HERC2/C-RAF complex (Fig. 5A); and (3) while HERC1 depletion regulates ERK signalling, HERC2 does not (Fig. 2D). By contrast, activation dependent on HERC2 affects the cellular response to oxidative and saline stresses. Although the precise mechanism explaining the differences between HERC1 and HERC2 should be explored further, differences could be explained by the different complexes formed between RAF proteins and large HERC proteins or by the pleiotropy of the p38 pathway [36]. Many p38 MAPK substrates have been described, both in the cytosol and the nucleus, and each large HERC family member appears to direct p38 signalling towards different downstream targets, suggesting the participation of different HERC1 and HERC2 complexes.

NRF2, a transcription factor encoded by the *NFE2L2* gene, is considered the master regulator of the cellular antioxidant response [37]. A critical regulatory step leading to its activation is its dissociation from Cullin 3 (CUL3) and the ubiquitin ligase Kelch-like ECH-associated protein 1 (KEAP1). CUL3 ubiquitylates NRF2, targeting it to proteasomal degradation, and upon exposure to oxidative stress, the NRF2-KEAP1 complex is disrupted and NRF2 is stabilised for translocation to the nucleus. Nevertheless, the precise mechanism by which cellular stress signals end up reaching NRF2 and causing its dissociation of the complex remains unclear [38]. Indeed, several studies have pointed out that some MAPK pathways are responsible for regulating this signal transduction. The p38 MAPK can regulate NRF2 activity through its activation [39–41] and its repression [42] depending on the context [43]. We observed NRF2 protein levels increasing after HERC2 depletion (Fig. 6C), consistent with p38 activating NRF2. Moreover, the mRNA levels of NRF2-regulated antioxidant genes also increased (e.g. *SOD1*, *SOD2* and *GPX1*) (Fig. 6B). The *NFE2L2* gene contains an antioxidant response element within its promoter region, providing NRF2 the ability to activate its own transcription [44]. This could explain why we observed increased mRNA levels of *NFE2L2* in addition to its protein levels. In addition, the fact that the inhibition of RAF or p38 activity, abolished upregulation of NRF2 in

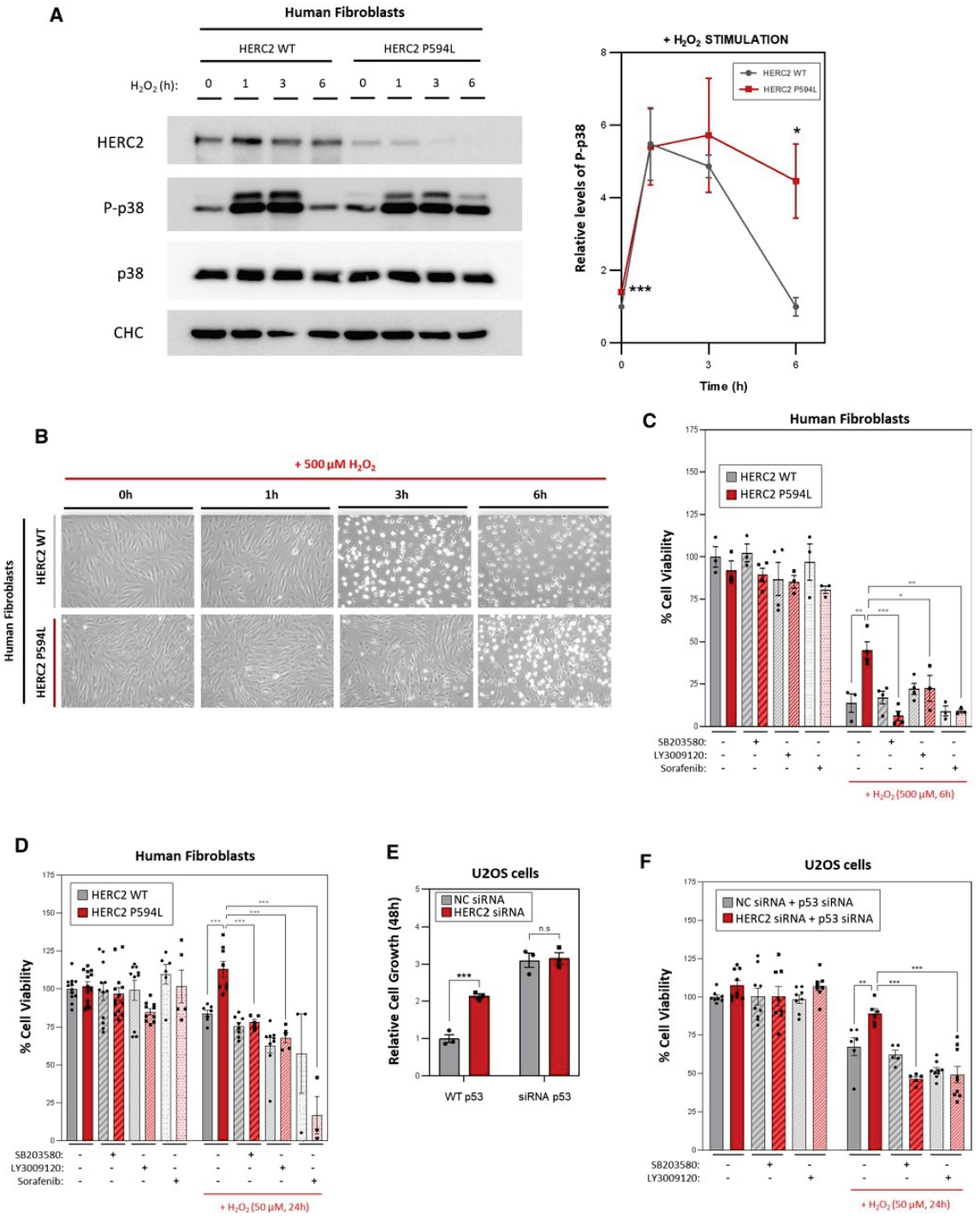
A
Human Fibroblasts
HERC2 WT
HERC2 P594L
H2O2 (h):
0 1 3 6 0 1 3 6
HERC2
P-p38
p38
CHC
+ H2O2 STIMULATION
HERC2 WT
HERC2 P594L
Relative levels of P-p38
Time (h)
B
+ 500 µM H2O2
0h
1h
3h
6h
Human Fibroblasts
HERC2 WT
HERC2 P594L
C
Human Fibroblasts
HERC2 WT
HERC2 P594L
% Cell Viability
SB203580:
LY3009120:
Sorafenib:
+ H2O2 (500 µM, 6h)
D
Human Fibroblasts
HERC2 WT
HERC2 P594L
% Cell Viability
SB203580:
LY3009120:
Sorafenib:
+ H2O2 (50 µM, 24h)
E
U2OS cells
NC siRNA
HERC2 siRNA
Relative Cell Growth (48h)
n.s
WT p53
siRNA p53
F
U2OS cells
NC siRNA + p53 siRNA
HERC2 siRNA + p53 siRNA
% Cell Viability
SB203580:
LY3009120:
+ H2O2 (50 µM, 24h)

◂**Fig. 7** HERC2 deficiency alters cellular resistance to H_2O_2-induced oxidative stress. **A** Human skin fibroblasts derived from an HERC2 wild-type individual (HERC2 WT) and an individual with the p.Pro594Leu HERC2 mutant variant (HERC2 P594L) were treated with 500 µM H_2O_2 to induce oxidative stress for the indicated time points and protein levels were analysed by immunoblot. Phospho-p38 (P-p38) levels were quantified, normalised based on total p38 protein levels and expressed relative to the non-treated control condition (HERC2 WT, $t=0$). Plots represent mean ± standard error of the mean of 4 independent experiments ($n=4$). **B** Human skin fibroblasts were treated as in (A) and images were acquired by optical microscopy after the indicated treatment times, with representative images shown from experiments repeated three times ($n=3$). **C**, **D** HERC2 WT and HERC2 P594L human skin fibroblasts were treated with 500 µM H_2O_2 for 6 h (**C**) or with 50 µM H_2O_2 for 24 h (**D**) as indicated. Cells were treated 1 µM LY3009120, 1 µM Sorafenib or 10 µM SB203580 in the specified conditions 1 h before adding H_2O_2. An MTT assay was performed. Data are presented as a percentage relative to the control and untreated condition. **E** U2OS were transfected with an siRNA negative control (NC) or an siRNA against HERC2. A p53 siRNA was added when indicated (siRNA p53). Subsequently, cells were plated in a 96-well plate and allowed to grow for 48 h to evaluate cell proliferation and an MTT assay was performed. Data are presented relative to the control condition (NC, WT p53). **F** U2OS cells were transfected with the NC or HERC2 siRNA along with p53 siRNA (NC + p53/HERC2 + p53). Cell viability was assessed by MTT assay (under the same conditions mentioned in **D**). Plots represent mean ± standard error of the mean. Representative results are shown from experiments repeated at least three times and the individual data points are plotted as single dots. Significance levels: ns = non-significance; $*p \leq 0.05$; $**p \leq 0.01$; $***p \leq 0.001$

HERC2-depleted cells, confirmed that p38 acts upstream of NRF2 activation. Still, given the variety of p38 substrates we cannot discard that other transcription factors, apart from NRF2, could also be involved in the regulation of the studied antioxidant genes. The transcription factor ATF-2 is another important mediator of p38 in the induction of *SOD2* expression upon H_2O_2-induced oxidative stress in MEFs [45]. This possible cooperation between NRF2 and ATF-2, or some other transcription factor targeted by p38, should be studied further.

Overall, our findings may have both physiological and clinical repercussions. Physiologically, we revealed a pro-survival function of p38 that is regulated by HERC2. HERC2 potentially fine-tunes the cellular response to oxidative stress by controlling protein levels of C-RAF and, therefore, C-RAF/MKK3/p38 signalling to regulate antioxidant gene expression. Clinically, these findings may be relevant to cancer, as well as individuals with HERC2 Angelman-like syndrome due to biallelic *HERC2* gene variants [16, 18].

Several *HERC2* mutations have been associated with a wide number of tumours [4]. In renal cancer, higher *HERC2* gene expression correlates with better patient prognosis [46], supporting the hypothesis that HERC2 may act as a tumour suppressor [4, 46]. We previously demonstrated that HERC2, and NEURL4, regulate the transcriptional activity of the tumour suppressor p53, facilitating its oligomerisation. HERC2 knockdown accordingly increases cell proliferation due to the impaired capability to arrest the cell cycle through p53 [10–12]. Equally, although the precise mechanism remains elusive, it is well established that the production of reactive oxygen species in tumour cells increases due to the higher metabolic rate, with the resulting excess being countered by an increased antioxidant cellular response [47]. Supporting this, in mice, oncogenic alleles of *Kras*, *Braf* and *Myc*, associated with increased *Nfe2l2* expression. This appear to stably enhance NRF2 antioxidant program and lower intracellular reactive oxygen species [48]. Furthermore, in p53 mutated cancer cells, the NRF2-dependent antioxidant response was selectively modulated to enhance cancer cell survival [49]. Our data reveal a new mechanism by which HERC2 deficiency may contribute to tumour malignancy by impairing p53 transcriptional activity, and also by boosting the cellular antioxidant response making cancer cells more resistant to oxidative stress (Fig. 8). In this context, combination treatments with drugs causing non-genotoxic activation of p53 oligomerisation and FDA-approved RAF inhibitors, such as Sorafenib, represent potential therapeutic candidates for tumours associated with HERC2 deficiency.

Finally, a previous proteomic analysis of human *HERC2* mutants (including the p.Pro594Leu variant studied here) has already identified an enrichment of the NRF2-mediated oxidative stress response in *HERC2* mutants compared to control group [20]. In addition, protein–protein interaction networks containing signal transduction proteins and MAPKs were found to be differentially expressed in *HERC2* mutants [20]. Our results add to these observations and, importantly, provide a possible molecular mechanism explanation. It would be interesting for further research to study the implication of a chronic activation of the C-RAF/MKK3/p38 signalling pathway in neuronal cells with HERC2 deficiency. Alterations in p38 MAPK signalling in neurons have been linked to neurodegenerative diseases including Parkinson's disease, Alzheimer's disease and amyotrophic lateral sclerosis (ALS) [50]. Therefore, we cannot discount the possibility that alterations in this pathway could be associated with clinical outcomes in HERC2 Angelman-like syndrome. Consistent with this, previous studies have shown that SOD1 overexpression, in which gene variants are associated with ALS and whose mRNA levels we found to be increased following HERC2 depletion, is associated with defects in the cerebellar architecture [51, 52]. In addition, while excessive ROS elicit oxidative stress, their persistent depletion, as observed in HERC2-deficient cells (Supplementary Fig. 4A), leads to an opposite condition called reductive stress. Persistent activation of antioxidant signalling can cause reductive stress and lead to pathology. In HERC2 P594L cells, the overactivation of NRF2 signalling could be one of the causes. In fact, NRF2 sustained activation has

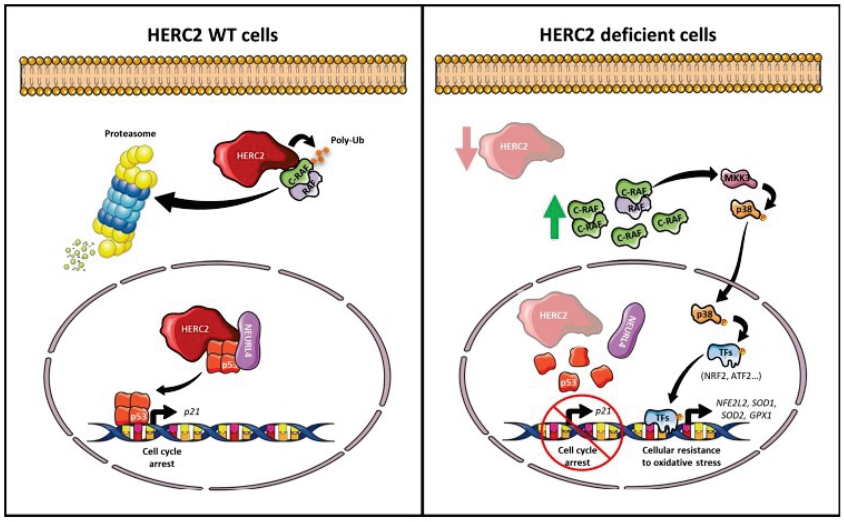

Fig. 8 Working model of HERC2 function in health and disease. In previous studies, we showed that independently of the ubiquitin ligase activity, HERC2 along with NEURL4, facilitates p53 oligomerisation to promote p53 transcriptional program activation. For example, the target gene p21 regulates the cell cycle and promotes cell cycle arrest. Under conditions of HERC2 deficiency or down-regulation, the transcriptional activation of p53 is impaired due to the compromised p53 oligomerisation process [10–13]. Now, with data presented in this study, we complement this working model by adding an important function of HERC2 dependent on its ubiquitin ligase activity. Under normal conditions, HERC2 controls C-RAF protein levels by regulating its ubiquitylation and targeting it to proteasomal degradation. Hence, in HERC2-deficient cells, C-RAF protein levels increase, which activates a crosstalk between the C-RAF and MKK3/p38 signalling pathways. Once p38 is activated by phosphorylation, it translocates to the nucleus and activates its target transcription factors (TFs). This eventually activates transcription of genes related to the oxidative stress response such as *NFE2L2*, *SOD1*, *SOD2* and *GPX1*, which predisposes cells to an enhanced resistance to oxidative stress. The combination of these effects in the p53/p21 and MKK3/p38 pathways may affect both tumorigenesis and neuronal cell homeostasis

already been linked to reductive stress [53]. Highlighting the importance of reductive stress on pathology, mutations in key components of the cellular reductive stress response can cause developmental diseases. For instance, FEM1B gain-of-function mutation, which cause a persistent activation of the reductive stress response, elicit developmental syndromes with some similarities to the HERC2 Angelman-like syndrome [33, 34]. An example of the damage that reductive stress can exert on cells is that it can induce mitochondrial dysfunction and impact on the correct cell function [54, 55]. Accordingly, we observed an increased number of fragmented mitochondria in HERC2 P594L cells, which is a common feature observed in neurodegeneration [56]. However, more experiments are needed to confirm these hypotheses and to associate these mechanisms with clinical outcomes in HERC2 Angelman-like syndrome. All things considered, the findings in this study identify p38 and RAF inhibitors as potential therapeutic options for individuals who present with such rare disease.

Supplementary Information The online version contains supplementary material available at https://doi.org/10.1007/s00018-022-04586-7.

Acknowledgements We would like to thank Dr. Benjamín Torrejón and Dr. Esther Castaño from "Centres Cientifics i Tecnològics de la Universitat de Barcelona" (CCiT-UB), and Ms. Esther Adanero for technical assistance. We also thank Dr. Ohta and Dr. Erazo for kindly providing us with plasmids. This research was supported by the following grants: JLR (*Agencia Estatal de Investigación:* PID2020-120344RB-I00/MCIN/AEI/10.13039/501100011033); and FV (PDC2021-121776-I00 and PID2020-117278GB-I00 from MCIN/AEI/10.13039/501100011033 and FEDER "*Una manera de hacer Europa*" "NextGenerationEU"/PRTR; and Grant 202038-30 from "*La Marató de TV3*"). As well, this article is based upon work from COST Action ProteoCure CA20113, supported by COST (European Cooperation in Science and Technology). J.S.-G. and A.M.-M. received FPU Fellowships (FPU17/02413 and FPU18/06325, respectively) from the Spanish Ministry of Universities.

Author contributions Conceived and designed the experiments: JSG, UM, FV, and JLR. Performed the experiments: JSG, LP, JR, AMM, and JLR. All the authors analysed the data. The first draft of the manuscript was written by JSG and JLR, and all the authors commented on previous versions of the manuscript. All the authors read and approved the final manuscript.

Funding Open Access funding provided thanks to the CRUE-CSIC agreement with Springer Nature. This study was funded by the following grants: JLR (Agencia Estatal de Investigación: PID2020-120344RB-I00/MCIN/AEI/10.13039/501100011033) and FV (PDC2021-121776-I00 and PID2020-117278 GB-I00 from MCIN/

AEI/10.13039/501100011033 and FEDER "Una manera de hacer Europa" "NextGenerationEU"/PRTR. And Grant 202038-30 from "La Marató de TV3"). As well, this article is based upon work from COST Action ProteoCure CA20113, supported by COST (European Cooperation in Science and Technology). JSG and AMM received FPU Fellowships (FPU17/02413 and FPU18/06325, respectively) from the Spanish Ministry of Universities.

Data availability All data analysed during this study to evaluate the conclusions are included within the article or available in supplemental information. Additional related data need to be requested from the corresponding author.

Declarations

Conflict of interest The authors declare no competing interests.

References

1. Parenti I, Rabaneda LG, Schoen H, Novarino G (2020) Neurodevelopmental disorders: from genetics to functional pathways. Trends Neurosci 43:608–621. https://doi.org/10.1016/j.tins.2020.05.004
2. García-Cano J, Martinez-Martinez A, Sala-Gaston J et al (2019) HERCing: structural and functional relevance of the large HERC ubiquitin ligases. Front Physiol. https://doi.org/10.3389/fphys.2019.01014
3. Husnjak K, Dikic I (2012) Ubiquitin-binding proteins: decoders of ubiquitin-mediated cellular functions. Annu Rev Biochem 81:291–322. https://doi.org/10.1146/annurev-biochem-051810-094654
4. Sala-Gaston J, Martinez-Martinez A, Pedrazza L et al (2020) Herc ubiquitin ligases in cancer. Cancers (Basel) 12:1–13. https://doi.org/10.3390/cancers12061653
5. Lee TH, Park JM, Leem SH, Kang TH (2014) Coordinated regulation of XPA stability by ATR and HERC2 during nucleotide excision repair. Oncogene 33:19–25. https://doi.org/10.1038/onc.2012.539
6. Peng Y, Dai H, Wang E et al (2015) TUSC4 functions as a tumor suppressor by regulating BRCA1 stability. Cancer Res 75:378–386. https://doi.org/10.1158/0008-5472.CAN-14-2315
7. Yuan J, Luo K, Deng M et al (2014) HERC2-USP20 axis regulates DNA damage checkpoint through Claspin. Nucleic Acids Res 42:13110–13121. https://doi.org/10.1093/nar/gku1034
8. Zhu M, Zhao H, Liao J, Xu X (2014) HERC2/USP20 coordinates CHK1 activation by modulating CLASPIN stability. Nucleic Acids Res 42:13074–13081. https://doi.org/10.1093/nar/gku978
9. Wu W, Rokutanda N, Takeuchi J et al (2018) HERC2 facilitates BLM and WRN helicase complex interaction with RPA to suppress G-quadruplex DNA. Cancer Res 78:6371–6385. https://doi.org/10.1158/0008-5472.CAN-18-1877
10. Cubillos-Rojas M, Amair-Pinedo F, Peiró-Jordán R et al (2014) The E3 ubiquitin protein ligase HERC2 modulates the activity of tumor protein p53 by regulating its oligomerization. J Biol Chem 289:14782–14795. https://doi.org/10.1074/jbc.M113.527978
11. Cubillos-Rojas M, Schneider T, Bartrons R et al (2017) NEURL4 regulates the transcriptional activity of tumor suppressor protein p53 by modulating its oligomerization. Oncotarget 8:61824–61836. https://doi.org/10.18632/oncotarget.18699
12. García-Cano J, Sánchez-Tena S, Sala-Gaston J et al (2020) Regulation of the MDM2-p53 pathway by the ubiquitin ligase HERC2. Mol Oncol 14:69–86. https://doi.org/10.1002/1878-0261.12592
13. Cubillos-Rojas M, Schneider T, Hadjebi O et al (2016) The HERC2 ubiquitin ligase is essential for embryonic development and regulates motor coordination. Oncotarget 7:56083–56106. https://doi.org/10.18632/oncotarget.11270
14. Pérez-Villegas EM, Ruiz R, Bachiller S et al (2021) The HERC proteins and the nervous system. Semin Cell Dev Biol. https://doi.org/10.1016/j.semcdb.2021.11.017
15. Puffenberger EG, Jinks RN, Wang H et al (2012) A homozygous missense mutation in HERC2 associated with global developmental delay and autism spectrum disorder. Hum Mutat 33:1639–1646. https://doi.org/10.1002/humu.22237
16. Harlalka GV, Baple EL, Cross H et al (2013) Mutation of HERC2 causes developmental delay with angelman-like features. J Med Genet 50:65–73. https://doi.org/10.1136/jmedgenet-2012-101367
17. Morice-Picard F, Benard G, Rezvani HR et al (2016) Complete loss of function of the ubiquitin ligase HERC2 causes a severe neurodevelopmental phenotype. Eur J Hum Genet 25:52–58. https://doi.org/10.1038/ejhg.2016.139
18. Elpidorou M, Best S, Poulter JA et al (2021) Novel loss-of-function mutation in HERC2 is associated with severe developmental delay and paediatric lethality. J Med Genet 58:334–341. https://doi.org/10.1136/jmedgenet-2020-106873
19. Vincent KM, Eaton A, Yassaee VR et al (2021) Delineating the expanding phenotype of HERC2-related disorders: the impact of biallelic loss of function versus missense variation. Clin Genet 100:637–640. https://doi.org/10.1111/cge.14039
20. Abraham JR, Barnard J, Wang H et al (2019) Proteomic investigations of human HERC2 mutants: Insights into the pathobiology of a neurodevelopmental disorder. Biochem Biophys Res Commun 512:421–427. https://doi.org/10.1016/j.bbrc.2019.02.149
21. Wu W, Sato K, Koike A et al (2010) HERC2 is an E3 ligase that targets BRCA1 for degradation. Cancer Res 70:6384–6392. https://doi.org/10.1158/0008-5472.CAN-10-1304
22. Schneider T, Martinez-Martinez A, Cubillos-Rojas M et al (2018) The E3 ubiquitin ligase HERC1 controls the ERK signaling pathway targeting C-RAF for degradation. Oncotarget 9:31531–31548. https://doi.org/10.18632/oncotarget.25847
23. Chan NC, Den Besten W, Sweredoski MJ et al (2014) Degradation of the deubiquitinating enzyme USP33 is mediated by p97 and the ubiquitin ligase HERC2. J Biol Chem 289:19789–19798. https://doi.org/10.1074/jbc.M114.569392
24. Erazo T, Moreno A, Ruiz-Babot G et al (2013) Canonical and kinase activity-independent mechanisms for extracellular signal-regulated kinase 5 (ERK5) nuclear translocation require dissociation of Hsp90 from the ERK5-Cdc37 complex. Mol Cell Biol 33:1671–1686. https://doi.org/10.1128/mcb.01246-12
25. Ramirez J, Prieto G, Olazabal-Herrero A et al (2021) A proteomic approach for systematic mapping of substrates of human

deubiquitinating enzymes. Int J Mol Sci 22:4851. https://doi.org/10.3390/ijms22094851
26. Moffat J, Grueneberg DA, Yang X et al (2006) A lentiviral RNAi library for human and mouse genes applied to an arrayed viral high-content screen. Cell 124:1283–1298. https://doi.org/10.1016/j.cell.2006.01.040
27. Casas-Terradellas E, Tato I, Bartrons R et al (2008) ERK and p38 pathways regulate amino acid signalling. Biochim Biophys Acta Mol Cell Res 1783:2241–2254. https://doi.org/10.1016/j.bbamcr.2008.08.011
28. Cubillos-Rojas M, Amair-Pinedo F, Tato I et al (2010) Simultaneous electrophoretic analysis of proteins of very high and low molecular mass using Tris-acetate polyacrylamide gels. Electrophoresis 31:1318–1321. https://doi.org/10.1002/elps.200900657
29. Pedrazza L, Schneider T, Bartrons R et al (2020) The ubiquitin ligase HERC1 regulates cell migration via RAF-dependent regulation of MKK3/p38 signaling. Sci Rep 10:824. https://doi.org/10.1038/s41598-020-57756-7
30. Raingeaud J, Gupta S, Rogers JS et al (1995) Pro-inflammatory cytokines and environmental stress cause p38 mitogen- activated protein kinase activation by dual phosphorylation on tyrosine and threonine. J Biol Chem 270:7420–7426. https://doi.org/10.1074/jbc.270.13.7420
31. Brummer T, McInnes C (2020) RAF kinase dimerization: implications for drug discovery and clinical outcomes. Oncogene 39:4155–4169. https://doi.org/10.1038/s41388-020-1263-y
32. Bellezza I, Giambanco I, Minelli A, Donato R (2018) Nrf2-Keap1 signaling in oxidative and reductive stress. BBA Mol Cell Res 1865:721–733. https://doi.org/10.1016/j.bbamcr.2018.02.010
33. Manford AG, Rodríguez-Pérez F, Shih KY et al (2020) A cellular mechanism to detect and alleviate reductive stress. Cell 183:46-61.e21. https://doi.org/10.1016/j.cell.2020.08.034
34. Manford AG, Mena EL, Shih KY et al (2021) Structural basis and regulation of the reductive stress response. Cell 184:5375-5390.e16. https://doi.org/10.1016/j.cell.2021.09.002
35. Galligan T, Martinez-noe G, Arndt V et al (2015) Proteomic analysis and identification of cellular interactors of the giant ubiquitin ligase HERC2. J Proteome Res 14:953–966. https://doi.org/10.1021/pr501005v
36. Canovas B, Nebreda AR (2021) Diversity and versatility of p38 kinase signalling in health and disease. Nat Rev Mol Cell Biol 22:346–366. https://doi.org/10.1038/s41580-020-00322-w
37. Rojo de la Vega M, Chapman E, Zhang DD (2018) NRF2 and the Hallmarks of cancer. Cancer Cell 34:21–43. https://doi.org/10.1016/j.ccell.2018.03.022
38. Suzuki T, Yamamoto M (2015) Molecular basis of the Keap1-Nrf2 system. Free Radic Biol Med 88:93–100. https://doi.org/10.1016/j.freeradbiomed.2015.06.006
39. Kang KW, Ryu JIH, Kim SG (2000) The essential role of phosphatidylinositol 3-kinase and of p38 mitogen-activated protein kinase activation in the antioxidant response element-mediated rGSTA2 induction by decreased glutathione in H4IIE hepatoma cells. Mol Pharmacol 58:1017–1025. https://doi.org/10.1124/mol.58.5.1017
40. Alam J, Wicks C, Stewart D et al (2000) Mechanism of heme oxygenase-1 gene activation by cadmium in MCF-7 mammary epithelial cells: role of p38 kinase and Nrf2 transcription factor. J Biol Chem 275:27694–27702. https://doi.org/10.1074/jbc.M004729200
41. Zipper LM, Mulcahy RT (2000) Inhibition of ERK and p38 MAP kinases inhibits binding of Nrf2 and induction of GCS genes. Biochem Biophys Res Commun 278:484–492. https://doi.org/10.1006/bbrc.2000.3830
42. Yu R, Chen C, Mo YY et al (2000) Activation of mitogen-activated protein kinase pathways induces antioxidant response element-mediated gene expression via a Nrf2-dependent mechanism. J Biol Chem 275:39907–39913. https://doi.org/10.1074/jbc.M004037200
43. Huang HC, Nguyen T, Pickett CB (2002) Phosphorylation of Nrf2 at Ser-40 by protein kinase C regulates antioxidant response element-mediated transcription. J Biol Chem 277:42769–42774. https://doi.org/10.1074/jbc.M206911200
44. He F, Ru X, Wen T (2020) NRF2, a transcription factor for stress response and beyond. Int J Mol Sci 21:1–23. https://doi.org/10.3390/ijms21134777
45. Gutiérrez-Uzquiza Á, Arechederra M, Bragado P et al (2012) p38α mediates cell survival in response to oxidative stress via induction of antioxidant genes: effect on the p70S6K pathway. J Biol Chem 287:2632–2642. https://doi.org/10.1074/jbc.M111.323709
46. Schneider T, Martinez-Martinez A, Cubillos-Rojas M et al (2019) Large HERCS function as tumor suppressors. Front Oncol 9:524. https://doi.org/10.3389/fonc.2019.00524
47. Perillo B, Di DM, Pezone A et al (2020) ROS in cancer therapy: the bright side of the moon. Exp Mol Med 52:192–203. https://doi.org/10.1038/s12276-020-0384-2
48. Denicola GM, Karreth FA, Humpton TJ et al (2011) Oncogene-induced Nrf2 transcriptionpromotes ROS detoxification and tumorigenesis. Nature 475:106–109. https://doi.org/10.1038/nature10189
49. Lisek K, Campaner E, Ciani Y et al (2018) Mutant p53 tunes the NRF2-dependent antioxidant response to support survival of cancer cells. Oncotraget 9:20508–20523. https://doi.org/10.18632/oncotarget.24974
50. Correa SAL, Eales KL (2012) The role of p38 MAPK and its substrates in neuronal plasticity and neurodegenerative disease. J Signal Transduct 2012:649079. https://doi.org/10.1155/2012/649079
51. Jaarsma D, Haasdijk ED, Grashorn JAC et al (2000) Human Cu/Zn superoxide dismutase (SOD1) overexpression in mice causes mitochondrial vacuolization, axonal degeneration, and premature motoneuron death and accelerates motoneuron disease in mice expressing a familial amyotrophic lateral sclerosis mut. Neurobiol Dis 7:623–643. https://doi.org/10.1006/nbdi.2000.0299
52. Afshar P, Ashtari N, Jiao X et al (2017) Overexpression of human SOD1 leads to discrete defects in the cerebellar architecture in the mouse. Front Neuroanat 11:22. https://doi.org/10.3389/fnana.2017.00022
53. Rajasekaran NS, Varadharaj S, Khanderao GD et al (2011) Sustained activation of nuclear erythroid 2-related factor 2/antioxidant response element signaling promotes reductive stress in the human mutant protein aggregation cardiomyopathy in mice. Antioxidants Redox Signal 14:957–971. https://doi.org/10.1089/ars.2010.3587
54. Ma WX, Li CY, Tao R et al (2020) Reductive stress-induced mitochondrial dysfunction and cardiomyopathy. Oxid Med Cell Longev. https://doi.org/10.1155/2020/5136957
55. Xiao W, Loscalzo J (2020) Metabolic responses to reductive stress. Antioxidants Redox Signal 32:1330–1347. https://doi.org/10.1089/ars.2019.7803
56. Knott AB, Perkins G, Schwarzenbacher R, Bossy-Wetzel E (2008) Mitochondrial fragmentation in neurodegeneration. Nat Rev Neurosci 9:505–518. https://doi.org/10.1038/nrn2417